Characterization of sncRNA7SL in neuroblastoma cell lines

Dissertation
zur Erlangung des Doktorgrades
der Biomedizinischen Wissenschaften
(Dr. rer. physiol.)

der
Fakultät für Medizin
der Universität Regensburg

vorgelegt von
Nina Weigert
aus
Burglengenfeld

im Jahr
2023

Characterization of sncRNA7SL neuroblastoma cell lines

Dissertation
zur Erlangung des Doktorgrades
der Biomedizinischen Wissenschaften
(Dr. rer. physiol.)

der
Fakultät für Medizin
der Universität Regensburg

vorgelegt von
Nina Weigert
aus
Burglengenfeld

im Jahr
2023

Dekan: Prof. Dr. Dirk Hellwig

Betreuer/in: PD Dr. Gunhild Sommer

Tag der mündlichen Prüfung:

Table of Contents

Zusammenfassung

Das RNA-bindende Protein La spielt eine wichtige Rolle bei der Verarbeitung und Reifung von Vorläufertranskripten der RNA-Polymerase III (Pol III), wie z. B. tRNA und die lange nicht-kodierende RNA 7SL. Die Deletion des La-Proteins in Krebszellen führt zu einer abweichenden Expression von kleinen nicht-kodierenden (snc) RNAs, die von RNA Pol III-Transkripten abgeleitet sind, wie kürzlich für tRNA-abgeleitete miRNAs nachgewiesen wurde.

In diesem Projekt wurde eine sncRNA identifiziert, die als sncRNA7SL bezeichnet wird und in La-depletierten Krebszellen um mehr als das Doppelte erhöht ist. Die Sequenz der sncRNA7SL ist identisch mit dem 3'-Ende des 7SL-RNA-Transkripts, dem Vorläufer aller Alu-Elemente.

Im Rahmen des ersten Ziels wurde gezeigt, dass die sncRNA7SL tumorsuppressive Eigenschaften in Neuroblastomzellen aufzeigt, da die Überexpression der sncRNA7SL zu einem Rückgang der Proliferation, der Vitalität, der Mobilität, des Sphäroidwachstums und der Expression von Protein BMI1 in Neuroblastomzellen führte und gleichzeitig einen G1-Arrest bewirkte. Darüber hinaus erhöhte die Hemmung von sncRNA7SL die Lebensfähigkeit in Neuroblastom- und Ewing-Sarkom-Zelllinien.

In einem zweiten Ziel zeigte die Anwendung von Molecular Beacons, dass die endogene sncRNA7SL hauptsächlich im Zellkern lokalisiert war, mit einem geringen Signal im Zytoplasma, während die endogene 7SL-RNA hauptsächlich im Zytoplasma lokalisiert war.

Das dritte Ziel bestand in der Optimierung synthetischer fluoreszenzmarkierter sncRNA7SL-Oligoribonukleotide, die sich für Lokalisierungs- und Bindungsstudien eignen. Es zeigte sich, dass die 5'- und 3'-Enden für die korrekte Lokalisierung von sncRNA7SL von entscheidender Bedeutung sind. Außerdem wurde gezeigt, dass Oligonukleotide, die am 3'- oder 5'-Ende markiert waren, sich im Zellkern als Kernkörperchen anreicherten, während intern markierte sncRNA7SL ein diffuses Signal im Zellkern zeigte und somit der endogenen Lokalisierung von sncRNA7SL ähnelte. Darüber hinaus akkumulierte intern markierte sncRNA7SL in gewissem Umfang auch in kleinen zytoplasmatischen Körpern. RNA-FISH- und Immunfluoreszenzstudien ergaben, dass es sich bei einigen dieser Kernkörperchen um Paraspeckle handelt. Interessanterweise sind Paraspeckle dafür bekannt, mRNAs zu speichern, die *invertierte Repeat-Alu-Elemente* enthalten. Da die sncRNA7SL-

Sequenz im Alu-Element des 7SL-Vorläufers gefunden wurde, sind diese Sequenzen potenzielle Ziele für sncRNA7SL. Um die Kolokalisation zwischen der FAM-sncRNA7SL und der KNL1 mRNA, die *IRAlu*-Elemente in ihrer 3'UTR enthält, zu analysieren, wurde diese untersucht. Eine partielle Kolokalisation von FAM-sncRNA7SL und KNL1 mRNA wurde bestätigt. Darüber hinaus wurde eine teilweise Kolokalisation zwischen sncRNA7SL-inte-FAM und EDC4-Protein festgestellt. Die Bindung der sncRNA7SL an zytoplasmatische Argonauten (siehe unten) und die Kolokalisation mit dem EDC4-Protein deuten auf die Bildung eines RNA-Silencing-Komplexes und eine mögliche Rolle der sncRNA7SL beim posttranskriptionalen Gen-Silencing hin. Diese Studien zeigen, dass intern fluoreszierend markierte sncRNA ein leistungsfähiges Instrument zur Untersuchung der zellulären Lokalisierung sowie der Kolokalisation mit anderen RNAs und Proteinen sind.

Als letztes Ziel wurde die Bindung von Argonauten, die bekannte Bindungspartner von kleinen nicht-kodierenden RNAs sind, an sncRNA7SL untersucht. Bindungstests zwischen HA-markierten Argonauten (Ago2-HA, Ago3-HA, PIWIL4-HA) und sncRNA7SL-inte-FAM zeigten eine starke *in vitro* Bindung zwischen Ago3-HA oder PIWIL4-HA und sncRNA7SL-inte-FAM. Auffallend ist, dass diese Bindung nicht beobachtet wurde, wenn die sncRNA7SL endmarkiert war, was die Bedeutung der freien 5'- und 3'-Enden unterstreicht und zeigt, dass synthetische und intern markierte sncRNA7SL sowohl in Lebendzell-Imaging als auch in Bindungsstudien verwendet werden können.

Zusammengenommen deuten die Ergebnisse darauf hin, dass die tumorsuppressive Funktion der sncRNA7SL zum Teil über posttranskriptionelles Gen-Silencing im Zytoplasma und, basierend auf der Kolokalisierung mit der Ziel-mRNA im Paraspeckle, über einen noch rätselhaften nukleären Mechanismus vermittelt wird. Die Entwicklung von sncRNA7SL-inte-FAM wird sich als Schlüssel für weitere Studien über die Rolle und Funktion der sncRNA7SL erweisen.

1. Introduction

1.1 sncRNA7SL in neuroblastoma

Cancer is a big health problem and new treatment options are urgently needed. Besides many other pathways such as proliferation, invasion, and metastasis (Hanahan and Weinberg, 2000) the aberrant regulation of the RNA metabolism plays an important role since it can often be used as a biomarker of cancer (Zhang et al., 2021 A; Hu et al., 2022; Xi et al., 2017). The class of small non-coding RNAs (sncRNAs) like transfer RNAs (tRNAs), microRNAs (miRNAs), small nuclear RNAs (snRNAs), and piwi-interacting RNAs (piRNAs) are known to contribute to cancer development (Xiong et al., 2022). The focus of this project lies on the functional characterization and the potential role in cancer of a so far enigmatic small non-coding RNA referred to as sncRNA7SL. As detailed below the functional characterization of this sncRNA7SL will be performed in neuroblastoma cancer cells, since sncRNA7SL is found in those cell lines. Therefore, in the following section, I will introduce the current knowledge about neuroblastoma, sncRNA7SL, and the potential mechanism of action.

Neuroblastoma, a nervous system tumor, is known for being the most common and the deadliest solid childhood tumor with the median age of diagnosis being at about 18 months. Part of the patients developing neuroblastoma tumors were found to have a genetic autosomal-dominant inherited predisposition for this type of cancer (reviewed in Brodeur, 2003). Interestingly, amplification of the so-called MYCN oncogene is found in a subpopulation of patients (Schwab et al., 1983). MYCN amplification correlates with poor prognosis for patients and rapid tumor progression (Seeger et al. 1985). Since only a few treatment options are currently applicable, the identification of novel therapeutic intervention points is urgently required.

A possible biomarker of neuroblastoma and an indicator of overall survival of neuroblastoma patients is the La protein overexpression (Kaess et al., 2023). The La protein is an RNA-binding protein that was first found in Lupus patients (Mattioli and Reichlin, 1974). Structurally, the La protein has three major parts. Two RNA Recognition Motifs (RRM1, RRM2) as well as the La motif (reviewed in Dock-Bregeon, 2021). The La module consisting of RRM1 and the La motif is a characteristic property found in all La-related proteins (Bousquet-Antonelli and Deragon, 2009). The La

module plays a role in binding the 3' uridine tail of RNA Polymerase III (Pol III) transcripts, while the RRM2 plays a role in binding target messenger RNAs' (mRNAs) internal RNA sequences (reviewed Maraia et al., 2017). Another important part of the La protein is its chaperone activity. With the help of its two RNA chaperone domains (RCD-1, RCD-2) (Naeeni et al., 2012; Kuehnert et al., 2015) La can also act independently of UUU-3'OH binding (Huang et al., 2006). In this case, RNA chaperone activity was found to help with the correct folding and maturation of pre-tRNAs (Bayfield and Maraia, 2009; Kucera et al., 2011). Furthermore, RNA chaperone activity was also indicated to play a role in the increased translation of mRNAs (Holcik and Sonenberg, 2005). Strikingly, La protein also plays a major role in cancer. Therefore, La protein levels were found to be elevated in several different cancer cell types, like myelogenous leukemia (Trotta et al., 2003), cervical squamous cell carcinoma (Sommer et al., 2011), primary myelofibrosis (Nakatake et al., 2012), and neuroblastoma (Kaess et al., 2023) as mentioned above. It was shown that elevated level of La mRNA in cancer cells correlates with poor patient survival in various different cancers like lung adenocarcinoma and even neuroblastoma. However, this fact cannot be applied to all cancers, since there is no correlation between high levels of La mRNAs and poor patient prognosis in bladder and ovarian cancer, suggesting La not to be an independent oncogene but in need of certain cellular conditions to promote cancer expression (reviewed in Sommer and Heise, 2021).

In yet-to-be-published data, our lab analyzed the aberrant expression of small non-coding RNA cancer cells by performing small RNA sequencing in La-depleted cancer cells (SK-N-MC). Among the most aberrantly expressed sncRNAs was a 32 nucleotide (nt) long sncRNA with more than a two-and-a-half-fold increase in La-depleted cells. This sncRNA is annotated in the NCBI gene bank under the accession number DQ571003 (https://www.ncbi.nlm.nih.gov/nucleotide/DQ571003) (Girard et al., 2006). According to the piRNA database piRBase this sncRNA is named piR-has-1254 (http://bigdata.ibp.ac.cn/piRBase/all.php?search_string=piR-hsa-1254&search_type=piRNA%20ID). Other aliases for piR-has-1254 are piR1254, piR-31278, and has_piRNA_30793. We assume that piR-has-1254 is annotated as piRNA mainly because of its length since the known piRNA biogenesis pathway occurs in the testis and so far, little is known of the biogenesis of piRNAs in other cell types. The genomic locus for piR1254 is found on chromosome 3 (UCSC Genome Browser on Human GRCh38/hg38). Moreover, BLAST search analysis revealed that the

sequences of piR-has-1254 are identical to the 3'-end of the long non-coding RNA RN7SL2 (RefSeq NR_027260; aliases: 7SL RNA, SRP RNA 2, or RNA, 7SL, cytoplasmic 2) the structural component of the signal recognition particle, as detailed below. Based on this information here,piR-has-1254 will be referred as sncRNA7SL. Since La protein was shown to foster tumor-promoting processes, might act as a non-oncogene addiction factor (reviewed in Sommer and Heise, 2021) in various cancers (Trotta et al., 2003; Sommer et al., 2011; Nakatake et al., 2012) and repressed the expression of sncRNA7SL, it was hypothesized that sncRNA7SL acts as a tumor suppressor in neuroblastoma cells. This inspired studying the impact of sncRNA7SL overexpression and depletion on tumor-promoting processes in various neuroblastoma cell lines. This approach is supported by evidence that sncRNA of the same length is known to play an important role in different types of cancer. Aberrant regulation of piRNAs was found to suppress oncogene expression in various cancers like breast and lung cancer (Moyano and Stefani, 2015; Chalbatani et al., 2019). An increase in oncogenic piRNAs and a decrease in tumor-suppressing piRNAs was found to promote metastasis, tumor growth, and anti-apoptotic factors (Cheng et al., 2011; Chu et al., 2015). Therefore, aberrantly regulated piRNAs are also used as biomarkers in various cancers like renal cell carcinoma (Li et al., 2015) and breast cancer (Tan et al., 2019).

To test tumor suppressive characteristics of sncRNA7SL, different methods could be used like proliferation and viability assays (Kozloski et al., 2016) or studies with molecular beacons to quantify sncRNA expression in cancer cells (Lee et al., 2016).

Furthermore, it is possible that sncRNA7SL acts in gene silencing as described for other sncRNAs such as piRNA (Czech et al., 2018), miRNA (Huntziger and Izaurralde, 2011), and small interfering RNAs (siRNAs) (Alshaer et al., 2021).

1.2 Localization of small non-coding RNAs

In case it is found that sncRNA7SL really exerts influence on tumor-promoting factors such as proliferation or viability in neuroblastoma cells, it is of importance in the next step to understand the mechanism behind these phenotypic results. For this, an important part is the localization of sncRNA7SL in cells, as it might be the first indicator of potential functional mechanisms.

If one considers the localization of other sncRNAs groups, mature miRNAs for example are known to be often localized in the cytoplasm, binding to Argonaute proteins like Ago2 and forming an RNA-induced silencing complex (RISC) (reviewed in Jie et al., 2021). Furthermore, inflammatory miRNAs were also found to accumulate in mitochondria-associated membranes in the human brain (Wang et al., 2020). However, there are also miRNAs that localize within the nucleus (Wong et al., 2014), playing a role in various cellular functions like splicing and activation of gene transcription (Dragomir et al., 2018), for example by binding to promoters, thereby prohibiting gene transcription (Fan et al., 2020).

Nevertheless, since the length of sncRNA7SL shows a closer resemblance to piRNAs compared to the shorter miRNAs, the localization of piRNAs in cells could be similar to sncRNA7SL localization.

piRNAs bind P-element-induced wimpy testis (PIWI) proteins in the germ line, therefore piRNA localization is linked to PIWI protein localization. In flies, it was found that PIWI proteins especially bind antisense strand piRNAs produced by Ago3 RNA cleavage to ensure PIWI-piRNA transport into the nucleus and transcriptional gene silencing of their targets (Wang et al., 2015). Furthermore, it was shown in mice that different piRNAs bind different Argonaute proteins (Aravin et al., 2008). piRNAs bound to MILI are found in cytoplasmatic pi-bodies, presumably playing a role in post-transcriptional silencing by the degradation of cytoplasmic repetitive elements, while MIWI2 preferred antisense piRNA binding was found to localize in the nucleus, playing a role in transcriptional gene silencing by target methylation or degradation of target retro transcripts (Gunawardane et al., 2007; Brennecke et al., 2007; reviewed in Bao and Yan, 2012). These studies suggest that piRNA localization is closely linked to PIWI protein localization.

Despite the focus of many studies being the role of the PIWI-piRNA pathway in the germ line, PIWI proteins were also found to be expressed in soma cells, like various cancers (sarcoma, (Taubert et al., 2007), gastric cancer (Liu et al., 2006)). As an example, it was found that inhibition of HIWI RNA expression led to a decrease in cell growth and to a G2/M cell cycle arrest (Liu et al., 2006). Furthermore, it was also shown that HIWI mRNA was expressed in hematopoietic progenitor cells, but not in their differentiated cell types. Artificial expression of HIWI mRNA in leukemia cell lines was shown to act as a negative regulator for proliferation and induced apoptosis into these

cancer cells (Sharma et al., 2001). These findings suggest the role of PIWI proteins in positive as well as negative cancer regulation.

To identify small non-coding RNA localization different approaches are already known like Northern blotting (Lee et al., 2002), next-generation sequencing (Turunen et al., 2019), and immunofluorescence (Vautrot et al., 2021) among others.

1.3 Argonaute proteins and RISC complexes

Since sncRNA7SL closely resembles the length of a piRNA, Argonaute proteins seem to be likely binding partners. Therefore, the formation of RISC could make sncRNA7SL a major factor in gene expression regulation. Argonaute proteins were first discovered in *Arabidopsis thaliana* in 1998 (Bohmert et al., 1998). Argonaute genes were found to be highly conserved across multicellular organisms (Bohmert et al., 1998, reviewed in Swarts et al. 2014). The eight members of the human Argonaute protein family can be divided into two distinct groups dependent on sequence similarities (Tolia and Joshua-Tor, 2007): the Ago and the PIWI family (Carmell et al., 2002). While all Argonauts are highly conserved, for a long time only Ago2 was shown to have cleavage activity (Meister et al., 2004). Since then, Ago3 has also been shown the ability to slice certain target RNAs, but only under the condition of association of specific small RNAs and if target RNAs furthermore hold flanking regions (Park et al., 2017). Ago proteins 1 and 4 do not have catalytic activity due to only having partial catalytic tetrads (Faehnle et al., 2013; Hauptmann et al., 2014). The Argonaute protein is composed of four distinct domains. The amino terminal or N domain, the PAZ domain, the MID domain, and the PIWI domain. These domains form two lobes that are divided by the so-called central cleft forming the perfect place for guide and target RNA binding (Wang et al., 2008). Interestingly, the MID domain was found to bind to the 5’ terminal nucleotide of the bound RNA (Boland et al., 2011; Frank et al., 2011), while the PAZ domain binds with the last 3’ nucleotides in order to ensure stable RNA binding (Lingel et al. 2003; Lingel et al., 2004; Yan et al.,2003; Duchaine and Fabian, 2019). Furthermore, some Ago proteins PIWI domains also have a catalytic tetrad consisting of Asp-Glu-Asp-His/Asp, allowing endonucleolytic cleavage of target RNAs (Nakanishi et al., 2012).

An especially interesting candidate for sncRNA7SL binding is Ago3, since it was already found to colocalize with and bind to sncRNAs of similar length (Hu et al., 2012). Furthermore, it was shown that interaction between these sncRNAs and Ago3 led to

post-transcriptional target regulation, while Ago1,2,4 and PIWI1-4 binding did not have the same effect (Hu et al., 2012). Depending on its localization, another interesting binding partner for sncRNA7SL is PIWIL4 since it is known to play a role in chromatin remodeling and therefore it could be a way for sncRNA7SL to be part of transcriptional gene silencing (Sugimoto et al., 2007).

Small RNA loading into a RISC can be performed by two different mechanisms: a Dicer-dependent and a Dicer-independent mechanism. In *Drosophila*, empty Ago2 binds to the chaperone Hsp70, which opens the Ago2 structure for RNA binding. Furthermore, Hsp90 stabilizes the open conformation of Ago2 and the small RNA duplex is able to bind Ago2 (Tsuboyama et al., 2018). However, Dicer-2 as well as its partner protein R2D2 were also found to be crucial to enable small RNA binding to Ago2 (Iwasaki et al., 2015). In contrast, human Ago2 RISC assembly was found to be Dicer—independent, but still required chaperone proteins, similar to the Dicer-dependent mechanism (Naruse et al., 2018). Since there are multiple Ago proteins with different functions, the specificity of small RNA is crucial. Therefore, Agos of different species have different criteria for small RNA binding like structural differences of Ago proteins, the identification of the 5' nucleotide, and the size of bound small RNAs (reviewed in Iwakawa and Tomari, 2022). Thereafter, the RISC complex is free to bind complementary target mRNAs, silencing their expression by slicing the activity of engagement of proteins mediating destabilization of target mRNA or its translational repression (reviewed in Iwakawa and Tomari, 2022).
For target RNA cleavage base pairing of the seed region (g2-g8) as well as the central region (g9-g12) of target RNA and small RNA is required (Ding et al., 2003). The cleavage activity of these RISC complexes is especially important as part of viral defense mechanisms (van Mierlo et al., 2012). In order to cleave complementary target RNAs, the Ago PIWI domain establishes the RNase H-like fold, which cleaves target RNAs with the help of the catalytic tetrad at positions 10 and 11 (Nakanishi et al., 2012).

For mRNA decay, small RNA-bound Argonauts were found to assemble with the RNA recognition motive containing GW182 protein among others (Meister et al., 2005). GW182 was found to promote the disassembly of poly(A)-binding protein (PABP) from its bound mRNA and helps to recruit the CCR4-NOT as well as the PAN2-PAN3 complexes (Fabian et al., 2011; Braun et al., 2011). In addition, CCR4-NOT has

deadenylation properties and recruits several decapping factors like the DCP1-DCP2 decapping complex and enhancer of mRNA decapping 4, stimulating DCP2 activity (EDC4) (Fenger-Grøn et al., 2005; Chang et al., 2014; Iwakawa and Tomari, 2022). Furthermore, XRN1, an exoribonuclease helps to degenerate the decapped and deadenylated mRNA (Rehwinkel et al., 2005).

A less understood method of RISC silencing is translational repression. Three pathways of translational repression have been proposed consisting of PABP displacement, eIF4A disjunction, and eIF4E or eIF4G inhibitor recruitment (reviewed in Iwakawa and Tomari, 2022). When the RISC complex dissociates PABP from the 3' poly-A-tail it hinders PABP-eIF4G interaction and therefore translation initiation (Moretti et al., 2012). When the RISC complex promotes eIF4E or eIF4G inhibitor recruitment, the CCR4-NOT complex element NOT1 binds to GW182. Translational repression is accomplished by GW182 interaction with decapping enhancer DDX6 (Chen et al., 2014). The only suggested GW182 independent pathway of RISC silencing was found in *Drosophila* and is the removal of eIF4A from the 5' cap structure resulting in translational repression (Fukaya et al., 2014), suggesting multiple possible pathways of RISC silencing.

While piRNA-dependent transcriptional silencing is often carried out in cooperation with catalytically inactive PIWI proteins (Sienski et al., 2012) the result of chromatin silencing by mechanisms like increased methylation, and post-transcriptional silencing often depends on PIWI proteins with cleavage activity (Fazio et al., 2011).

It was shown that piRNAs use a seed region for target recognition similar to miRNAs (Zhang et al., 2018), however, the piRNAs recognition mechanism must fit the consistently changing transposable elements (Brennecke et al., 2007). While piRNAs binding to PIWI proteins also show a seed region at g2 to g8 their binding affinity is significantly lower compared to miRNAs with Ago2 (Anzelon et al., 2021). Extending the target complementary with piRNAs, strengthened target binding (Anzelon et al., 2021). Nevertheless, piRNA binding to PIWI proteins leaves a central cleft that is tolerant to sequence complementarity imperfections allowing piRNAs to adapt to changing transposable elements (Anzelon et al., 2021).

1.4 target RNAs

In case sncRNA7SL is engaged in gene silencing, it has to be postulated that a sncRNA7SL:Ago clade protein complex binds to target sequences located in specific RNAs. Hence, it would be important to identify potential target RNA containing the more or less degenerated complementary sequence to the sncRNA7SL sequence.
The signal recognition particle (SRP) in humans is made up of six polypeptides or protein subunits (SRP9, SRP14, SRP19, SRP54, SRP68, and SRP72), and its backbone is the 7SL RNA (Walter and Blobel, 1983). Functionally it is known to guide the traffic of membrane proteins as well as secreted proteins across the endoplasmatic reticulum (Walter and Johnson, 1995).

High levels of 7SL RNA were found to be present in various cancer cell types (e.g., breast cancer, and lung cancer) (Abdelmohsen et al., 2014). 7SL RNA depletion was also shown to reduce proliferation in various cancer cell types like cervical carcinoma and pancreatic carcinoma (Abdelmohsen et al., 2014). 7SL RNA was found to interact with the 3' untranslated region (UTR) of TP53 mRNA and therefore decrease the p53 translation level in various cancer cells (Abdelmohsen et al., 2014). As a polymerase III (Pol III) transcript, 7SL RNA is in one category with for example U6 RNA, 5S RNA, and tRNA (reviewed in Willis, 1993).

Interestingly, 7SL RNA, a 300 nt long non-coding RNA, was found to be the ancestor of all Alu sequences (Ullu and Tschudi, 1984). With over one million copies within the human genome, Alu elements are considered the most widespread transposable elements (Lander et al., 2001). Alu elements are part of the class of retroelements, called short interspersed elements (SINES), which are considered to be non-autonomous. This means they require LINE-1, an autonomous human retroelement trans-acting factor for their amplification (Dewannieux et al., 2003). Structurally Alu elements are formed by two dimers, which are separated by an A-rich region (Kramerov et al., 1982; Ullu and Tschudi, 1984; Kramerov and Vassetzky, 2011). Another, even longer, rich region is in the 3' end. While they do have an RNA polymerase III promoter, they do not have a terminator sequence for transcriptions (reviewed in Deininger, 2011). It is suggested that their transcription ends by using a TTTT sequence for termination. Interestingly, while Alu sequences are found to be located in both the 5' and the 3' UTRs of mRNAs, 5 to 10 % of all mRNAs have Alu elements in their 3' UTR (reviewed in Deininger, 2011).

Since 7SL RNA is the ancestor of all Alu elements and the exact sequence of sncRNA7SL was found in the 3' UTR of the 7SL RNA precursor, mRNAs containing Alu elements are potential target RNAs of sncRNA7SL. Alu elements are often expressed as *inverted repeat Alu* (*IRAlu*) elements, which are not only present in a sequence in a sense but also in their complementary sequence and thus lead to the formation of a double structure (Gussakovsky and Kenna, 2021). Therefore, Alu elements have not only the potential of containing degenerated sncRNA7SL sequence but also its degenerated target sequences.

Indeed, this aspect leads to another mechanism for how sncRNA7SL might be involved in gene silencing since *IRAlu* elements are frequently affected by adenosine to inosine RNA editing (Häsler and Strub, 2006). There adenosine is deaminated to inosine by adenosine deaminase acting on RNA (ADAR) protein (Nishikura, 2016). Interestingly, A-to-I editing was also found to play a role in cancer progression as reduction of A-to-I editing was linked to various cancer types like brain tumors (Paz et al.,2007), kidney cancer, and lung cancer among others (reviewed in Gussakovsky and Kenna, 2021).

A-to-I edited mRNAs are often stored in paraspeckles leading to nuclear retention and inhibition of translation (reviewed in Pisani and Baron, 2019). As one of the more recently identified nuclear bodies, paraspeckles were described in 2002 (Andersen et al., 2002). There are about 5 to 20 irregularly distributed paraspeckles per cell (Fox et al., 2002). Furthermore, paraspeckles were shown to have a diameter of about 0.5 to 1 µM (Cardinale et al., 2007). The only mammalian cell type found to not contain paraspeckles to date are human embryonic stem cells (Chen and Carmichael, 2009). Paraspeckles consist of RNA as well as several proteins. The major proteins allowing paraspeckle formation are PSF, NONO (also known as p54NRB), and PSPC1 (reviewed in Fox and Lamond, 2010). While depletion of PSPC1 does not influence paraspeckle assembly (Sasaki et al., 2009), PSF and NONO are essential to the paraspeckle formation (Fox et al., 2005). Interestingly NONO plays a role in the adenosine-to-inosine editing of double-stranded RNA by binding inosine-containing RNA and retaining it within the nucleus (Zhang and Carmichael, 2001). While some proteins are essential to paraspeckle formation, NEAT1 RNA is known as the backbone of paraspeckles and is also essential for paraspeckle formation (Clemson et al., 2009). It is even suggested that early paraspeckle formation at the beginning of the G1 phase is localized near the NEAT1 gene further strengthening the importance of

NEAT1 for paraspeckle formation (Clemson et al., 2009). Interestingly NEAT1 RNA has two distinct isoforms (NEAT1_1 (short), and NEAT1_2 (long)). While paraspeckles were shown to form under the NEAT1_1 knockdown condition, NEAT1_2 is essential for paraspeckle formation (Naganuma et al., 2012; Modic et al., 2019).

In the lab, a number of *IRAlu*-containing mRNAs were found, which have degenerated target sites for sncRNA 7SL in their 3'-UTR. One of those mRNAs is KNL1 mRNA, which will be studied in the work. Interestingly, KNL1 was also found to have negative effects on patient survival in cancer (Bai et al., 2019) and is associated with poor survival of neuroblastoma patients (Fig 1). Therefore, negative regulation of protein expression of MDM2 and KNL1 could further strengthen sncRNA7SL as a tumor suppressor in neuroblastoma.

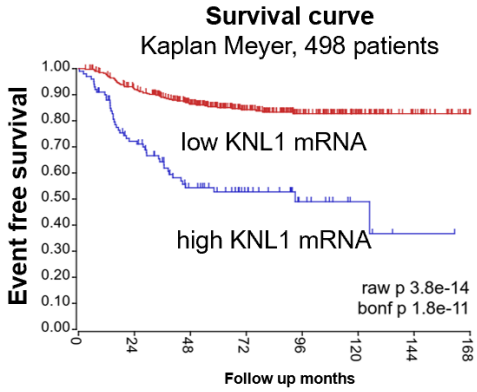

Figure 1. KNL1 expression correlates with poor survival of patients.
Kaplan Meyer survival curve of RNA sequencing analysis of 498 patient samples. The graph shows a correlation between high KNL1 mRNA levels and poor patient survival. Source: R2: Genomics Analysis and Visualization Platform (https://hgserver1.amc.nl/cgi-bin/r2/main.cgi?open_page=login).

To confirm target RNAs of small non-coding RNAs, RNA sequencing of small RNA transfected cells compared to controls (Shiromoto et al., 2020) could be performed as well as Western Blot analysis after transfection of small RNAs or knockdown of small RNAs (Shiromoto et al., 2020). Furthermore, the pull-down of small RNAs could lead to identifying bound protein complexes (Dash et al., 2018) or the pull-down of possible target proteins with subsequent qPCR analysis to confirm small RNA binding of the target protein (Barnes and Kanhere, 2016).

1.5 Objective

The main objective of this study is to demonstrate the tumor-suppressive properties of scnRNA7SL in neuroblastoma and to draw conclusions on the underlying mechanisms by which sncRNA7SL acts. Therefore, sncRNA7SL's role and function will be characterized in neuroblastoma cell lines. The experiments are designed to 1) test the assumptions that sncRNA7SL acts as a tumor suppressor, 2) to define the cellular localization of sncRNA7SL, 3) establish that specifically labeled synthetic sncRNA7SL are powerful tools, useful for studying the subcellular localization and the colocalization of sncRNA7SL with other cellular RNAs and proteins, and 4) set up fluorescence-based sncRNA7SL binding assays. If successfully completed our knowledge about this yet uncharacterized sncRNA will be strongly advanced and will lay the ground for future experiments designed to establish the mechanism of action.

2. Material and Methods

2.1 Material

2.1.1 Chemicals

Table 1. Chemicals and materials used in this study.

Name	Provider	Number
1 kb Extended	NEB	#N32395
Albumin (BSA) Fraction VpH 7,0 for Western Blotting	PanReac Appli Chem	#A6588-0100
Amersham Protran WB Membrane Nitrocellulose 0,45 µm	Sigma	#GE10600002
Ammoniumpersulfat (APS)	Serva	#13375.01
Ampicilin	Carl Roth	#HP62.1
Biozym LE Agarose	Biozym	#A840004
Blue Prestained Protein Standard, Broad Range (11-190 kDa)	NEB	#P7706S
4-Bormoanisole	Sigma	#B56501-100G
BSA 100x 10 mg/l	NEB	#B9001S
Bromphenol blue sodium salt	Sigma	#111746
cOmplete Protease Inhibitor cocktail EasyPack	Sigma	#4693116001
Cut smart Buffer	NEB	#B7204S
DharmaFECT1 Transfection Reagent 0,2 mL	horizon discovery	#T-2001-01
DMEM	Gibco Life Technologies	#21969-035
DMSO HybriMax sterile	Sigma	#D2650-100ML
DTT	Sigma	#D0632-10G
EDTA	Applichem	#A4892,0100
EMEM	Lonza	#12-125F
ER Tracker Green	thermo fisher	#E34251
Ethanol puriss p.a. absol. 99,8% 2,5l	Sigma	#32221-2,5L-M
Fetal bovine serum	Sigma	#F7524
2xFormamide,deionized, bioscience grade, Rnase/Dnase free	Carl Roth	#P040.1
FuGene HD Transfektion Reagent	Promega	#E2311
G418 disulfate, cell culture reagent	AlfaAesar/thermo fisher	#J62671
Gel Loading Dye Purple (6x)	NEB	#B7024A

GelRed Nucleic Acid Gel Stain	Biotium/Linaris	#41003
Gene Ruler DNA Ladder Mix, ready to use	Thermo Fisher Scientific	#SM0334
GlycoBlue	Thermo fisher/life technologies	#AM9516
Gylcerol BioXtra	Sigma	#56-81-5
Glycin>98.5%	Carl Roth	#T873.2
Ham's F12	Biochrom, Schaffhausen, Switzerland	#F0815
HCl (25%)	Carl Roth	#6331.1
HEPES (1M)	Thermo Fisher Scientific	#15630080
Immersol 518 F	Zeiss	#12737327
IsopropanolSigma	Sigma	#I9516-1L
KCl (2M)	Thermo Fisher Scientific	#AM9640G
LB Agar	Sigma	#1102830500
L-glutamine	Gibco Life Technologies	#25030081
Light Cycler 480 SYBR Green I Master	Roche	#04887352001
Lipofectamine 3000/P3000	Thermo Fisher Scientific	#L3000001
Lipofectamine RNAiMAX	Thermo Fisher Scientific	#13778030
magnesium chloride solution, 1.00M	Sigma	#4693116001
2-Mercaptoethanol	Carl Roth	#4227.1
Molecular Probe DAPI, Hochest 33342	Thermo Fisher Scientific	#R37605
NaCl	Carl Roth	#3957.1
NaCl (5M)	Thermo Fisher Scientific	#AM9760G
Nail polish	trent it up	#010
NP-40 Surfact-Amps™ Detergent Solution	Thermo Fisher Scientific	#85124
Natriumacid	Carl Roth	#K305.1
nuklease free water, for mol biology	Sigma	#W4502-10x50ML
OptiMEM I	gibco/Thermo Fisher	#11058-021
1xPBS	gibco/life technologies	#14190-169
Penecilin/Streptomycin	Sigma	#P0781
10x phosphate buffered sline, RNase-free	invitrogen	#AM9624
PhosSTOP EASY pack	Roche	#04906837001
Pierce Anti HA magnetic beads	Thermo Fisher Scientific	#88836
Pierce 16% methanolfree Formaldehyd	Thermo Fisher Scientific	#28906
Poly-D-Lysine	Thermo Fisher Scientific	#A3890401
ProLong Gold Antifade Mountant with DAPI	Thermo Fisher Scientific	#P36941
Propidium iodide	Sigma	#P4864-10ML

Protein Assay Dye Reagent Concentrate	Bio-Rad	#5000006
QIAfilter Plasmid Maxi Kit	Qiagen	#12262
QIAprep Spin Miniprep Kit	Qiagen	#27104
QuantiTect Reverse Transcription Kit	Qiagen	#205311
recombinant RNAsin reibonuclease inhibibtor	promega	#N251B
Ribonuclease A	Sigma	#R6513
RNaseOUT™ Recombinant Ribonuclease Inhibitor	Thermo Fisher Scientific	#10777019
RNAzol RT	Sigma	#R4533-200ML
Rotiphhorese 50x TAE Buffer	Carl Roth	#CL86.1
RPMI 1640	Gibco Life Technologies	#31870-025
RPMI 1640 without Phenolred	Gibco Life Technologies	#32404-014
Saponin	Sigma	#47036-50G
SDS ultra pure, f. Elektroph,Biochem &Molbio, powder >99,0%	Carl Roth	#2326.2
SOC-Medium	invitrogen	#15544-034
Sodium acetate solution (3M)	Thermo Fisher Scientific	#R1181
Sodium Dodecyl Sulfate Reagent Plus	Sigma	#L4509-100G
Stellaris RNA FISH Hybridization Buffer	Biosearch Technologies	#SMF-HB1-10
StellarisRNA FISH 5x Wash Buffer A	Biosearch Technologies	#SMF-WA1-60
StellarisRNA FISH Wash Buffer B	Biosearch Technologies	#SMF-WB1-20
Sucrose, Mol. Biol	Sigma	#S0389-500G
Super Signal West Dura, WB Susbtrat	Thermo Fisher Scientific	#37071
SuperSignal™ West Pico PLUS Chemiluminescent Substrate	Thermo Fisher Scientific	#34577
TEMED (≥99 %, p.a., für die Elektrophorese)	Roth	#2367.3
Thiazolyl Blue Tetrazolium Bromide	SIGMA	#M5655-100MG
Trichostatin A	Cell Signaling	#9950S
Tris-(hydroxymethyl)-aminomethan	Sigma	#77861
TRIS, pro analysis	Sigma	#108383.0500
Triton X-100, for molecular biology	Sigma	#t8787-100ML

6x TriTrack Loading Dye Solution	Fermentas	#R1161
Trypan Blue	Thermo Fisher Scientific	#15250061
6x Trypsin/EDTA Solution, sterile, for cell culture	Sigma	#T3924-100ML
Tryptone/Peptone	Carl Roth	#8952.3
Tween 20	Sigma	#P9416
Ultra-Pure 1M Tris-HCl Buffer pH7.5	Thermo Fisher Scientific	#15567027
Urea	Sigma	#57-13-6
Wash Buffer B	Biosearch Technologies	#SMF-WB1-20
Western Blot Filter Paper, 8x10.5cm	Thermo Fisher Scientific	#88600
Yeast Extract	Carl Roth	#2363.3
Yeast tRNA (10 mg/ml)	Thermo Fisher Scientific	#AM7119

2.1.2 Expendable Materials

Table 2. Expendable materials and plastic products used.

Name	**Provider**	**Number**
µSlide, 8 well	ibidi	#80826
6-Well plates	Falcon/Omnilab	#353046
14 ml Polypropylene Round-Bottom Tube	Corning	#352059
12 well TC Platte	Omnilab	#353043
24WP, TC treated, flat bottom, steril	Sarstedt	#83.3922
96 well cell culture plate	Omnilab	#FALC353072
Amersham Protran Western Blot Membran, Nitrocellulose	Sigma	#GE10600002
Cover Slips	epredia	#CB00180RA120MNZ0
Eppendorf Cups 1,5 m	Sarstedt	#72.706.400
Eppendorf Cups 2 ml	Sarstedt	#72.695.400
Falkon, 15 ml	Sarstedt	#62.554.502
Falkon, 50 ml	Sarstedt	#62.547.254
Laboratory film	Parafilm	#PM-992
Menzel-glas cut edges frosted end	Thermo Fisher Scientific	#ISO8037/1
PCR Plate full skirt LP white	Sarstedt	#72.1980.010
PCR Single Cap 8er-Stripes	Biozym	#710976
Petri Dish	Falcon	#351029
Pipettenspitzen mit Filter	Sarstedt	#655076
Plate, Black, 96 Well Fluotrac 200	greiner bio-one	#781076
Plate, Black 384-well med. binding	greiner bio-one	#352235
Polystyrene Round bottom tube (FACS) with cell strainer	Falcon	#710176
Reaction tube low binding 1,5 ml	Biozym	#844-70045-0

Sealing Tape, optically clear	analytic jena	#FALC353136
Serolog. Pipetten	Sarstedt	#FALC353108
TC Flasche T75	Omnilab	#FALC353136
TC Fasche T25	Omnilab	#FALC353108
Tissue Culture Plate 12 Well Flat Bottom with Low Evaporation Lid	Falcon	#353043
ultra-low-attachment 96-well plates with round bottoms	Corning	#7007
Western Blotting Filter Paper	Thermof Scientific	#88600

2.1.3 Cell lines

Table 3. Mammalian cell lines.

Cell line	Provider
HEK293	Deutsche Sammlung von Mikroorganismen und Zellkulturen
Kelly	Deutsche Sammlung von Mikroorganismen und Zellkulturen
SK-N-AS	American Type Culture Collection
SK-N-MC	American Type Culture Collection
SK-N-SH	American Type Culture Collection
U2-OS	Deutsche Sammlung von Mikroorganismen und Zellkulturen

2.1.4 Bacteria

Table 4. Bacteria used for transformation.

Bacteria	Provider
JM109 Competent Cells	Aglient #200235
TOP10 Bacteria	Thermo Fisher #C404003

2.1.5 Instruments

Table 5. Instruments used for analsis.

Instruments	Provider
96-pin woundmaking tool	Satorius
Autoclav	Sanoclav
Centrifuge 5804R with Cooling	Eppendorf
Certomat R	B. Braun Biotech international
ChemiDoc Imaging-System	BioRad
CLARIOStar® Plate Reader	BMG Labtech
Clean Bench HERAsafe	Heraeus
CO_2Incubator HERA Cell 150i	Heraeus
Compact M Biometra System	analytik jena

Incucyte	Satorius
Integra Pipetboy Acu 2	Inegra
Keyence BZ-X810 fluorescence microscope	Keyence
Leica TCS SP5 confocal laser scanning microscope	Leica
MACS Quant Analyser 10	Miltenyi Biotec
Magnetic Mixer with Heater VMA-C4	VWR
Microscop Nikon Eclipse TS100	Nikon
Microscop camera Nikon DS-Vil	Nikon
Micro centrifuge cooled Micro Star 17R	VWR
Milli-Q EQ 7000	Sigma
Mini-PROTEAN TETRA Cell	Bio-Rad
Mini Trans-Blot Cell	Bio-Rad
Mini Vortex	VWR
Multipipette research 300 µl	Eppendorf
Nanodrop 2000 Spectrophotometer	Thermo scientific
Neubauer Cell Counting Chamber	Brand
pH-Meter Phenomenbal PH1100L	VWR
Pipettes Eppendorf research plus 2 µl, 10 µl, 20 µl, 100 µl, 200µl, 1000 µl	Eppendorf
Power Pack P25T	Biometra
qTOWER2.2	analytik jena
Roller Phoenix instrument RS TR05	Carl Roth
Scale	Kern EW
SonoPuls	Bandelin
Sorvall RC 6 Plus	Thermo electron corporation
Thermomixer R 1.5 ml	Eppendorf
Tube revolver	Thermo Scientific
Water Bath	Julaba
ZOE Fluorescent Cell Imager	Bio-Rad

2.1.6 Software

Table 6. Software used for analysis.

Programm	**Provider**
Adobe Photoshop	Adobe Inc.
BLAST	National Center for Biotechnology Information
BZ-X800 Analyzer software package (Version 1.1.2.4)	Keyence
Cell Migration Analysis software module	Satorius
Citavi 6	Swiss Academic Software
CLARIOStar MARS Analysis Software	BMG Labtech
GraphPad Prism 8.4	GraphPad Software, Inc.

Image J Win-64 (Version 0.10.5)	NIH, Waayne Rasband
IncuCyte 2019B Rev2	Satorius
MACSQuantify™ Software	Miltenyi Biotec
Microsoft Excel	Microsoft Corporation
Microsoft PowerPoint	Microsoft Corporation
Microsoft Word	Microsoft Corporation
NCBI gene bank	https://www.ncbi.nlm.nih.gov/nucleotide/DQ571003
piRBase	http://bigdata.ibp.ac.cn/piRBase/all.php?search_string=piR-hsa-1254&search_type=piRNA%20ID
R2: Genomics Analysis and Visualization Platform	https://hgserver1.amc.nl/cgi-bin/r2/main.cgi?open_page=login
The UNAFold Web Server	http://www.unafold.org
UCSC Genome Broser on Human	University of California

2.1.7 Enzymes

Table 7. Enzymes used.

Enzyme	Provider	Number
APAI	NEB	#R0114S
ECORI	NEB	#R0101S
XCMI	NEB	#R05335

2.1.8 Antibodies

Table 8. Antibodies used for Western Blot and Immunofluorescence.
WB= Western Blot, IF= Immunofluorescence.

Antibodies	Provider	Number	Dilution IF	Dilution WB
Ago3	Cell Signaling Technology	#5054S	1:300-1:600	1:1000
BMI1	Cell Signaling Technology	#5856	-	1:1000
Casp3	Cell Signaling Technology	#9665	-	1:1000
Coilin (H-300)	Santa Cruz	#sc-32860	1:1000	-
EDC4	Cell Signaling Technology	#2548	1:400-1:1000	1:1000
GAPDH	Santa Cruz	#sc-47724	-	1:2000
HA	Cell Signaling Technology	#3724T	1:1000	1:500-1000
Lamin	Cell Signaling Technology	#4777S	-	1:3000

NONO	Cell Signaling Technology	#90336	1:200-1:1000	1:1000
PIWIL4	Abcam	#ab182760	-	1:1000
PSPC1	Abcam	#ab214012	1:3000 – 1:6000	-
SC35	Abcam	#ab11826	1:500	-
α-Tubulin	Calbiochem	#CP06	-	1:1000
anti-mouse IgG, HRP	Cell Signaling Technology	#7076	-	1:3000 – 1:6000
anti-rabbit IgG, HRP	Cell Signaling Technology	#7074	-	1:3000
anti-rabbit IgG (H+L), $F(ab')_2$ Fragment (Alexa Fluor555 Conjugate)	Cell Signaling	#4413	1:1000	-
anti-mouse IgG (H+L), $F(ab')_2$ Fragment (Alexa Fluor 647 Conjugate)	Cell Signaling	#4410	1:1000	-
anti-mouse IgG (H+L), $F(ab')_2$ Fragment (Alexa Fluor 555 Conjugate)	Cell Signaling	#4409	1:1000	-

2.1.9 DNA and RNA Oligos

Table 9. Oligonucleotides used.
The target transcript of siRNAs is indicated by the NCBI Gene ID.

Name	**Provider**	**Number**
control sncRNA	Dharmacon/ Horizon Discovery	#HEITC-000002
sncRNA7SL	Dharmacon/ Horizon Discovery	#HEITC-000001
sncRNA7SL inhibitor	Integrated DNA Technology (IDT)	#226450556
control inhibitor	Integrated DNA Technology (IDT)	#226450557
MBcontrol	Integrated DNA Technology (IDT)	#231760697
MBsncRNA7SL	Integrated DNA Technology (IDT)	#231760696
MBsncRNA-1	Integrated DNA Technology (IDT)	#224943600
MBsnRNA-2A	Integrated DNA Technology (IDT)	#232951542
MB7SL	Integrated DNA Technology (IDT)	#226910439
MB6145	Integrated DNA Technology (IDT)	#224943601
MB7SL-Quencher	Integrated DNA Technology (IDT)	#234660432
MBsncRNA7SL-Quencher	Integrated DNA Technology (IDT)	#234660431
FAM-sncRNA7SL	Dharmacon/ Horizon Discovery	#HEITC-000003
FAM-sncRNActrl	Dharmacon/ Horizon Discovery	#HR1ZN-009289
sncRNA7SL-FAM	Dharmacon/ Horizon Discovery	#HEITC-0000007
sncRNActrl-FAM	Dharmacon/ Horizon Discovery	#HEITC-000008

Cy5-sncRNA7SL	Dharmacon/ Horizon Discovery	#HR1ZN-012090
sncRNA7SL-inte-FAM	Dharmacon/ Horizon Discovery	#HEITC-000009
Cy5-sncRNA7SL-Δ1	Dharmacon/ Horizon Discovery	#HR1ZN-012091
Cy5-sncRNA7SL-Δ2	Dharmacon/ Horizon Discovery	#HR1ZN-012092
sncRNA7SL-Δ2-inte-Cy5	Dharmacon/ Horizon Discovery	#HEITC-000012
RNA FISH Probe KNL1 ORF	BIO SEARCH Technologies	SS851720_01_48
RNA FISH Probe Human NEAT1_m	BIO SEARCH Technologies	SS848739_01_48
siLa/SSB	siTOOLS Biotech	NCBI Gene ID: 6741
siNEAT1-1 long human	siTOOLS Biotech	NCBI Gene ID: 283131
siPIWIL4 human	siTOOLS Biotech	NCBI Gene ID: 143689
sicontrol	siTOOLS Biotech	NCBI Gene ID: control sequence
NEAT1_2 fw	Integrated DNA Technology (IDT)	#225695006
NEAT1_2 rv	Integrated DNA Technology (IDT)	225695007
Hs_GAPDH_1_SG	Qiagen	QT00079247

2.1.10 Plasmide

Table 10.Plasmids used.

Name	**Provider**
Ago2-HA	AG Gunter Meister, Universität Regensburg
Ago3-HA	AG Gunter Meister, Universität Regensburg
PIWIL4-HA	AG Gunter Meister, Universität Regensburg
VP5-HA	AG Gunter Meister, Universität Regensburg

2.2 Methods

2.2.1 Cell culture

Cell lines (Neuroblastoma, Ewing's sarcoma, Osteosarcoma, and embryonic kidney cells) were originally purchased from the American Type Culture Collection, ATCC (SK-N-AS, SK-N-SH, SK-N-MC) or from the Deutsche Sammlung von Mikroorganismen und Zellkulturen, DSMZ (Kelly, HEK293, U2-OS). SK-N-AS and SK-N-SH cells were cultivated in 1:1 EMEM (Lonza, #12-125F) and Ham's F12 (Biochrom, Schaffhausen, Switzerland, #F0815), combined with 2 mM L-glutamine (Gibco Life Technologies, #25030081),1% Penicillin/Streptomycin (Sigma #P0781) and 10% heat-inactivated fetal bovine serum (FBS, Sigma #F7524). SK-N-MC cells were cultured in DMEM (Gibco Life Technologies, #21969-035) containing 2 mM L-glutamine, 1% Penicillin/Streptomycin, and 10% heat-inactivated FBS. Kelly and U2-OS cells were cultivated in RPMI 1640 (Gibco Life Technologies, #31870-025) containing 2 mM L-glutamine (Kelly) or 1.5 nM L-glutamine (U2-OS), 1% Penicillin/Streptomycin, and 10% heat-inactivated FBS. HEK293 cells were cultured in DMEM containing 2 mM L-glutamine, 1% Penicillin/Streptomycin, and 10% heat-inactivated FBS. HA-tagged stable cell HEK293 cell lines were furthermore incubated with 50 µg/ml G418 (AlfaAesar/Thermo Fisher, #J62671). All cell lines were cultivated at 5% CO_2 atmosphere and 37°C. Cell lines were tested for mycoplasma contamination on a regular basis. Cells were split two times a week as a rule. The medium was removed, the cells were washed with 1xPBS (gibco/life technologies, #14190-169), the PBS was removed and the cells were incubated briefly with Trypsin/EDTA (Sigma, #T3924-100ML) to detach them. The cells were then taken up again in medium and distributed in a new T75 or T25 bottle with freshly prepared medium according to the respective split ratios.

2.2.2 DNA and RNA oligonucleotides and Molecular Beacon (MB)

All DNA oligonucleotides were purchased from (Integrated DNA Technology (IDT)) and all RNA oligonucleotides from Horizone/Dharmafect. All oligonucleotides were solved in nuclease-free water to a stock concentration of 100 µM.

<u>RNA oligonucleotides:</u>

RNA modifications: * = Phosphorothioate bond, m = 2’-O-methylation of RNA bases, 3’cholesterol-TEG=3CholTEG

sncRNA7SL (32 nts, sncRNA7SL mimics):

5’-P-
rA*rG*rC*rC*rU*rG*rA*rG*rC*rA*rA*rC*rA*rU*rA*rG*rC*rG*rA*rG*rA*rC*rC*rC*rC*rG*
rU*rC*rU*rC*rU*mA-3’

sncRNActrl (32 nts, reverse sequence of sncRNA7SL):

5‘-P-
rA*rU*rC*rU*rC*rU*rG*rC*rC*rC*rC*rA*rG*rA*rG*rC*rG*rA*rU*rA*rC*rA*rA*rC*rG*rA*r
G*rU*rC*rC*rG*mA-3‘

FAM-sncRNA7SL (32 nts):

5’-FAM-
A*G*C*C*U*G*A*G*C*A*A*C*A*U*A*G*C*G*A*G*A*C*C*C*C*G*U*C*U*C*U*mA-3’

Cy5-sncRNA7SL (32 nts):

5’-Cy5-
A*G*C*C*U*G*A*G*C*A*A*C*A*U*A*G*C*G*A*G*A*C*C*C*C*G*U*C*U*C*U*mA-3’

FAM-sncRNActrl (32 nts):

5’-FAM-
A*U*C*U*C*U*G*C*C*C*C*A*G*A*G*C*G*A*U*A*C*A*A*C*G*A*G*U*C*C*G*mA-3’

sncRNA7SL-FAM (32 nts):

5’-P-A*G*C*C*U*G*A*G*C*A*A*C*A*U*A*G*C*G*A*G*A*C*C*C*C*G*U*C*U*C*U*A-
FAM-3’

sncRNActrl-FAM (32 nts):

5’-P-A*U*C*U*C*U*G*C*C*C*C*A*G*A*G*C*G*A*U*A*C*A*A*C*G*A*G*U*C*C*G*A-
FAM-3’

sncRNA7SL-inte-FAM (32 nts):

5’-P-A*G*C*CmUmGmAmGmCmAmAmCmAU-FAM-
AmGmCmGmAmGmAmCmCmCmCmGmU*C*U*C*U*mA-3’

Cy5-sncRNA7SL (32 nts):

5’-Cy5-
A*G*C*C*U*G*A*G*C*A*A*C*A*U*A*G*C*G*A*G*A*C*C*C*C*G*U*C*U*C*U*mA-3’

Cy5-sncRNA7SL-Δ1 (21 nts):

5’-Cy5-A*G*C*C*U*G*A*G*C*A*A*C*C*C*C*G*U*C*U*C*U*mA-3’

Cy5-sncRNA7SL-Δ2 (22 nts):

5’-Cy5-A*G*C*C*U*G*A*G*C*A*A*C*A*U*A*G*C*G*A*G*A*C*mA-3’

sncRNA7SL-Δ2-inte-Cy5 (22 nts):

5’-PA*G*C*mCmUmGmAmGmCmAU-Cy5-mCmAmUmAmGmCmG*A*G*ACmA-3’

sncRNA7SL inhibitor:

5`-
rU*rA*rG*mAmGmAmCmGmGmGmGmUmCmUmCmGmCmUmAmUmGmUmUmG
mCmUmCmArG*rG* rC*rU*/3CholTEG

sncRNActrl inhibitor:

5’-rU*rC*rG*
rGmAmCmUmCmGmUmUmGmUmAmUmCmGmCmUmCmUmGmGmGmGmCmA
mGrA*rG* rA*rU*/3CholTEG

Molecular Beacon: (FAM = fluorescein, excitation peak at 493 nm, emission peak at 517 nm; DAB = Dabcyl (quenching range: 400–550 nm); Cy5 = Cyanine5: excitation peak at 651 nm, emission peak at 670 nm; BHQ2 = Black Hole Quencher 2, Quenching range: 520-650 nm)

MBsncRNA7SL:

5’-FAM-cgcgAGAGACGGGGTCTCGCTATGTTGCTCAGGCTcgcg-DAB-3’

MBsncRNA7SL-1:

5’-FAM-cgcgcgAGAGACGGGGTCTCGCTATGTTGCTCAGGCTcgcgcg-DAB-3’

MBsncRNA7SL-2A:

5’FAM-cgcgca----ACGGGGTaTCGaTATGTTGCTCAGGC-agcgcg-DAB-3’

(MB-snc7SL-Mut: grey indicates nucleotide deletions or changes (small letters) when compared to wildtype snc7SL RNA)

MBcon:

5’FAM-cgcgTCGGACTCGTTGTATCGCTCTGGGGCAGAGATcgcg-DAB-3’

MB7SL:

5’Cy5-cgcgaGATCGGCATAGCGCACTACAGCCCAGAACTcgcg-BHQ2-3’

MB6145:

5‘FAM-cgcgcgTGAGGCGAACGTGATAACCACTACACTACGGAcgcgcg-DAB-3’

MBsncRNA7SL-Quencher:

5’-FAM-cgcgAGAGACGGGGTCTCGCTATGTTGCTCAGGCTcgcg-3’

MB7SL-Quencher:

5’Cy5-cgcgaGATCGGCATAGCGCACTACAGCCCAGAACTcgcg-3’

Primer used for qPCR analysis:

NEAT1_2 fw:

5’-GTCTTTCCATCCACTCACGTCTATTT-3’

NEAT1_2 rv:

5’-GTACTCTGTGATGGGGTAGTCAGTCAG-3’

2.2.3 Cell transfection

RNA and DNA Oligonucleotides were transfected using various transfection reagents. Cells were transfected either on the day of seeding or the following day, depending on the condition of the cells and the cellular stress caused by transfection.

Table 11. Cell seeding, usage, and density in different cell culture formats.

Format	**Cells Seeded per Well**	**Usage**	**Cell density on the day of the experiment**	**Manufacturer**
6-Well	150.000 (SK-N-AS)-800.000 (Kelly)	Western Blot, RNA	~70-95 %	Falcon/Omnilab (#353046)
12-Well	50.000 - 300.000,	Immunofluorescence, Cell cycle analysis	~50-95 %	Omnilab (#353043)
24-Well	50.000 – 300.000	Live Cell Imaging	~50-95 %	Sarstedt (#83.3922)
96-Well	5.000-75.000	Proliferation, Viability, Mobility, Spheroid assays	~30-95 %	Omnilab (#FALC353072)
Live Cell Imaging Chambers	10.000-70.000	Live Cell Imaging	~40-80 %	ibidi (#80826, 1.5 polymer coverslip bottom)

2.2.4 Transfection with RNAiMAX

All modified RNAs and Molecular Beacons (DNA Oligonucleotides) were transfected into cells using Lipofectamine RNAiMAX Transfection Reagent (ThermoFisher Scientific, #13778030).

Lipofectamine RNAiMAX Transfection Reagent was used for all depletion experiments using siRNAs (see 2.2.20) as well as for microscopy experiments and RNA overexpression and inhibitor experiments.

In most experiments, a final oligo concentration of 12.5 nM was used. For single transfection 100 µM stock solution was diluted to 1 µM in H_2O. Then further diluted to 125 nM with Opti-MEM (gibco/Thermo Fisher, #11058-021) (Reaction A). Furthermore, Lipofectamine RNAiMAX was also mixed with Opti-MEM (1:50) according to the manufacturer's instructions to have an equal amount of solution in a second Eppendorf tube (Reaction B). The contents of Reaction A and Reaction B were then mixed together (1:1) and incubated at room temperature for 5 minutes. Then transfection solution was mixed with 1:5 with medium-containing cells or pipetted into medium and put onto pre-plated cells. In 6-well plates, a transfection mix end volume of 500 µl was used, while in 12-well plates 400 µl was used, in 24-well plates 200 µl and in 96-well plates, 20 µl of transfection mix per well was used per well. For the Ibidi-chamber slides, 60 µl of transfection mix per well was prepared and transfected., For a final concentration of 12.5 nM. For other concentrations, dilutions were adjusted accordingly. Cells were then incubated at 37°C in a 5% CO_2 atmosphere for the needed amount of time. If incubation at 37°C exceeded 48 h medium exchange was performed 48 h after transfection.

Table 12. Volumes used for transfection of 12.5 nM RNA in different plate types.

Plate type	Final Volume [µl]	TF-Mix Volume [µl]	RNAi Max [µl]	Optimem for RNAiMax -Dilution [µl]	1 µM RNA [µl]	Optimem for RNA-Dilution	Final RNA Concentration
6-well	2000	500	4	246	31.25	218.75	12.5
12-well	1000	200	2	98	12.5	87.5	12.5
24-well	500	100	1	49	6.25	43.75	12.5
96-well	100	20	0.2	9.8	1.25	8.75	12.5
Live Cell Imaging Chambers	300	60	0.6	29.04	3.75	26.25	12.5

Table 13. Volumes used for transfection of different final concentrations of RNA in Live Cell Imaging Chambers.

Plate type	Final Volume [µl]	TF-Mix Volume [µl]	RNAi Max [µl]	Optimem for RNAiMax -Dilution [µl]	1 µM RNA [µl]	Optimem for RNA-Dilution	Final RNA Concentration
Live Cell Imaging Chambers	300	60	0.6	29.4	1.9	28.2	6.25
Live Cell Imaging Chambers	300	60	0.6	29.4	3.75	26.25	12.5
Live Cell Imaging Chambers	300	60	0.6	29.4	7.5	22.5	25
Live Cell Imaging Chambers	300	60	0.6	29.4	15	15	50
Live Cell Imaging Chambers	300	60	0.6	29.4	22.5	7.5	75

2.2.5 Transfection with DharmaFECT I

Modified RNAs were transfected into cells using DharmaFECT transfection reagent I (horizon discovery, #T-2001-01).

In most experiments, a final oligo concentration of 12.5 nM was used. For single transfection 100 µM stock solution was diluted to 1 µM in an antibiotic-free serum-free medium. Then further diluted to 125 nM with serum-free medium. In a second Eppendorf tube DharmaFECT transfection reagent I was diluted 1:66.5 in serum-free medium to match the volume of solution in Eppendorf tube 1. The final concentration of DharmaFECT transfection reagent I should be 0.2 µl per well. Contents of both Eppendorf tubes were mixed separately and incubated for 5 minutes at room temperature. Afterward, contents were mixed with each other, incubated for 20 minutes at room temperature, and mixed with four volumes of pre-plated cells or cell medium-containing cells. For a final concentration of 12.5 nM. In 6-well plates, a transfection mix end volume of 500 µl was used, while in 24-well plates 200 µl and in 96-well plates, 20 µl of transfection mix was used per well. For other concentrations, dilutions were adjusted accordingly. Cells were then incubated at 37°C in a 5% CO_2 atmosphere for

the needed amount of time. If incubation at 37°C exceeded 48 h medium exchange was performed.

Table 14. Volumes used for transfection of different final concentrations of RNA in 96-Well plates.

Plate type	Final Volume [µl]	TF-Mix Volume [µl]	RNAi Max [µl]	Optimem for RNAiMax -Dilution [µl]	1 µM RNA [µl]	Optimem for RNA-Dilution	Final RNA Concentration
96	100	20	0.2	9.8	2.5	7.5	25
96	100	20	0.2	9.8	1.9	8.1	18.75
96	100	20	0.2	9.8	1.25	8.75	12.5
96	100	20	0.2	9.8	0.6	9.4	6.25
96	100	20	0.2	9.8	0.3	9.7	3.125

2.2.6 Transfection with FuGENE

Molecular Beacons and Argonaute and PIWI protein expression Vectors were transfected into cells using FuGENE HD Transfection Reagent (Promega, #E2311).
For the plasmid vectors, cells were plated 24 h prior to transfection and transfected at a confluence between 50% and 80 %. For single transfection 2 µg DNA was diluted 1:3 with FuGENE HD Transfection Reagent. Hence, for a final volume of 100 µl, 2 µg DNA was mixed with Opti-MEM and FuGENE and incubated for 15 min at room temperature. Afterward, the solution was mixed with pre-plated cells drop by drop. Cells were then incubated at 37°C in a 5 % CO_2 atmosphere for the needed amount of time. If incubation at 37°C exceeded 48 h medium exchange was performed.
For the molecular beacon transfection, cells were also plated 24 h prior to transfection and transfected at a confluence between 50% and 80%. Per well, 12.5 nM Molecular Beacon was diluted with 0.75 µl FuGENE HD Transfection Reagent, and Opti-MEM was added to fill the volume to 60 µl. The solution was mixed carefully and incubated for 15 min at room temperature. Afterward, the solution was given drop by drop on pre-plated cells which were then incubated at 37°C in a 5% CO_2 atmosphere for 24h.

2.2.7 Transfection with Lipofectamine 3000

Molecular Beacons were transfected using Lipofectamine 3000 (Thermo Fisher #L3000001).

For transfection of the final 12.5 nM concentration, this Oligo stock solution (100 µM) was diluted to 1 µM in H_2O. Afterwards, for a final volume of 60 µl transfection reagent 1 µM Oligo was diluted 1:16 to a concentration of 62.5 nM with Opti-MEM and 0.9 µl Lipofectamine 3000 plus 1.2 µM P3000. Transfection reagents were mixed and incubated at room temperature for 15 min. Afterward, the transfection mix was diluted 1:5 in cell medium, the solution was put onto pre-plated cells and incubated at 37°C for 24 hours.

2.2.8 Viability Assays

To determine the viability of sncRNA7SL transfected cells compared to control transfected cells Thiazolyl Blue Tetrazolium Bromide (Sigma, #M5655-100MG) (MTT) was used based on metabolic activity. In principle, in this assay, the water-soluble MTT reagent is converted to water-insoluble blue formazan by the metabolic components, pyridine nucleotide NADH and NADPH (Berridge and Tan, 1993), therefore quantifying metabolic activity in a cell population. To see the effect the transfection reagent alone caused on the cells a mock control was used. A mock control was used to see the effect the transfection reagent alone caused on the cells; therefore, the cells were transfected not with RNA but with water as a placeholder.

Therefore, 10.000 to 75.000 cells were seeded and transfected 48h, 72h, or 96h prior to MTT analysis in a 96-well plate. A day before the experiments 100 mg MTT stock solution was solved in 20 ml 1xPBS. On the day of the analysis, the medium was taken off the cells and replaced by 100µl of the solved stock solution that was again diluted (1:5) with colorless RPMI (Gibco Life Technologies, #32404-014) medium. Three empty wells also were included to serve as blank controls. Cells were incubated for 2 hours at 37°C. Afterward, 100 µl 100% Isopropanol was added to each well and mixed thoroughly. Cells were incubated for 30 minutes at room temperature. After the incubation period, the precipitate built at the bottom of the wells needed to be solved thoroughly by pipetting up and down for more than ten times. Wells were checked for air bubbles and analyzed in the CLARIOStar Plate Reader. CLARIOSTAR MARS analysis software was used for evaluation. Viability was calculated by normalizing the measured viability against blank controls.

2.2.9 Proliferation Assays

Proliferation assays were performed using a 96-Well cell culture plate (Omnilab, #FALC353072). In these assays, wells were photographed at a specific point every two hours for several days, and cell numbers were counted and compared to control cells. 10.000 to 50.000 cells were seeded onto cell culture plates and transfected immediately. For transfection of cells with 12.5 nM RNA in a 96-Well format, 1 µl RNA Stock (100 µM) was mixed with 99 µl sterile H_2O to create 1 µM RNA solution. Next, two fresh 1.5 ml Eppendorf tubes were used to first mix diluted RNA to 125 nM with antibiotic-free medium to a final volume of 10 µl. Furthermore, DharmaFECT-1 was diluted at 1:50 with an antibiotic-free medium to a final volume of 10 µl. After 5 min incubation at room temperature contents of both tubes were mixed by pipetting to a final volume of 20 µl and incubated for 20 min at room temperature. Afterward, the sample was mixed 1:5 with cell solution (20.000 to 30.000 cells per well) and seeded into one 96-well plate. All numbers given here are for one well. The transfected cells were incubated in the Incucyte (Satorius) for up to 72 hours to analyze proliferation over several days. Cell numbers were counted every two hours and compared. Measurement data were analyzed using IncuCyte 2019B Rev2 (Sartorius).

2.2.10 Mobility Assays

To see if cells' capability of migrating into a cell-free area was influenced by RNA transfection, 50.000 to 80.000 Kelly cells were transfected with 12.,5 nM sncRNA7SL mimics or its respective control using DharmaFECT-1 (see subsection 2.2.5). Cells were plated on a 96-Well plate and allowed to grow for 24 hours to about 80 to 90% confluence. A "wound" was scratched into the cell layer using the 96-pin wound-making tool (Incucyte WoundMaker). Cells were put back into the Incucyte System and analyzed for up to 68 hours. The size of the cell-free scratched area was measured and compared to control samples. Measurements of the scratched area were quantified using the Cell Migration Analysis software module (Sartorius, #4400).

2.2.11 Spheroid Assays

To see if sncRNA7SL also has an effect in 3D cell culture, closer to the shape of an actual tumor, spheroid assays were performed. For spheroid assay analysis cells were transfected with 12.5 nM (Kelly) or 25 nM (SK-N-SH) sncRNA7SL or control RNA respectively using DharmaFECT-1 (see subsection 2.2.5). 24 hours after transfection

cells were taken off the 96-well plate, counted, and about 5.000 cells were replated in ultra-low-attachment (ULA) 96-well plates with round bottoms (Corning, #7007). Three, seven, and ten days after replating of cells pictures were taken with the Microscope Nikon Eclipse TS100 (Nikon) and the Microscope camera Nikon DS-Vil (Nikon). Measurement and analysis of growth were done with ImageJ-win64 (Version 0.10.5).

2.2.12 Cell cycle assays

To see if RNA transfection leads to a cell cycle arrest, 400.000 cells were transfected with sncRNA7SL mimics or respective controls on 12- Well plates. 72h after transfection cells were washed once with 1 ml 1x PBS and incubated for about 5 minutes in 0.3 ml Trypsin-EDTA per well. 400.000 cells were then harvested in 1 ml of sample buffer (1x PBS containing 1% FBS). The cell suspension was transferred to FACs tubes (Falcon, #710176) and centrifuged at 300 rcf for 5 min at 4°C. Cells were kept on ice. The supernatant was discarded and the cells were resuspended in 2 ml Sample Buffer (1x PBS containing 1% FBS). The centrifugation step was repeated, 1.9 ml of the supernatant was discarded and the pellet was solved in the rest volume of about 100 µl. Cells were vortexed for 10 seconds and fixed with 70% ice-cold Ethanol (EtOH) by vortexing Eppendorf Tubes carefully and adding 500 µl/tube of EtOH dropwise to a final volume of about 0.6 ml. Eppendorf Tubes were closed and incubated at 4°C in the dark overnight. The staining solution was prepared by mixing 0.4 ml Sample Buffer with 25 µg Propidium iodide (Sigma, #P4864-10ML) and 50 µg RNase A (Sigma, #R6513). The fixed cells were mixed with 2 ml Sample Buffer and centrifugated at 400 rcf for 10 min at 4°C. The supernatant was discarded. Rest volume was used to solve the pellet and 0.4 ml Staining Solution was added per sample. Cells were mixed gently and incubated for 30 min at room temperature in the dark. Afterward, cell cycle phases were sorted by measuring the DNA quantity of the cells by measuring DNA bound Propidium iodide signal with the MACS Quant Analyser 10 (Miltenyi Biontec).

2.2.13 Western blot analysis for protein detection

Cells were lysed in SDS-Loading Buffer (5 ml 0.5 M Tris/HCl pH 6.8; 8 ml 10% SDS; 4 ml Glycerol; 21 ml Millipore water and some Bromphenol Blue; 500.000 cells per 400 µl SDS-Loading Buffer). After lysis, cells were sonified using basic settings of SonoPuls

for about 15 to 30 seconds, mixed with 5% 2-mercaptoethanol, and shaken for 10 min at 95°C and 550 rpm. Lysates were analyzed on a 7,5% or 12,5% SDS-polyacrylamide gel (SDS-Gel).

Table 15. Composition of the running gel.
APS= Ammoniumperoxodisulfat; TEMED= Tetramethylethylendiamin.

Running gel 4.5 ml/gel	**7.50%**	**12.50%**
Milipore water	4.9 ml	3.2 ml
1.5 M Tris pH 8.8	2.5 ml	2.5 ml
Acryl/Bisacrylamide	2.5 ml	4.2 ml
10% SDS	100 µl	100 µl
TEMED	30 µl	30 µl
10 % fresh APS	40 µl	40 µl

Table 16. Composition of the stacking gel.
APS= Ammoniumperoxodisulfat; TEMED= Tetramethylethylendiamin.

Stacking gel 2.0 ml/gel	**2 gels**
Milipore water	2.27 ml
0.5 M Tris pH 6.8	1.0 ml
Acryl/Bisacrylamide	0.65 ml
10% SDS	40 µl
TEMED	2 µl
10 % fresh APS	30 µl

SDS-PAGE and western blot analysis were performed according to the manufacturer's instructions, using Blue Prestained Protein Standard (NEB, #P7706S). Filling assemble electrophoresis module with 1x SDS-PAGE running buffer (900 mL H_2O with 100 ml 250 mM Tris with 1.92 M Glycine and 1% SDS solved in 1L H_2O) to just under the edge of outer gel plate and fill the tank to just under 1 cm of the top of the plate. Load gel and run at 200 V and 350 mA for 45 to 55 min. Afterward, gels are taken from the electrophoresis module. Amersham Protran 0.45 µM Nitrocellulose membrane and Whatman paper are pre-soaked in cold 1x Transferbuffer (700 ml H_2O plus 200 ml EtOH and 100 ml 250 mM Tris, 1.92 M Glycin solved in 1L H_2O). The transfer cassette is set up with the transparent colored cassette at the bottom. Filter Pads, Whatman paper, and Membrane are put onto a cassette with gel on top of the membrane, and

another Whatman paper and filter pad on top of that. The transfer cassette is closed and put into Transfer pox. An ice cube is put in the transfer box and the box is filled with 1x Transferbuffer. Transfer run is performed with 100 V and 350 mA for 90 min. After the Transfer run is completed, membrane is blocked in 2% BSA solved in 1x Wash buffer (900 ml H_2O mixed with 100 ml of 200 mM Tris and 1.5 M Sodium Chloride solved in 1 L H_2O and 1 ml Tween 20) for 30 min at room temperature. Afterward, the blocked membrane is incubated with primary antibodies, diluted in 2% BSA solved in 1x Wash buffer overnight at 4°C. The day after the membrane is washed three times with 1x Wash buffer, incubated for 5 min at room temperature, and incubated for 1 h with a secondary antibody diluted in 2% BSA solved in 1x Wash buffer. Afterward, the membrane is again washed three times and incubated for 5 min at room temperature each time before being analyzed with the ChemiDoc Imaging System.

The following antibodies were applied: Ago3 (Cell Signaling Technology, #5054S, dilution 1:1000), BMI1 (Cell Signaling Technology, #5856, dilution 1:1000), Casp3 (Cell signaling Technology, #9665, dilution 1:1000), GAPDH (Santa Cruz, #sc-47724, dilution 1:2000), HA (Cell Signaling Technology, #3724T, dilution 1:1000), EDC4 (Cell Signaling Technology, #2548, dilution 1:1000), Lamin (Cell Signaling Technology, #4777S, dilution 1:3000), NONO (Cell Signaling Technology, #90336, dilution 1:1000) α-Tubulin (Calbiochem, #CP06, dilution 1:1000), PIWIL4 (abcam, #ab182760, dilution 1:1000), the secondary antibodies used were anti-mouse IgG, HRP (Cell Signaling Technology, #7076, dilution 1:3000 to 1:6000), anti-rabbit IgG, HRP (Cell Signaling Technology, #7074 dilution 1:3000).

Table 17. RNA concentrations used in different cell culture experiments.

RNA concentration [nM]	Cell line	Experiment	Comment
3.125	Kelly	Viability	Less effect than 12.5 nM
6.25	Kelly	Viability	Less effect than 12.5 nM
12.5	Kelly	Viability, Proliferation, Mobility, Spheroid growth, Cell cycle, Casp 3, and BMI1 protein expression	Biggest effect on Viability
18	Kelly	Viability	Many dead cells also in controls

25	Kelly	Viability	Many dead cells also in controls
12.5	SK-N-AS, SK-N-SH, SK-N-MC	Viability	Significant decrease in Viability
12.5	SK-N-MC	Viability RNA inhibitors	Biggest effect on Viability
12.5	SK-N-SH	Spheroid growth	Significant decrease in Spheroid growth
25	Kelly, SK-N-AS	Viability RNA inhibitors	Biggest effect on Viability

2.2.14 *In vitro* MB analysis

All reagents used in these reactions as well as the 384-well plates (Perkin Elmer) were pre-chilled on ice. MBs and target RNA or DNA oligonucleotides were assembled on ice in 1x ICN buffer (10 mM Tris/HCl pH=7.5, 100 mM NaCl, 0.75 mM MgCl2, 0.0001 % NP-40) and transferred into the pre-warmed to 37°C CLARIOStar® Plate Reader. Reactions (20 µl) were recorded over time at 37°C with CLARIOStar® Plate Reader (gain set at 1000). Detailed in Weigert et al. (manuscript under revision).

2.2.15 Live cell imaging

In order to avoid distortions of the natural localization state, e.g., by fixation reagents, as far as possible live cell imaging was used. For live cell imaging, different microscopes were used. The Bio-Rad ZOE cell imager, a brightfield channel, a green channel (excitation: 480/17 nm; emission: 517/23 nm), and a LED light source were used. For live cell imaging analysis with the Bio-Rad ZOE cell imager, from our department, cells were plated on 24-Wells, while for all other live cell imaging, cells were plated on µ-Slide 8 well chamber slides (ibidi, #80826).

Also, the KEYENCE BZ-X810 fluorescence microscope with a LED light source, at the department of human genetics, was used, while exposure times varied between 1/35s to 3 seconds magnifications varied between 20 x (Objective: Plan Fluor 20x Na 0.45), 40 x (Objective: Plan Apo 40x NA 0.95) and 100 x (Objective: Plan Apo 100x 1.45, Oil). The following filters were used: BZ-X filter GFP (excitation 470 nM; emission 525 nM); BZ-X filter Cy5 (excitation 620 nM; emission 700 nM), BZ-X filter TxRED (excitation 560 nM; emission 630 nM), BZ-X filter DAPI (excitation 360 nM; emission 460 nM). Z-stacks in the range of 0.2 to 0.8 µM were generated. Furthermore, line profiles were performed by using the KEYENCE measurement module. To avoid false negative

signals, untransfected or control transfected (MBcon) cells were used to adjust the signal that no signal was to be seen in control cells. BZ-X800 Analyzer software package (Version 1.1.2.4) was used for data analysis.
Furthermore, live cell imaging was performed using the Leica TCS SP5 confocal laser scanning microscope, from the department of microbiology, with a laser as a light source (Argon ion laser for 458 nm, 476 nm, 488 nm, 496 nm, 514 nm; Helium-neon laser for 633 nm; Diode laser for 561 nm and Pulsed UV laser (including B&H control system)). While magnification varied between 40x (oil) and 63x (oil), lasers were set on the range of FAM (470 nM to 525 nM), on the range of Cy5 (620 nM to 700 nM) and on the range of DAPI (360 nM to 460 nM) for detection of those signals. Furthermore, Z-stacks were generated and the background signal was adjusted as described above. Leica Application Suite (Version 2.7.3.9723) and the Adobe software package Elements were used for data analysis.

2.2.16 Staining of the endoplasmatic reticulum

To confirm colocalization between MB7SL and the endoplasmatic reticulum (ER) co-staining of 7SL RNA and the ER was performed. Therefore, ER Tracker Green stock (100 µg, Thermo fisher #E34251, dye BODIPY® FL (EX/EM 504/511) was dissolved to a concentration of 1 mM in 128 µl DMSO. Stock solution (1 mM) was further diluted in 1x PBS to 100 nM. 300 µl of this solution was put onto pre-plated cells in Live Cell Imaging Chambers and incubated at 37°C for 20 min. The solution was then discarded and replaced with 300 µl 1x PBS. Afterward, cells were analyzed using the KEYENCE BZ-X810 fluorescence microscope (BZ-X filter GFP (excitation 470 nM; emission 525 nM)).

2.2.17 DAPI staining in live cell imaging

DAPI staining was done directly before microscopy was performed. Therefore, cells were washed in 1x PBS once, and afterward, 1x PBS was replaced by 1x PBS mixed with DAPI solution (one to two drops per ml, Thermo Fisher Scientific, #R37605) and this solution was incubated for 10 to 20 min at room temperature. Afterward, 1x PBS with DAPI was replaced by fresh 1x PBS and cells were ready for microscopy.

2.2.18 RNA FISH

Fluorescence in situ hybridization (FISH) is used to visualize messenger RNA (mRNA) or DNA. Thereby, an RNA:RNA, DNA:DNA or DNA:RNA duplex is generated by two complimentary sequences (Felsenfeld and Miles, 1967). The probes have fluorescent labels attached and are able to bind to their targets very specifically (Young et al., 2020). The signals of the fluorescent FISH probe can now be detected by fluorescence microscopy (Young et al., 2020). Our NEAT1_m probe is designed to detect the long isoform of NEAT1 (NEAT1_2) but not the short one (NEAT1_1).

To ensure sterilization of the 12-well coverslips (epredia, # CB00180RA120MNZ0; 0.13 to 0.16 µm), they were first incubated in 70% ethanol for 5 to 10 minutes. The coverslips were then washed once in 1x PBS and irradiated with UV light for at least 20 minutes. Subsequently, the coverslips were transferred to the 12-well plates.

For fixation of RNA FISH cells, SK-N-SH cells were plated onto the coverslips 24 hours prior to transfection with FAM-sncRNA7SL (see 2.2.4). 24 hours after transfection cells were carefully washed twice with 1 ml of 1x PBS. For each of the washing steps in this protocol, the different Wash solutions (1x PBS; Wash Buffer A (Biosearch Technologies, #SMF-WA1-60); Wash Buffer B (Biosearch Technologies, # SMF-WB1-20) were incubated on the cells for 5 min at room temperature. Afterward, 1 ml of Fixation Buffer (2.3 ml 16% Formaldehyde solution, 1 ml 10x Phosphate Buffered Saline, RNase-free, 6.7 mL Nuclease-free water) was put onto cells and incubated for 1 h at room temperature. Cells were washed twice with 1 ml 1x PBS. In order to permeabilize cells, 70% Ethanol was put on top of coverslips and incubated for at least 1 h at 4°C.

RNA FISH probes (RNA FISH Probe Human NEAT1_m or RNA FISH Probe KNL1 ORF) were dissolved in 400 µl TE buffer (10 mM Tris-HCL, 1 mM EDTA, ph 8.0), thereby creating a probe stock of 12.5 nM. Ethanol was discarded and permeabilized cells were washed with 1 ml Wash Buffer A (2mL Stellaris RNA FISH 5x Wash Buffer A, 7 ml Nuclease—free water, 1 ml Deionized Formamide (Carl Roth, #P040.1)) and incubated for 5 minutes at room temperature. To assemble a humidified chamber empty pipette tip boxes were lined evenly with flat water-saturated paper towels. Parafilm was evenly placed on top of the paper towel. Then 1 µl RNA FISH Probe was mixed with 100 µL Hybridization Buffer (90 µl Stellaris RNA FISH Hybridization Buffer, and 10 µl Deionized Formamide) plus an appropriately diluted antibody (NONO 1:1000) and placed onto parafilm into the humidified chamber. Cover glass was placed with cells side down onto the Hybridization Buffer mix within the humidified chamber

and the chamber was sealed with Parafilm. Afterward, the chamber with RNA FISH probes was incubated in the dark at 37°C for 16 hours. After incubation cover glass was transferred into a fresh 12-well plate (cells side up) and washed with 1 ml Wash Buffer A (2 mL Stellaris RNA FISH 5x Wash Buffer A, 7ml Nuclease-free water, 1 ml deionized formamide) plus secondary antibody (anti-rabbit IgG (H+L), $F(ab')_2$ Fragment (Alexa Fluor555 Conjugate) 1:1000). Cells were incubated for 1 h at 37°C in the dark. Afterward, cells were washed with 1 ml Wash Buffer B (Biosearch Technologies, #SMF-WB1-20) and incubated for 5 min at room temperature in the dark. ProLong Gold Antifade Mountant with DAPI (Thermo Fisher Scientific, #P36941) was put on a Microscope slide and Cover Slide was put onto the slide, cell side down. The cover slide was incubated in the dark at room temperature for 45 minutes to let Mounting Medium dry before sealing Cove Slide to Microscope slide with nail polish.
KEYENCE BZ-X810 fluorescence microscope was used for analyzing RNA FISH probes.

2.2.19 RNA Immunofluorescence

For immunofluorescence cover slips were sterilized as mentioned in the RNA FISH protocol.
Different cover slip treatments were tested to optimize cell growth conditions. First, the cover slips were incubated with 1 M HCl for two hours at RT to roughen them. Afterward, the coverslips were washed twice with 1xPBS and once with water and then sterilized. Since this method did not lead to an improvement in the grip of the cells on the coverslips, this method was not carried out further.
Second, the coverslips were coated with Poly-D-lysine. For this purpose, the Poly-D-lysine was first diluted 1:1 with 1x PBS to reach a final concentration of 50 µg/µl. The coverslips were then sterilized and washed with sterile 1x PBS. Subsequently, the coverslips were placed in a 24-well plate and each was coated with 300 µl of 50 µg/µl of Poly-D-lysine. After an incubation period of 1 h at RT with a closed lid, the Poly-D-lysine was then removed and the coverslips were washed three times with sterile water (500 µl) and then dried for 2 h at RT under the sterile bench with an open lid. However, since this method did not improve the growth of the cells, sterile untreated coverslips were used in the following experiments.

Afterward, SK-N-SH or HEK293 cells were plated on top of coverslips and eventually transfected with sncRNA oligos. As soon as cells reached a confluence of about 80 % or 24 h after sncRNA transfection, cells were fixed.

For fixation, cells were first washed twice in 1x PBS and incubated each time at room temperature for 5 min. Afterward, PBS was discarded and 1 ml 4% PFA (16% PFA 1:4 diluted in 1xPBS) per well was put on top of the cells. 4% PFA was incubated for 1 h at room temperature. Incubation for 1 h was very important, as a shorter time period resulted in incomplete fixation of sncRNAs, causing them to localize to the cytoplasm rather than the nucleus. Cells were again washed three times with 1x PBS and incubated for 5 min at room temperature each time. Afterward, cells were incubated in 500 µl PBS with 0.5% Triton X for 10 min at room temperature to permeabilize cells. Using Triton X is also crucial to this protocol since the usage of 0.1 % Saponin again led to an incomplete fixation of sncRNAs, causing them to localize completely in the cytoplasm. Afterward, Triton X was discarded and cells were washed three times with 1x PBS, and incubated for 5 min at room temperature. 5% Bovine Serum Albumin (BSA) was solved in 1x PBS and put on cells for 1 h at room temperature for blocking. Cells were again washed thrice with 1x PBS, and incubated for 5 min at room temperature. Primary Antibodies (Ago3 1:300 to 1:600, Coilin 1:1000, EDC4 1:400 to 1:1000, HA 1:1000, NONO 1:200 to 1:1000, PSPC1 1:3000 to 1:6000, SC35 1:500) were diluted appropriately in 1% BSA solved in 1xPBS and 1 ml of this solution was put on top of cells. Incubation was performed overnight at 4°C with a closed lid. On the next day, cells were again washed three times in 1x PBS which was incubated for 5 min at room temperature, secondary antibodies (anti-rabbit IgG (H+L), $F(ab')_2$ Fragment (Alexa Fluor555 Conjugate); anti-mouse IgG (H+L), $F(ab')_2$ Fragment (Alexa Fluor 647 Conjugate); anti-mouse IgG (H+L), $F(ab')_2$ Fragment (Alexa Fluor 555 Conjugate)) were diluted 1:1000 in 1% BSA solved in 1x PBS and put on top of cells. Antibody incubated for 2 h at room temperature in the dark before cells were washed three times with 1x PBS, and incubated for 5 min at room temperature in the dark. One droplet of ProLong Gold Antifade Mountant with DAPI (Thermo Fisher Scientific, #P36941) was put on a Microscope slide. Next, the coverslip was taken out of the plate and the edge of the coverslip was briefly and very carefully dabbed on a piece of paper, to remove excess fluid, before putting it onto the ProLong Gold Antifade Mountant droplet, cell side down. The cover slide was incubated in the dark at room temperature

for 45 minutes to let Mounting Medium dry before sealing Cove Slide to Microscope slide with nail polish.

KEYENCE BZ-X810 fluorescence microscope was used for analyzing RNA FISH probes.

Table 18. Antibody combinations and Keyence filters used in immunofluorescence analysis.

Name	AB Dilution	Keyence Filter 1	Exitation/ Emission Filter 1	Combined with	Keyence Filter 2/3	Exitation/ Emission Filter 2/3
Ago3	1:300-1:600	BZ-X filter TxRED	560 nM/ 630 nM	-	-	-
Coilin	1:1000	BZ-X filter TxRED	560 nM/ 630 nM	FAM-sncRNA7SL	BZ-X filter GFP	470 nM/ 525 nM
EDC4	1:400-1:1000	BZ-X filter TxRED	560 nM/ 630 nM	sncRNA7SL-inte-FAM or sncRNA7SL Δ2-inte-Cy5	BZ-X filter GFP BZ-X filter Cy5	470 nM/ 525 nM 620 nM/ 700 nM
HA	1:1000	BZ-X filter TxRED	560 nM/ 630 nM	-	-	-
NONO	1:200-1:1000	BZ-X filter TxRED	560 nM/ 630 nM	NEAT1 mRNA Probe (Cy5) or KNL1 mRNA Probe (Cy5) and FAM-sncRNA7SL	BZ-X filter Cy5 BZ-X filter Cy5 BZ-X filter GFP	620 nM/ 700 nM 620 nM/ 700 nM 470 nM/ 525 nM
PSPC1	1:3000-1:6000	BZ-X filter TxRED	560 nM/ 630 nM	FAM-sncRNA7SL	BZ-X filter GFP	470 nM/ 525 nM
SC35	1:500	BZ-X filter TxRED	560 nM/ 630 nM	FAM-sncRNA7SL	BZ-X filter GFP	470 nM/ 525

2.2.20 NEAT 1_2 or La knockdown

To establish NEAT1_2 knock down 150.000 to 800.000 cells were seeded into a 6-Well. Cells were transfected with 3 nM, 6 nM, and 9 nM final siRNA concentration.

Hence, a final concentration of 3 nM 10 µM siPOOL Stock (siNEAT1_2 or control) was diluted 1:66.5 to 0.15 µM with nuclease-free H_2O (3 µl 10 µM siPOOL stock plus 197 µl nuclease-free water). The solution was vortex and centrifuged shortly. Furthermore, 210 µl Opti-MEM were mixed with 40 µl diluted 0.15 µM siPOOL stock. In a second Eppendorf tube, 4 µl Lipofectamin transfection reagent RNAiMAX was diluted with 246 µl Opti-MEM. All reagents were vortex and centrifuged shortly. Afterward, solutions of both Eppendorf tubes were mixed together for a final volume of 500 µl, vortexed, centrifuged shortly, and incubated at room temperature for 5 minutes. After incubation transfection mix was mixed with 1500 µl cell solution and plated onto a 6-Well plate. For the final siPOOL concentration of 6 nM and 9nM dilutions were adjusted accordingly. Cells were incubated for 48h, 72h, or 96h at 37°C and 5% CO_2. If the incubation period was longer than 48h cell medium was changed once 48h after transfection.
After incubation, RNA was isolated (see 2.2.22), cDNA synthesis (see 2.2.23) was performed and RNA levels were measured by qPCR analysis.
For live cell imaging analysis of NEAT knockdown cells, volumes were adjusted to suit the ibidi live cell imaging chamber format.

2.2.21 Fractionation

For fractionation five to ten million cells were harvested using trypsinization. Cells were centrifuged at 300 xg for 5 min at 4°C and then washed once with ice-cold PBS and centrifuged again. Afterward, cells were resuspended in 1 ml fresh 1x PBS and transferred into a 1.5 ml low attachment Eppendorf tube (Biozym #844-70045-0). Cells were centrifuged at 300 xg for 5 min at 4°C and the supernatant was discarded. Cells were dissolved in 100 µl Hypotonic buffer (10 mM Tris/HCl pH=7.4, 15 mM KCl, 2.5 mM $MgCl_2$, 1 mM EDTA pH=8.0, 0.5 mM DTT, 1x protease inhibitor (40 µl/ml), and 1x Phospho stop (100 µl/ml), add H_2O to a final volume of 100 µl) and 40 units RNase Inhibitor were added. Cells were incubated on Ice for 5 minutes. 100 µl 2x Detergent Cytoplasmic Membrane lysis buffer ((DCML) 20 mM Tris/HCl pH=7.4, 30 mM KCl, 5 mM $MgCl_2$, 2 mM EDTA pH=8, 0.2% NP40, 1 mM DTT, 2x protease inhibitor (40 µl/ml), add H_2O) buffer was added. The solution was mixed very carefully by flipping the Eppendorf tube five times. Cells were incubated for no longer than 3 min on ice. 500 µl of 24% Sucrose solution (10mM Tris/HCl pH=7.4, 15 mM KCl, 1 mM EDTA pH=8.0, 24% Sucrose, and 0.5 mM DTT, 1x protease inhibitor (40 µl/ml)) was put into a fresh

1.5 low attachment Eppendorf tube. Lysate was collected with a 1000 µl pipette and layered dropwise on a sucrose cushion. Lysate was centrifuged at 6000 xg for 10 min at 4°C. The top 400 µl, comprising the cytoplasmic fraction, of the supernatant was removed and placed in a fresh Eppendorf tube, 30 µl supernatant was put in another Eppendorf tube, and mixed with 20 µl SDS-Loading Buffer the rest was stored at -20°C till usage. The rest of the supernatant was discarded. The nuclear pellet was dissolved in 100 µl 1x PBS and the pellet was carefully transferred into a fresh 1.5 ml Eppendorf tube. A white pellet color, in contrast to yellow, was considered a sign of intact nuclei. 1 ml 1x PBS was added and the tube was inverted carefully until the pellet dissolved completely. The now dissolved nuclei were centrifuged at 6000 xg for 2 min at 4°C, and the supernatant was discarded. 100 µl Glycerol Buffer (20 mM Tris/HCl pH=7.5, 75 mM NaCl, 0.5 mM EDTA pH=8.0, 50% Glycerol, 0.85 DTT, and 1x protease inhibitor (40 µl/ml), 1x Phospho stop (100 µl/ml), and water added for a final volume of 100 µl) was added to the pellet of nuclei and pellet was centrifuged for 1 s. Eppendorf tube was inverted until Pellet dissolved completely, 40 units RNase Inhibitor was added and 100 µl Cold Nuclei Lysis Buffer (20 mM HEPES pH=7.6, 1M Urea, 7.5 mM $MgCl_2$, 0.2 mM EDTA pH=8, 300 mM NaCl, 1% NP-40, and 1mM DTT, and 1x Protease inhibitor (40 µl/ml)) was added. Lysate was mixed by vortexing for two seconds twice and sonicated for five seconds twice. 20 µl nucleic lysate was put in a fresh Eppendorf tube and mixed with 30 µl SDS-Loading Buffer, while the rest was stored at -20 °C until usage.

2.2.22 RNA isolation

Total RNA from SK-N-SH cells was isolated using RNAzol (Sigma, #R4533-200ML), following the manufacturer's instructions.
Concentrations were measured and the purity of RNA was verified using ND spectrophotometer NanoDrop.

2.2.23 cDNA-synthesis

Complementary DNA (cDNA) was reverse-transcribed using Quiatec Reverse Transcription Kit (Quiagen, #205311), with contained primers, according to the manufacturer's instructions. As negative controls for each template RT (-) control, not

containing any templates, was performed. The Thermocycler system (Analytik, Jena) was used for the PCR run.

2.2.24 Quantitative qPCR

To test NEAT1_2 depletion in SK-N-SH cells, SYBR Green Master Mix (Roche, #0488735001) was used on a thermocycler system (Analytik Jena). Primers used were NEAT1_2 fw (IDT, #225695006; 5'-GTCTTTCCATCCACTCACGTCTATTT-3') and NEAT1_2 rv (IDT, #225695007; 5'-GTACTCTGTGATGGGGTAGTCAGTCAG-3'), and GAPDH (QuantiTect, Qiagen, #QT00079247). Quantification of PCR products was measured using GAPDH as a reference gene to normalize the NEAT1_2 level. For negative control, a no template control was performed for each run. For quantification purposes the relative quantification method first performed by Livak and Schmittgen, 2001 was used.

2.2.25 Binding assay-Lysates

To receive total cell lysates for binding assays, about two to five million cells were harvested by trypsinization. Cells were centrifuged at 300 xg for 5 min at 4°C. And washed twice with 1 ml ice-cold PBS. Cells were again centrifuged as described above and taken in 1 ml lysis buffer (100 mM KCl, 5 mM $MgCl_2$, 10 mM HEPES pH=7.0, 0.5 % NP-40) added with 40 µl 25x protease inhibitor cocktail (Sigma, #4693116001) as well as 1 µl 100 mM DTT (Sigma, #D0632-10G) and 2 µl RNase-OUT (40 U/ µl, Thermo Fisher Scientific, #10777019) per 1 ml lysis buffer. Lysates were incubated on ice for 10 min. Cells were sonified twice for 3 seconds on ice to ensure cell lysation and centrifuged for 10 min at 13.000 rpm at 4°C to clear the lysates. Afterward, the supernatant was collected in fresh 1.5 ml Eppendorf tubes and protein concentration was determined using Bradford assay.

2.2.26 Bradford Analysis

For protein concentration measurement Bradford assays were performed. Hence, Protein Assay Dye Reagent (Bio-Rad, #5000006) was diluted 1:5 with water and 200 µl of that solution was submitted per clear 96-Well. Protein samples were also diluted 1:5 in water and pipetted with increasing volume (2 µl, 4 µl, 6 µl, 8 µl, and 10 µl) on top of the protein assay dye reagent into a 96-well respectively. For the standard BSA

(NEB, #B9001S) was diluted with water into several increasing concentrations (0 µg/ µl, 0.93 µg/ µl, 1.86 µg/ µl, 2.8 µg/ µl, 3.73 µg/ µl, 5.6 µg/ µl, 7.46 µg/ µl, 9.3 µg/ µl). Three wells with protein assay dye reagents were used as blanks. The 96-well plate was incubated while shaking for at least 5 min at room temperature. Air bubbles within wells were removed and protein concentration was measured using CLARIOStar® Plate Reader. The CLARIOSTAR MARS analysis software was used for evaluation. Raw data was calculated by normalizing the measured concentrations against blank controls. Raw data of the protein concentrations were converted to concentrations per 1 µl and mean values were then related to the standard curve using a regression line (y=mx+t).

2.2.27 sncRNA7SL binding assay

On the day before the actual experiment, 20 µl of Pierce HA-magnetic beads (Thermo Fisher Scientific, #88836) were added to a 1.5 ml low-binding Eppendorf tube and washed twice with 500 µl 1x PBS. The beads were then taken up in 500 µl 1x PBS and 500 nM Yeast tRNA (Thermo Fisher Scientific, #AM7119), to block unspecific small RNA binding, was added to each. The Eppendorf tubes were incubated overnight at 4°C rolling. The next day, the beads were washed again three times with 500 µl 1x PBS, then the 1x PBS was discarded and the beads were taken up in 100 µg protein lysate each. The beads were incubated with the lysate for two hours rolling at 4 °C and the supernatant was then removed and saved for later western blot analysis. The beads were carefully washed three times with 500 µl 1x PBS and rolled at 4 °C for 5 min each time. The PBS was discarded and the beads were taken up in 50 µl Binding Buffer (20 mM Tris/HCl, 0.5 M NaCl (pH=7.5), 1 mM EDTA, add H_2O) mixed with 50 pmol sncRNA7SL-inte-FAM. Incubation was performed rolling for 30 min at room temperature. The supernatant was then removed and the beads were washed three times in 500 µl Wash Buffer 1 (20 mM Tris/HCl, 150 mM NaCl, 0.05% NP-40). The beads were incubated again for 5 min at 4 °C. The supernatant was discarded and the beads were taken up in 30 µl SDS loading dye without bromophenol blue mixed with 5% β-mercaptoethanol. The beads were then incubated at 70°C for 10 min and the supernatant was transferred first into black 96-Well plates (greiner bio-one, #781076) for fluorescence measurement on the CLARIOStar® Plate Reader and later for western blot analysis to check the efficiency of the pulldown. The CLARIOSTAR MARS

analysis software was used for evaluation. As controls empty vector (VP5) plasmid was used.

2.2.28 Cultivating bacteria

For LB_{Amp} medium, 0.5 % Yeast Extract (Carl Roth, #2363.3) was mixed with 1% Tryptone (Carl Roth, #8952.2) and 1% NaCl (Carl Roth, #2957.1) and dissolved in 1 L ddH_2O. For sterilization purposes solution was autoclaved, and cooled, and 100 µg/ml Ampicillin (Carl Roth, #HP62.1) was freshly added before use.
For LB_{Amp} plates, 3.7 % LB Agar (Sigma, #1102830500) was dissolved in 500 ml ddH_2O. For sterilization purposes solution was autoclaved, cooled to at least below 50°C, 100 µg/ml Ampicillin added, and poured into a 10 cm Petri dish (Falcon, #351029). Afterward, they were dried overnight at room temperature in the dark and stored at 4 °C until use.

2.2.29 Transformation of *Escherichia coli*

For Plasmid multiplication purposes Plasmids Ago2-HA, PIWIL4-HA, and VP5-HA were transformed in TOP10 Bacteria (Thermo Fisher, #C404003), while Plasmid Ago3-HA was transformed in JM109 Component Cells (Aglient #200235).
For Transformation with TOP10 Bacteria, cells were thawed on ice. 5 µl template DNA (Ago2-HA, PIWIL4-HA, VP5-HA) was added and cell solution was incubated for 30 min on ice before being heat shocked at 42 °C for 30 sec on a thermos block and again incubated for 2 min on ice. 250 µl SOC-Medium was added and cells were shaken at 225 rpm for 1 h at 37°C. Afterward, 100 µl of cells were plated on LB_{Amp} plates and incubated at 37°C overnight.
Since the previous approach did not work for Ago3-HA plasmids, JM109 Competent Cells were used. For Transformation with JM109 Competent Cell, cells were thawed on ice. A fresh Eppendorf was chilled on ice and SOC-Medium was pre-heated to 42°C. 50 µl JM109 Competent cells were put into a pre-chilled Eppendorf tube. 0.8 µl 2-mercaptoethanol was added and the solution was mixed carefully. The solution was incubated for 10 min on ice and mixed every two minutes carefully. 50 ng Ago3-HA template DNA was added and the contents were mixed carefully. The solution was incubated on Ice for 30 minutes and then heat-shocked at 42°C for 45 s. Cells were again incubated on ice for 2 min and 900 µl pre-heated SOC-Medium was added. Cells

were shaken at 225 rpm for 1 h at 37°C. Afterward, 100 µl of cells were plated on LB_{Amp} plates and incubated at 37°C overnight.
Afterwards, a single colony was picked from the plates and incubated overnight in 5 ml LB_{Amp} Medium at 37°C shaking at 225 rpm and mini-preps were performed as a control.

2.2.30 Mini preparation

For Mini prep, 1 colony was picked off plates and incubated overnight in 5 ml LB_{Amp} Medium at 37°C shaking at 225 rpm and QIAprep Spin Mini Kit (Qiagen, #27104) was used according to manufacturer's instructions, and DNA concentrations were measured using Nanodrop.

2.2.31 Maxi preparation

For Maxi prep, 100 µl of Mini prep culture was incubated in 100 ml LB_{Amp} shaking at 225 rpm at 37°C overnight. QIAfilter Plasmid Maxi Kit (Qiagen, #205311) was used according to the manufacturer's instructions and DNA concentration was measured using Nanodrop.

2.2.32 Digestion

Digestion of DNA Plasmids: Ago2-HA: XcmI, Ago3-HA XcmI, EcoRI, PIWIL4-HA: XcmI, ApaI, VP5-HA, EcoRI), 2 µl Cutsmart Buffer (NEB, #B7204S) was mixed with 0.5 µl Enzyme and 500 ng Vector and water was added to fill 20 µl. The solution was incubated for 1h at 37°C and 300 rpm. For the purpose of having a negative control, the same protocol was performed without adding any enzymes to the solution mix.

2.2.33 Gels

1% Agarose gels were used to check Plasmid length. Hence, 1.3 g Agarose was mixed with 130 ml 1x TAE and heated. The liquid gel was cooled slightly, and 5 µl GelRED (Biotium/Linaris, #41003) was added and poured into the mold. After 20 min, the gel was cured and ready for loading. After positioning in the gel chamber and layering with 1x TAE, the gel was loaded. For this purpose, 5 µl of the digested vector DNA or control was mixed with 1 µl of 6x Gel Loading dye (NEB, #B7024A) and applied to the gel. As standard 1 kb Extended (NEB, #32395), as well as Gene Ruler Mix (Thermo Fisher

Scientific, #SM0334), was used according to the manufacturer's instructions. Gels were run for 2 h at 90 V and analyzed using the ChemiDoc Imaging System.

3. Results

sncRNA7SL is a 32 nt long small RNA annotated as piRNA based on its similar length to 24 to 33 nucleotides long piRNAs (Czech et al., 2018). However, it is unclear if sncRNA7SL is indeed part of the piRNA family. piRNAs are known to be 2'-O-methylated at the 3'-end and 5'-monophosphorylated (Kirino and Mourelatos, 2007). For sncRNA7SL 3' as well as 5' modifications are yet to be analyzed. sncRNA7SL was found not only in gonad cell tissues like the testis (Girard et al., 2006) or ovaries (Roovers et al., 2015) but also in somatic cells tissues like the lung (Mei et al., 2015) or neuroblastoma (Roy and Bibekanand, 2018). The main function of sncRNAs such as piRNAs and miRNAs is to induce transcriptional or posttranscriptional gene silencing, leading to the assumption that sncRNA7SL also plays a role in gene silencing.

A)

Modifications: * = Phosphorothioate Bond m = 2'O-Methyl RNA bases

sncRNA7SL mimic design:

5'-P-
rA*rG*rC*rC*rU*rG*rA*rG*rC*rA*rA*rC*rA*rU*rA*rG*rC*rG*rA*rG*rA*rC*rC*rC*rC*rG*rU*rC*rU*rC*rU*mA-3'

sncRNActrl design:

5'-P-
rA*rU*rC*rU*rC*rU*rG*rC*rC*rC*rC*rA*rG*rA*rG*rC*rG*rA*rU*rA*rC*rA*rA*rC*rG*rA*rG*rU*rC*rC*rG*mA-3'

B)

Modifications: * = Phosphorothioate Bond m = 2'O-Methyl RNA bases 3CholTEG = 3'cholesterol-TEG

sncRNA7SL inhibitor design:

5`-
rU*rA*rG*mAmGmAmCmGmGmGmGmUmCmUmCmGmCmUmAmUmGmUmUmGmCmUmCmArG*rG* rC*rU*/3CholTEG/

sncRNActrl inhibitor design:

5'-rU*rC*rG*
rGmAmCmUmCmGmUmUmGmUmAmUmCmGmCmUmCmUmGmGmGmCmAmGrA*rG* rA*rU*/3CholTEG/

Figure 2. sncRNA7SL mimics and inhibitor design.
(A) Oligonucleotide design of sncRNA7SL and sncRNActrl. **(B)** Oligonucleotide design of sncRNA7SL inhibitor and sncRNActrl inhibitor.

To uncover the role and function of sncRNA7SL, cell culture experiments were performed in this study. Therefore, sncRNA7SL was either overexpressed by transfection of a synthetic sncRNA7SL mimics, or endogenous sncRNA7SL was depleted by transfection of a sncRNA7SL inhibitors (Figure 2).

3.1 sncRNA7SL acts as a tumor suppressor in neuroblastoma and Ewing sarcoma cell lines

3.1.1 sncRNA7SL mimics reduce viability and proliferation in neuroblastoma and Ewing sarcoma cell lines

To determine whether sncRNA7SL has tumor-suppressive effects on both, neuroblastoma (Kelly, SK-N-AS, SK-N-SH) and Ewing sarcoma cells (SK-N-MC), various cell culture analyses were performed. For this, a sncRNA7SL oligonucleotide carrying the exact sequence of sncRNA7SL as well as a control oligonucleotide (sncRNActrl) of similar length carrying the reverse sequence of sncRNA7SL were designed. The Oligonucleotides were 5'-phosphorylated as well as 3'-2-O-methylated to resemble the modifications of piRNAs. Moreover, Phosphorothioate bonds were incorporated between the individual base pairs for stability purposes (Figure 2 A).
First, the viability of the different cell lines was assessed using MTT assays (see 2.2.8).

For optimization purposes, the viability of Kelly cells, transfected with different concentrations of sncRNA7SL mimics or sncRNActrl, was determined at various time points after transfection (Figure 3 A-C). These studies revealed a decrease in viability in sncRNA7SL transfected cells compared to sncRNActrl transfected cells. It was shown that the viability was strongly impaired 72 h after transfection of 12.5 nM sncRNA7SL (Figure 3 B). The decrease of viability in sncRNA7SL treated cells was still significant 96 h after transfection (Figure 3 C). Nonetheless, it was not as strong as 72 hours after transfection, suggesting a decrease in the effect of sncRNA7SL over time. Upscaling of sncRNA7SL mimics transfection concentration to 18.5 nM and 25 nM also led to a strong reduction of viability 96 h after transfection (Supplementary Figure 1 A). However, those high sncRNA7SL and sncRNActrl concentrations caused severe damage to the cells, which was evident by the rounding off of many cells as well as a strongly reduced growth of sncRNA7SL and control transfected cells (Supplementary Figure 1 B). Therefore, in the following experiments, 12.5 nM

sncRNA7SL mimics or sncRNActrl were transfected and analyzed 72 h after transfection (Kelly, SK-N-AS, SK-N-MC, SK-N-SH).

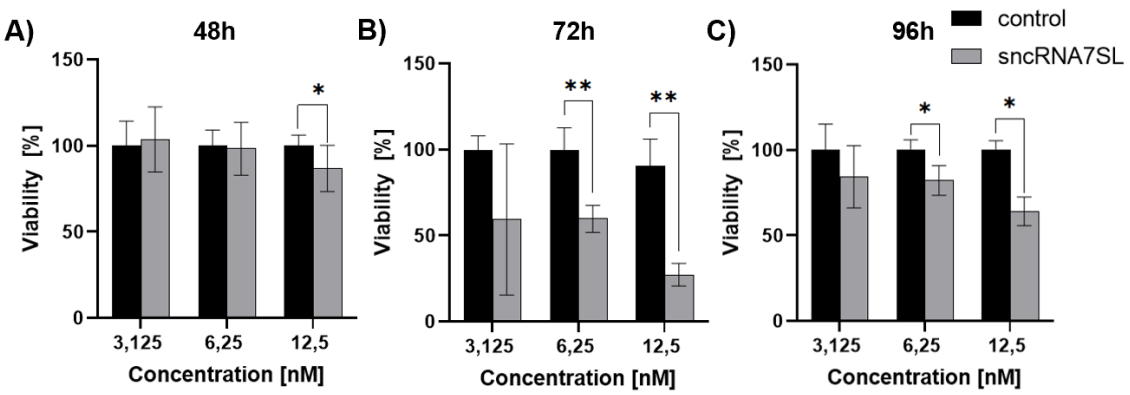

Figure 3. sncRNA7SL mimics reduce cell viability.
(A) Transfection of 12.5 nM sncRNA7SL mimics correlates with decreased viability in Kelly cells after 48 h while the lower level of sncRNA7SL does not have that effect as determined in three independent experiments performed in triplicates. **(B)** 72 h after transfection viability of Kelly cells is significantly decreased by 12.5 nM and 6.25 nM sncRNA7SL. There is no significant decrease in cells transfected with 3.125 nM as determined in two independent experiments performed in triplicates. **(C)** 12.5 nM and 6.25 nM sncRNA7SL lead to a significant decrease of Kelly cell viability 96 h after transfection compared to corresponding control transfected cells. This effect could not be shown using 3.125 nM to transfect the cells as determined in 2 independent experiments. Control = transfection of sncRNActrl.
All results were determined as mean SD (error bars). P value * ≤ 0.05 and ** ≤ 0.01 was determined using paired t-test with Prism 8.4 (Graph Pad Software).

Determination of viability in various neuroblastoma as well as an Ewing Sarcoma cell lines showed a correlation between high levels of sncRNA7SL and significantly decreased viability (Figure 4 A). The strength of this effect was dependent on the cell line. While in Kelly and SK-N-AS cells, a more than 50 % reduction of viability was observed, in SK-N-SH and SK-N-MC cells a decrease of about 20 % was detected.
Following these results, depletion of endogenous sncRNA7SL was performed to detect a possible corresponding effect on viability. Therefore, levels of endogenous sncRNA7SL were decreased, by transfection of single-stranded modified RNA oligonucleotide inhibitors with 100 % of nucleotide complementarity to sncRNA7SL (sncRNA7SL inhibitor (Figure 2 B)) or sncRNActrl (sncRNActrl inhibitor (Figure 2 B) into Kelly, SK-N-AS, and SK-N-MC cells (Figure 4 B). Inhibitor oligonucleotides were designed to carry the exact target sequence of sncRNA7SL as well as the target sequence of sncRNActrl, which is not naturally occurring in cells. To help with cellular uptake and for stability purposes, the Oligonucleotides were labeled at the 3'-end with a Cholesterol-TEG group and Phosphorothioate bonds were placed between

nucleotides. 96 h after transfection a small but significant increase of viability was estimated in all three cell lines, showing that the previously seen phenotype of sncRNA7SL overexpression could be reversed by a decrease of endogenous sncRNA7SL level in cancer cells (Figure 4 B).

To further verify the potential cancer-suppressive properties of sncRNA7SL, the proliferation rate of sncRNA7SL transfected neuroblastoma cells was measured using the Incucyte Live-Cell Analysis System (see 2.2.9). For this, sncRNA7SL and sncRNActrl transfected Kelly cells were photographed every two hours for 3 days and an increase in cell numbers was determined and compared. The proliferation rate was significantly reduced between 48 h and 72 h after transfection of 12.5 nM sncRNA7SL in Kelly cells (Figure 4 C), suggesting that a high level of sncRNA7SL lead to about 20% slower growth of cells compared to control-treated cells.

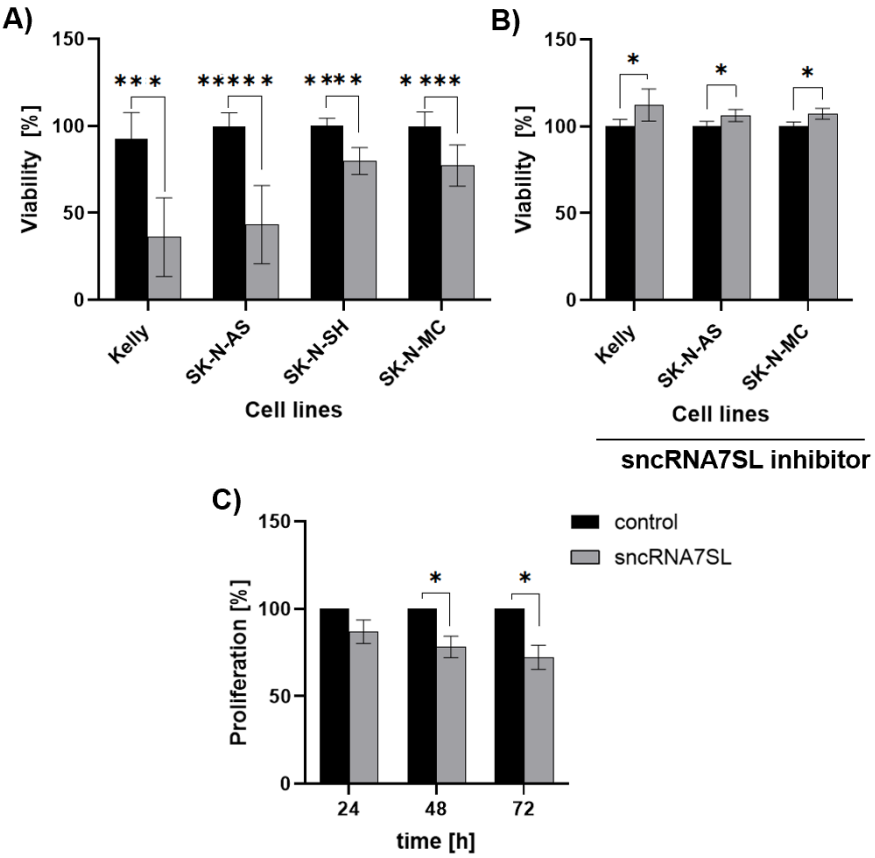

Figure 4. sncRNA7SL mimics reduce viability and proliferation in different cancer cell lines while sncRNA7SL inhibitor increases viability.

(A) Overexpression of sncRNA7SL correlates with a decrease in viability in different cancer cell lines 72 h after transfection of 12.5 nM sncRNA7SL mimics or sncRNActrl (control), as determined in two (Kelly) or three (SK-N-AS, SK-N-SH, SK-N-MC) independent experiments performed in triplicates. **(B)** Transfection of 12.5 nM (SK-N-MC) or 25 nM (SK-N-AS, Kelly) sncRNA7SL inhibitors cause an increase of viability in all tested cell lines 72 hours (SK-N-AS, Kelly) or 96 hours (SK-N-MC) after transfection, as determined in two (SK-N-MC) or three (SK-N-AS, Kelly) independent experiments performed in triplicates. Experiments for SK-N-AS and Kelly were done by coworkers in our laboratory. **(C)** Significantly reduced cell proliferation in

Kelly cells with an increased level of sncRNA7SL (12.5 nM) after 48h and 72h as determined in 2 independent experiments.
All results were determined as mean SD (error bars). P value * ≤ 0.05, ** ≤ 0.01, *** ≤ 0.001 and, **** ≤ 0.0001 was determined using paired t-test with Prism 8.4 (Graph Pad Software).

Taken together, these data demonstrate that overexpression of sncRNA7SL has a negative effect on viability and proliferation, while a reduction of free sncRNA7SL increases viability in various cancer cell lines.

3.1.2 sncRNA7SL mimics reduce mobility in neuroblastoma

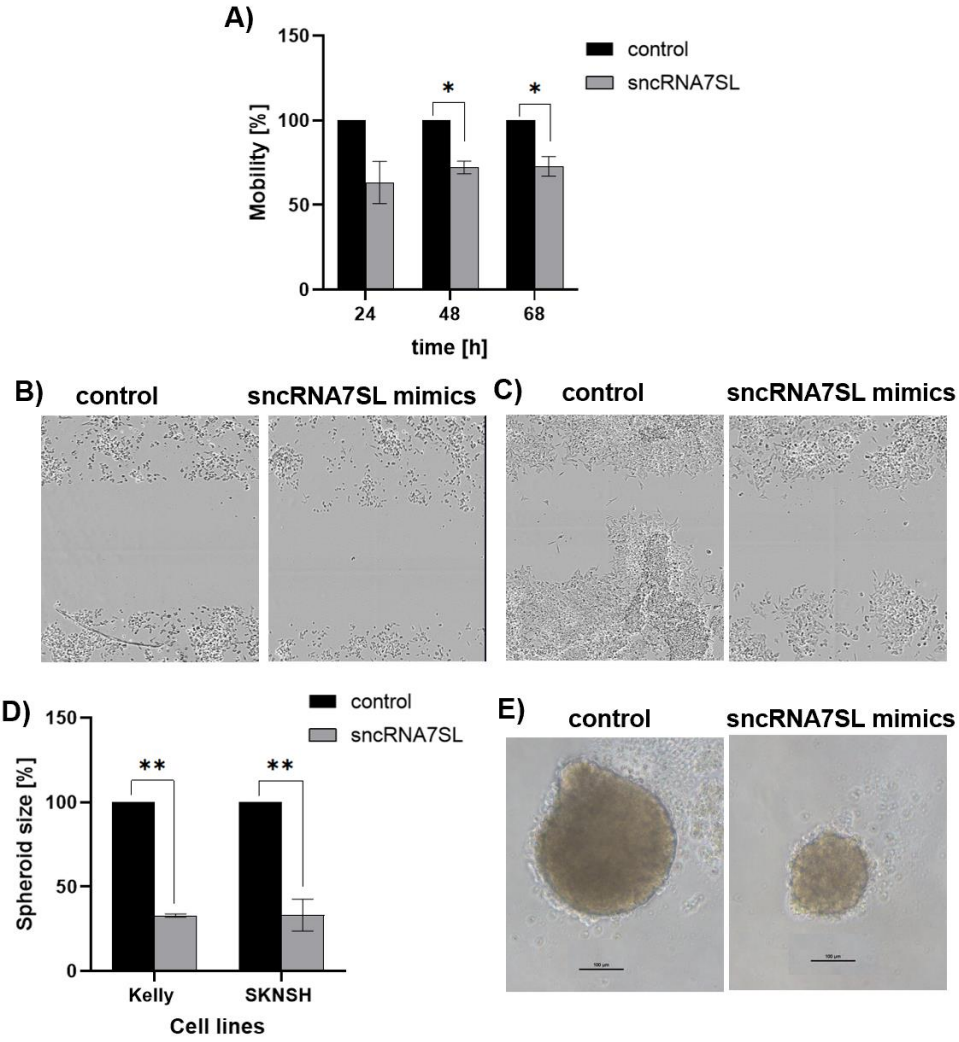

Figure 5. sncRNA7SL mimics reduces mobility and spheroid growth in neuroblastoma. **(A)** Overexpression of sncRNA7SL correlate with a decrease of mobility in Kelly cells 48h and 68h after transfection of 12.5 nM sncRNA7SL mimics or control RNA (sncRNActrl), as determined in two independent experiments. **(B)** Picture of control and sncRNA7SL transfected cells 0 h after scratching. **(C)** 48 h after scratching mobility of cells transfected with 12.5 nM sncRNA7SL was visibly reduced compared to controls. **(D)** Transfection of 12.5 nM sncRNA7SL mimics led to a decrease of spheroid growth three days after transfection, as determined in three (Kelly) and two (SK-N-SH) independent experiments performed in triplicates. **(E)** Seven days after transfection of 12.5 nM sncRNA7SL mimics or control RNA significant decrease of spheroid growth in SK-N-SH cells compared to sncRNActrl transfected

cells was observed. Mean SD (error bars) and P Values were determined using the paired t-test (Prism 8.4, Graph Pad Software). P value * ≤ 0.05 and ** ≤ 0.01. Spheroid scopes were measured with ImageJ-win64.

Next, the effect of sncRNA7SL overexpression on the mobility of neuroblastoma cell lines was studied. Kelly cells were transfected with 12.5 nM sncRNA7SL mimics and plated on 96-Well cell culture plates. 24 h after transfection a scratch was drawn through the cell layer. The width of the scratched cell-free area was measured every two hours over a time period of 68 h with an Incucyte instrument and compared to control transfected cells (Figure 5 B and C). Concurring with previous experiments, sncRNA7SL mimics decreased mobility of Kelly cells at all tested time points (24h to 68h, Figure 5 A) with an attained reduction of about 20 %. While the decrease in mobility was already visible 24 h after scratching of sncRNA7SL mimics transfected Kelly cells, the reduction of mobility turned out to be significant after 48 and 68 hours.

Concisely, overexpression of sncRNA7SL impaired cell viability, and proliferation, and furthermore significantly decreased the mobility of neuroblastoma cells.

3.1.3 Spheroid growth is reduced by sncRNA7SL mimics in neuroblastoma

As a next step, the impact of sncRNA7SL overexpression on three-dimensional (3D) cell cultures was investigated. Contrary to 2D cell cultures, 3D cell cultures have a variety of physiological markers that are important for the characteristics of the tumor such as treatment resistance in cancer therapies (Friedrich et al., 2009; Nunes et al., 2019). Furthermore, 3D models are regarded to better reflect *in vivo* properties of tumors due to their similarities in structural and biological features (Pampaloni et al., 2007). Therefore, 3D cell cultures are considered to give insight into proliferation properties and cell-cell contacts of *in vivo* tumors (Nolan et al., 2020).
To confirm the previously described negative effects of sncRNA7SL overexpression on proliferation (Figure 4 C) in 3D cell culture, Kelly and SK-N-SH cells were transfected with sncRNA7SL mimics or its reverse control RNA and transferred to a low attachment plate 24 h post-transfection. The spheroid size was analyzed three, seven, and ten days later as recently described in Käss et al., 2023. Analysis showed a significant decrease in spheroid growth at day three after sncRNA7SL transfection (Figure 5 D), with about 70 % spheroid size reduction in both tested cell lines. While

the reduction in size in sncRNA7SL transfected spheroids compared to controls was significant throughout the measurement period, the strength of the effect decreased over the measured time period (data not shown). While the effect could be best seen on day three, even on day seven the size reduction in sncRNA7SL transfected neuroblastoma cells was distinct (Figure 5 E).

In summary, 3D cell culture is an important tool to gain a clearer insight into real tumor proliferation processes in cancer cells. sncRNA7SL mimics in Kelly and SK-N-SH cells resulted in a significant reduction of spheroid growth, in line with previous experiments, strengthening sncRNA7SL as a tumor suppressor.

3.1.4 sncRNA7SL mimics lead to a cell cycle arrest in neuroblastoma

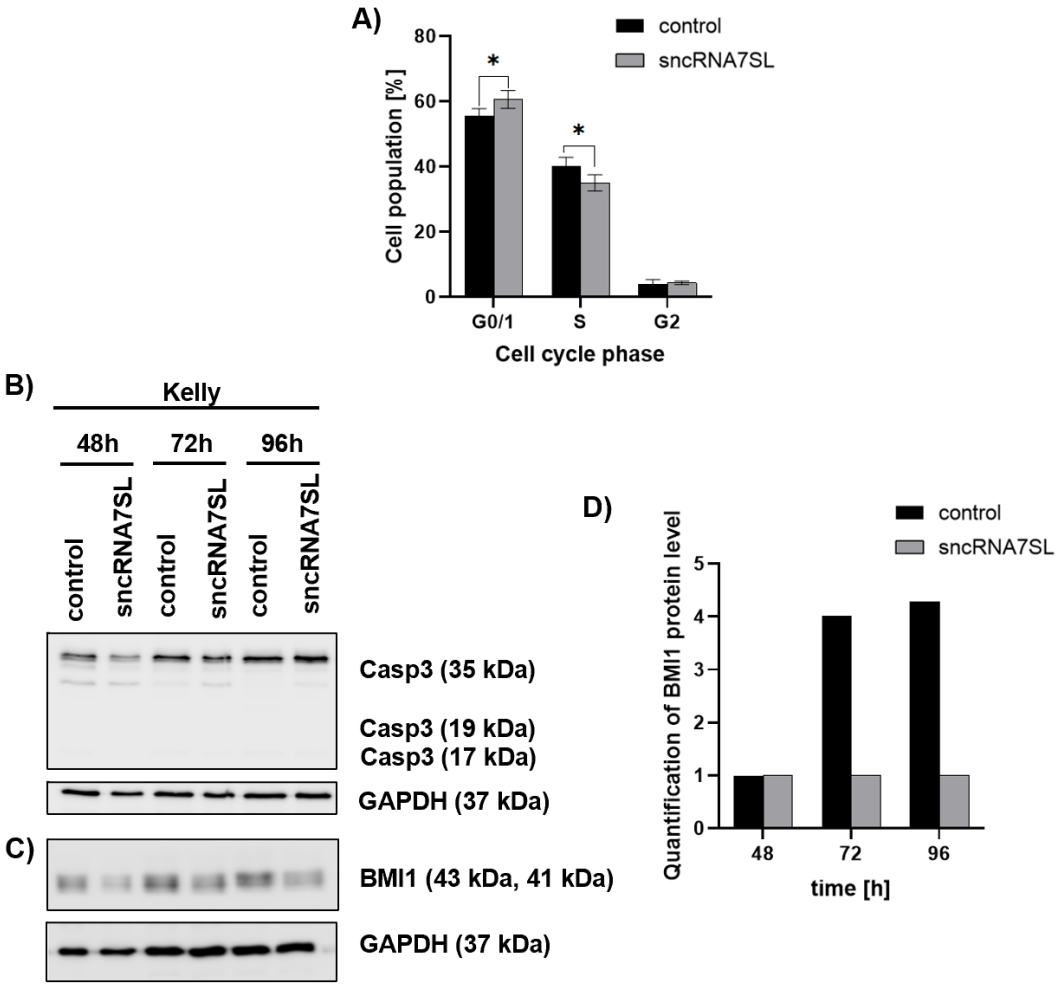

Figure 6. sncRNA7SL mimics cause a G1 arrest and decrease BMI1 protein expression in Kelly cells.
(A) Overexpression of sncRNA7SL correlate with a G1 arrest in Kelly cells 72h transfection of 12.5 nM sncRNA7SL mimics or a respective control RNA (sncRNActrl), as determined in three independent experiments performed in triplicates. The results were determined as mean SD (error bars). P value <0.05 was determined using paired t-test with Prism 8.4 (Graph Pad

Software). **(B)** Transfection of 12.5 nM sncRNA7SL mimics had no effect on the apoptosis marker Casp3, however, decreased BMI1 protein expression in Kelly cells at all tested time points **(C)**. **(D)** Quantification of BMI1 protein level normalized with GAPDH. P value <0.05 was determined using paired t-test with Prism 8.4 (Graph Pad Software).

sncRNA7SL overexpression reduced cell viability, proliferation, mobility, and spheroid growth (Figure 3,4,5). To identify the cause of these effects, a look at the cell cycle in sncRNA7SL overexpressed cells was essential, to elicit a possible cell cycle arrest. Kelly cells were transfected with 12.5 nM sncRNA7SL mimics. 72 hours after transfection cells were fixed and DNA was stained with Propidium iodide. Cell cycle analysis evaluated the amount of DNA via fluorescence measurement. The amount of DNA in individual cells provided information about the cell cycle phase in which the respective cells were situated and hence cells were sorted in different stages of the cell cycle by the MACS Quant Analyzer 10. It was found that sncRNA7SL overexpression led to a slight but significant increase in cells in the G1 phase and a corresponding decrease in the cell in the S phase (Figure 6 A).

Taken together these results suggest that sncRNA7SL overexpression cause a defect in the G1 to S phase transition and thereby reduces cell proliferation.

3.1.5 sncRNA7SL mimics have no impact on Casp3 protein level

Another important question to address is whether sncRNA7SL regulates apoptosis.
Caspase-3 (Casp3) is one of the best-studied factors in cell death. The protein's active form consists of two subunits (12 kDa and 17 kDa), while the inactive precursor is visualized by 32 kDa and plays a key role in breaking down apoptotic cells (Miller 1997).
Therefore, protein levels of apoptosis marker Casp3 were used to test whether overexpression of sncRNA7SL induces apoptosis in Kelly cells 48 h, 72 h, and 96 h after transfection (Figure 6 B). Western blot analysis showed no induction of proteolytic cleavage of Casp3 in sncRNA7SL overexpressed Kelly cells compared to controls. This finding suggests that apoptosis is not induced by overexpression of sncRNA7SL.

Taken together, the tumor suppressive function of sncRNA7SL overexpression does not include the induction of apoptosis by activating Casp3-dependent apoptotic pathways.

3.1.6 sncRNA7SL mimics reduce BMI1 protein expression

B-lymphoma Moloney murine leukemia virus insertion region-1 (BMI1) is a known oncogene and part of the Polycomb repressor complex 1. BMI1 plays a role in chromatin remodeling by increased methylation of histones and therefore functions as an epigenetic repressor (reviewed in Bhattacharya et al., 2015). Furthermore, it was found to promote stem cell renewal (Molofsky et al., 2005) and helps with DNA break repair (Ginjala et al., 2011). Among other factors, it is known to correlate with a poor prognosis for patients with various cancers including neuroblastoma (Nowak et al., 2006). To test whether sncRNA7SL can impair BMI1 expression, Kelly cells were transfected with 12.5 nM sncRNA7SL mimics and analyzed protein levels of BMI1 via Western blot analysis. Overexpression of sncRNA7SL led to a decrease in BMI1 protein level at all measured time points (Figure 6 C). Quantification of Western blots revealed an about four times lower level of BMI1 proteins in sncRNA7SL transfected cells 72h and 96h after transfection. This effect became even stronger over time (Figure 6 D), further strengthening the role of sncRNA7SL as a tumor suppressor in neuroblastoma.

In sum, results suggest that overexpression of sncRNA7SL reduces the protein level of the oncogene BMI1, by a yet unknown mechanism.

3.1.7 Summary sncRNA7SL as a tumor suppressor in cell culture

In summary, overexpression of sncRNA7SL reduces cell viability, and cell proliferation by hindering the G1- to S-phase transition during the cell cycle. Although, it has only a small effect on the cell cycle progression and because apoptosis is not induced by overexpression of sncRNA7SL, the data suggest that sncRNA7SL regulates factors supporting G1 to S-phase transition. Based on these findings, the results of the wound healing experiment suggesting the sncRNA7SL impairs cell mobility is not conclusive, until the mobility of individual cells would be recorded. The strong reduction in BMI1 expression by overexpression of sncRNA7SL is striking and suggests other important cellular mechanisms driven by BMI1 such as stem cell self-renewal and DNA repair, being impaired and contributing to the reduced spheroid formation seen by overexpression of sncRNA7SL. Strikingly, the depletion of sncRNA7SL results in an

increase in viability. The data suggest that sncRNA7SL negatively regulates tumor-promoting processes such as cell cycle progression, stem cell renewal, and DNA repair.

These results, as visualized in Figure 7, suggest that sncRNA7SL indeed acts as a tumor suppressor.

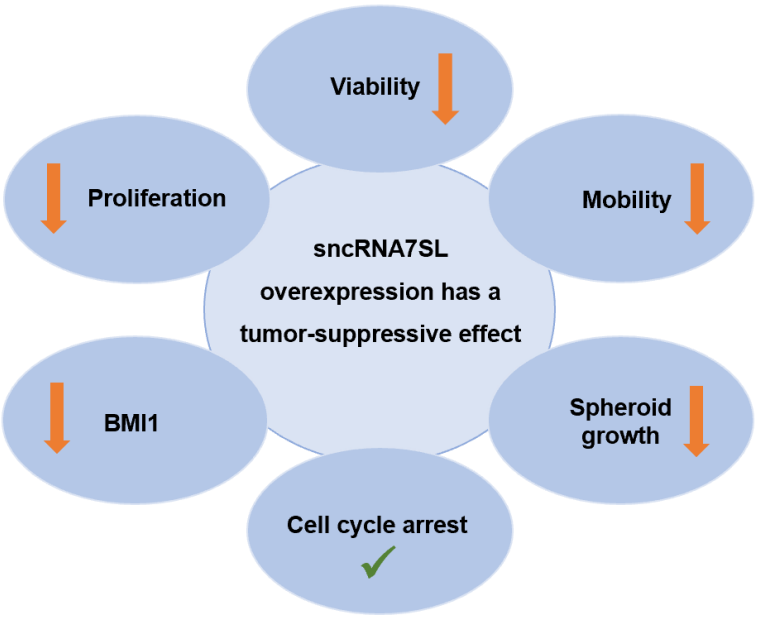

Figure 7. Graphical summary of the phenotype of sncRNA7SL overexpressing cancer cells.
Overexpression of sncRNA7SL results in a decrease in proliferation, viability, mobility, spheroid growth, and BMI1 protein expression. It also leads to a G1 arrest but does not have an effect on apoptosis. Meanwhile, depletion of sncRNA7SL results in an increase in viability, suggesting the role of sncRNA7SL as a tumor suppressor in cancer cells.

3.2 Detection of sncRNA7SL localization in neuroblastoma

In cell-based assays, overexpression of sncRNA7SL was found to disturb critical cellular mechanisms in neuroblastoma cells, suggesting a tumor-suppressive function of sncRNA7SL. However, the mechanisms of action of sncRNA7SL in neuroblastoma are unknown. To this end, a first look was taken at the localization of sncRNA7SL, as this can give good indications not only towards the mechanisms of action of sncRNA7SL but also to its possible cellular functions. First, a Molecular Beacon-based (MB) detection method to localize the endogenous sncRNA7SL and its precursor 7SL RNA was developed (see 3.2.1 (Weigert et al., manuscript under revision).

3.2.1 Cellular localization of endogenous sncRNA7SL

First, the cellular localization of endogenous sncRNA7SL was investigated. For this purpose, the system of a Molecular Beacon (MB) was applied, described in Tyagi and Kramer, 1996. The principle here is that the MB consists of a stem-loop structure. The stem is formed by G-C base pairs (here: four to six) bringing the 3'- and the 5'-ends in close proximity. The 3'-end terminates with a quencher (here: DAB or BHQ), while the 5'-end terminates with a fluorophore (here: FAM or Cy5). As long as the G-C base pairing the stem remains closed, the excited fluorophore is in the immediate vicinity of the quencher. The quencher can absorb the fluorophore's energy and prevent an emission signal of the fluorophore. The second component of the Molecular Beacon is the loop structure. This consists of the target sequence of the RNA that is to be bound, for example by endogenous sncRNA7SL. If the MB is transfected into the cell, the endogenous RNA binds to the target sequence of the loop and thus opens the stem. The fluorophore is no longer in the immediate vicinity of the quencher and a fluorescence signal is in the cell site where the endogenous RNA has bound (Figure 8 A). Therefore, the length of the stem is a decisive factor. A stem that is too long will make the MB construct too stable and it will not open upon binding to its target RNA, while a stem that is too short will result in an MB that is too unstable and could lead to the spontaneous opening of the MB without binding to its endogenous target sequence, causing a strong background signal.

To exclude non-specific signals, several MBs with different characteristics and sequences were tested (Figure 8 B; Supplementary Figure 2 A). First, *in vitro* experiments, performed by members of our lab, investigated whether the individual molecular beacons are both specific (Supplementary Figure 2 B) and sensitive.

Based on the *in vitro* studies aiming the detailed characterization of the different MB, as described in detail in Weigert et al., 2023 (manuscript under revision), the following MB were tested in cell-based assays: targeting sncRNA7SL (MBsncRNA-1, MBsncRNA, MBsncRNA-2A), targeting the endogenous 7SL RNA (MB7SL), the endogenous piR6145 (MB6145-1) and as control an MBcon, directed against the reverse sequence of sncRNA7SL.

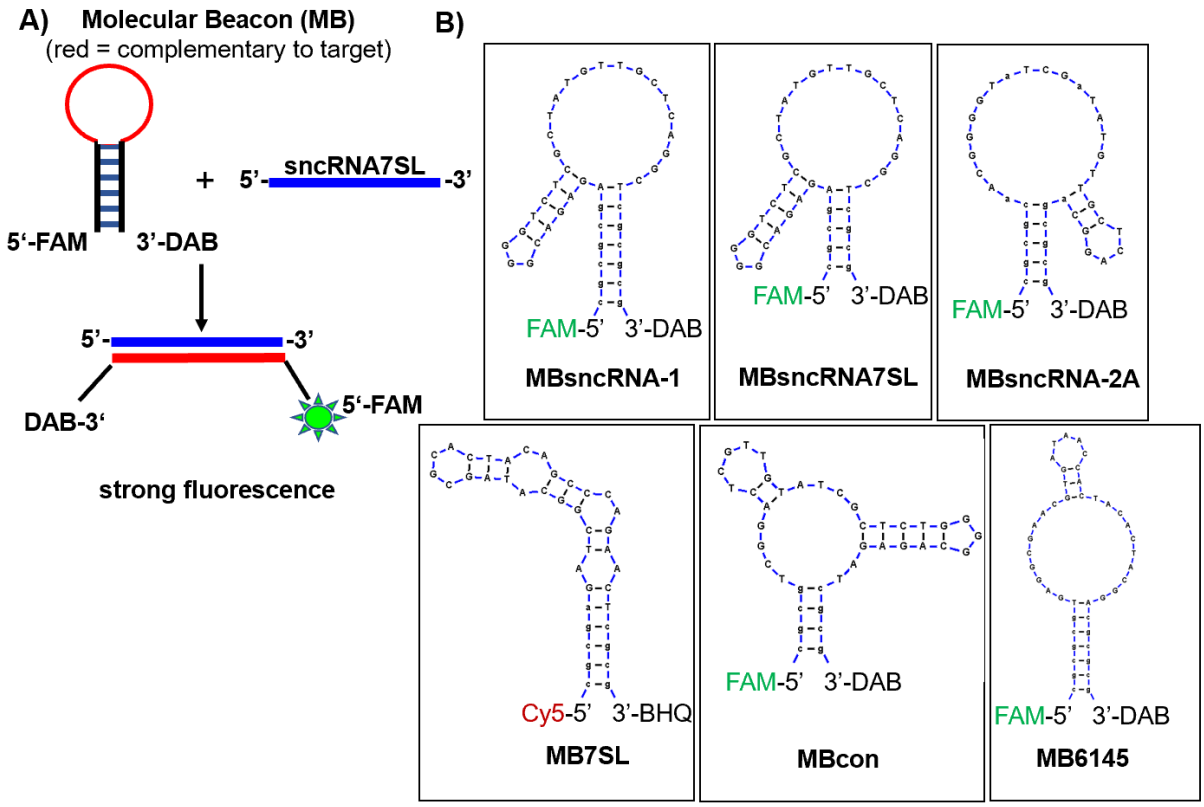

Figure 8. Molecular Beacon (MB) concept of a function and different structures of MB were used in this study.
(A) Endogenous target RNA binds to MB loop target sequence and opens MB stem. Fluorophore is freed from quencher proximity. A fluorescence signal can be detected**. (B)** Predicted folding of MBs MBsncRNA-1, MBsncRNA, MBsncRNA-2A, MB7SL, MB con and MB6145. Structures were predicted using DNA fold (http://www.unafold.org; Zuker, 2003). CT-values were imported into jViz.RNA 4.0 (http://jviz.cs.sfu.ca/). FAM = Fluorescein; DAB = Dabcyl quentcher; Cy5 = Cyanine5; BHQ = Black hole quencher. Figure adapted from Weigert et al., manuscript under revision.

3.2.1.1 Endogenous sncRNA7SL is mainly localized in the nucleus, endogenous 7SL RNA is mainly localized in the cytoplasm

Preliminary *in vitro* experiments proved the MBs to be sensitive and specific (Supplementary Figure 2). Hence, as a next step localization of MB was investigated *in vivo* in live cells using fluorescence microscopy. Therefore, cells were seeded 24 h prior to transfection into live cell imaging chambers and incubated overnight at 37°C. On the following day, these cells were transfected with 12.5 nM MB. 24h later cell nuclei were stained with DAPI and cells were visualized using the Keyence BZ-X810 fluorescence microscope. To avoid identifying background signals as false positives, the first step was always to view MBcon transfected cells and adjust signal strengths

so no signal was seen in the MBcon transfected cells before investigating MBsncRNA7SL and other MB signals with the same microscopic adjustments (Figure 9).

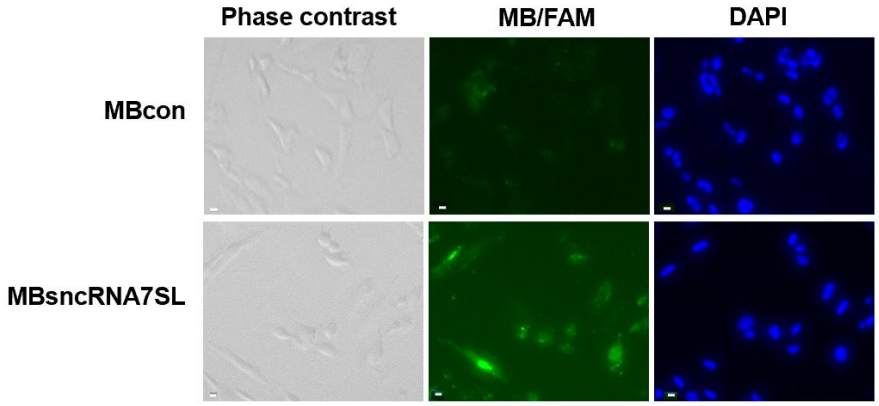

Figure 9. Endogenous sncRNA7SL mainly localizes in the nucleus while MBcon does not show any signal.
SK-N-SH cells were transfected with 12.5 nM MBcon or MBsncRNA7SL respectively and visualized 24h after transfection using the Keyence BZX fluorescence microscope with a magnification of 40x. The scale bar measures 10 µm.

Fluorescence microscopy of MBsncRNA samples showed the main localization of endogenous sncRNA7SL to be in the nucleus visualized as a diffuse green signal. While there was also a slight signal found in the cytoplasm it was much weaker (Figure 9, 10 A).

Since the sequence of sncRNA7SL is found in the Alu element of the 7SL RNA precursor, it was essential to confirm the specificity of MBsncRNA7SL *in vivo*. Hence, MB7SL was used to visualize endogenous 7SL RNA localization in live cells. It was shown that MB7SL was mainly visualized as a diffuse red signal in the cytoplasm (Figure 10 A, red signal). Since the 7SL RNA is a key member of the Signal Recognition Particle (SRP) and therefore localizes around the ER (Gundelfinger et al., 1983) these findings were not unexpected and additionally strengthened confidence in MB signaling. There was only a slight overlap between signals of MB7SL and MBsncRNA7SL in co-transfected SK-N-SH cells (Figure 10 A, arrows), shown in the lower part of Figure 10 A, suggesting that both MB bind specifically to their target sequences. Line Profiles, measuring fluorescence signals within a drawn line through the Z-Stacks, confirmed the majority of endogenous sncRNA7SL (green signal, Figure 10 B) to be localized in the nucleus (blue signal, Figure 10 B), while there was also a spike of sncRNA7SL signal in the cytoplasm it was located in the proximity of the 7SL RNA (red signal, Figure 10 B) signal, suggesting recognition of the endogenous 7SL

RNA by MB sncRNA7SL. Endogenous 7SL RNA barely showed any signal in the nucleus localizing in the cytoplasm instead (Figure 10 B).

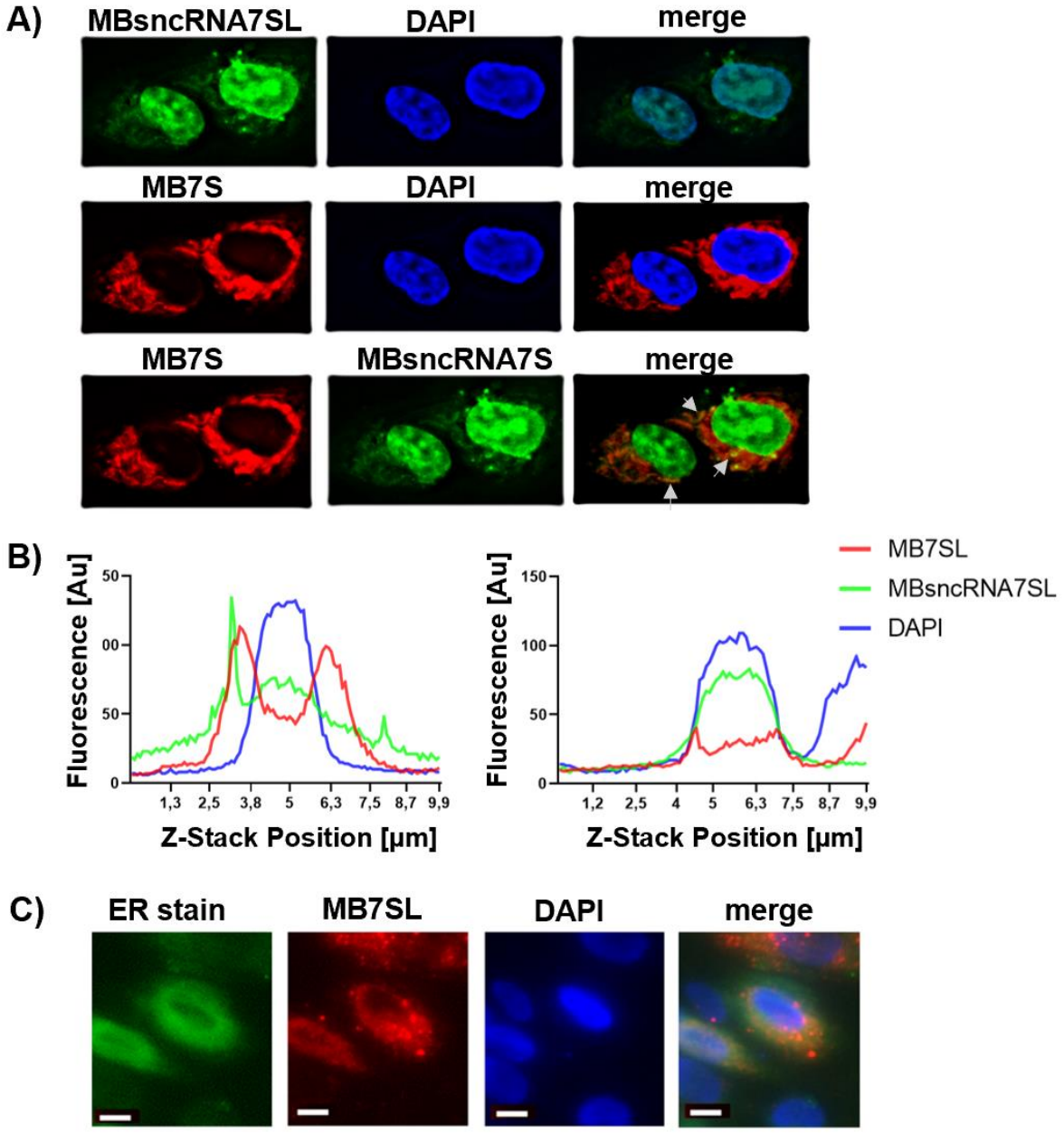

Figure 10. Endogenous sncRNA7SL mainly localizes in the nucleus while endogenous 7SLRNA is mainly localized in the cytoplasm.
(A) Staining of sncRNA7SL and 7SLRNA via Molecular Beacon (MB). Endogenous sncRNA7SL is visualized as a diffuse signal, primarily localized in the nucleus of SK-N-SH cells. Endogenous 7SLRNA is visualized as a diffuse signal in the cytoplasm, there is a slight overlap between sncRNA7SL and 7SLRNA signals in the cytoplasm (arrows). Pictures were processed using Adobe software package Elements. **(B)** Line Profiles of SK-N-SH cells transfected with MBsncRNA7SL and MB7SL (pictures not shown). MBsncRNA7SL is localized in the cytoplasm and nucleus and colocalizes with MB7SL. MB7SL is localized in the cytoplasm. **(C)** Endoplasmatic reticulum (ER) stain (ER tracker green) in MB 7SLRNA transfected cells shows a large overlap between ER and 7SLRNA signals.

All images were taken 24 hours after transfection of Molecular Beacon in live cells with a Keyence BZX fluorescence microscope, with a magnification of 40x or 100x. The scale bar measures 10 µm.
Adapted figure from Weigert et al., manuscript in revision.

Furthermore, to confirm the localization of MB7SL at the ER, neuroblastoma cells were transfected with MB7SL and ER tracker green (fisher scientific, #E24351). 24 hours after transfection cells were stained with DAPI and live cell fluorescence microscopy was performed. The high amount of overlapping signal between MB7SL and ER tracker green suggests that the signal of MB7SL is indeed highly specific in live cells (Figure 10 C).
Interestingly, many more cells showed an MB7SL signal than an MBsncRNA7SL signal which could either indicate reduced transfection efficiency of MBsncRNA7SL or could be related to the amount of respective endogenous RNA present in the cell. Further investigations will be described later in the course of this work.

Taken together, endogenous sncRNA7SL was mainly localized in the nucleus while MB7SL showed a diffuse signal in the cytoplasm, which was overlapping with the localization of ER, as to be expected. Signals of MBsncRNA7SL and MB7SL overlapped only slightly in the cytoplasm.

3.2.1.2 Transfection of MB sncRNA7SL with RNAiMAX is preferable for localization studies

Since MBsncRNA7SL transfection efficiency seemed to be quite low, different transfection reagents were tested. Cells were transfected 24 h after seeding with 12.5 nM MB sncRNA7SL using various transfection reagents (RNAiMAX, FuGENE, and Lipofectamine 3000). MB transfection with RNAiMAX yielded the results already obtained in previous experiments with a quite low transfection efficiency of MBsncRAN7SL (Supplementary Figure 3 A). However, transfection with Lipofectamine 3000 led to very low signal emission (Supplementary Figure 3 B) close to the signal in control transfected cells and was therefore discarded as a possible transfection reagent. FuGENE, often used for plasmid transfection was considered next. FuGENE transfection of MBsncRNA7SL yielded a very high signal level, however, upon close inspection, the signal did not occur in the nucleus (Supplementary Figure 3 C). Often MBsncRNA7SL signal seemed not even to be accumulated in huge unspecific dots in

the cytoplasm or even next to cells, suggesting the opening of the MB stem without target binding.

In short, RNAiMAX could be confirmed as the best transfection reagent.

3.2.1.3 Different types of MBs in SK-N-SH cells

To further prove the specificity of MBs in live cells, several different types of MBs were tested in SK-N-SH cells. For this purpose, pre-seeded cells were transfected with 12.5 nM MB and visualized 24 hours later via the Keyence BZ-X810 fluorescence microscope. MBsncRNA7SL and MBcon (data not shown) were transfected as a transfection efficiency and background signal control respectively. MBsncRNA7SL showed a strong signal mainly localized in the nucleus confirming previous results (Figure 11 A). MBsncRNA-1, containing a six-base pair stem, barely showed any signal, indicating that six base pairs as a stem structure are too strong to be opened by endogenous sncRNA7SL binding to the loop target sequence (Figure 11 B). Similar to MBsncRNA-1, MB sncRNA-2A which includes a four-base pair stem structure but three mismatches as well as five deletions in the sncRNA7SL target sequence loop showed noticeably less signal than MBsncRNA7SL did (Figure 11 C). This suggests MB to be highly specific to its target. These data are in line with *in vitro* studies described in detail in Weigert et al. (under revision).
MB6145 shows a strong diffuse signal mainly localized in the nucleus (Figure 11 D), similar to MBsncRNA7SL, indicating that the size of the target might play a role in the localization in the nucleus. Interestingly, MB6145 has six base pairs as a stem structure, suggesting RNA 6145 is a stronger target. Whether this is due to the amount of RNA 6145 in SK-N-SH cells cannot be confirmed at this time.

Concisely, sncRNA7SL can only be visualized with an MB with a stem consisting of four G-C base pairs, while RNA 6145 can open MBs with a stem consisting of at least six G-C base pairs. Both small RNAs were found to be mainly localized in the nucleus and seen as diffuse signals. MB also seem to be highly specific toward their target since three mismatches in the target sequence were enough to prevent the MB from opening.

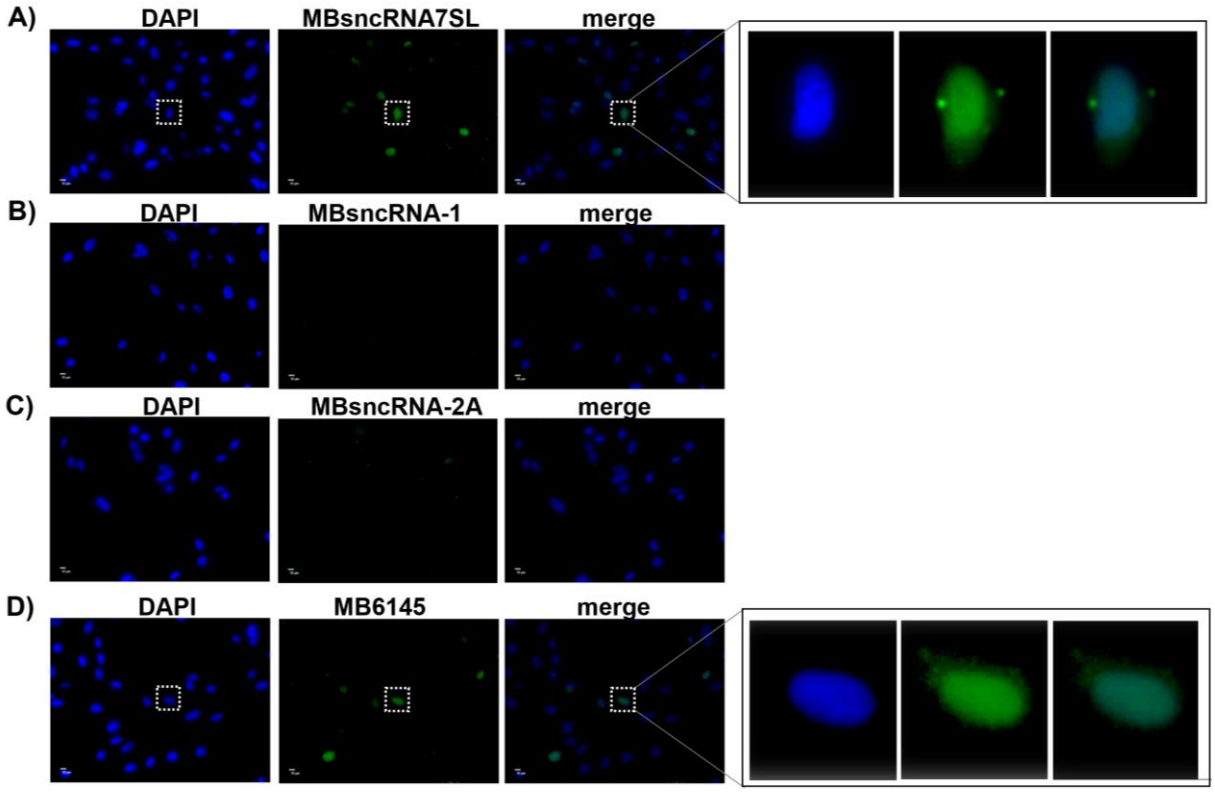

Figure 11. Detection of sncRNA7SL by MBsncRNA7SL but not by MBsncRNA-1 or MBsncRNA-2A in SKNSH cells.
SK-N-SH cells were transfected with 12.5 nM **(A)** MBsncRNA7SL, **(B)** MBsncRNA-1, **(C)** MBsncRNA-2A, and **(D)** MB6145.
Enlarged nuclei are shown for A and D. 24 h after transfection pictures were taken with a KEYENCE BZ-X810 fluorescence microscope. Z stack was taken, magnification=40x, Plan apochromat Scale bar = 10 µM All pictures were processed using Adobe software, Elements. Figure submitted for Weigert et al., manuscript under revision.

3.2.1.4 Comparison of transfection efficiency of MBsncRNA7SL and MB7SL

In previous experiments, it was shown that MBsncRNA7SL mainly localizes in the nucleus, while MB7SL gives a diffuse signal in the cytoplasm (Figure 10). Strikingly, while almost all transfected cells showed a fluorescent signal in the cytoplasm when transfected with MB7SL, transfection with MBsncRNA7SL was much less productive. Two causes could be involved in this phenomenon. First, sncRNA7SL could occur endogenously in much lower concentrations or only be abundant enough in certain cell stages to be detected by MB, and second, the transfection efficiency with MB sncRNA7SL could be much lower than that with MB7SL. To check the transfection efficiency, MBsncRNA7SL, and MB 7SL were designed without a quencher (Figure 12). The reason was to be able to visualize the fluorescence signal in the cells at any given time, even if it was not bound to a target.

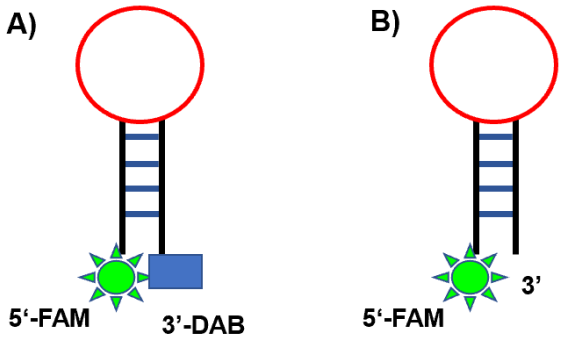

Figure 12. Different structures of MB were used to investigate transfection efficiency in this study.
(A) MB sncRNA7SL, MB 7SL, with a stem of 4 base pairs used for the majority of this study. **(B)** MB sncRNA7SL-Quencher, MB 7SL-Quencher, MB with a 4 base pair stem without a quencher at the 3' end. FAM = Fluorescein; DAB = Dabcyl quentcher.

SK-N-SH cells were transfected with MBcon, MBsncRNA7SL, and MB7SL. MBsncRNA7SL-Quencher and MB7SL-Quencher respectively and visualized using the KEYENCE BZ-X810 fluorescence microscope 24 hours after transfection. MBcon cells were again used for background determination.

Interestingly, the percentage of transfected cells did not seem to differ much between MBsncRNA7SL and MBsncRNA7SL-Quencher or between MB7SL and MB7SL-Quencher (Figure 13). It was apparent that MB7SL transfected cells with and without quencher have a very high transfection efficiency while MBsncRNA7SL transfected cells with and without quencher have only a very low rate of transfected cells. Quantifications show that MBsncRNA7SL transfected cells with and without quencher are at a transfection rate of about 20 % (Figure 13 A), whereas MB7SL transfected cells with and without quencher have rates above 85 % (Figure 13 B). This suggests that the reason for the low signaling rate in MBsncRNA7SL cells is at least not exclusively the insufficient presence of endogenous sncRNA7SL at a particular cell stage. Interestingly, the folding of MB7SL is significantly different from all other MBs tested (Figure 8 B). This leads to the assumption that folding is an important factor in transfection efficiency.

Taken together, it was found that MBsncRNA7SL has a significantly lower transfection efficiency than MB7SL. It does not matter whether a quencher is used or not.

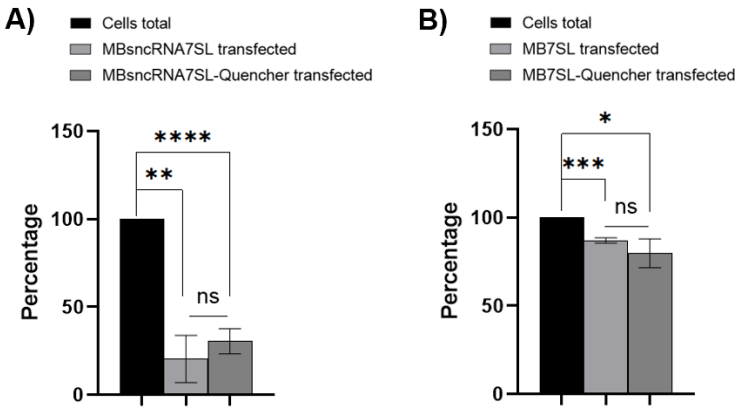

Figure 13. Transfection efficiency of MBsncRNA7SL and MB7SL compared to their counterparts without a quencher.
(A) Transfection efficiency was not significantly different in MBsncRNA7SL compared to MBsncRNA7SL-Quencher. Transfection levels were at about 20 to 30 % 24 hours after transfection of 12.5 nM Molecular Beacon, respectively. As determined in two (MBsncRNA7SL) or three (MBsncRNA7SL-Quencher) overview pictures with a magnification of 20x. **(B)** Transfection efficiency was not significantly different in MB7SL compared to MB7SL-Quencher. Transfection efficiency was at about 80% 24 hours after transfection of 12.5 nM Molecular Beacon, respectively. As determined in three overview pictures with a magnification of 20x.
Transfection efficiency was normalized to the total number of counted cells and converted into percent.
All results were determined as mean SD (error bars). P value * ≤ 0.05,** ≤ 0.01, *** ≤ 0.001 and,**** ≤ 0.0001 was determined using paired t-test with Prism 8.4 (Graph Pad Software).

3.2.1.5 Summary endogenous localization of sncRNA7SL

In summary, endogenous sncRNA7SL was found to be mainly localized in the nucleus with a weak diffuse signal in the cytoplasm as well as some accumulated bright dots in the cytoplasm. While MB7SL is mainly localized in the cytoplasm as expected for an architectural component of the SRP. MB proved to be sensitive and specific in live cell imaging with only three mismatches and five deletions in the target sequence enough to prohibit the binding of MB to sncRNA7SL. Furthermore, localization in the nucleus may be influenced by RNA length since it was shown that sncRNA7SL as well as RNA 6145, an RNA of similar length, were mainly localized in the nucleus as visualized in Figure 14. However, transfection efficiency was low in MBsncRNA7SL (about 20 %) compared to MB7SL (about 80 %, Figure 13). Using MB without Quencher did not improve the overall number of transfected cells, suggesting that not only the target abundance is responsible for the low signal transmission in MBsncRNA7SL transfected cells but also that the transfection efficiency of MBsncRNA7SL is low.

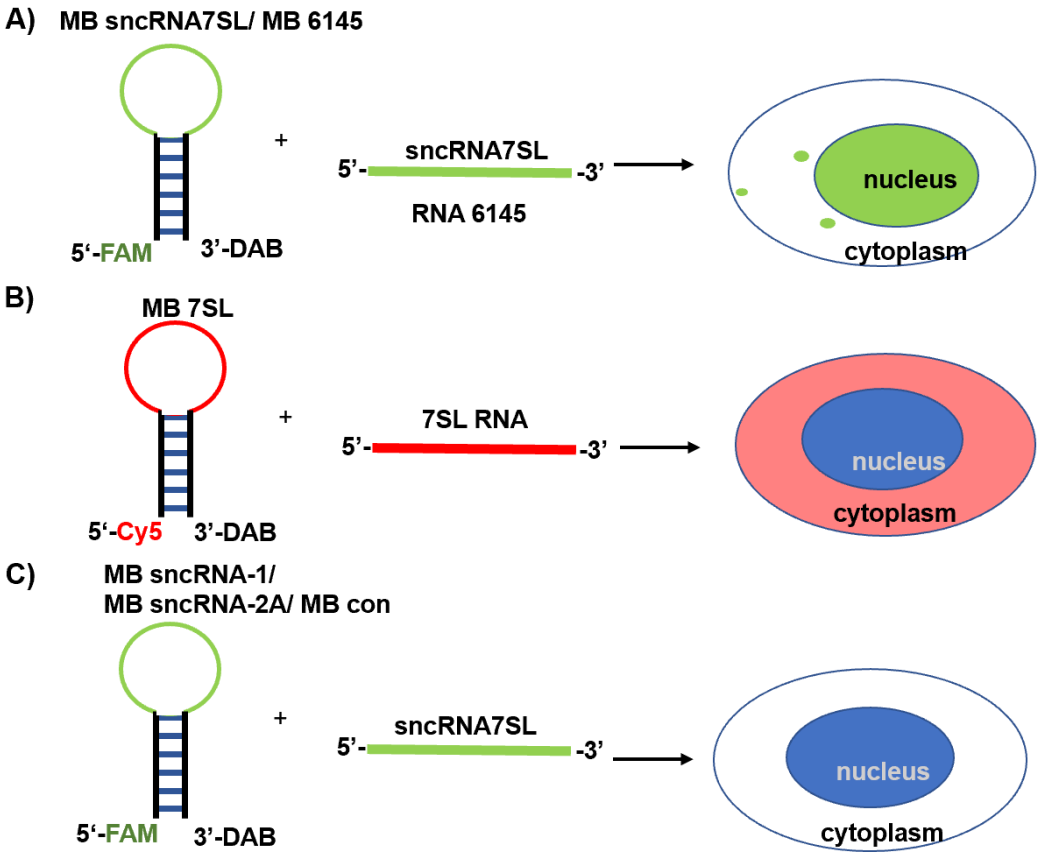

Figure 14. Graphical summary of endogenous localization of sncRNA7SL.
Localization of MB signals in the cell **(A)** MB sncRNA7SL and MB 6145 are mainly localized in the nucleus. **(B)** MB 7SL signal is mainly visualized in the cytoplasm **(C)** MB sncRNA-1, MB sncRNA-2A and MB con barely showed any signal.

3.2.2 Establishment of fluorescence-labeled synthetic sncRNA7SL as a powerful tool for studying the subcellular localization and the colocalization of sncRNA7SL with other cellular RNAs and proteins

3.2.2.1 Rational of synthetic sncRNAs

Molecular beacon experiments revealed that endogenous sncRNA7SL mainly localizes to the nucleus. Nucleic endogenous sncRNA7SL is evenly distributed and not concentrated in specific areas (Figure 10). This discovery raised the question, about the underlying mechanism leading to the nuclear localization of sncRNA7SL.

The biogenesis of sncRNA7SL is not known yet. However, it seems possible that the 7SL RNA is either cleaved by Drosha/DGCR8 in the nucleus or by Dicer in the cytoplasm. These assumptions are based on the finding that Drosha can also cleave RNAs much bigger than miRNA precursors (Knuckles et al., 2012) and Dicer can indeed process the 7SL RNA into small RNAs of various lengths (Ren et al., 2012). Furthermore, Dicer was found to possess a nuclear localization sequence (Doyle et

al., 2013) and was affirmed to be localized in the nucleus at low levels (White et al., 2014).

If sncRNA7SL is generated by Dicer in the cytoplasm it could be postulated that the sncRNA7SL is imported to the nucleus via a binding partner, presumably an RNA binding protein (RBP). Studies of the nucleic import of sncRNA7SL-protein complexes could be performed by knockdown of various nuclear import factors monitored by immunofluorescence studies.

In case sncRNA7SL is generated in the nucleus by nuclear Dicer or Drosha/DCGR8, it would fit well with the main nuclear localization of endogenous sncRNA7SL. The finding that endogenous sncRNA7SL is also detectable in the cytoplasm suggests that sncRNA7SL can be exported to the cytoplasm and might shuttle between the nucleus and cytoplasm. A fluorescence-labeled synthetic sncRNA7SL would be a great tool to test the notion of whether sncRNA7SL is bound by an RBP and shuttles between the nucleus and cytoplasm. This was described for other small RNAs like miRNAs using Importin 8 for nucleic import (Wei et al., 2014) and Exportin 5 playing a huge role, among others, in miRNA biogenesis as a transporter from the nucleus in the cytoplasm (Yi et al., 2003).

Hence a fluorescence-labeled synthetic sncRNA7SL would be a great tool to test the notion that sncRNA7SL shuttles between the nucleus and cytoplasm. Others studied the subcellular localization of siRNAs by cellular fractionation, RNA fluorescent *in situ* hybridization (FISH), or by introducing a fluorescence group to the 3'-end of synthetic RNA (Jakymiw et al., 2005.; Pitchiaya et al., 2012;2013;2017;2018; Leung et al., 2006)**.** However, it is well established that 5'- and 3'-ends of miRNAs are crucial for binding by Argonaute proteins. Argonaute protein 3 was shown to bind 28 nt to 65 nt long RNAs (Hu et al., 2012), similar to the 32 nt long sncRNA7SL, while Ago2 protein is known to bind smaller RNAs like microRNAs in order to build RISCs (Meister et al., 2004). The PIWI and the MID domain of said proteins bind the 5'-phosphate and the 5'-terminal nucleotide (Figure 15; Boland et al., 2011; Frank et al., 2010, 2011), while the MID domain needs access to the last nucleotides of the 3'-end for binding (Lingel et al., 2003, 2004; Song et al., 2003; Yan et al., 2003; Ma et al., 2004; Kidner and Martienssen, 2004; reviewed in Duchaine and Fabian, 2019). These studies raise the question of to which extent terminal fluorescent groups affect the binding of labeled sncRNA7SL by Ago proteins and result in artificial subcellular localizations.

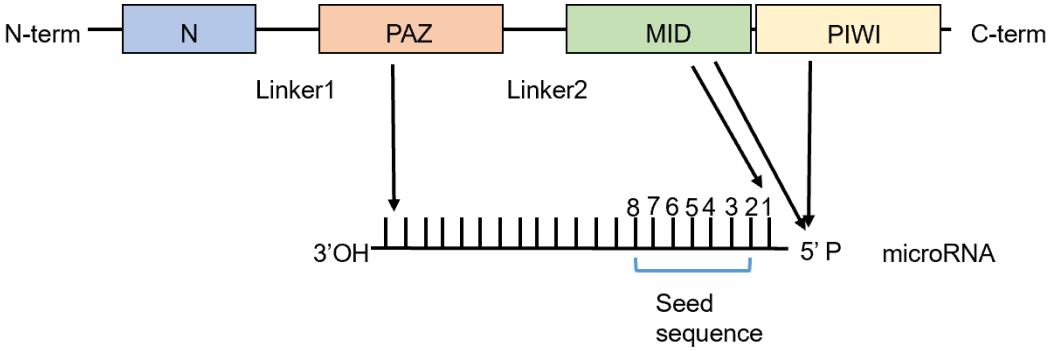

Figure 15. Structure of human Argonauts interacting with RNA.
The figure shows the domains of human Ago2. With N, PAZ, MID, and PIWI domains as well as the two linkers connecting those domains. Interactions with guide RNA are with the MID domain binding to the very first nucleotide, as well as the PAZ domain binding to the last nucleotides of the 3' tail (Figure is altered from Duchain and Fabian, 2019).

Hence, several different fluorescence-labeled synthetic RNAs were designed (Table 19). First fluorescence labels were linked to the 5'-end (FAM-sncRNA7SL, FAM-sncRNActrl, Cy5-sncRNA7SL) or the 3'-end (sncRNA7SL-FAM, sncRNActrl-FAM) and analyzed by live cell imaging. Furthermore, an internal fluorescence tag was placed after position 14 within the sncRNA7SL sequence. Since Literature showed, piRNAs have a seed region at nucleotides 2 to 8 extending up to nucleotide 12 (Anzelon et al., 2021), the fluorescence label after position 14 was deemed safe to ensure optimal RNA protein binding conditions. Furthermore, it was found that for Argonaute binding RNA nucleotides 14 to 18 were excluded from base-pairing (reviewed in Duchaine and Fabian, 2019) making position 14 an excellent position for undisruptive fluorescence labeling.

To exclude that the type of label instead of RNA sequence, determines localization, both FAM and Cy5 fluorescence groups were compared.

As already suggested due to the localization of both endogenous sncRNA7SL and endogenous RNA 6145, and the reported cytoplasmic localization of labeled miRNAs (Sonoda et al., 2021) length may play a major role in the localization of sncRNA7SL in the nucleus. Consequently, smaller RNA Oligos with lengths closer to miRNAs, 22 nts and 23 nts respectively, were designed by deleting nucleotides of sncRNA7SL. Fluorescence labels were tagged at the 5'-end as well as integrated into the sequence after position 11 to avoid seed sequence interference (Cy5-sncRNA7SL-Δ1, Cy5-sncRNA7SL-Δ2, sncRNA7SL-Δ2-inte-Cy5 (Table 19)). Shorter RNA oligos were tagged with Cy5 to make co-staining with full-length FAM-tagged sncRNA7SL oligos possible.

Table 19. Fluorescence labeled RNA oligos used in this study.

Name	Sequence
FAM-sncRNA7SL	5'-FAM-AGCCUGAGCAACAUAGCGAGACCCCGUCUCUmA-3'
FAM-sncRNActrl	5'-FAM-AUCUCUGCCCCAGAGCGAUACAACGAGUCCGmA-3'
sncRNA7SL-FAM	5'-P-AGCCUGAGCAACAUAGCGAGACCCCGUCUCUA-FAM-3'
sncRNActrl-FAM	5'-P-AUCUCUGCCCCAGAGCGAUACAACGAGUCCGA-FAM-3'
sncRNA7SL-inte-FAM	5'-P-AGCCUGAGCAACAU-FAM-AGCGAGACCCCGUCUCUmA-3'
Cy5-sncRNA7SL	5'-Cy5-AGCCUGAGCAACAUAGCGAGACCCCGUCUCUmA-3'
Cy5-sncNRA7SL-Δ1	5'-Cy5-AGCCUGAGCAACCCCGUCUCUmA-3'
Cy5-sncNRA7SL-Δ2	5'-Cy5-AGCCUGAGCAACAUAGCGAGACmA-3'
sncRNA7SL-Δ2-inte-Cy5	5'-PAGCCUGAGCAU-Cy5-CAUAGCGAGACmA-3'

3.2.2.2 Synthetic sncRNA7SL and control RNA both accumulate in the nucleus as nuclear bodies in different cell lines

As the first step in this series of experiments, different neuroblastoma cell lines (Kelly, SK-N-AS, SK-N-SH) and U2-OS cells were plated on live cell imaging slides and transfected with 12.5 nM FAM-sncRNA7SL or FAM-sncRNActrl. 24 h after transfection, cell nuclei were stained with DAPI, and cells were analyzed using the Keyence BZ-X810 fluorescence microscope (Kelly, SK-N-AS, SK-N-SH) or the Leica TCS SP5 confocal laser scanning microscope (U2-OS). Live cell imaging microscopy showed an accumulation of both: the FAM-sncRNA7SL and FAM-sncRNActrl signal in

the nucleus in all examined cell lines (Figure 16 A and B). Both RNA oligos, FAM-sncRNA7SL and FAM-sncRNActrl, localized mainly to the cell nucleus and to a minor extent to the cytoplasm, similar to the localization of endogenous sncRNA7SL (Figure 8, 10). The nuclear fluorescence signal shows that a fraction of the RNA oligos were evenly distributed in the nucleoplasm, such as the endogenous sncRNA7SL detected by molecular beacons (Figure 9-11). However, another fraction of the RNA oligos accumulated in several nuclear bodies per cell nucleus. No difference was apparent between the number of FAM-sncRNA7SL or FAM-sncRNActrl nuclear bodies in transfected cells. Quantification also showed no significant difference in the number of nuclear bodies in different cell lines or between FAM-sncRNA7SL and FAM-sncRNActrl transfected cells, with an average of about seven bodies per nucleus (Supplementary Figure 4).

To see if not the position of the label, but its type is responsible for creating accumulations as dots in the nucleus, 5'-Cy5 labeled RNA Oligos were used. 12.5 nM Cy5-sncRNA7SL were transfected in U2-OS cells. 24 after transfection cells were stained with DAPI and live cell imaging was performed using the Leica TCS SP5 confocal laser scanning microscope. Analysis showed that the signal was again mainly accumulated in the nucleus as nuclear bodies (Figure 16 C).

Subsequently, the influence of the position of the fluorescence label on the localization was investigated. Therefore, sncRNA7SL and sncRNActrl were labeled with a FAM fluorescence tag at the 3'-end of the RNA. U2-OS (sncRNA7SL-FAM) and SK-N-SH (sncRNActrl-FAM) cells were transfected with 12.5 nM of the respective RNA Oligos and 24 h after transfection stained with DAPI. Live cell imaging was performed using the Leica TCS SP5 confocal laser scanning microscope (U2-OS) or the Keyence BZ-X810 fluorescence microscope (SK-N-SH). Signals were again detected mainly in the nucleus (Figure 16 D). They also accumulated in nuclear dots. No visual difference could be identified between sncRNA7SL-FAM and sncRNActrl-FAM. These findings suggest that not the type or the terminal position of the fluorescence label or the RNA oligo sequence triggers the concentration of sncRNA7SL or sncRNActrl in nuclear bodies.

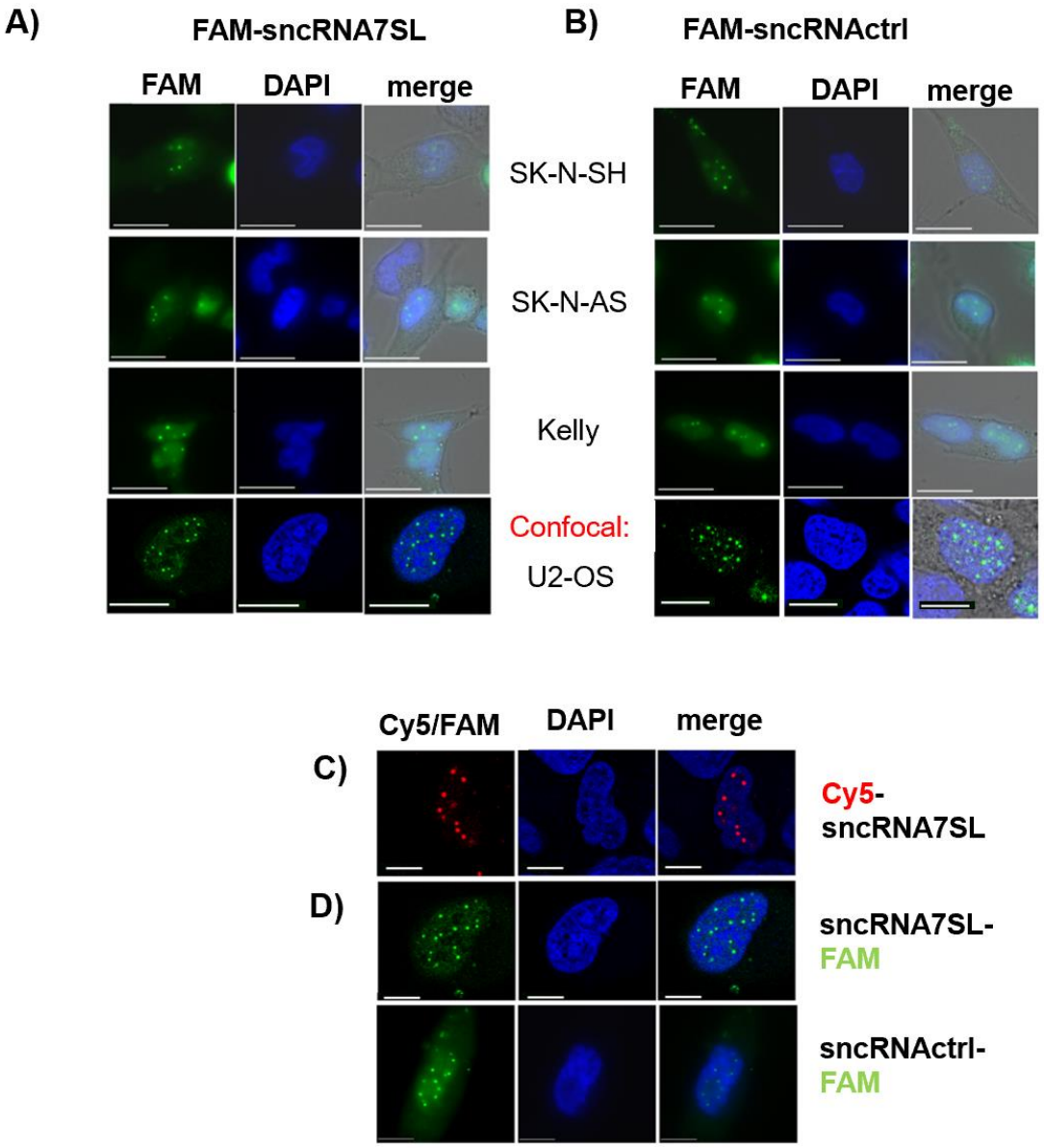

Figure 16. Localization of fluorescent-labeled sncRNA7SL and its control in nuclear bodies.
(A) Live cell fluorescence microscopy of 12.5 nM FAM-snRNA7SL transfected various cell lines (SK-N-SH, SK-N-AS, Kelly, U2-OS) shows localization of FAM-sncRNA7SL in the nucleus where it accumulates as nuclear bodies. Images were taken with the Keyence BZX fluorescence microscope or Leica confocal microscope. **(B)** Live cell fluorescence microscopy of 12.5 FAM-snRNActrl transfected cells also shows an accumulation of the signal in nuclear bodies. Images were taken with the Keyence BZX fluorescence microscope or Leica confocal microscope. **(C)** Live cell fluorescence microscopy of 12.5 nM Cy5-snRNA7SL transfected U2-OS cells shows localization of sncRNA7SL in the nucleus where it accumulates as nuclear bodies. Images were taken with Leica confocal microscope, with a magnification of 60x. **(D)** Live cell fluorescence microscopy of 12.5 nM sncRNA7SL-FAM transfected U2-OS cells taken with the Leica confocal microscope with a magnification of 60X. 3' labeled FAM cells show an accumulation of the signal in nuclear bodies. Images were taken with Leica TCS SP5 confocal laser scanning microscope with a magnification of 60x. SK-N-SH cells were transfected with sncRNActrl-FAM and also show nuclear accumulations of the sncRNActrl-FAM signal. Images were taken with the Keyence BZX fluorescence microscope, with a magnification of 100x.
All images were taken 24 h after transfection in live cells. All scale bars measure 10 µm.

Taken together, similar to endogenous sncRNA7SL synthetic sncRNA7SL, either labeled at the 5'- or 3'-end or with FAM or Cy5 localized to the nucleus. However, contrary to the diffuse nuclear localization of endogenous sncRNA7SL (Figure 10), synthetic sncRNA7SL and sncRNActrl accumulate in part also in nuclear bodies. Interestingly, this data show that longer sncRNAs are imported to the nucleus when compared to the localization of 3'-end labeled miRNAs (Lu et al., 2016). Furthermore, in my study it was shown that the nuclear import of sncRNA7SL and sncRNActrl is not hindered by 5'- or 3'- fluorescence groups. However, the subnuclear localization is likely to be affected by 5'- or 3'-terminal labeling, since the 5'- or 3'-labeled sncRNAs accumulate, sncRNA7SL as well as control RNA, in nuclear bodies.

3.2.2.3 sncRNA7SL is mainly localized in the nucleus while shorter RNAs are localized in the cytoplasm

As shown, terminally fluorescence-labeled sncRNA7SL or sncRNActrl are imported to the nucleus and accumulate to some extent in nuclear bodies (Figure 16) in contrast to the cytoplasmic localization of fluorescence-labeled miRNAs (Lu et al., 2016). To test, whether the length of sncRNA7SL is a determinant for subcellular localization two shorter 5'-end labeled RNAs were designed. In the case of Cy5-sncRNA7SL-Δ1, nine nucleotides were deleted from the middle of full-length sncRNA7SL, and in the case of Cy5-sncRNA7SL-Δ2 ten nucleotides were deleted from the 3'-end of full-length sncRNA7SL (Figure 17 A, Table 19). To assure that change in localization was not the result of the deletion of specific nucleotides, deletions were performed in two different parts of the sequence.

Hence, SK-N-SH cells were co-transfected with 12.5 nM FAM-sncRNA7SL and Cy5-sncRNA7SL-Δ1 or Cy5-sncRNA7SL-Δ2, respectively, 24 h prior to DAPI staining and live cell imaging microscopy using the Keyence BZ-X810 fluorescence microscope. Analysis showed FAM-sncRNA7SL still accumulated in the nucleus in nuclear bodies (green signal, Figure 17 B), however, both short RNA oligos Cy5-sncRNA7SL-Δ1 and Cy5-sncRNA7SL-Δ2 mainly localized in the cytoplasm, as many small cytoplasmic bodies with some minor nuclear staining (Figure 17 B). Interestingly, some of the nucleic signals could be colocalized with nuclear bodies formed by sncRNA7SL-FAM (Figure 17 B orange arrows). Indicating that a small fraction of both short RNA oligos were transported not only in the nucleus but also accumulated in nuclear bodies as full-length sncRNA7SL.

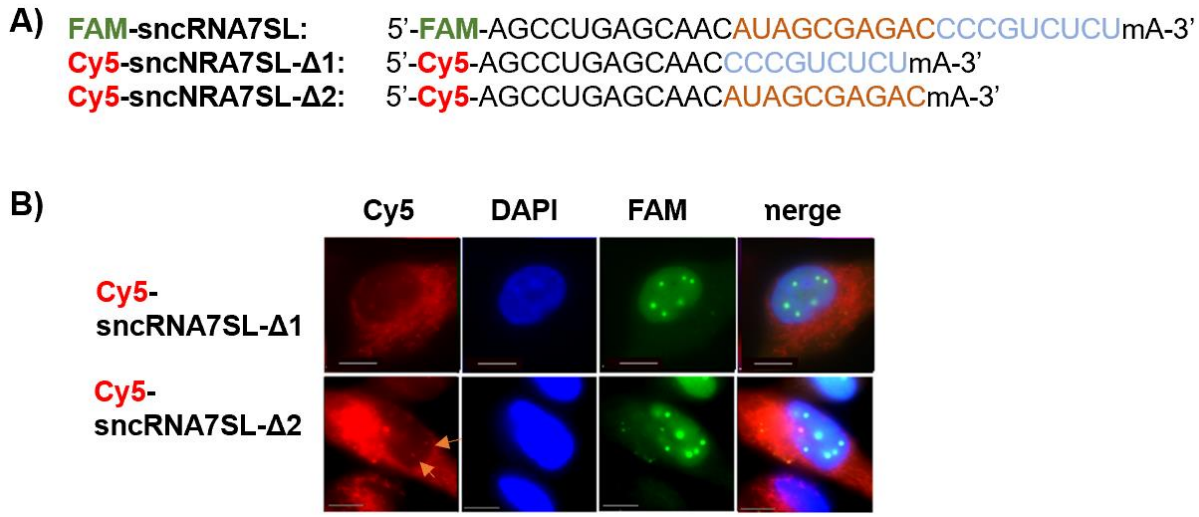

Figure 17. Localization of shortened fluorescently labeled sncRNA7SL in the cell.
(A) Sequence of RNA oligos FAM-sncRNA7SL, or Cy5-snRNA7SL-Δ1 and or Cy5-snRNA7SL-Δ2. **(B)** Live cell fluorescence microscopy of 12.5 nM Cy5-snRNA7SL-Δ1 and FAM-sncRNA7SL or Cy5-snRNA7SL-Δ2 and FAM-sncRNA7SL co-transfected SK-N-SH cells shows localization of FAM-sncRNA7SL in the nucleus where it accumulates in both cases as nuclear bodies while Cy5-sncRNA7SL-Δ1 and -Δ2 are mainly localized in the cytoplasm and visualized as a diffuse signal. Slight signal in the nucleus overlapping with FAM-sncRNA7SL nuclear bodies (indicated by orange arrows). Images were taken with the Keyence BZX fluorescence microscope with a magnification of 100x. All images were taken 24 h after transfection in live cells. All scale bars measure 10 µm.

In summary, it was shown that the length of sncRNAs determines their subcellular localization. Fluorescence groups at the 5'- or 3'-ends are not interfering with the nuclear import mechanism and the differential localization of short and full-length transfected sncRNAs.

3.2.2.4 Internal labeling of synthetic sncRNA7SL recapitulates the diffuse nuclear localization of endogenous sncRNA7SL

As shown, the cytoplasmic or nuclear localization of fluorescence-labeled sncRNAs is determined by their length (Figure 16, 17). However, the subnuclear localization of sncRNA7SL or sncRNActrl in nuclear bodies could be caused by the terminal fluorescence group. As already described (see above 3.2.2.1) it is likely that fluorescence groups at the 5'- or 3'-end might block the efficient binding by Argonaute clade proteins and therefore affect the localization and/or functionality of sncRNAs. To further test the possibility that terminal fluorescence groups might lead to miss-localizations of sncRNA7SL, a fluorescence group was attached to nucleotide 14 of the sncRNA7SL sequence, referred to as sncRNA7SL-inte-FAM (Figure 18 A, Table 19). The internal position was chosen based on Schirle et al., 2014, where they show

that during Ago2 binding miRNA nucleotides 14 to 18 pass through a channel formed between the N domain and the PAZ domain, suggesting nucleotides 14 to 18 are not essential for Argonaute binding and some space for bulky fluorescence groups.
Furthermore, the seed regions of piRNAs span nucleotides 2 to 8 extending even up to nucleotide 12 (Anzelon et al., 2021), therefore, a fluorescence label after position 12 was considered not to interfere with the binding by Argonaute proteins.
Since the signal strength of sncRNA7SL-inte-FAM was quite low, 25 nM of sncRNA7SL-inte-FAM were transfected into SK-N-SH cells. 24 h after transfection, cells were stained with DAPI and analyzed using the Keyence BZ-X810 fluorescence microscope. Strikingly, sncRNA7SL-inte-FAM was evenly distributed in the nucleoplasm and recapitulated the diffuse localization of endogenous sncRNA7SL signal (Figure 18 B). These findings suggest that terminal fluorescence groups interfere with the interaction between sncRNA7SL and nuclear factors leading to a diffuse localization of synthetic and endogenous sncRNA7SL.
Although, most sncRNA7SL-inte-FAM molecules accumulated in the nucleus, a distinct fraction localized to small cytoplasmic bodies (Figure 18 B).
Because of the significant impact of terminal-fluorescence groups on the subnuclear localization of sncRNA7SL, I wondered, whether the cytoplasmic location of short sncRNAs was also changed by terminal fluorescence groups. Hence, sncRNA7SL-Δ2 was internally labeled with Cy5 at nucleotide 11 at position 12 referred to as sncRNA7SL-Δ2-inte-Cy5. Again, the terminal fluorescence groups had a major impact on the localization. Whereas Cy5-sncRNA7SL-Δ2 concentrated in small cytoplasmic bodies, almost appearing as a diffuse signal as shown before (Figure 17 B) sncRNA7SL-Δ2-inte-Cy5 accumulated in large cytoplasmic bodies (Figure 18 C).
These data suggest that both full-length sncRNA7SL and sncRNA7SL-Δ2 require their natural 5'- and 3'-ends for binding to binding-partners and determining their localization and probably their function as well.

Taken together, the position of the fluorescent label is of major importance for the localization of synthetic short and long sncRNA7SL to cellular structures such as nuclear or cytoplasmic bodies. This section aimed to develop a tool to study the cellular localization of dynamics of sncRNA7SL. With RNA oligos sncRNA7SL-inte-FAM and sncRNA7SL-Δ2-inte-Cy5, those tools are now available and will be used later in this

study (see. 3.3) for analyzing colocalization with components of cytoplasmic silencing complexes.

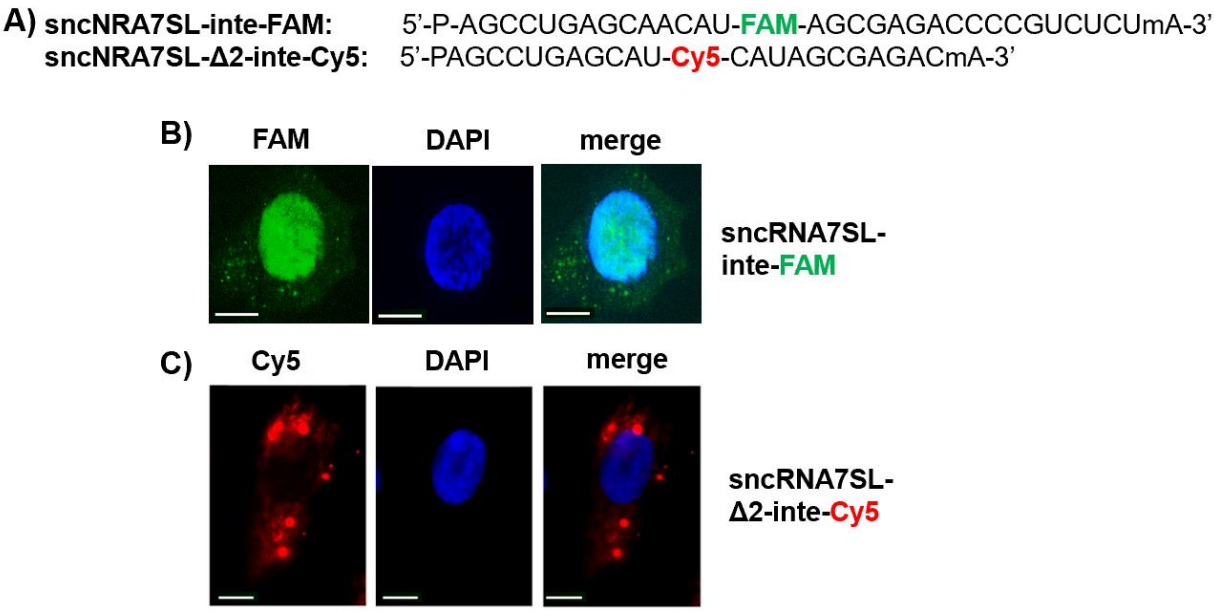

Figure 18. Localization of shortened and full-length internal fluorescent labeled sncRNA7SL in the cell.
(A) Sequences of sncRNA7SL-inte-FAM and sncRNA7SL-Δ2-inte-Cy5. **(B)** sncRNA7SL-inte-FAM localizes to the nucleoplasm. Live cell fluorescence microscopy of 12.5 nM sncRNActrl-FAM transfected SK-N-SH cells as well as 25 nM snRNA7SL-inte-FAM transfected SK-N-SH cells. sncRNA7SL-inte-FAM labeled cells show localization of sncRNA7SL in the nucleus as a diffuse signal. And a slight accumulated signal in the cytoplasm. **(C)** sncRNA7SL-Δ2-inte-Cy5 localizes to cytoplasmic bodies. Fluorescence microscopy of live SK-N-SH cells transfected with 25 nM snRNA7SL-Δ2-inte-Cy5 shows localization of snRNA7SL-Δ2-inte-Cy5 in cytoplasmic foci, most likely representing processing bodies, in which Argonaute proteins accumulate Images were taken with Keyence BZX fluorescence microscope, with a magnification of 100x. All images were taken 24 h after transfection in live cells. All scale bars measure 10 µm.

3.2.2.5 Partial colocalization of FAM-sncRNA7SL with several nuclear bodies

As described above, terminally labeled sncRNA7SL accumulated presumably in some type of nuclear bodies (Figure 16). The aim of this section was to characterize the nature of FAM-sncRNA7SL containing nuclear bodies. The mammalian nucleus is a highly structured organelle. Specialized structures of different sizes and numbers and with various functions are present there (reviewed in Spector, 2001, 2011). For clarification purposes, splicing speckles, found to play a role in the pre-mRNA splicing, nucleoli where ribosomal RNA synthesis and processing takes place, PML bodies,

suggested to play a role in transcriptional regulation, Cajal bodies, in which the snRNP biogenesis takes place, and paraspeckles known to store mRNAs, all are found here (reviewed in Spector, 2001). Common to all those nuclear bodies (NB) is that they are biomolecular condensates and do not have a membrane. Their formation is very dynamic and triggered by liquid-liquid-phase separation (Handwerger et al., 2005; reviewed in Sawyer et al., 2016, 2018).

Since terminally fluorescently labeled sncRNA7SL forms nuclear bodies, the subsequent challenge was to determine in which nuclear structures FAM-sncRNA7SL accumulates.

Hence, one of the most common nuclear structures, referred to as splicing speckle, was taken into consideration. Splicing speckles can be identified by immunofluorescence microscopy using antibodies against the serine/arginine-rich splicing factor 2 (SC35) (Misteli et al., 1997). SK-N-SH cells were transfected with FAM-sncRNA7SL, fixed, and stained with DAPI and SC35 antibodies. Microscopy using the Keyence BZ-X810 fluorescence microscope did not show colocalization between SC35 antibody and FAM-sncRNA7SL further confirmed by line profiling (Figure 19 A and B), however, signals of FAM-sncRNA7SL and the splicing speckle were in many cases directly next to each other, indicating close proximity of FAM-sncRNA7SL nuclear bodies and splicing speckles.

Furthermore, Coilin is the best-known marker for Cajal bodies as it appears to be essential for Cajal body formation (Bauer and Gall, 1997). However, it is also known that not the entire amount of coilin is set in Cajal bodies and most of it is diffusely distributed within the nucleus (Carmo-Fonseca et al., 1993, Platani et al., 2000). Colocalization studies between Coilin protein and FAM-sncRNA7SL indicate rare partial colocalization between the two components (Figure 19 C). Line profiling (position indicated as the orange arrow) further proves colocalization between Coilin protein and accumulated FAM-sncRNA7SL (Figure 19 D). It is known that two to three Cajal bodies accumulate in one nucleus at a time (Morris, 2008). Since antibody staining of Coilin showed many small dots but only two larger dots per cell, it is likely that the large dots represent Cajal bodies, which have a diameter of about 0.5 µm (Matera, 1999). Colocalizations of FAM-sncRNA7SL and Coilin were found in these larger nuclear bodies, indicating indeed a partial colocalization between Cajal bodies and FAM-sncRNA7SL. However, most of the FAM-sncRNA7SL-containing bodies did not colocalize with Cajal bodies.

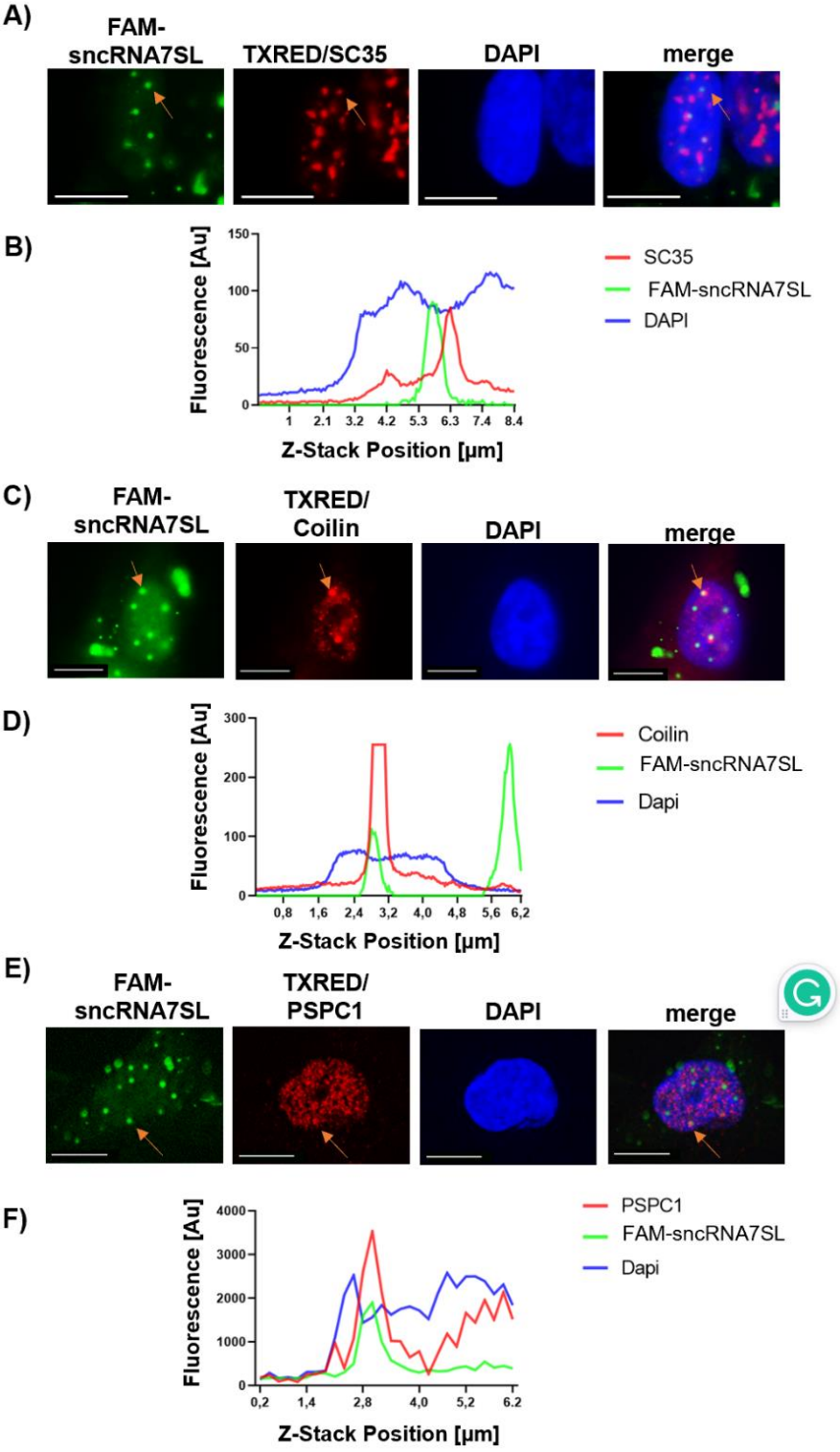

Figure 19. Partial colocalization of FAM-sncRNA7SL with Coilin protein, and PSPC1 protein in the nucleus of SK-N-SH cells but not SC35.
Fluorescence microscopy of 12.5 nM FAM-sncRNA7SL transfected SK-N-SH cells. **(A)** Fluorescence microscopy of cells stained with SC35 antibody. The line used for line profiling is indicated in orange. **(B)** Line Profile of the close proximity of FAM-sncRNA7SL with SC35 protein. **(C)** Fluorescence microscopy of cells stained with Coilin antibody. The line used for line profiling is indicated in orange. **(D)** Line Profile of colocalized FAM-sncRNA7SL with Coilin protein. **(E)** Fluorescence microscopy of cells stained with PSPC1 antibody. The line used for

line profiling is indicated in orange. **(F)** Line Profile of colocalized FAM-sncRNA7SL with PSPC1 protein.
Images were taken with the Keyence BZX fluorescence microscope. With a magnification of 100x. All images were taken 2 days after transfection of sncRNA7SL in fixed cells. All scale bars measure 10 µm.

Lastly, another possible nuclear localization point for FAM-sncRNA7SL paraspeckles was considered. Paraspeckle numbers vary per cell between five and twenty (Fox et al., 2002), consistent with the number of FAM-sncRNA7SL bodies observed in different cell lines. As a marker for paraspeckles, Paraspeckle Component 1 (PSPC1) was used. SK-N-SH cells were transfected with FAM-sncRNA7SL, fixed, PSPC1 protein stained with antibody, and nuclei stained with DAPI. Microscopy using the Keyence BZ-X810 fluorescence microscope showed a partial colocalization of FAM-sncRNA7SL and PSPC1 protein (Figure 19 E). The line profile is indicated by the orange arrow within the merge picture and also confirmed a colocalization between those two components, indicating FAM-sncRNA7SL localization within paraspeckles (Figure 19 F). Since paraspeckle occurrence matches the number of FAM-sncRNA7SL nuclear bodies best, further experiments were conducted to study interactions between the two components. Furthermore, measurement of FAM-sncRNA7SL sizes revealed a size range of about 0.8 to 1 µm, since paraspeckles are calculated to have a diameter of 0.5 to 1 µm (Cardinale et al., 2007), the sizes of both nuclear bodies also match.

Taken together, the colocalization studies with SC35, Coilin, and PSPC1 antibodies were not conclusive. However, paraspeckles consist of NEAT1 RNA as well as various RNA-binding proteins like NONO, PSF, PSPC1, and FUS (reviewed in Fox and Lamond, 2010; Fox et al., 2005). These membrane-less domains hold onto mRNAs containing, for example, inverted repeat Alu elements (*IRAlus*), in their 3' UTR (reviewed in Chen and Yang, 2017; Chen et al., 2008). As mentioned before 7SL RNA is the precursor of all Alu elements (Ullu and Tschudi, 1984). Therefore, inverted repeat Alu element containing mRNA harbor possible target sites for sncRNA7SL. More than 300 mRNAs were found to contain *IRAlu* elements, which are often found in the 3' UTR of mRNAs (Chen et al., 2008).
Because of the high complementarity between an Alu element and an inverted Alu element, *IRAlus* form long double-stranded RNA structures. These structures can be Adenosine to Inosine (A-to-I) edited, meaning Adenosine gets deaminated to an Inosine, therefore, being read as a Guanin, by Adenosine Deaminase acting on RNA

(ADAR). Those A-to-I edited *IRAlu* containing mRNAs can be retained in the nucleus and can have an RNA stabilizing effect (Brümmer et al., 2017; reviewed in Maquat, 2020). The RBP NONO is a component of paraspeckle (reviewed in Fox and Lamond, 2010) and binds to hyper-edited RNA (Zhang and Carmichael, 2001), which leads to localization of A-to-I edited *IRAlu*-containing mRNAs in paraspeckle and temporary silencing of those mRNAs (Chen et al., 2008, reviewed in Chen and Yang, 2017). Therefore, to test the assumption that sncRNA7SL accumulates in paraspeckle we decided to deplete the structural component, NEAT1_2 RNA, to reduce the number of paraspeckle and possibly also the number of sncRNA7SL bodies.

3.2.2.6 NEAT1_2 knockdown decreases nuclear sncRNA7SL bodies

As suggested above sncRNA7SL could accumulate in paraspeckles. Therefore, next depletion of NEAT1_2 RNA, the essential structural component of paraspeckle, was performed to reduce the number of sncRNA7SL bodies.

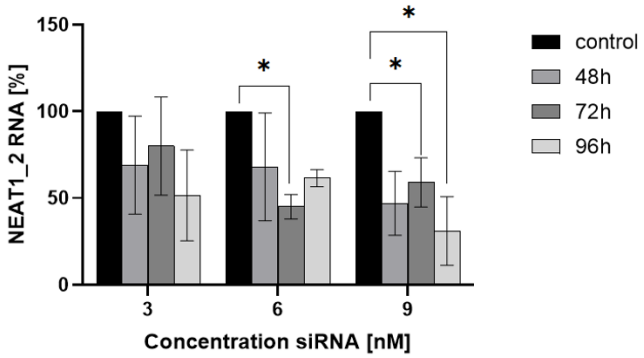

Figure 20. Titration of siRNAs for NEAT1_2 depletion in SK-N-As cells.
Higher concentrations of siNEAT1_2 result in a lower level of NEAT1_2 in NEAT1_2-depleted SK-N-AS cells. Later time points result in a lower level of NEAT1_2. The lowest level of NEAT1_2 is reached with 9nM of si transfection tools 96 h after transfection, as determined in two independent experiments performed in triplicates. All results were determined as mean SD (error bars) with Prism 8.4 (Graph Pad Software).

NEAT1 RNA is expressed in two isoforms (NEAT1_1, NEAT1_2). While it was shown that NEAT1_1 (short isoform) is not essential to paraspeckle formation, NEAT1_2 (long isoform) is an essential part and its deletion prohibits paraspeckle formation (Naganuma et al., 2012; Modic et al.,2019).

To further characterize the nuclear bodies visible by 5'- or 3'-end labeled sncRNA7SL NEAT1_2 depletion was tested and optimized in SK-N-AS cells via qPCR (Figure 20). SK-N-AS cells were used for optimization since growth was prominently faster compared to SK-N-SH growth. The ideal concentration of siRNA used for knockdown

was determined 9 nM and the strongest NEAT1_2 depletion levels of about 60 % were found to be 96 h after depletion.

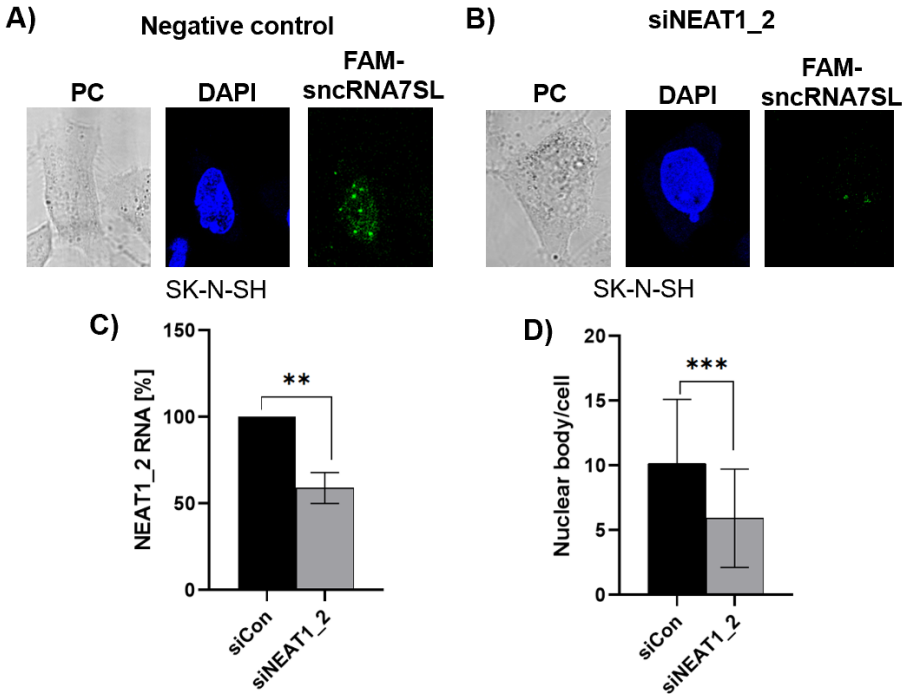

Figure 21. Figure 21. NEAT1_2 RNA knockdown decreases sncRNA7SL nuclear body formation.
(A) Live cell imaging of 9nM control knockdown SK-N-SH cells transfected with 12.5 nM FAM-sncRNA7SL. FAM-sncRNA7SL signal shows accumulation in nuclear bodies. **(B)** Live cell imaging of 9 nM NEAT1_2 knockdown SK-N-SH cells transfected with 12.5 nM FAM-sncRNA7SL 72h after the knockdown. FAM-sncRNA7SL signal shows less accumulation in nuclear bodies compared to control cells. © qPCR analysis of NEAT1_2 RNA knockdown efficiency in SK-N-SH cells, as determined in three independent experiments performed in triplicates. The results were determined as mean SD (error bars). P value ** ≤ 0.01 was determined using paired t-test with Prism 8.4 (Graph Pad Software). **(D)** NEAT1_2 RNA knockdown results in a significant decrease in the number of FAM-sncRNA7SL nuclear bodies as determined in three independent experiments. The results were determined as mean SD (error bars). P value *** ≤ 0.001 was determined using paired t-test with Prism 8.4 (Graph Pad Software).
All pictures were taken 24 hours after FAM-sncRNA7SL transfection and 96 h after initial knockdown with a Leica TCS SP5 confocal laser scanning microscope with a magnification of 60x.

Hence, for further experiments NEAT 1_2 knockdown was performed with 9 nM in SK-N-SH cells. 72 h after transfection of NEAT1_2 specific siRNAs or control siRNAs, SK-N-SH cells were transfected with 12.5 nM FAM-sncRNA7SL and 24 h later cells were visualized using the Leica TCS SP5 confocal laser scanning microscope. NEAT1_2 RNA level decreased by 30 to 40 % in NEAT1_2 RNA-depleted cells, verified by qPCR analysis (Figure 21 C). Microscopy showed a noticeable decrease of FAM-sncRNA7SL

nuclear bodies in NEAT1_2 depleted cells compared to untransfected controls (Figure 21 A and B).
Quantification of the number of sncRNA7SL bodies revealed a reduction of about 40 % in NEAT1_2 depleted cells (Figure 21 D). These findings suggest that at least a part of the found FAM-sncRNA7SL nuclear bodies were indeed dependent on paraspeckle formation. Since only about 40 % of NEAT1_2 RNA was depleted, it is reasonable to assume that there is still paraspeckle formation in the cells, explaining the few remaining FAM-sncRNA7SL bodies.

In summary, the reduction of NEAT1_2 mRNA levels by about 40 % led to a significant decrease in FAM-sncRNA7SL nuclear bodies, indicating that 5'- or 3'-end labeled sncRNA7SL accumulates in paraspeckles.

3.2.2.7 Synthetic sncRNA7SL colocalizes with NEAT1_2 RNA and NONO protein

To further prove a colocalization between FAM-sncRNA7SL and NEAT1_2 RNA and the paraspeckles component NONO protein, RNA FISH experiments were established. SK-N-SH cells were transfected with 12.5 nM FAM-sncRNA7SL. 24 h after transfection cells were fixed, mRNA FISH for NEAT1 RNA (designed to detect NEAT1_2 (long variant), but not NEAT1_1 (short variant)) was performed and NONO protein was stained with an antibody. The colocalization of NEAT1 RNA and NONO protein was used to visualize paraspeckles. Colocalization between NEAT1 RNA and the NONO protein was critical since the NONO protein is not only a part of the paraspeckle but is also involved in RNA stability (Kim et al., 2020) and has many other functions within the nucleus (Zhang and Carmichael, 2001; Mircsof et al., 2015). For example, it is also involved in the splicing process (reviewed by Feng et al., 2020). Cells were DAPI stained and analyzed using the Keyence BZ-X810 fluorescence microscope. Microscopy showed a partial colocalization between FAM-sncRNA7SL, NONO protein, and NEAT1 RNA (Figure 22 A, C).

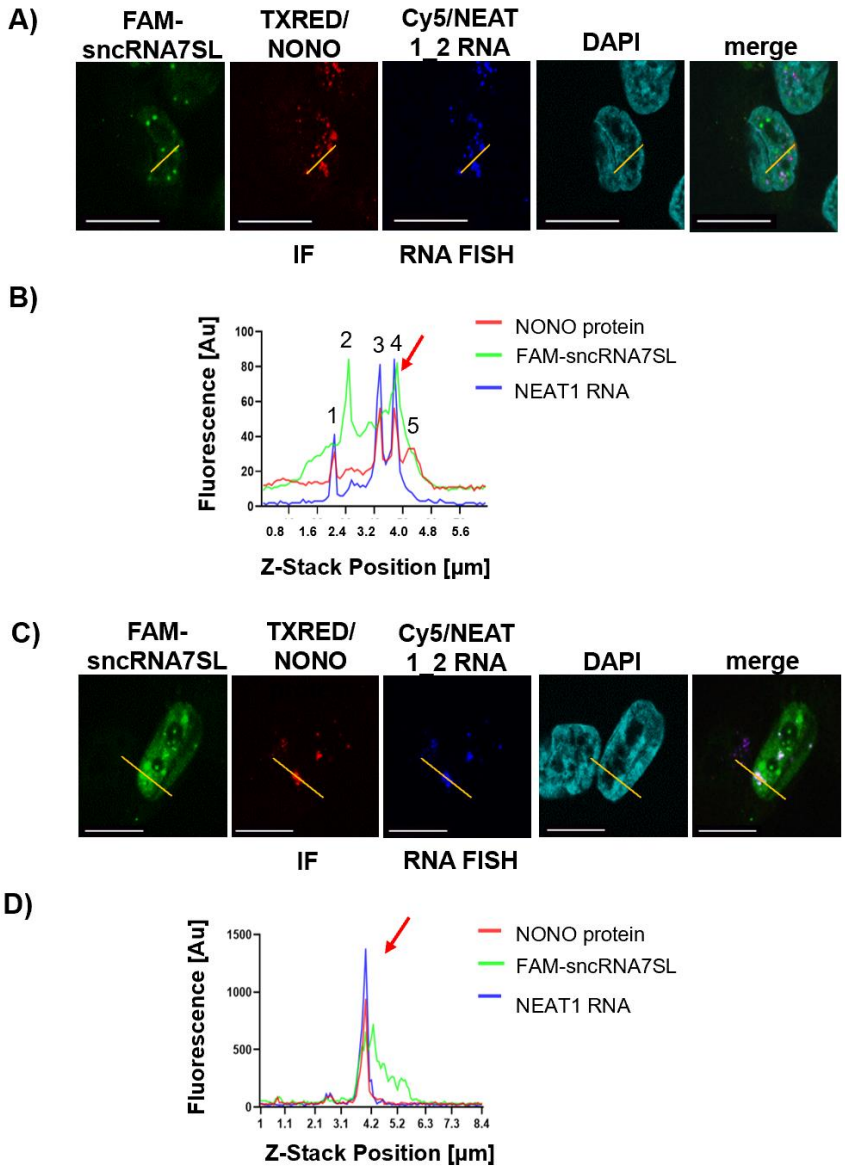

Figure 22. Partial colocalization of FAM-sncRNA7SL with NONO protein and NEAT1_2 mRNA in the nucleus.
(A, C) RNA FISH analysis shows a partial colocalization of FAM-snRNA7SL with NONO protein and NEAT1_2 mRNA in SK-N-SH cells. Line used for line profiling indicated in orange. Images were taken with Keyence BZX fluorescence microscope. With a magnification of 100x. All images were taken 3 days after transfection of sncRNA7SL in fixed cells. All scale bars measure 10 µm.
(B, D) Line Profile of colocalized FAM-sncRNA7SL, NONO protein, and NEAT1_2 mRNA in the nucleus of SK-NSH cells. The red arrow indicates the point of colocalization.

To further prove the colocalization of NONO protein, NEAT1 RNA, and FAM-sncRNA7SL a line profile was drawn and five peaks were recorded. As mentioned above, the first focus was on the colocalization of the NEAT RNA signal (blue line, peaks 1, 3, 4) and the NONO signal (red line, peaks 1, 3, 4, 5). Inspecting the line profile, it reveals a strong colocalization of Neat RNA and NONO in peaks 1, 3, and 4,

indicating paraspeckles. The weak peak 5 represents only NONO in nuclear bodies (NB) different from paraspeckle. For FAM-sncRNA7SL two peaks were recorded (green line, peaks 2 and 4). Strikingly in peak four, all three signals were recorded, demonstrating the FAM-sncRNA7SL localizes to some paraspeckle. However, peak two only showed the FAM-sncRNA7SL signal, strongly suggesting that FAM-sncRNA7SL localizes to another type of NB, not containing the NONO protein and NEAT RNA, like the Cajal bodies shown above (Figure 18 C). Figure 22 C shows another cell expressing colocalization between FAM-sncRNA7SL with NEAT1 RNA and NONO protein. The line profile (indicated by the orange line) further confirms the partial colocalization of FAM-sncRNA7SL with NEAT1 RNA and NONO protein, showing all three signals strongly expressed in a single peak (Figure 22 D).

Taken together, NEAT1_2 knockdown experiments showed a significant decrease of FAM-sncRNA7SL nuclear bodies indicating that terminally labeled FAM-sncRNA7SL could concentrate in paraspeckles, as further supported by the partial colocalization of FAM-sncRNA7SL, NEAT1_2 RNA and NONO protein. There is also to consider the well-known dynamics of nuclear body formation, growth, and disappearance (Sasaki and Hirose, 2009; Fox et al., 2005; Tripathi and Parnaik, 2008; Platani et al., 2000) in interpreting the microscopic pictures probably explaining the only partial colocalization of sncRNA7SL with those different nuclear bodies.

3.2.2.8 FAM-sncRNA7SL colocalizes with KNL1 mRNA and NONO protein

As mentioned above, *IRAlus* are likely to contain degenerated sncRNA7SL RNA binding sites and might be retained in paraspeckle (Chen et al., 2008, reviewed in Chen and Yang, 2017). To test whether an *IRAlu* mRNA localizes to paraspeckle and colocalizes with FAM-sncRNA7SL, the *IRAlu* containing Kinetochor Scaffold 1 (KNL1) mRNA was chosen to be studied (Figure 23). KNL1 is important for chromosome alignment during mitosis, helping chromosomes to separate correctly, therefore it is a major part of the cell cycle (Cheeseman et al., 2008), furthermore, it was found to play a major role in the mitotic checkpoint (Kiyomitsu et al., 2007).

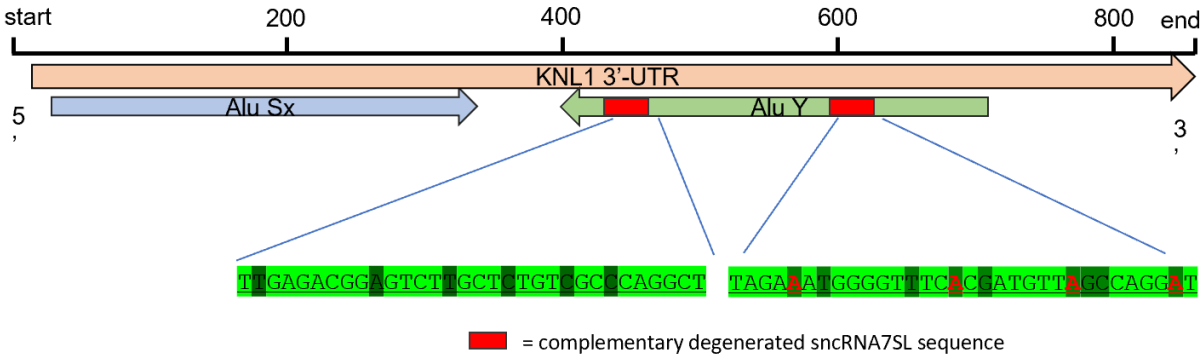

Figure 23. KNL1 3'-UTR.
KNL1 3' UTR with AluY (green arrow) and Alu Sx (blue arrow) forming a double-stranded structure. Close-up of KNL1 3' UTR degenerated sncRNA7SL target sites sequences (red boxes) with seven or nine mismatches.

To visualize the colocalization of FAM-sncRNA7SL and KNL1 mRNA in the cell and eventually prove that this colocalization takes place within paraspeckles, RNA FISH analysis in FAM-sncRNA7SL transfected SK-N-SH cells was performed and the cells were furthermore stained with NONO antibody. FAM-sncRNA7SL was used to further characterize possible colocalization partners for the nuclear bodies. NONO antibody was chosen as it is an essential part of the paraspeckle formation and therefore a marker of those. FISH analysis indeed showed a partial colocalization between FAM-sncRNA7SL, KNL1 mRNA, and NONO protein (Figure 24 A), the line profile was showing a spike of all three signals at the same place within the Z-stack. This result was further confirmed by the line profile (Figure 24 B) indicated by the orange bar. While a majority of NONO protein and FAM-sncRNA7SL signal was localized in the nucleus, KNL1 mRNA was mostly localized in the cytoplasm, as to be expected for a translated mRNA. Cytoplasmatic KNL1 mRNA signal was seen as small cytoplasmatic bodies mainly localized in close proximity to the nucleus. Colocalization between KNL1 mRNA and NONO indicates, the localization of part of the KNL1 mRNA to be in paraspeckles, while colocalization between KNL1 mRNA and FAM-sncRNA7SL indicates binding between those to RNAs. Figure 24 C shows another microscopic picture of FAM-sncRNA7SL transfected cells with Immunofluorescence of NONO protein and KNL1 mRNA FISH analysis. There is quite little distinct KNL1 mRNA signal, however, in the zoomed image on the left, the position where all three signals overlap is highlighted with orange arrows, indicating a co-localization, this observation is further confirmed by the peak of all three signals at the same time in the line profile (Figure 24 D).

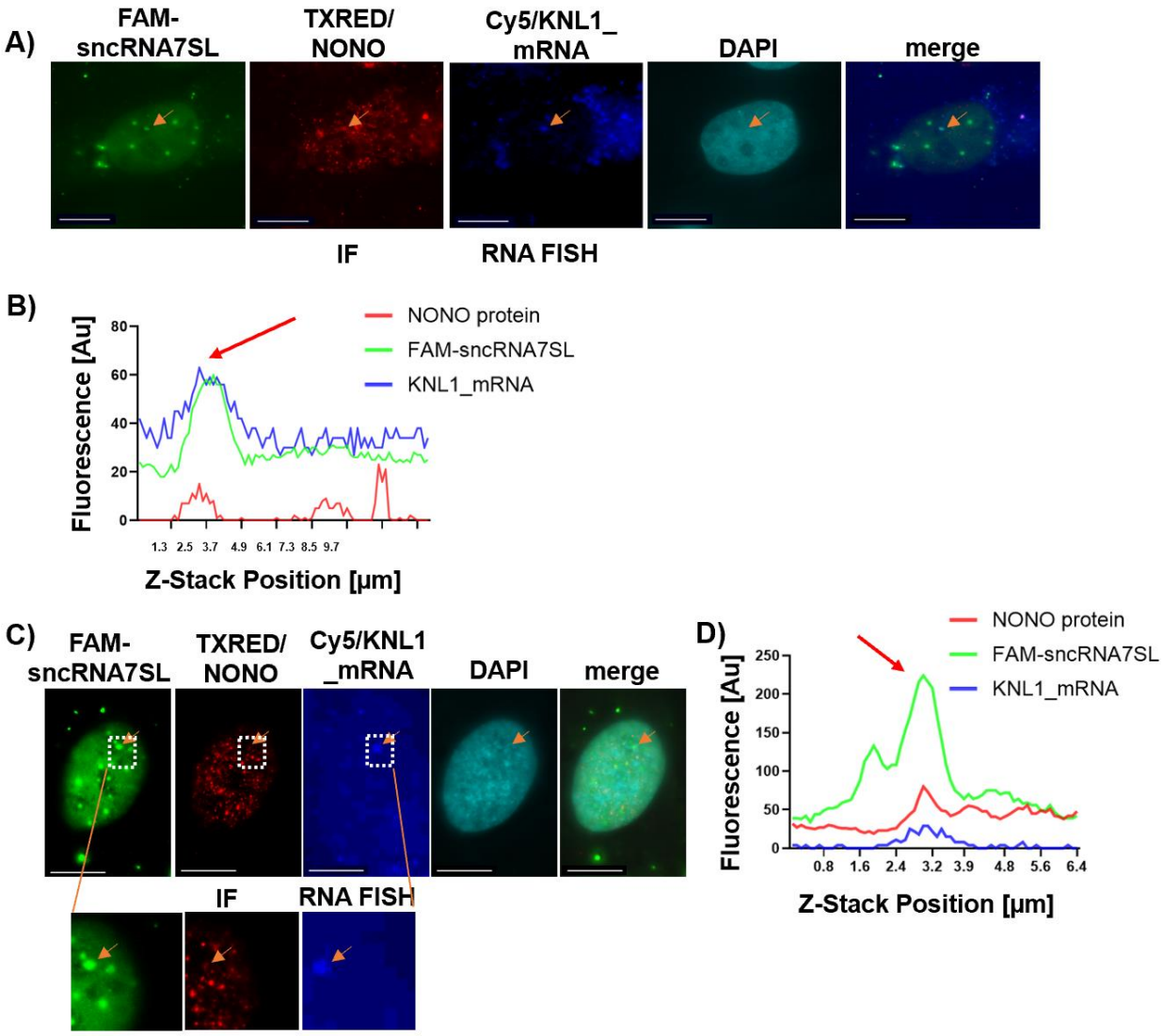

Figure 24. Partial colocalization of FAM-sncRNA7SL with NONO protein and KNL1 mRNA in the nucleus.
(A, C) RNA FISH analysis shows a partial colocalization of FAM-snRNA7SL with NONO protein and KNL1 mRNA in SK-N-SH cells. Orange arrows indicate the point of colocalization shown in line profiling **(B, D)**. Line Profile shows colocalization of FAM- sncRNA7SL, NONO protein, and KNL1 mRNA in the nucleus of SK-NSH cells.
Images were taken with a Keyence BZX fluorescence microscope. With a magnification of 100x. All images were taken 3 days after transfection of sncRNA7SL in fixed cells. All scale bars measure 10 µm.

Succinctly, while most KNL1 mRNA signal is localized in the cytoplasm there still is partial colocalization between KNL1 mRNA, FAM-sncRNA7SL, and NONO protein in the nucleus. In future experiments, it would be interesting to see if sncRNA7SL transfection without a fluorescence marker leads to a shift of KNL1 mRNA from cytoplasmic to nuclear localization since most endogenous sncRNA7SL is localized in the nucleus (Figure 10).

3.2.2.9 NEAT1_2 RNA levels are elevated in sncRNA overexpressing cells

It was shown that NEAT1_2 knockdown decreased FAM-sncRNA7SL nuclear bodies in neuroblastoma cells (Figure 21). Hence it could be suggested that sncRNA7SL is localized in paraspeckles. As a next step to see what factors would increase paraspeckle formation, neuroblastoma cells were exposed to different kinds of cellular stress.

It is known that treatment of cells with Trichostatin A (TSA), an HDAC inhibitor, increases NEAT1_2 RNA level and therefore promotes paraspeckle formation (Shelkovnikova, 2018). To confirm these results in neuroblastoma cell lines, Kelly cells were treated for 24 h with 500 nM TSA. Subsequently, RNA was isolated and NEAT1_2 RNA levels were checked by qPCR in comparison with untreated Kelly cells. qPCR analysis showed an about 2.5 increase in NEAT1_2 RNA level in TSA-treated cells compared to untreated control Kelly cells (Figure 25), confirming TSA as a NEAT1_2 RNA stimulant. Transfection of FAM-sncRNA7SL and treatment with directly subsequent TSA treatment were attempted to see if increased paraspeckle formation increases nuclear body formation of FAM-sncRNA7SL. Unfortunately, TSA and FAM-sncRNA7SL co-transfection damaged cells too much for microscopic analysis (data not shown). In future experiments, this method should be further optimized by trying different intervals between FAM-sncRNA7SL transfection and TSA treatment time points to produce the greatest possible increase in NEAT1_2 level while exerting as little stress on the cells as possible.

Since paraspeckles are known to be stress-responsive and therefore can increase in a variety of cellular stress states (An et al., 2019), it is likely that sncRNA7SL overexpression causes cellular stress because sncRNA7SL transfection led to a decrease in cell viability, proliferation, mobility, and spheroid growth. Therefore, our next objective was to see if sncRNA7SL has an effect on the NEAT1_2 RNA level. Kelly cells were transfected with 12.5 nM sncRNA7SL. 24 h after transfection RNA was isolated and qPCR analysis of NEAT1_2 RNA level with GAPDH as loading control was performed. qPCR analysis confirmed a more than twofold increase in NEAT1_2 RNA level in sncRNA7SL transfected cells (Figure 25 A) compared to untransfected Kelly cells, indicating an effect of sncRNA7SL on paraspeckle formation.

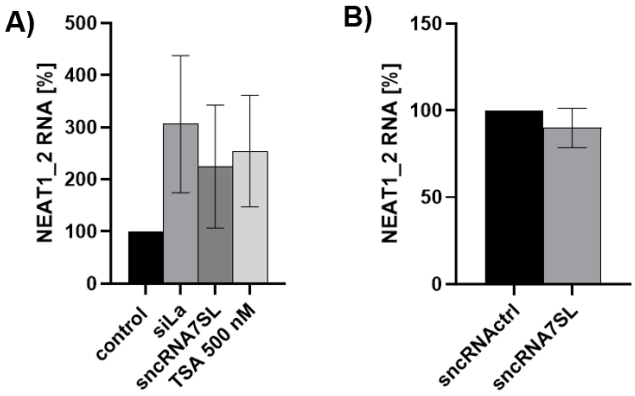

Figure 25. NEAT1_2 RNA level in siLa knockdown cells, sncRNA7SL or sncRNActrl transfected and TSA 500 nM treated cells.
Kelly cells were treated with 500 nM TSA and control cells remained untreated. 24h after transfected cells were harvested and RNA was isolated and NEAT1_2 levels were mapped. NEAT1_2 level increased almost threefold 24 h after TSA transfection, as determined in three independent experiments. Furthermore, La depletion was performed in Kelly cells control siRNA transfected cells were used as controls. 96 h after depletion cells were harvested, RNA isolated and NEAT1_2 levels were determined. NEAT1_2 increased threefold in La-depleted cells as determined in two independent experiments. Lastly, sncRNA was transfected with 12.5 nM sncRNA7SL, harvested 24 h after transfection, RNA was isolated and NEAT1_2 level was determined. Control cells remained untransfected. NEAT1_2 increased about 2.5-fold in sncRNA7SL transfected cells compared to untransfected controls, as determined in three independent experiments. **(B)** Kelly cells were transfected with 12.5 nM sncRNA7SL or sncRNActrl, harvested 24 h after transfection and RNA was isolated. NEAT1_2 showed no significant difference between the two samples, as determined in two independent experiments.
In all experiments, GAPDH levels were used as loading controls
The results were determined as mean SD (error bars). P value *** ≤ 0.001 was determined using paired t-test with Prism 8.4 (Graph Pad Software).

To determine whether these observations were a specific effect of sncRNA7SL or if RNAs of the same length can present a similar effect, cells were transfected with sncRNA7SL or sncRNActrl, and their NEAT1_2 RNA levels were checked 24 h after transfection. In fact, qPCR analysis showed little difference in NEAT1_2 RNA levels in a direct comparison of the two transfected cell lines to each other (Figure 25 B). This suggests that not the specific sncRNA7SL but possibly stress on the cells in general leads to an increase in paraspeckle formation.

Furthermore, our preliminary experiments showed La depletion to have an increasing effect on the sncRNA7SL level. To see if La depletion also has an effect on NEAT1_2 RNA level, La depletion was performed in Kelly cells. 96 h after depletion RNA was isolated and NEAT1_2 RNA levels were measured. These experiments showed the largest increase of NEAT1_2 RNA yet, with an about threefold elevation of NEAT1_2 RNA level, 96 h after La depletion (Figure 25 A).

Taken together, NEAT1_2 RNA depletion impairs paraspeckle formation and concomitantly reduces the number of FAM-sncRNA7SL-containing nuclear structures. The findings suggest that terminal-labeled sncRNA7SL and sncRNActrl accumulate in some paraspeckles.

Furthermore, an increase of NEAT1_2 RNA and therefore an increase in paraspeckle formation can be achieved by TSA treatment as well as transfection of 12.5 nM sncRNA7SL or sncRNActrl as well as La depletion in Kelly cells, indicating that stress, not specifically sncRNA7SL promotes paraspeckle formation.

3.2.2.10 Summary: synthetic sncRNA7SL accumulates often as bodies in the nucleus

In summary, fluorescent labeling on the 3'- or 5'-end of sncRNA7SL led to an accumulation of the signal in nuclear bodies. While the type of label did not have an impact on its localization, the position of the label did. Internally labeled sncRNA7SL did not show an accumulation in nuclear bodies. However, it was still mainly localized in the nucleus showing a diffuse signal there and a less bright accumulated signal in the cytoplasm. The internally labeled sncRNA7SL looked quite similar to the MBsncRNA7SL signal, indicating the 3'- and 5'-end to play a major role in the localization and possible binding of binding partners. A major factor in localization in the nucleus also seems to be the length, as already suggested during endogenous localization studies. While RNAs with 32 nt of length are mainly localized in the nucleus, fluorescence labels RNAs with a length of 22 nt or 23 nt respectively showed their main localization to be in the cytoplasm as expected of small RNAs similar in length to miRNAs, as visualized in Figure 26.

To further characterize the nuclear bodies formed by sncRNA7SL labeled at the 3'- or 5'-end NEAT1_2 depletion was performed in SK-N-SH cells and showed a reduction of the number of nuclear sncRNA7SL bodies per cell. This indicates at least partial localization of sncRNA7SL nuclear bodies in paraspeckles. Furthermore, partial colocalization of FAM-sncRNA7SL with NEAT1 RNA and NONO protein, two essential components of paraspeckles, strengthened this suggestion. As well as the colocalization between PSPC1 and FAM-sncRNA7SL.

As a result of TSA treatment as well as sncRNA transfection and La depletion, the NEAT1 RNA level increased, suggesting cellular stress to be a major factor in paraspeckle formation. Furthermore, Coilin, a Cajal body marker, showed isolated

colocalization with FAM-sncRNA7SL, while SC35, a nuclear speckle marker, did not show colocalization with FAM-sncRNA7SL. Another potential target RNA of sncRNA7SL, KNL1 mRNA was shown by FISH analysis to be mainly localized in the cytoplasm. However, slight signals were found in the nucleus, partially colocalizing with NONO protein and FAM-sncRNA7SL nuclear bodies, indicating KNL1 to be a potential binding partner of sncRNA7SL.

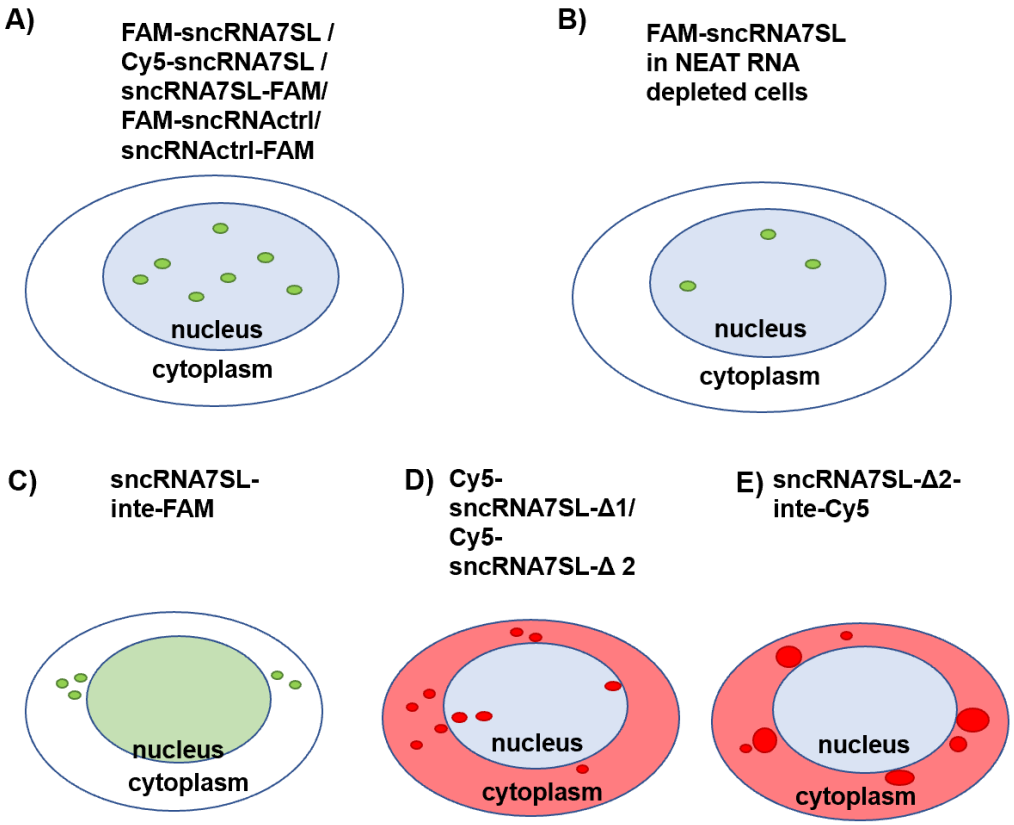

Figure 26. Graphical summary of synthetic sncRNA7SL localization.
(A) 3'- and 5'-labeled sncRNA7SL signal is mainly localized in the cytoplasm accumulated as nuclear bodies. **(B)** NEAT1 RNA depletion in FAM-sncRNA7SL reduced the number of nuclear bodies. **(C)** sncRNA7SL-inte-FAM shows a diffuse signal in the nucleus and an accumulated signal in the cytoplasm. **(D)** shortened sncRNA7SL mainly accumulates in the cytoplasm as many really small cytoplasmatic bodies that almost show as a diffuse signal (FAM-sncRNA7SL-Δ1 and –Δ2) and individual small nuclear bodies **(E)** sncRNA7SL-Δ2-inteCy5 accumulate in fewer larger cytoplasmic bodies and a bit diffuse cytoplasmic background signal.

These experiments still open up several unresolved questions. It is yet unknown why sncRNA7SL-inte-FAM does not lead to accumulation in nuclear bodies like FAM-sncRNA7SL and the other fluorescently labeled full-length sncRNA7SL oligos do. Furthermore, since there was only partial colocalization between paraspeckle markers and FAM-sncRNA7SL it is also still unresolved where in the nucleus FAM-sncRNA7SL signals that do not show colocalization with investigated nuclear body markers localize.

3.3 Ago clade family members binding sncRNA7SL

In the cell culture experiments previously described in 3.1, a tumor suppressive effect of sncRNA7SL in neuroblastoma could be seen, expressed by decreased proliferation, mobility, spheroid growth, and viability among others upon sncRNA7SL overexpression (Figure 3, 4, and 5). It is yet not established how sncRNA7SL operates in the cell to cause these effects. sncRNA7SL could be involved in cellular silencing mechanisms like other sncRNAs (miRNAs, siRNAs, and piRNAs) are known to be (reviewed in Kutter and Svoboda, 2008). This could take place in the cytoplasm as well as the nucleus since sncRNA7SL was shown to be localized in both cellular compartments (Figure 10). Assembly of an RNA-induced silencing complex similar to those of piRNAs would presuppose the binding of Argonaute family proteins.

In the cytoplasm, the protein expression might be silenced so-called posttranscriptional gene silencing (PTGS), by binding of sncRNA7SL to Ago clade proteins leading to the formation of a silencing complex as detailed in the introduction (reviewed in Treiber, Treiber, and Meister, 2019). Furthermore, in the nucleus, transcriptional gene silencing (TGS) by nuclear Ago proteins could be executed. However, since mRNAs are often found to be retained in paraspeckles (Fox and Lamond, 2010), A-to-I editing might be another possible silencing mechanism.

An interesting aspect is that Ago3 binds RNAs of a length of 28 nt to 65 nt and forms a functional silencing complex (Hu et al., 2012).

Since sncRNA7SL has a length of 32 nt, Ago3 is especially interesting as a potential binding partner for sncRNA7SL. Hence, the formation of a silencing complex between sncRNA7SL and an Argonaute protein may be an explanation for the tumor suppressive effect of sncRNA7SL overexpression. This may occur in the cytoplasm by binding of Ago3 as well as the nucleus by binding of PIWIL4, since immunofluorescence with sncRNA7SL-inte-FAM transfected cells showed that sncRNA7SL localizes in the nucleus as well as in the cytoplasm.

Therefore, the localization of Argonaute clade proteins by fractionation as well as immunofluorescence was performed to see where within the cell silencing complexes might be formed. Furthermore, RNA and protein expression of Argonaute clade proteins was compared in different cell lines to evaluate their expression level in order to consider RNA immunoprecipitation (RIP) experiments aiming to show the binding of sncRNA7LS by Argonaute clade proteins.

3.3.1 Argonaute expression in Kelly cells

To verify Argonaute RNA expression in neuroblastoma cells, RNA sequencing was performed on Kelly cells by a former member of the laboratory. This sequencing showed that while Ago 1 to 4 were expressed in Kelly cells RNA levels of PIWIL1 to 4 were extremely low (Supplementary Figure 5 A). This was quite surprising since protein expression of PIWIL4 was shown to be quite high in various tested cell lines (Supplementary Figure 5 B). To verify PIWIL4 antibody specificity our technical assistant performed a PIWIL4 depletion in Kelly cells over various time points (24 h to 7 days). PIWIL4 depletion experiments showed no difference in PIWIL4 protein expression between PIWIL4 depleted and control cells (Supplementary Figure 5 C), confirming that the PIWIL4 antibody is not specific. This excluded the PIWIL4 antibody for further localization studies by immunofluorescence as well as further protein expression studies.

Taken together, Kelly cells showed very low RNA levels of PIWIL1 to 4 while Ago 1 to 4 RNA expression was much higher. Accordingly, endogenous Ago3 was specifically detected in Western blot analysis, however, the test PIWIL4 antibody cannot be used for immunoprecipitation since PIWIL4 deletion and western blot analysis showed that the PIWIL4 antibody does not recognize PIWIL4 protein.

3.3.2 Expression of Argonaute proteins and EDC4 in neuroblastoma and other cell lines

Enhancer of decapping protein 4 (EDC4) is part of the decapping complex (Chang et al., 2014) and is known to associate with cytoplasmatic processing bodies (P-bodies) that are known to be the place of RISC complex activity (Yu et al., 2005; Parker and Sheth, 2007). Therefore, EDC4 is a good marker for potential RISC complex assembly. Hence, in order to see if sncRNA7SL binds to Ago3 and builds a silencing complex, at first expression of Ago3 and silencing complex component EDC4 in neuroblastoma cells had to be confirmed.

To further verify the expression of Ago3 and EDC4, which is part of the RNA silencing complex, in cell lines, Western Blot analysis was performed on multiple neuroblastoma cell lines (Kelly, SK-N-AS, SK-N-SH) and SK-N-MC and HEK293 cell lines. While the

expression level of the two tested proteins varied in the different cell lines, all cell lines showed at least some level of Ago3 and EDC4 protein expression (Figure 27 A). The highest level of EDC4 expression was found in HEK293 as well as Kelly cells, while the least amount of expression was shown in SK-N-MC cells. Ago3 protein levels were found to be SK-N-AS and SK-N-SH cells, with Kelly cells showing the least amount of Ago3 protein expression.

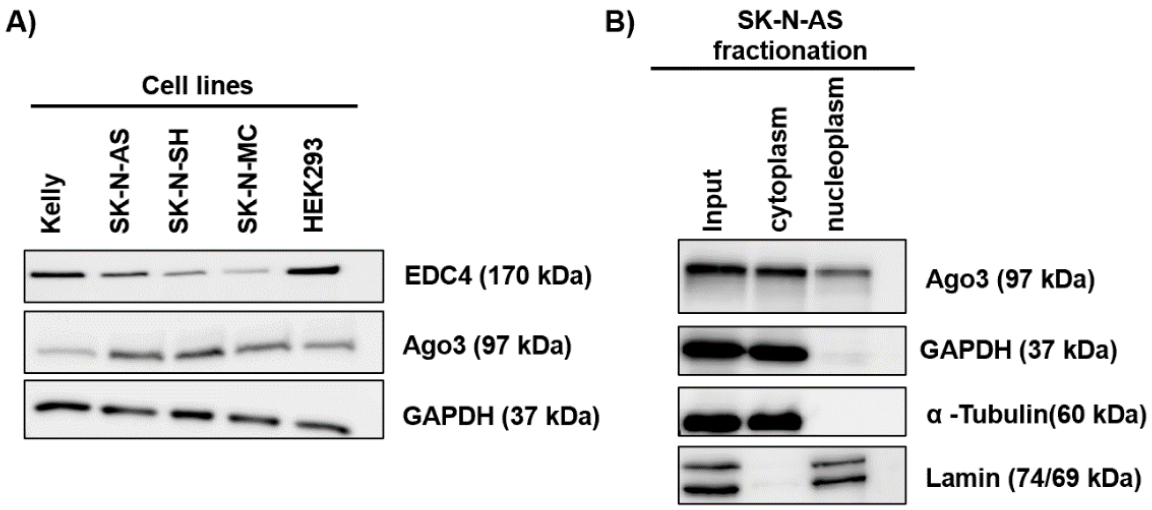

Figure 27. EDC4 and Ago3 expression level in different cell lines and localization of Ago3 protein within SK-N-AS cells.
(A) Western Blot analysis shows the expression of EDC4 and Ago3 protein in various cell lines with GAPDH used as a loading control. **(B)** Western Blot analysis of fractionated SK-N-AS cells shows endogenous Ago3 to be mainly localized in the cytoplasm but also present in the nucleus. Lamin and α-Tubulin were used as fractionation controls.

Taken together Ago3 and EDC4 protein levels varied in the different tested cell lines with HEK293 and Kelly cells expressing the highest amounts of EDC4, while SK-N-AS and SK-N-SH cells showed the highest amount of Ago3 protein levels. Ago3 immunofluorescence could not provide clear information about Ago3 localization, as the antibody gave a non-specific signal. However, fractionation suggests Ago3 proteins to be mainly localized in the cytoplasm, while also being partially localized in the nucleus.

3.3.3 Localization of HA-tagged proteins in HEK293

To visualize Argonaute proteins in cells, indicating where sncRNA7SL binding might occur within the cell, plasmids were used. Plasmids with HA-tagged Argonaute proteins provided by AG Meister (Ago2, Ago3, PIWIL4, and empty vector VP5;

Supplemental Figure 6 for plasmid maps) were multiplied and HEK293 cell lines stably expressing the HA-tagged Argonaute clad proteins or the empty expression vector were created and Western blot analysis is shown (Figure 28 A).

Next, to visualize the localization of HA-tagged Argonauts, immunofluorescence using HA antibody was performed with the Keyence BZ-X810 fluorescence microscope. Fluorescence microscopy showed that all HA-tagged Argonaute proteins were mainly localized to multiple small cytoplasmic dots (Figure 28 B). Antibody titration did not decrease the amount of HA antibody signal, suggesting that a large number of cytoplasmic HA dots is due to the high overexpression of the respective Argonaute proteins in the cell. Interestingly, only Ago2-HA showed an accumulation of signal in the cytoplasm to form larger dots (Figure 28 B). HA antibody specificity was confirmed by negative control, empty vector VP5, which did not show any signal.

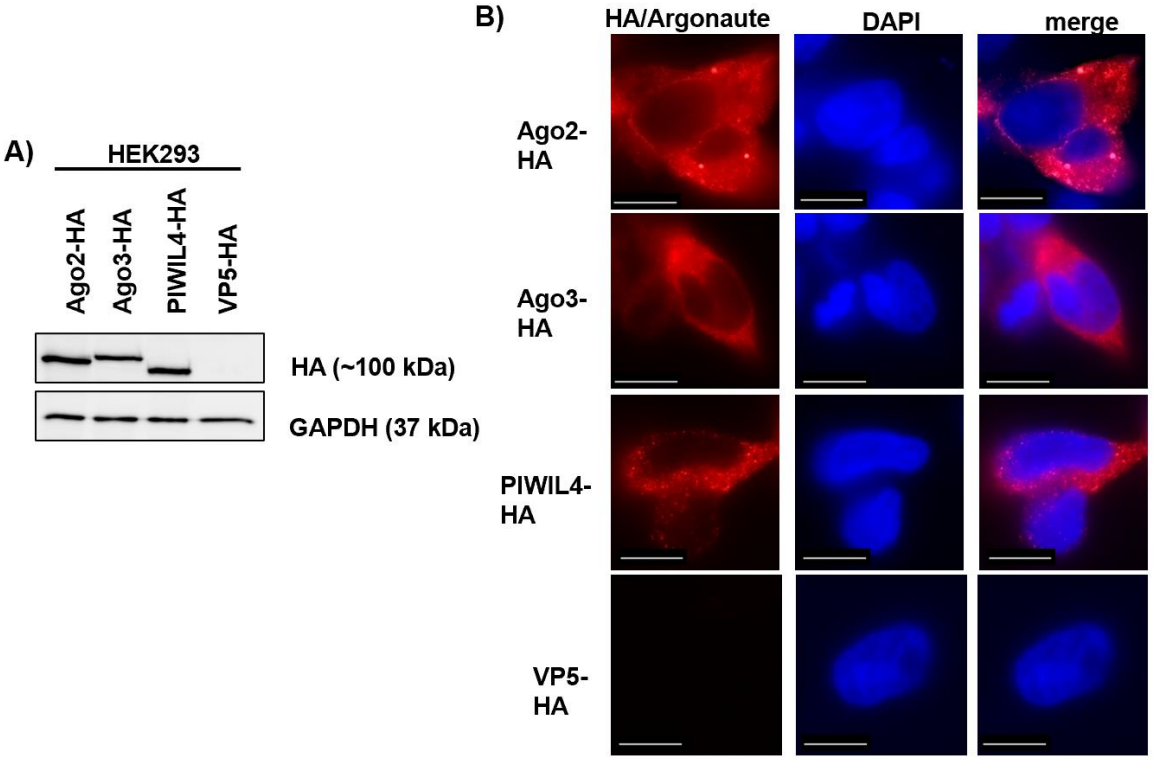

Figure 28. The HA expression level of stably transfected cell lines and HA-tagged Argonaute proteins mainly localize in the cytoplasm.
(A) Western Blot analysis of HEK293 cell lines stably transfected with HA-tagged Argonaute proteins shows an even expression of HA-tagged proteins in all tested cell lines. **(B)** Fluorescence microscopy of HA antibody-stained HEK293 cells transfected with various HA-tagged Argonaute proteins (Ago2-HA, Ago3-HA, PIWIL4-HA), showed their main localization to be in the cytoplasm. Negative control empty vector VP5-HA did not show a signal.
Images were taken with the Keyence BZX fluorescence microscope. With a magnification of 100x. All scale bars measure 10 µm.

Subsequent, visualization of endogenous Ago3 was tested. Immunofluorescence showed Ago3 to be mainly localized in the nucleus in SK-N-SH cells (Supplementary Figure 7 B, upper part). To be certain antibody-specificity verification by Ago3 depletion was performed. Hence, Ago3 depletion was performed in SK-N-SH cells and verified at different time points (24 h to 96 h) using western blot analysis. Western Blot analysis showed barely any depletion of Ago3 protein level 24 h after the knockdown. Depletion rates increased 48 h after knockdown and peaked at 72 h and 96 h (Supplementary Figure 7 A). Therefore, 72 h after depletion of Ago3 SK-N-SH cells were fixed and stained with DAPI and Ago3 antibody. Fluorescence microscopy was performed using the Keyence BZ-X810 fluorescence microscope. Unfortunately, no difference in Ago3 antibody staining could be visualized using Immunofluorescence in Ago3-depleted cells compared to non-depleted controls (Supplementary Figure 7 B), suggesting unspecific antibody staining. However, fractionation experiments showed the localization of Ago3 to be about two-thirds localized in the cytoplasm while one-third was localized in the nucleus (Figure 27 B). GAPDH and α-Tubulin were used as cytoplasmic markers, while Lamin was used as a nuclear marker.

Taken together all HA tagged Argonaute proteins show a similar mainly cytoplasmic localization in HEK293 cells. While endogenous Ago3 antibody was not specific enough for immunofluorescence, fractionation shows a divide of endogenous Ago3 between the cytoplasm (about two-thirds) and the nucleus (about one-third). These experiments indicate that possible binding between Ago3 and sncRNA7SL could occur in the cytoplasm and nucleus.

3.3.4 Development of a fluorescence based sncRNA7SL binding assays

As delineated above, it was assumed that sncRNA7SL is likely to be bound by Ago3 and PIWIL4, due to their documented ability to bind longer sncRNAs such as the 32 nucleotides long sncRNA7SL and to be required for the formation of gene silencing complexes such as Ago3 in the cytoplasm's (PTGS). Due to the very low expression of endogenous PIWIL4 in neuroblastoma cells, a role in gene silencing by PIWIL4 appears unlikely in neuroblastoma cells. However, the potential interaction between PIWIL4 and sncRNA7SL is of interest in the scenario that sncRNA7SL might be expressed in testis, ovary, and monocytes or cancer types (like cervical cancer (Su et

al., 2012)) with high PIWIL4 expression (https://www.genecards.org/cgi-bin/carddisp.pl?gene=PIWIL4&keywords=piwil4#proteins).

In order to develop a sncRNA7SL binding assay, which allows testing of the binding by various proteins, two tools were applied: 1) stable HEK293 cells expression HA-tagged Ago2, Ago3, and PiwiL4 protein (Figure 28) and 2) sncRNA7SL-inte-FAM the fluorescence-labeled synthetic sncRNA7SL. As shown above, the fluorescence-labeled sncRNA7SL-inte-FAM molecule localizes similarly to the endogenous sncRNA7SL (Figure 18 B), most likely because of the 5'- and 3'-ends accessible for binding by Argonaute clade proteins.

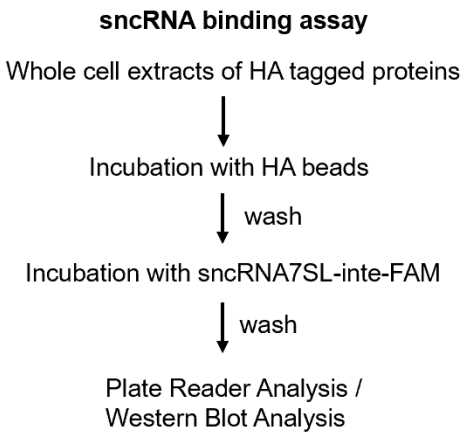

Figure 29. Experimental setup of sncRNA binding assays.
Experimental setup of sncRNA binding assays with stably transfected cell lines.

For the sncRNA7SL binding assays (Figure 29), HEK293 cell lines stably transfected with Ago2-HA, Ago3-HA, PIWIL4-HA, or the negative control empty vector (VP5-HA) respectively, were used. HA protein expression was verified using western blot analysis (Figure 28 A). Afterward, stably transfected cell lines were harvested and lysed to prepare protein extracts. Bradford analysis was used for the determination of protein concentration. HA antibody-labeled magnetic beads (20 µl per sample) were prepared and incubated for 2 h with 100 µg protein Lysate at 4°C in rotation. Afterward, beads were washed thrice and incubated for 30 min with 50 pmol sncRNA7SL-inte-FAM. Thereafter, the supernatant was taken down, and the beads were again washed three times. Beads were taken in 30 µl clear SDS-Loading buffer and 5% β-mercaptoethanol and incubated for 10 min at 70°C to dissolve protein complexes from the beads (Figure 29). Two sets were generated per protein: one for fluorescence measurement the other for western blot analysis to determine individual HA protein pull-downs. Fluorescence measurements showed a high signal with Ago3-HA protein samples, indicating the strongest binding between Ago3 and sncRNA7SL, closely

followed by PIWIL4-HA protein samples (Figure 30 B, C). Ago2-HA samples showed an average of three times lower signal compared to Ago3 and PIWIL4. Negative controls always showed the least amount of signal. After normalization with western blots (Figure 30 A) and therefore the efficiency of pull downs of individual Proteins, Ago3 and PIWIL4 showed almost the same binding to sncRNA7SL-inte-FAM with PIWIL4 binding being only slightly stronger (Figure 30 C).

Interestingly, using end labeled sncRNA7SL in this assay led to inconclusive results and shows that 5'-labeling of sncRNA7SL hinders stable binding of sncRNA7SL to Argonaute proteins, showing the importance of free 5'-and 3'-ends for binding (supplementary Figure 8).

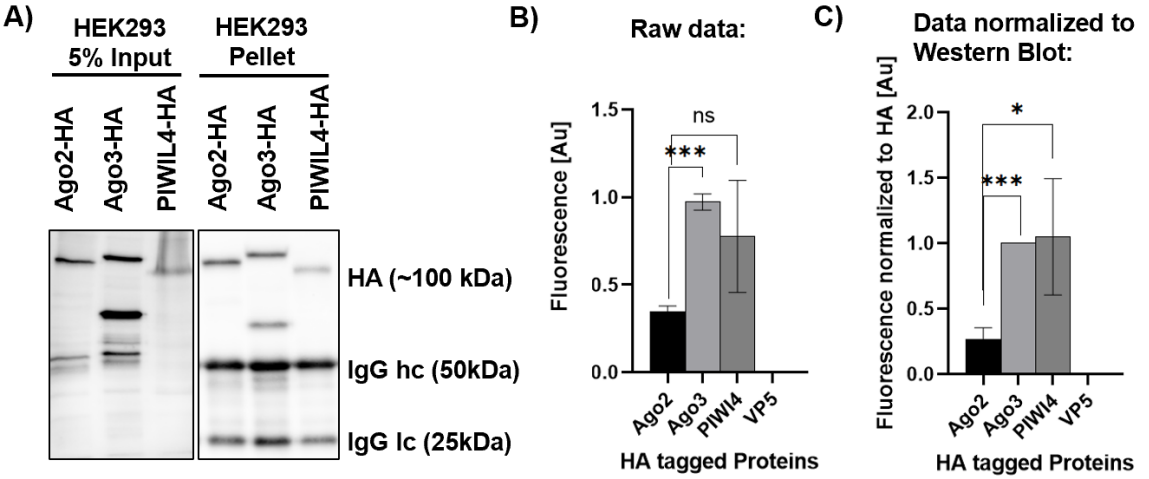

Figure 30. Argonaute proteins pull-down efficiency and binding of sncRNA7SL-inte-FAM to several Argonaute proteins.

(A) Western Blot Analysis showed variations in pull-down efficiency among the different HA-tagged Argonaute proteins. Pull-down efficiency is similar in Ago2-HA and Ago3-Ha while decreasing in PIWIL4-HA. **(B)** Results of fluorescence measurements of sncRNA7SL-inte-FAM binding assays prior to normalization against pull-down efficiency analyzed in Western Blot (A). Ago3-HA protein binds significantly better to sncRNA7SL-inte-FAM compared to Ago3-HA protein. PIWI4-HA also binds better to sncRNA7SL-inte-FAM compared to Ago2-HA, but the difference is not significant. Negative control VP5 showed the least fluorescence signal, as determined in 3independent experiments. **(C)** Results of sncRNA7SL-inte-FAM binding assays after normalization against pull-down efficiency. PIWI4-HA shows the best binding to sncRNA7SL-inte-FAM, closely followed by Ago3-HA. Ago2-HA shows about three to fourfold less binding than the other tested proteins, while the negative control is still negative, as determined in 3 independent experiments.

All results were determined as mean SD (error bars). P value * ≤ 0.05,** ≤ 0.01, and *** ≤ 0.001 was determined using paired t-test with Prism 8.4 (Graph Pad Software).

All in all, this suggests sncRNA7SL-inte-FAM binds best to PIWIL4 and Ago3 *in vitro*, while Ago2 binding is not as strong. This suggests that sncRNA7SL could actually be part of different RISC complexes, indicating a role of sncRNA7SL in gene silencing.

3.3.5 sncRNA7SL-inte-FAM partially colocalizes with EDC4 proteins in neuroblastoma cells

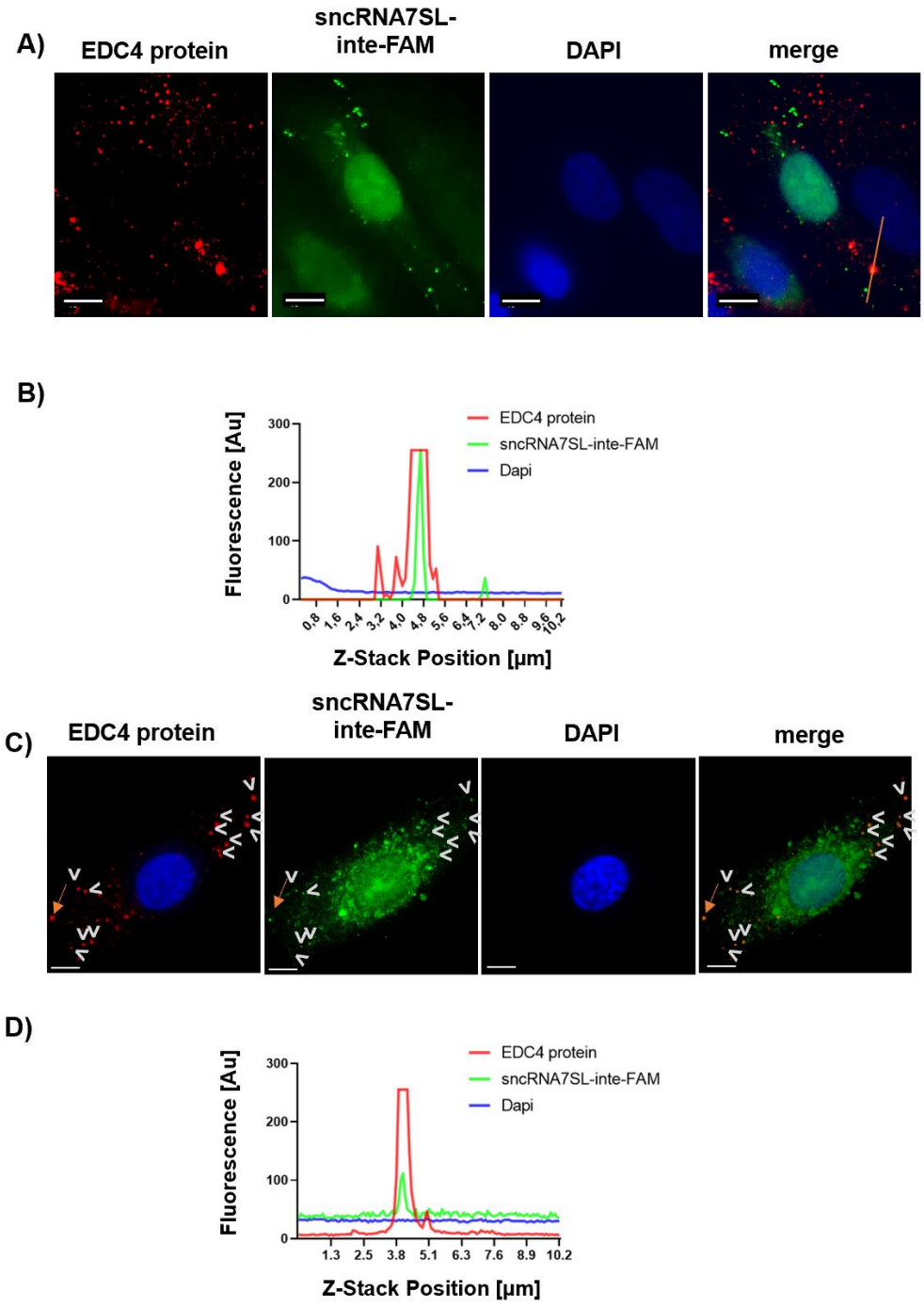

Figure 31. Partial colocalization of internally fluorescent labeled sncRNA7SL and EDC4 protein.
(A) Fluorescence microscopy of fixed and 25 nM snRNA7SL-inte-FAM transfected SK-N-SH cells dyed with EDC4 antibody. Pictures show partial colocalization between sncRNA7SL-inte-FAM and EDC4 protein. The line used for line profiling is indicated in orange. Images were taken with the Keyence BZX fluorescence microscope. With a magnification of 100x. All images were taken 2 days after transfection in fixed cells. All scale bars measure 10 µm. **(B)** Line Profile of colocalized sncRNA7SL-inte-FAM and EDC4 protein in the cytoplasm of SK-NSH cells. **(C)** Fluorescence microscopy of fixed and 25 nM snRNA7SL-inte-FAM transfected SK-N-SH cells dyed with EDC4 antibody. Pictures show partial colocalization between

sncRNA7SL-inte-FAM and EDC4 protein. White arrows indicate colocalization between EDC4 protein and sncRNA7SL-inte-FAM in the cytoplasm. **(D)** Line Profile of colocalization of sncRNA7SL-inte-FAM and EDC4 protein in the cytoplasm of SK-N-SH cells indicated by orange arrow.

Since sncRNA7SL-inte-FAM was shown to bind mainly to Ago3 and PIWI4 (Figure 30) and therefore potentially form a silencing complex, P-body marker EDC4 was used to analyze possible colocalization between sncRNA7SL-inte-FAM and EDC4 protein in the cytoplasm. Hence, SK-N-SH cells were transfected with sncRNA7SL-inte-FAM. 24 h after transfection cells were fixed, stained with EDC4 protein antibody, and nuclei were stained with DAPI.

Partial colocalization between EDC4 protein and sncRNA7SL-inte-FAM could be confirmed using immunofluorescence microscopy using the Keyence BZ-X810 fluorescence microscope. EDC4 protein (Figure 31, red signal) is visualized mainly in the cytoplasm forming small cytoplasmatic dots, while sncRNA7SL-inte-FAM (Figure 31, green signal) is mainly visualized as a diffuse signal in the nucleus, but also shows slight accumulation in dots in the cytoplasm (Figure 31 A, C). Colocalization was further confirmed using line profiling (Figure 31 B, D). White arrows in Figure 31C indicate colocalization between a majority of sncRNA7SL-inte-FAM accumulated cytoplasm bodies and EDC4 protein, line profiles of several of these dots confirm colocalizations (Figure 31 D, Supplementary Figure 9)

Concisely, colocalization between EDC4 protein and sncRNA7SL-inte-FAM indeed indicates the formation of an Argonaute-sncRNA7SL silencing complex within the cytoplasm.

3.3.6 sncRNA7SLΔ2-inte-Cy5 partially colocalizes with EDC4 proteins in neuroblastoma cells

As shown before, sncRNA7SLΔ2-inte-Cy5 also accumulates in the cytoplasm as dots (Figure 18 C), considered likely to be P-bodies since miRNAs, which are roughly of the same length as sncRNA7SLΔ2-inte-Cy5, are known to build RISC complexes together with Argonauts forming so-called P-bodies in the process (Parker and Sheth, 2007). Therefore sncRNA7SLΔ2-inte-Cy5 and EDC4 protein colocalization was analyzed. Using the Keyence BZ-X810 fluorescence microscope to perform immunofluorescence on sncRNA7SLΔ2-inte-Cy5 SK-N-SH cells which were fixed and stained with EDC4

antibody as well as DAPI. sncRNA7SLΔ2-inte-Cy5 and EDC4 protein showed partial colocalization, similar to full length sncRNA7SL-inte-FAM and EDC4 protein (Figure 32).

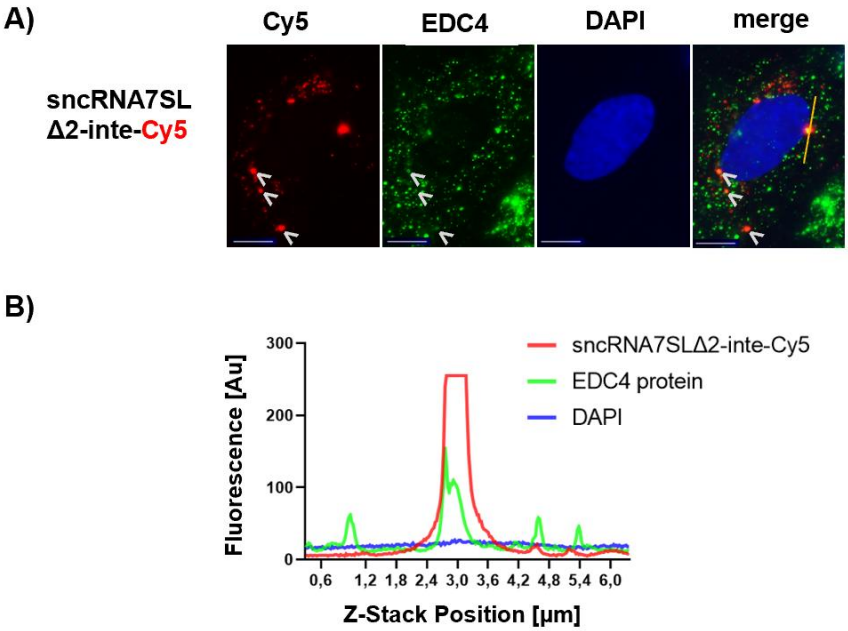

Figure 32. sncRNA7SLΔ2-inte-Cy5 accumulates in the cytoplasm and partially colocalizes with the EDC4 protein.
(A) Fluorescence microscopy of fixed and 25 nM snRNA7SLΔ2-inte-Cy5 transfected SK-N-SH cells dyed with EDC4 antibody. Nuclei were stained with DAPI. Pictures show partial colocalization between sncRNA7SLΔ2-inte-Cy5 and EDC4 protein. Images were taken 2 days after transfection. The line used for line profiling is indicated in orange. All images were taken with a Keyence BZX fluorescence microscope. With a magnification of 100x. All scale bars measure 10 µm. Arrowhead indicate colocalizing signals.**(B)** Line Profile of colocalized sncRNA7SLΔ2-inte-Cy5 and EDC4 protein in the cytoplasm of SK-NSH cells.

In summary, these experiments suggest that sncRNA7SLΔ2-inte-Cy5 builds an RNA silencing complex with Argonaute proteins similar to those complexes' miRNAs built with Ago2.

3.3.7 Summary: Argonaute proteins binding sncRNA7SL

Taken together, sncRNA7SL-inte-FAM was found to bind Ago3 and PIWIL4 proteins better than Ago2 proteins. EDC4 and endogenous Ago3 proteins were found to be expressed in all tested cell lines. HA-tagged Argonauts were shown to be mainly localized in the cytoplasm with Ago2-HA being the only tested protein to accumulate into bigger cytoplasmic dots, resembling probably P-bodies. Furthermore sncRNA7SL-

inte-FAM as well as the shortened version sncRNA7SL-Δ2-inte-Cy5 both partially localized with endogenous EDC4 protein in SK-N-SH cells, indicating accumulation in P-bodies. For future experiments, RNA immunoprecipitation for Ago3 and PIWIL4 should be performed and samples sequenced to confirm Ago3 and PIWIL4 binding to sncRNA7SL.

3.4 Summary

To summarize, as a first objective,it was shown that overexpression of sncRNA7SL had a tumor suppressive effect in neuroblastoma cells indicated by decreased viability, proliferation, mobility, and spheroid growth as well as a cell cycle arrest in the G1 phase and reduction of the protein expression level of BMI1 protein. Low levels of sncRNA7SL reversed the previously described effect on viability and lead to increased viability. This strong tumor suppressive effect of sncRNA7SL raises the question of how this small RNA functions. The most likely functional mechanism is through the formation of a gene-silencing complex. Furthermore, it would be important to study the biogenesis and to identify conditions upregulating the biogenesis of this tumor-suppressive small RNA.

In the second objective, Molecular beacons were found to be highly sensitive and specific *in vivo* and *in vitro* localization studies. Endogenous sncRNA7SL was found to be mainly localized in the nucleus, visualized as a diffuse signal, while endogenous 7SL RNA was mainly localized in the cytoplasm at the ER. However, partial colocalization of sncRNA7SL and 7SL RNA in the cytoplasm suggests that MB sncRNA7SL partially recognized 7SL RNA as a target.

The finding that sncRNA7SL predominantly localizes to the nucleus raises important questions about its biogenesis and cellular trafficking. As a third objective fluoresce-tagged sncRNAs were established as powerful tools to analyze sncRNA localization and colocalization with other pRNAs and proteins. Fluorescence-tagged sncRNA7SL showed a close resemblance to the Molecular beacon signal if the fluorescence tag was attached within the sequence, being visualized as a diffuse signal in the nucleus and less intense accumulated in dots in the cytoplasm. However, fluorescence tagging on the 3’- or 5’-end leads to an accumulation in the nucleus as nuclear dots. These nuclear dots seem to be, at least partly, localized in paraspeckles, since NEAT1_2 RNA depletion led to a reduction of those nuclear dots. Furthermore, FAM-sncRNA7SL immunofluorescence showed partial colocalization with paraspeckle markers NONO

and NEAT1 RNA. Moreover, length seems to have a strong impact on RNA localization, since depletion of 9 nt or 10 nt out of sncRNA7SL leads to a shift in localization into the cytoplasm. In future studies, it would be interesting to study whether sncRNA7SL-inte-FAM also localizes to paraspeckle, due to the interaction with *IRAlu*-containing mRNAs. Furthermore, it might be a powerful tool to study the potential shuttling of sncRNA7SL-inte-FAM between the nucleus and the cytoplasm.

The colocalization between KNL1 mRNA and sncRNA7SL in some paraspeckle is very promising since KNL1 mRNA contains two target sites for sncRNA7SL in the 3'-UTR. In addition, it will be interesting to test whether the colocalization with sncRNA7SL-inte-FAM might be even stronger and also occurs in the cytoplasm since sncRNA7SL-inte-FAM localizes to cytoplasmic bodies and colocalizes with EDC4 the component of the decapping complex.

In the last objective a fluorescence based sncRNA binding assay was developed to study binding between sncRNA7SL-inte-FAM and different Argonaute proteins. sncRNA7SL-inte-FAM was found to strongly bind Ago3 and PIWIL4 proteins, while only lightly binding Ago2 protein. Furthermore, sncRNA7SL-inte-FAM was found to colocalize to EDC4 protein, indicating the formation of an RNA silencing complex with its Argonaute binding partners. These striking data lay the ground for functional assays focusing on the formation of sncRNA7SL:Ago3 and sncRNA7SL:PiwiL4 gene silencing complex.

Figure 33 summarizes all colocalizations and *in vitro* bindings of fluorescence-labeled sncRNA7SL.

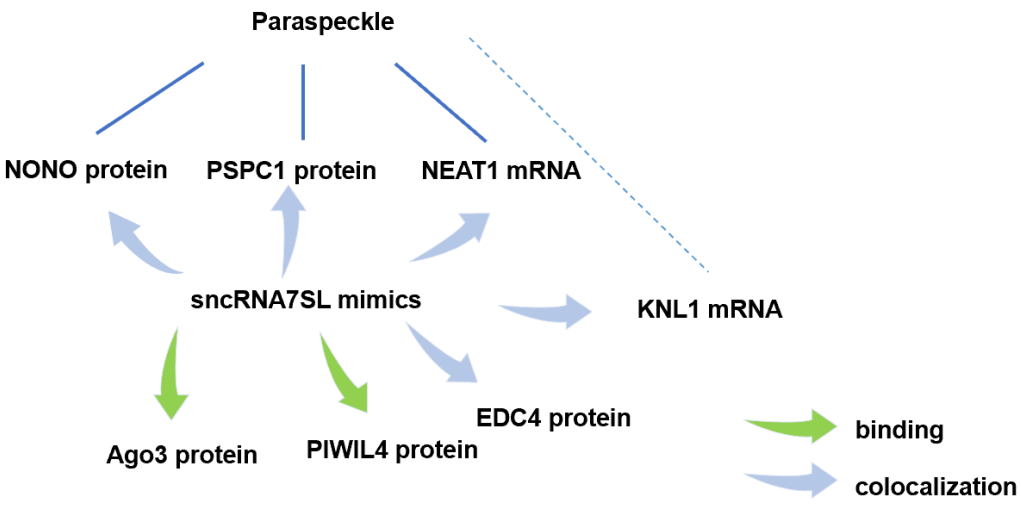

Figure 33. Graphical summary of colocalization and binding of fluorescence-labeled sncRNA7SL.

3’- and 5’-labelled sncRNA7SL colocalizes with paraspeckle marker NONO protein, PSPC1 protein and NEAT1 mRNA. They also colocalize KNL1 mRNA. Internally labeled sncRNA7SL binds to Ago3 and PIWIL4 protein in in vitro experiments and colocalizes with P-body marker EDC4.

4. Discussion

4.1 sncRNA7SL acts as a tumor suppressor in neuroblastoma and Ewing Sarcoma cell lines

Taken together, this study indicates that sncRNA7SL has tumor-suppressive properties in neuroblastoma as well as SK-N-MC cell lines. sncRNA7SL overexpression leads to a decrease in viability, proliferation, mobility, and spheroid growth. sncRNA7SL overexpression also led to a G1 arrest and a decrease in BMI protein expression but there was no effect on Casp3 protein level (Figure 7). Furthermore, inhibition of endogenous sncRNA7SL led to an increase in viability, reversing the effect of overexpression, albeit the effect was smaller. However, the underlying mechanisms of these shifts are yet to be identified.

The decrease of proliferation in neuroblastoma cell lines by sncRNA7SL (Figure 4 C) is especially interesting since proliferation pathways are critical targets of treatments able to decrease the malignant potential of cancers (Stafman and Beierle, 2016). Although the mobility assay showed that the overexpression of sncRNA7SL results in a reduction of mobility in neuroblastoma cells (Figure 5 A), it cannot be excluded that this is not a direct reduction of mobility but only a reduction of proliferation. Further tests would be in order to distinguish these two mechanisms since proliferation and invasion or mobility are distinctive by a change in the cytoskeleton of cells. While proliferative cells build an actomyosin ring during mitosis, invading cells use their actomyosin network to form invadopodia, actin-rich projections helping with invasion (Lattmann et al., 2020). The mechanisms behind sncRNA7SL overexpression leading to a G1 arrest also need to be investigated further. An interesting pathway could be the upregulation of p21 protein expression. Sine p21 is one of the key targets of p53 (el-Deiry, et al., 1993), p21 overexpression results in cyclin-dependent kinases (CDK) inhibition and was found to lead to G1 arrest in neuroblastoma cells treated with a p53 activator (Gamble et al., 2012). Therefore, p21 also plays a major role in the regulation of proliferation (Harper et al., 1993). Furthermore, while several CDK inhibitors were shown to be influenced by cellular stress, and increase of p21 expression was found during a broad range of cellular stress conditions (Gerospe et al., 1999).

Moreover, the BMI1 protein, which was also reduced in sncRNA7SL treated cells (Figure 6), was found to play a role in the invasion of glioma cells, a highly invasive cancer. Here, the downregulation of BMI1 leads to an increase in cyclin-dependent

kinase inhibitor p16INK4A (p16) expression, a known tumor suppressor and cell cycle regulator, and a decrease in cell invasion (Liang et al., 2015). p16INK4A (p16) expression was further found to lead to a G1 arrest in leukemia cells (Ausserlechner et al., 2005). This suggests that BMI1 downregulation by sncRNA7SL in neuroblastoma cell lines might lead to the found G1 arrest and further strengthens sncRNA7SL as a tumor suppressor.

However, BMI1 also has many more functions including in spheroid cultures. Among solid tumors, neuroblastoma has established a higher expression of cancer stem cell markers like BMI1, compared to 2D cell cultures (Nunes et al., 2019; Bahmad et al., 2019). This might suggest that sncRNA7SL might have an even bigger effect on spheroids compared to 2D cell culture cells.

Furthermore, it was also found that BMI1 plays a role in the MYC-N pathway in MYC-N amplified tumors. In MYC-N overexpressed mice, an increase in BMI1 expression was also observed and it was suggested that BMI1 decreases apoptosis in these cells acting as an oncogenic partner to MYC-N (Cui et al., 2007). Also, BMI1 depletion led to an increase in Schwannian stroma, a factor that is linked to better prognosis (Cui et al., 2007), showing the major importance of BMI1 as an oncogenic factor in neuroblastoma and the cruciality of BMI1 downregulation after sncRNA7SL transfection to suggest sncRNA7SL as a good tumor suppressor. However, looking at the sequence of BMI1, it is apparent that BMI1 does not contain Alu elements. Furthermore, no target sites for sncRNA7SL are found, neither in the 5’ nor in the 3’-UTR, indicating an indirect regulation of BMI1 expression by sncRNA7SL.

As already mentioned, MYC-N is also an important factor in neuroblastoma tumors and it was found that amplification of MYC-N correlates with therapy resistance and poor patient prognosis (Seeger et al. 1985). In my studies, MYC-N amplified (Kelly) and non-MYC-N amplified (SK-N-AS, SK-N-SH) neuroblastoma cell lines were tested. Interestingly, sncRNA7SL overexpression often had stronger effects on MYC-N amplified cells compared to MYC-N non-amplified cells (Figure 4 A). These results suggest that sncRNA7SL may exert a particularly strong effect on MYC-N amplified neuroblastoma cells, suggesting it is a tumor suppressor in highly aggressive neuroblastoma cells.

In conclusion, sncRNA7SL showed tumor-suppressive characteristics in various neuroblastoma cell lines (Figure 4,5,6). sncRNA7SL overexpression decreased proliferation, viability, mobility, and spheroid growth, led to cell cycle arrest in neuroblastoma cells, and was shown to specifically lower the expression of BMI1 protein.

4.2 Endogenous localization of RNAs in neuroblastoma

One important objective of this project was, to reveal the cellular localization of sncRNA7SL. Since the exact sequence of scnRNA7SL is found in the Alu element of 7SL RNA, localization studies using fractionation followed by qPCR analysis proved to be difficult. Hence, other methods needed to be explored to determine the endogenous localization of sncRNA7SL.

Studies of endogenous localization of sncRNA7SL and 7SL RNA were done using Molecular Beacons. Since MBs carry the target sequence of the analyzed RNA in a loop and have a stem ending in a fluorescent tag and a quencher, a fluorescence signal should only be seen by binding the RNA to the loop target sequence and subsequently opening the stem (Figure 8 A). Several differently built MBs were tested and it was found that stem length was critical for stability (Figure 8 B). *In vitro*, experiments already showed that two additional G:C base pairs prolonging the stem (MBsncRNA-1) drastically decreased MB sensitivity. *In vivo*, the longer stem MB did not show any signal (Figure 11). *In vitro,* experiments also demonstrated low background fluorescence, yet high sensitivity and specificity of shorter stemmed MBs deeming them appropriate for *in vivo* experiments (Weigert et al., manuscript under revision).

Strikingly, the predicted structure of MB7SL showed base pairing in the target sequence of the MB, leading to a highly extended stem and no real loop region (Figure 8 B). However, *in vitro* as well as *in vivo* experiments showed an exceptionally good sensitivity of MB7SL compared to MBsncRNA7SL (Weigert et al., manuscript under revision). This suggests that not only an extended loop for appropriate target binding and stem length are critical factors of MB stability and sensitivity but that additional components must play a critical role in the opening of MBs. As an example, it has been shown that cations play a role in forming a double-stranded structure (Nakano et al., 1999), which affects MBs stem stability and the binding of target RNA to the MB target

sequence. Furthermore, it is likely that the ratio between transfected MB in the cells and endogenously occurring target RNA contributes to MB stability and sensitivity.
The difference in transfection efficiency between MB7SL and MBsncRNA7SL was especially striking *in vivo* (Figure 13). There may be two possibilities for such different strengths and frequencies of the signal. First, the molecules per se may have been transfected with different efficiency; second, endogenous 7SL RNA, unlike endogenous sncRNA7SL, may simply be present in greater amounts in the cell, which would facilitate MB signal development; and 7SL RNA may also be present in more cell cycle stages, whereas sncRNA7SL may only be present in some specific cell cycle stages enough for detection with MB. Since it was suggested that sncRNA7SL derives from a precursor of the 7SL RNA sncRNA7SL expression could be dependent on incomplete maturation of 7SL RNA. Since the La protein associates with 7SL RNA (Hashimoto and Steitz, 1983), stabilizes the RNA and chaperones maturation of Pol III transcripts (reviwed in Mariaia and Intine, 2002), depletion of La could lead to an alternative pathway, resulting in expression of sncRNA7SL. Similar processes were already found for tRNAs. There, La was found to prevent pre-tRNA fragment association with Ago proteins, therefore inhibiting potential functional tRNA fragments from the formation of a silencing complex with Argonauts (Hasler et al.,2016)

Hence, MB of sncRNA7SL and 7SL without a quencher were designed. Thus, these fluorescence-labeled MB should always light up as soon as they are transfected into the cells and not only when they are opened by an endogenous target RNA. Strikingly, there was no significant difference between the transfection efficiency of MB7SL with and without a quencher and MBsncRNA7SL with or without a quencher (Fig. 13). This result indicates that it is not only the potential lower amount of endogenous sncRNa7SL in the cells that leads to a weaker and less abundant signal of MBsncRNA7SL compared to MB7SL but that the MBsncRNA7SL per se is less transfected into the cell. The mechanisms behind this process are as yet unclear and would need to be investigated in more detail by further experiments.

The tested MBs were highly specific as observed *in vitro* and *in vivo* (Weigert et al., manuscript under revision). MBsncRNA-2A had three mismatches and five deletions in their sncRNA7SL target sequences. This significantly reduced opening of MB *in vitro* even with five-fold excess of sncRNA7SL target RNA. *In vivo* MBsncRNA-2A showed almost no signal at all similar to MBcon transfected cells (Figure 11). MBs were

previously shown to be highly specific. They could even distinguish between the perfect target sequence and a single nucleotide mismatch (Kostrikis et al., 1998; Tyagi et al., 1998).

Experiments in living cells are always more difficult since various cellular factors can play a role in the opening of the MB that can be excluded in *in vitro* experiments. One difficulty was that sncRNA7SL might not be the only possible target of MBsncRNA7SL since 7SL RNA contains the perfect target sequence of MBsncRNA7SL, furthermore, several mRNAs containing 3'-UTRs of Alu elements might also contain the sncRNA7SL sequence. Hence, *in vitro* experiments with the degenerated sncRNA7SL sequence contained in several Alu elements containing mRNAs and MBsncRNA7SL were performed. These experiments indicate that *in vivo* MBsnc7SL will not be opened by degenerated target sequences.

The 7SL RNA could potentially be more likely to open MBsncRNA7SL since its expression in cells is quite high and the exact sequence of sncRNA7SL is found in the 3' UTR of 7SL RNA. However, *in vivo* experiments with live cells showed that endogenous sncRNA7SL mainly localizes in the nucleus with only a little signal in the cytoplasm while 7SL RNA mainly localizes in the cytoplasm (Fig. 10 A). The two signals only overlap slightly in the cytoplasm (Fig. 10 A). As mentioned before 7SL RNA is the backbone of the signal recognition particle (SRP) and therefore was expected to be mainly localized in the cytoplasm, colocalizing with the endoplasmatic reticulum (ER) to be more specific (Kellogg et al., 2021; Walter and Lingappa, 1986). Staining of ER indeed showed colocalization of the majority of MB7SL signal with ER signal (Figure 10 B). The slight signal of MBsncRNA7SL in the cytoplasm cannot be ruled out as detected 7SL RNA. However, since this signal is only very weak it suggests that MBsncRNA7SL cannot bind 7SL RNA very well, suggesting steric obstruction of MBsncRNA7SL binding to 7SL RNA by folding or association with different signal recognition particles.

MBs were already shown to be transfected into cells by various methods like membrane pore formation using streptolysin (Santangelo et al., 2004), electroporation (Mao et al., 2020), microinjection (Bratu et al., 2003), and lipid-based transfection methods (Nitin et al., 2004). Here, different lipid-based transfection reagents (RNAiMax, Lipofectamin3000, RNAiMax) were tested. RNAiMax a transfection reagent recommended for RNA transfection worked best for DNA MB transfection. While

Lipofectamin3000 transfection did only yield extremely weak signals, FUGENE transfection usually used for DNA and Plasmid transfection resulted in big bright spots within the cells and outside of cellular compartments, indicating a premature opening of the MBs by the transfection reagent.

Transfecting higher concentrations of MB (50 nM and 75 nM) did not result in a brighter MBsncRNA7SL signal, but led to a higher background signal of MBcon (data not shown), suggesting more MB to be opened erroneously. These findings suggested 12.5 nM MB transfected with RNAiMax to yield the best results in live cell imaging.

It is unclear if sncRNA7SL is processed in the nucleus by e.g., the DROSHA-DGCR8 complex or maybe exported into the cytoplasm and processed there by the endonuclease DICER in a similar fashion as other small non-coding RNAs like miRNA-producing tRNA fragments (Hasler et al., 2016). If this small RNA is indeed processed in a similar process, it is possible that it also binds to Argonaute proteins in the same process as DR2 Alu repeat-induced small RNAs derived from DR2 Alu repeats of similar length (Hu et al., 2012).

Taken together, MB was confirmed as a sensitive and specific tool for endogenous RNA detection. 7SL RNA was confirmed to be localized at the ER and sncRNA7SL as well as RNA 6145 were shown to be mainly localized in the nucleus with a slight signal in the cytoplasm.

4.3 Localization of synthetic sncRNA7SL

Fluorescence labeling of small RNA is common practice, however, not many studies actually investigated the effects of labeling on the localization of those RNAs. Studies with endogenous sncRNA7SL showed that a majority of endogenous sncRNA7SL was localized in the nucleus and visualized as a diffuse signal, while the signal in the cytoplasm was only very weak (Figure 10 A) and it was unclear if it was a true sncRNA7SL signal or if it was a false positive signal from the 7SL RNA.

To investigate the potential dynamics and the trafficking of sncRNA7SL in the cells sncRNA7SL oligos with various fluorescence groups and label positions were designed. Those synthetic sncRNAs were transfected into cells to test their applicability to study sncRNA7SL dynamics and trafficking in living cells.

Firstly, it was investigated if the length of sncRNA7SL plays a role in its nuclear localization, since MBsncRNA7SL as well as MB6145, two MBs targeting RNAs of similar length, both showed majorly nuclear localization (Figure 11). Indeed, while full-length FAM-sncRNA7SL mainly localized in the nucleus and accumulated to nuclear bodies (Figure 16), a deletion of ten or eleven nucleotides (Cy5-sncRNA7SL-Δ1, Cy5-sncRNA7SL-Δ2) within the sncRNA7SL sequence led to a predominant cytoplasmic localization (Figure 17). This matches the localization of miRNAs, which have similar lengths of 20 to 22 nucleotides and are also known to be mainly localized in the cytoplasm to regulate mRNA silencing (reviewed in Jie et al., 2021). Internal labeling of sncRNA7SL-Δ2 (sncRNA7SL-Δ2-inte-Cy5) still resulted in a predominant cytoplasmic localization (Figure 18 C), however, the formerly almost diffuse signal now partially accumulated into larger cytoplasmic bodies. Since sncRNA7SL-Δ2-inte-Cy5 is similar to miRNA in length and also localizes in the cytoplasm, this suggests that those large cytoplasmatic bodies are processing bodies, or P-bodies that are also known to colocalize with miRNA and Argonaute proteins (Liu et al., 2005). Another possible process is that the overexpression of sncRNA7SL leads to the initiation of liquid-liquid phase separation (LLPS) which was found to be triggered by high-concentration non-coding RNAs (Lin et al., 2015; Pessina et al., 2019).

Furthermore, the comparison of FAM-sncRNA7SL and the shorter labeled sncRNAs (Cy5-sncRNA7SL-Δ1, Cy5-sncRNA7SL-Δ2) revealed the likely existence of a nuclear sncRNA nuclear import pathway specialized on sncRNAs with at least the length of 32 nts, for example by binding PIWI-proteins (Li et al., 2021). Although little is known about the nuclear transportation process of MIWI2 (murine PIWIL4) it is certain, that it plays a role in the methylation of DNA and hence in transcriptional gene regulation in fetal testes (Kuramochi-Miyagawa et al., 2008).

Strikingly, sncRNA7SL with fluorescence labels at the 3’- and 5’-end led to an accumulation of the fluorescence signal to nuclear bodies (Figure 16). While internally labeled full-length sncRNA7SL still had diffuse signals within the nucleus and weaker accumulations in the cytoplasm (Figure 18 B), resembling the endogenous signal of sncRNA7SL. These results suggest that the 3’- and the 5’-end of sncRNA7SL is important for its correct localization purposes, possibly for binding to binding-proteins that are crucial for the endogenous localization of sncRNA7SL.

Interestingly, literature shows that small non-coding DR2 Alu repeat-induced RNA that are derived from DR2 Alu repeats of similar length to sncRNA7SL (28 nts to 65 nts) bind to Argonaute proteins, especially Ago3 (Hu et al., 2012). Which suggests sncRNA7SL to also possibly bind Ago3. Furthermore, it was found that for Argonaute binding the 3'- end and the 5'-end of the bound RNA are critical, since the MID domain needs to be able to bind the 5'-terminal nucleotide and the PAZ domain the last 3'-nucleotides (Boland et al., 2011; Yan et al., 2003; Duchaine and Fabian, 2019). This potentially leaves only a small middle part of the RNA reaching out of the central cleft of Argonaute RNAs for a functionally non-compromising fluorescence label.
These findings again cast doubt on the accuracy of studies on the localization of sncRNAs performed with a fluorescent label at the 5' or 3' end of the small RNAs under investigation. An example of studies done like this is Du et al., 2017, where they quantified colocalizations between a Cy5 labeled siRNA and PTMS, a pH-dependent nanomicelle, polyplexes. Here, it is possible that the quantification of colocalization between PTMS and the siRNA could shift if the Cy5 label prevents stable binding of siRNA with other binding partners. A similar case is Sonoda et al., 2021 where localization of fluorescence-labeled miRNAs was observed, and nucleic miRNA accumulation was quantified.

Another factor that shows how important the 3' end of miRNAs is for stable Argonaute binding is the binding of miRNAs to Ago1, which is already significantly impaired by a 2'-O-methylation at the 3' end (Tian et al., 2011). This further strengthens the suggestion that fluorescence labeling at the 3' end is likely to interfere with binding and thus with correct localization in the cell.

In my studies, it was shown that the accumulation of 3'- or a 5'-fluorescence labeled sncRNA7SL in nuclear bodies colocalize with Coilin protein in isolated cases (Figure 19 C,D), a known marker for Cajal bodies, and with NEAT1_2 RNA and NONO protein, both markers for paraspeckles.

Cajal bodies are known to have several functions, but one of the most studied is the modification of small nuclear RNAs (snRNAs), one of those modifications is the 2'-O-methylation of RNAs, protecting the RNA against alkaline hydrolysis as a result (Meier, 2017). This is especially interesting since sncRNA7SL was also annotated as piR1254. Even tough the endogenous modifications of this sncRNA are not yet known it was dubbed a piRNA due to its length, however, piRNAs are known to have a 5' phosphate

and a 2'-O-methylated at their 3' ends (Kirino and Mourelatos, 2007). Colocalization of sncRNA7SL and Cajal bodies could indicate that sncRNA7SL also gets 2'-O-methylated in those Cajal bodies, further linking sncRNA7SL to actual piRNAs. Furthermore, Cajal bodies were found to play a role in the regulation of gene expression by forming chromosomal gene clusters (Sawyer et al., 2016), hence colocalization of sncRNA7SL and Cajal bodies could indicate also a role of sncRNA7SL in the regulation of gene expression.

On the other hand, paraspeckles are also known to play a role in gene expression. They are able to retain A-to-I edited mRNAs in the nucleus, impairing translation processes (Darling and Uversky, 2023) this is especially interesting here since many possible target mRNA of sncRNA7SL contain inverted Alu repeat (*IRAlu)* elements. As double-stranded RNAs, *IRAlus* have the potential to be A-to-I edited and therefore to be stored in paraspeckles. Therefore, colocalization between paraspeckles (Figure 19, E and D; Figure 22) and sncRNA7SL further indicates that sncRNA7SL plays a role in gene expression.

A-to-I RNA editing is a global event in the human genome. It is the process of deamination of an Adenosine to an Inosine mediated by Adenosine Deaminase Acting on RNA (ADAR) (Nishikura, 2016). Due to these post-transcriptional modifications of mRNAs, the gene products are diversified (Maas et al., 2003). The most common targets of A-to-I editing are *IRAlus*, which are double-stranded structures that are located in but are not limited to untranslated regions of mRNAs (Athanasiadis et al., 2004). A-to-I editing was also linked to gene conservation and genes with A-to-I editing sites were shown to be increasingly expressed in various cancers like breast cancer and glioblastoma (Bahn et al., 2012). Interestingly the NONO ($p54^{nrb}$) protein, an essential part of paraspeckle formation was found to identify and bind inosine-containing RNAs resulting in the nuclear retention of those bound mRNAs in paraspeckles (Zhang and Carmichael, 2001). Furthermore, as mentioned before many degenerated sequences of sncRNA7SL and degenerated target sequences of sncRNA7SL are localized in *IRAlu* elements. In unpublished data, our laboratory looked into the 3' UTR of possible target mRNAs including *IRAlus* to see if there were A-to-I editing sites. Indeed, several A-to-I editing sites were found within or in close proximity to sncRNA7SL degenerated sequences and degenerated target sequences. This suggests that sncRNA7SL binding to those target sites may have an effect on A-

to-I editing and therefore on the expression of certain target sites containing mRNAs. However, it was also found that since A:U matched base pairs, as well as A-C mismatched base pairs, get A-to-I edited, RNA editing can have a stabilizing as well as a destabilizing effect on mRNAs (Shiromoto et al., 2020). Nevertheless, it was also found that these effects might cancel each other out depending on how many edition sites are present (Shiromoto et al., 2020).

Treatment of SK-N-SH cells with TSA, sncRNA7SL, sncRNActrl, or La depletion led to an increase in NEAT1_2 RNA, (Figure 25) suggesting an increase in paraspeckle formation in those cells. Unfortunately, localization studies with FAM-sncRNA7SL transfected and TSA, sncRNA7SL, sncRNActrl, or La depleted cells were not successful as co-transfection of these two components severely damaged the cells. However, all these tested conditions did indeed increase NEAT1_2 RNA expression, suggesting cellular stress, to be a major factor in increased paraspeckle formation, which is unsurprising, since paraspeckles are known as stress granulates (McCluggage and Fox, 2021). It is of interest that paraspeckles are widely known to play a role in various cancers. NEAT1 RNA was found to act as an oncogene in a variety of cancers like breast cancer, ovarian cancer, pancreatic cancer, and glioma among others, there NEAT1 RNA was found to be severely upregulated compared to healthy controls (Dong et al., 2018; Yu et al., 2017). In those cancers, NEAT1 is suggested to be a biomarker and is often linked to poor patient prognosis (Dong et al., 2018). However, in acute promyelocytic leukemia, NEAT1 was found to have tumor-suppressive characteristics, as it was down-regulated compared to healthy controls (Yu et al., 2017). Interestingly, in MYC-N amplified, so high-risk, neuroblastoma cells, were found to form low numbers of paraspeckles (Naveed et al., 2021). It was also found that an increase in NEAT1_2 RNA as well as a simultaneous decrease of NEAT1_1 RNA led to a decrease in cell proliferation, an increase in paraspeckle formation, and an increase in differentiation pathways (Naveed et al., 2021). As already mentioned, while NEAT1_2 was found to be essential for the paraspeckle formation, NEAT1_1 is not (Li et al., 2017). Furthermore, NEAT1_1 was found to localize outside of paraspeckles so-called micro speckles, suggesting to have paraspeckle independent functions (Li et al., 2017). Since this study found that sncRNA7SL increases NEAT1_2 level (Figure 25), this would further confirm sncRNA7SL as a tumor suppressor, as they affect cellular stress on neuroblastoma cells. Furthermore, it matches the previously made observation that sncRNA7SL exerts a particularly high

effect on high-risk neuroblastoma cell lines since an increase in NEAT1 RNA level would have an even stronger effect if base line NEAT1 RNA levels were really low.

Taken together, 3’ and 5’ ends were confirmed to be important for sncRNA7SL localization, indicating an important role of the 3’- and 5’-binding of this RNA. Fluorescence labels at the 3‘- or the 5‘-end led to an accumulation of sncRNA7SL signal to nuclear bodies, most likely being localized in Cajal bodies and paraspeckles. sncRNA7SL was also indicated in the regulation of the NEAT1 level. Internal fluorescence labeled sncRNA7SL was also mainly localized in the nucleus, now visualized as a diffuse signal, similar to the endogenous signal measured with MBs. This makes internally labeled sncRNA7SL a great tool for further studies about possible binding partners and functional mechanisms of sncRNA7SL in the cell. Furthermore, a cytoplasmic signal was also found, visualized as small cytoplasmic bodies, indicating not only nuclear functions of sncRNA7SL but cytoplasmic functions as well. Shortened sncRNA7SL of 22 nt or 23 nt of length was shown to be mainly localized in the cytoplasm, internal fluorescence labeling also revealed a slight shift in localization, with larger cytoplasmic bodies now forming. These results indicate that the nuclear import of sncRNA may be length dependent.

4.4 Potential binding partners of sncRNA7SL

KNL1 mRNA as well as Argonaute proteins were shown to be potential binding partners of sncRNA7SL (Figure 23, 30).

While KNL1 mRNA was mainly localized in the cytoplasm, there was still partial colocalization to be found between FAM-sncRNA7SL, NONO protein, and KNL1 mRNA within the nucleus, indicating localization in paraspeckles. Furthermore, members of our laboratory showed overexpression of sncRNA7SL to decrease KNL1 protein expression as well as mRNA level, compared to control transfected cells, indicating KNL1 mRNA to be indeed an interaction partner of sncRNA7SL. While a decrease of about 20% of KNL1 mRNA was shown to be caused by a high level of sncRNA7SL, sncRNA7SL inhibitors increased KNL1 mRNA level dramatically in SK-N-AS cells, but could not reverse the effect of sncRNA7SL on KNL1 mRNA level in Kelly cells. Furthermore, KNL1 protein levels were shown to decrease in sncRNA7SL overexpressed SK-N-AS and Kelly cells, 72 h after transfection (data not shown). Inhibition of KNL1 mRNA and protein expression further confirms sncRNA7SL as a

tumor suppressor, since a high level of KNL1 is a marker of various cancers, increasing their cells' ability to proliferate and invade therefore increasing metastasis and even often associated with poor patients' prognosis like in colorectal cancer (Bai et al., 2019), uterine corpus endometrial cancer (He et al., 2023) and neuroblastoma (Figure 1) among others.
Ago3-HA proteins, as well as Ago2-Ha and PIWIL4-HA proteins, were shown to be mainly localized in the cytoplasm visualized as hundreds of tiny nuclear bodies within one cell (Figure 28 B). This is interesting since sncRNA7SL-inte-FAM is mostly localized in the cytoplasm.

Since Ago2-HA, Ago3-HA, and PIWIL4-HA were all found to localize in the cytoplasm, the binding of sncRNA7SL would likely indicate a role in post-transcriptional silencing. Ago proteins are known to bind to small non-coding RNA like miRNA as well as siRNA in the cytoplasm, building an RNA-induced silencing complex, and controlling mRNA expression (Nakanishi, 2016). Another indication for sncRNA7SL to be involved in post-transcriptional silencing and be part of an RNA-induced silencing complex is the partial colocalization found between sncRNA7SL-inte-FAM and EDC4 protein in the cytoplasm of neuroblastoma cells (Figure 31; Supplementary Figure 9). EDC4 protein plays a role in post-transcriptional silencing and is a crucial part of P-bodies (Seto et al., 2015). Moreover, sncRNA7SL-Δ2-inte-Cy5, mimicking miRNAs with its similar length, was also shown to partially colocalize with EDC4 protein (Figure 32). Hence, a possible mechanism for sncRNA7SL to play a role in post-transcriptional gene silencing would be for sncRNA7SL to bind to an Argonaute protein in the cytoplasm, which would lead to a RISC assembly and degradation of targets by decapping.

Another important mechanism to influence gene expression is transcriptional gene silencing (reviewed in Weinberg and Morris, 2016). piRNAs of similar length to sncRNA7SL are known to bind PIWI proteins, influencing transcriptional as well as post-transcriptional gene silencing (Rojas-Ríos and Simonelig, 2018). However, piRNAs were also found to bind nuclear PIWI proteins in mice (MIWI2), binding to nuclear nascent RNAs and thereby repressing the transcription of transposable elements by DNA methylation as well as histone modification (Ernst et al., 2017). Therefore, a possible mechanism for sncRNA7SL to play a role in transcriptional gene silencing could be by binding of PIWIL4, thereby being transported into the nucleus and playing a role in target methylation. However, since PIWIL4-HA was mainly shown

to localize in the cytoplasm (Figure 28 B), the next step would be to find a way to localize endogenous PIWIL4 in the cell.

In vitro RNA binding assays showed a strong binding between sncRNA7SL-inte-FAM and Ago3 as well as PIWIL4 while binding to Ago2 was much weaker (Figure 30 B, C). However, as mentioned above PIWIL4 RNA levels are very low in neuroblastoma cells compared to Ago1-4 RNA level (Supplementary Figure 5 A). Hence, in a cellular context sncRNA7SL-inte-FAM binding to Ago3 is likely more important in neuroblastoma compared to sncRNA7SL-inte-FAM binding to PIWIL4. There are different possible causes for lower Ago2 binding to sncRNA7SL-inte-FAM compared to Ago3 and PIWIL4. First of all, is the length of sncRNA7SL-inte-FAM, since it was already shown for Ago3 to bind sncRNA between 28 nt and 65 nt (Hu et al., 2012), while PIWIL4 is known to bind piRNAs that range between 24 and 32 nts in length (Li et al., 2021), while Ago2 binds smaller RNAs like miRNAs, helping them in their maturation process (Bossé and Simard, 2010). Furthermore, the sncRNA7SL-inte-FAM Oligo was modified to carry a 5’ phosphate as well as a 2’-O-methlyation at its 3’-end, mimicking piRNA modifications (Tian et al., 2011). PIWIL proteins are known to preferentially target piRNAs with a 3’-O-methyl group, compared to small RNA with 2’OH ends like miRNAs. The reason for this is the structure of their binding pocket, while the binding pocket of human PIWIL1 displays a hydrophobic cleft, allowing 2’-O-methylation binding, human Ago1 shows a more restricted binding pocket resulting in the preferential binding of a 2’-OH group over a 2’-O-methylation, avoiding steric incompatibility between the two components (Tian et al., 2011). However, while Ago3 binding of sncRNA7SL was identified as a good candidate for post-transcriptional gene silencing, PIWIL4 binding of sncRNA7SL might indicate transcriptional silencing mechanisms. PIWIL4 was already shown to play a role in chromatin remodeling by histone methylation of specific loci, resulting in the downregulation of transcription in human somatic cells (Sugimoto et al., 2007). Furthermore, the first epigenetic data produced in our laboratory, showed a decrease of Acetylation at H3K9 48 h after sncRNA7SL transfection, indicating sncRNA7SL to indeed play a role in transcriptional repression of certain mRNAs (data not shown).

Taken together sncRNA7SL was shown to bind KNL1 mRNA *in vivo* as well as Ago3 and PIWIL4 proteins *in vitro*. In first experiments in our workgroup KNL1 mRNA as well as protein level were shown to decrease in sncRNA7SL overexpressed cells,

strengthening KNL1 as a target of sncRNA7SL and further confirming sncRNA7SL as a tumor suppressor. All HA-tagged Argonaute proteins were found to localize in the cytoplasm, therefore binding of sncRNA7SL to Argonaute proteins indicates a possible role of sncRNA7SL in post-transcriptional gene silencing. Compared to Ago 1-4 RNA level, RNA sequencing showed a very low expression level of PIWIL4 RNA, indicating a bigger *in vivo* relevance of sncRNA7SL and Ago3 protein binding in neuroblastoma cell lines. Furthermore, binding between Ago2 protein and sncRNA7SL-inte-FAM was quite weak, which could be a result of Ago2 preferably binding shorter RNAs, or because of the modifications, attached to the synthetic sncRNA7SL.

4.5 Outlook

To better understand the mechanisms of how sncRNA7SL acts in neuroblastoma cells, this study needs to be continued. For this purpose, the sncRNA-binding assays should be repeated and sequenced to confirm sncRNA7SL binding with Ago3 and PIWIL4. Also colocalization studies could be performed between sncRNA7SL-inte-FAM and the various HA-tagged Argonaute proteins. Furthermore, sncRNA7SL oligos should be designed with an internal fluorescence group but with a 2'-OH instead of a 2'-O-methylation at its 3'-end. To see if binding of Argonaute proteins shifts among this modification change. In addition, the binding between sncRNA7SL and KNL1 mRNA should be investigated in more detail, and further studies investigating the effect of sncRNA7SL level on KNL1 complexes are already ongoing in our laboratory. In addition, colocalization studies between sncRNA7SL-inte-FAM and KNL1 mRNA could be performed and the effect of sncRNA7SL on more potential targets should be analyzed. Lastly, it would be exciting to extend the studies in the field of epigenetics to gain further insights into possible sncRNA7SL-dependent transcriptional silencing.

5. Abstract

The RNA-binding protein La plays a major role in the processing and maturation process of RNA polymerase III (Pol III) precursor transcripts, such as tRNA and the long non-coding RNA 7SL. Depletion of the La protein in cancer cells causes aberrant expression of small non-coding (snc) RNAs derived from RNA Pol III transcripts, as recently demonstrated for tRNA-derived miRNAs.

Herein a sncRNA was identified, referred to as sncRNA7SL, which is more than twofold upregulated in La-depleted cancer cells. The sncRNA7SL sequence is identical to the 3'-end of the 7SL RNA transcript, the ancestor of all Alu elements.

In the first objective, sncRNA7SL was shown to have tumor suppressive properties in neuroblastoma, since sncRNA7SL overexpression showed a decrease in proliferation, viability, mobility, spheroid growth, and BMI1 protein expression in neuroblastoma cells, while also resulting in a G1 arrest. Moreover, inhibition of sncRNA7SL increased viability in neuroblastoma and Ewing sarcoma cell lines.

In a second objective, the application of Molecular beacons revealed that endogenous sncRNA7SL mainly localized in the nucleus with a slight signal in the cytoplasm, while endogenous 7SL RNA was mainly localized in the cytoplasm.

The third objective aimed to optimize synthetic fluorescence-labeled sncRNA7SL oligoribonucleotides as toop applicable for localization and binding studies. It was revealed that 5'- and 3'-ends are of critical importance the correct localization of sncRNA7SL, showing that oligonucleotides labeled at the 3'- or 5'-end accumulated in the nucleus as nuclear bodies, while internally labeled sncRNA7SL showed a diffuse signal in the nucleus and therefore resembled the endogenous localization of sncRNA7SL. In addition, internally labeled sncRNA7SL accumulated also to some extent in small cytoplasmic bodies. RNA FISH and immunofluorescence studies revealed that some of those nuclear bodies are paraspeckles. Interestingly paraspeckles are known to store mRNAs containing *inverted repeat Alu elements*. Since the sncRNA7SL sequence was found in the Alu element of the 7SL precursor those sequences are potential targets for sncRNA7SL. To analyze colocalization between FAM-sncRNA7SL and KNL1 mRNA, containing *IRAlu* elements in its 3'UTR, was investigated. Partial colocalization of FAM-sncRNA7SL and KNL1 mRNA was confirmed. Furthermore, partial colocalization between sncRNA7SL-inte-FAM and EDC4 protein was found. sncRNA7SL binding of cytoplasmic Argonauts (see below) and colocalization with EDC4 protein indicates the formation of an RNA silencing

complex and a potential role of sncRNA7SL in post-transcriptional gene silencing. These studies demonstrate that internally fluorescent labeled sncRNA are powerful tools to study cellular localization as well as colocalization with other RNAs and proteins.

As a last objective, the binding of Argonauts, which are known binding partners of small non-coding RNAs, to sncRNA7SL was investigated. Binding assays between HA-tagged Argonauts (Ago2-HA, Ago3-HA, PIWIL4-HA) and sncRNA7SL-inte-FAM revealed strong *in vitro* binding between Ago3-HA or PIWIL4-HA and sncRNA7SL-inte-FAM. Strikingly, this binding was not observed when the sncRNA7SL was end labled, underscoring the importance of free 5'- and 3'-ends and demonstated that synthetics and internal labeled sncRNA7SL can be used in live cell imging as well as in binding studies.

Taken together, the results suggestes that the tumor suppressive function of sncRNA7SL is mediated in part via posttranscriptional gene silencing in the cytoplamsn and, based on the colocalization with target mRNA in paraspeckle, a yet enigmatic nuclear mechanism. The development of sncRNA7SL-inte-FAM will prove to be key for further studies on the role and function of sncRNA7SL.

6. Supplements

6.1 Supplemental Figures

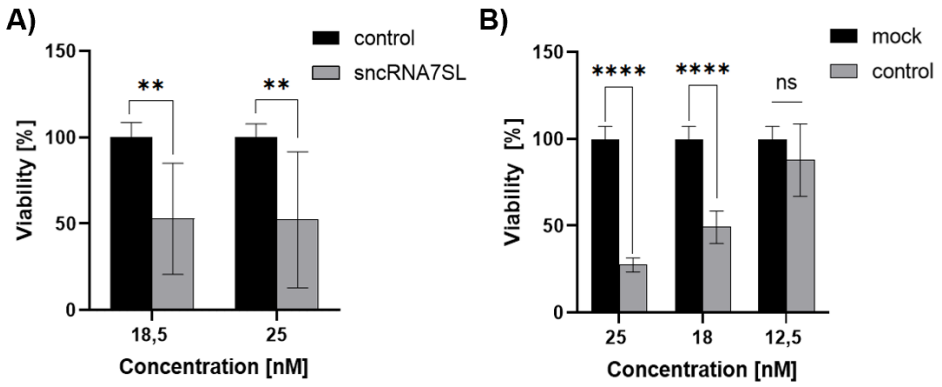

Supplementary Figure 1. sncRNA7SL mimics reduce viability in Kelly cells overexpression of RNA reduces viability.
(A) Overexpression of sncRNA7SL correlates with a decrease in viability in different cancer cell lines 96 h after transfection of 18.5 nM and 25 nM sncRNA7SL mimics compared to transfection with 18.5 nM or 25 nM sncRNActrl, as determined in three independent experiments performed in triplicates. **(B)** 25 nM and 18 nM of sncRNActrl transfection significantly reduced viability compared to mock transfection controls only treated with transfection reagent, as determined in two independent experiments performed in triplicates. All results were determined as mean SD (error bars). P value * ≤ 0.05,** ≤ 0.01, *** ≤ 0.001 and,**** ≤ 0.0001 was determined using paired t-test with Prism 8.4 (Graph Pad Software).

A)

Molecular beacons:

MBsncRNA-1	5'-FAM-cgcgcg**AGAGACGGGGTCTCGCTATGTTGCTCAGGCT**cgcgcg-3'-DAB
MBsncRNA	5'-FAM- cgcg**AGAGACGGGGTCTCGCTATGTTGCTCAGGCT**cgcg---3'-DAB
MBsncRNA-2A	5'-FAM-cgcgca----**ACGGGGTaTCGaTATGTTGCTCAGGC-a**gcgcg-3'- DAB
MB7SL	5'-Cy5-cgcga**GATCGGCATAGCGCACTACAGCCCAGAACT**cgcg-3'- BHQ2
MBcon	5'-FAM-cgcg**TCGGACTCGTTGTATCGCTCTGGGGCAGAGAT**cgcg-3'-DAB
MB6145	5'-FAM-cgcgcg**TGAGGCGAACGTGATAACCACTACACTACGGA**cgcgcg-3'-DAB

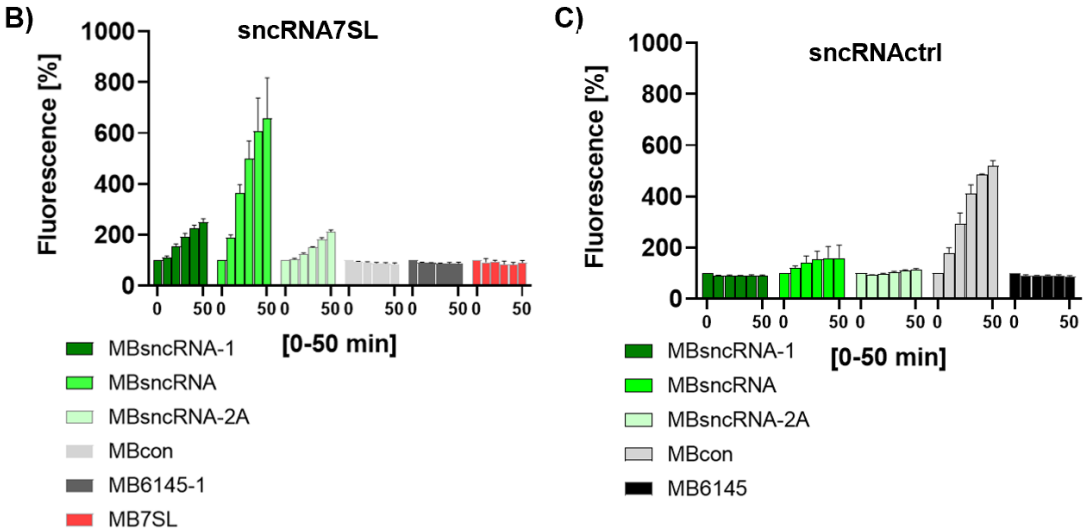

Supplementary Figure 2. MB Sequences and target specificity of MBs.

(A) Sequences of MB used in this study. **(B)** 100 nM of MBs were incubated with 500 nM of sncRNA7SL. **(C)** 100 nM of MBs were incubated with 500 nM of sncRNA con.
All reactions were incubated for 0, 10, 20, 30, 40, 50 min at 37°C in ICN buffer and determined in three independent experiments performed in triplicates. All results were determined as mean SD (error bars) using paired t-test with Prism 8.4 (Graph Pad Software). Experiments were performed by the laboratory technician. Figure submitted for Weigert et al., manuscript under revision.

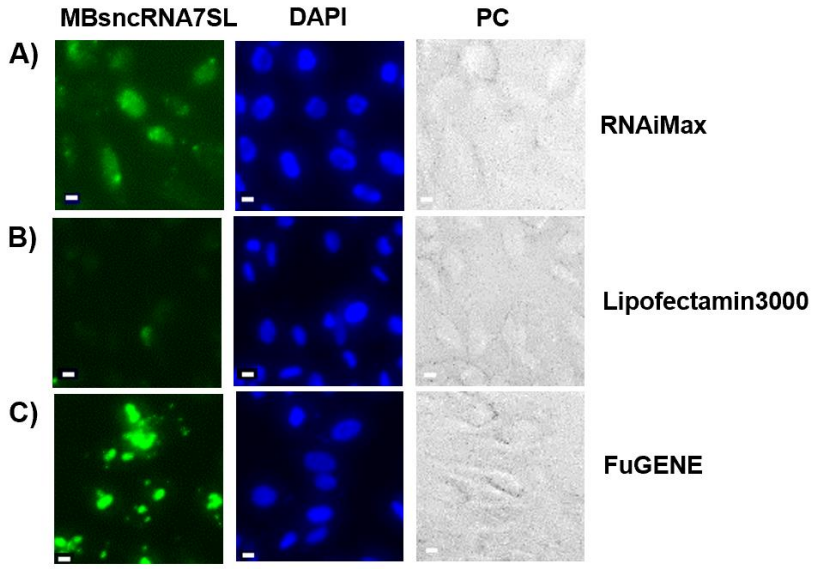

Supplementary Figure 3. Transfection of MBsncRNA7SL with different transfection reagents.
(A) SK-N-SH cells were transfected with 12.5 nM MBsncRNA7SL using RNAiMAx. The signal was mainly concentrated in the nucleus. **(B)** SK-N-SH cells were transfected with 12.5 nM MBsncRNA7SL using Lipofectamine 300 as a transfection reagent. Very low signal strength was detected. **(C)** SK-N-SH cells were transfected with 12.5 nM MBsncRNA7SL using FuGENE. The signal is very strong but unspecific. Accumulation of fluorescent signal in the cytoplasm or even outside of cells.
All images were taken 24 hours after transfection of Molecular Beacon in live cells with a Keyence BZX fluorescence microscope, with a magnification of 20x. The scale bar measures 10 µm.

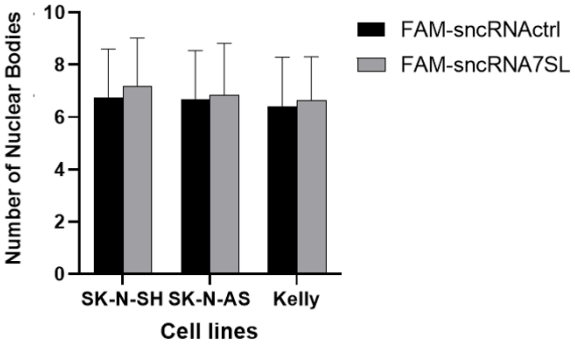

Supplementary Figure 4. Quantification of nuclear dots per cell in different neuroblastoma cell lines.
Different neuroblastoma cell lines were transfected with 12.5 nM FAM-sncRNA7SL of FAM-sncRNActrl. 24 h after transfection nuclei were stained and live cell imaging microscopy was done using a Keyence BZX fluorescence microscope. Nuclear dots of several cells were quantified and compared between different cell lines. There was no significant difference in the number of nuclear dots in the different cell lines. An average of 7 nuclear dots per cell was quantified. All results were determined as mean SD (error bars) with Prism 8.4 (Graph Pad Software).

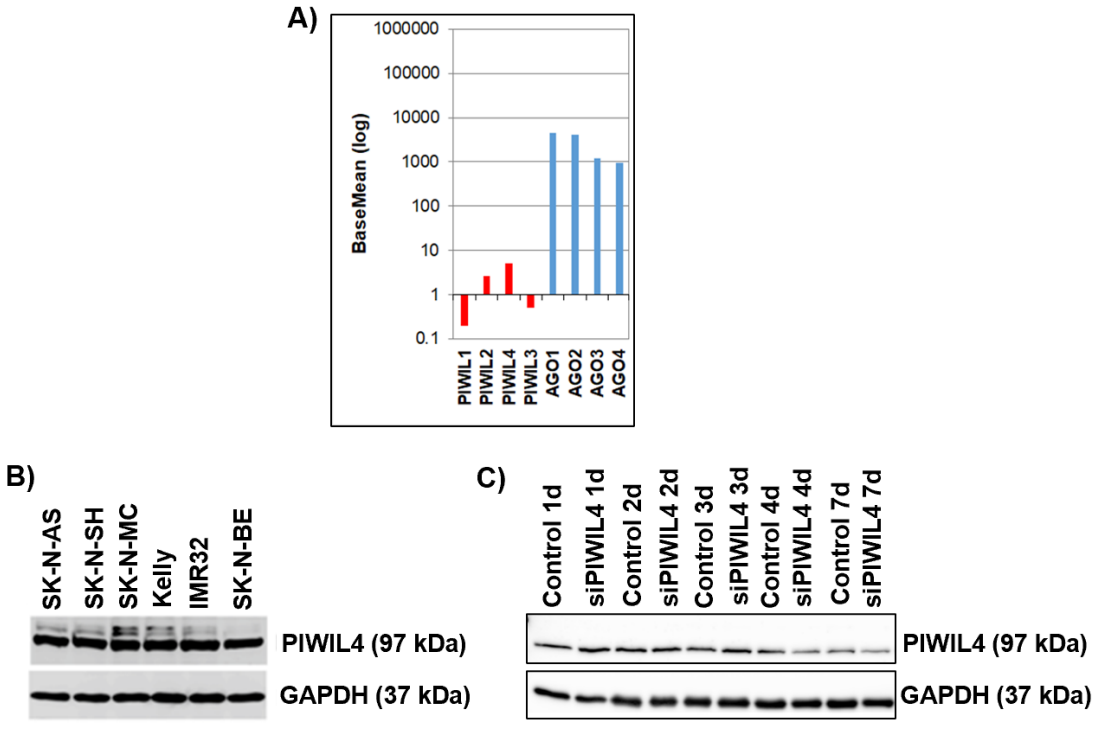

Supplementary Figure 5. RNA seq shows a low level of PIWIL but a high level of Ago RNA. Western Blot analysis shows a high level of PIWIL4.
(A) RNA seq of Kelly cells shows quite low RNA levels of PIWIL1-4 and high levels of Ago1-4. **(B)** Western blot analysis shows high protein expression of PIWIL4 in various cell lines. **(C)** Depletion of PIWIL4 in Kelly cells proves PIWIL4 antibody as unspecific. All experiments were performed by our technical assistant and former lab members.

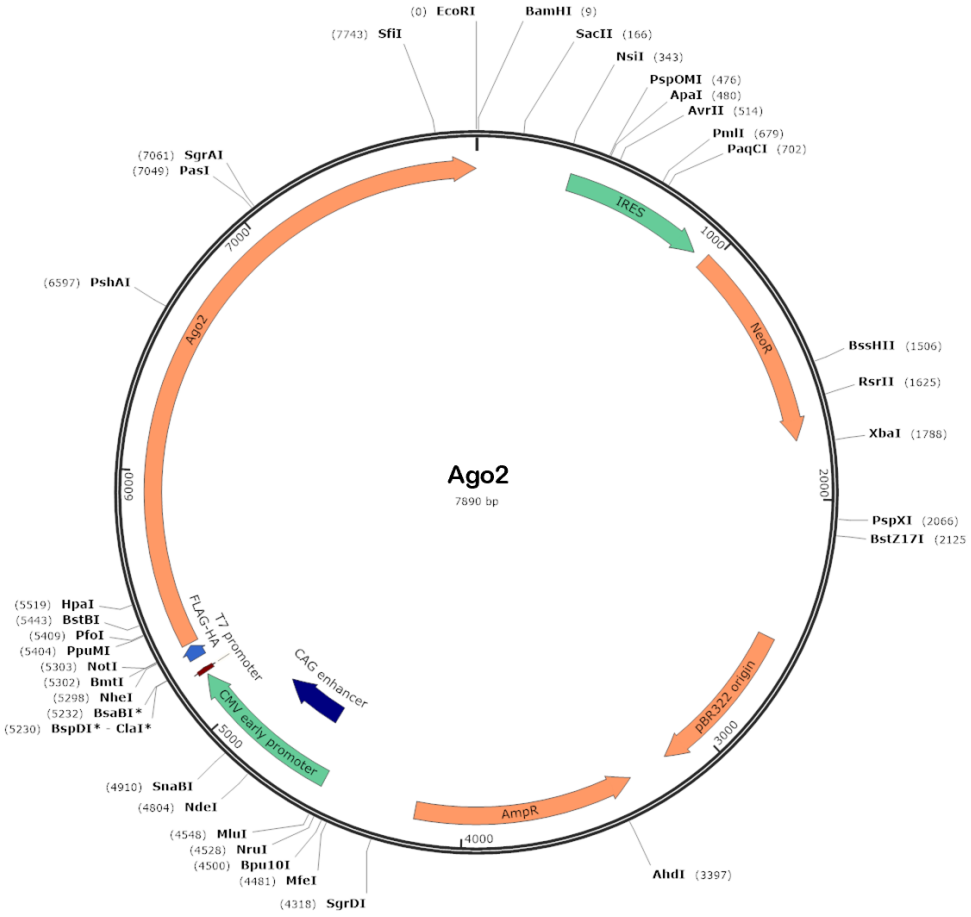
Ago2
7890 bp
(0) EcoRI
BamHI (9)
(7743) SfiI
SacII (166)
NsiI (343)
PspOMI (476)
ApaI (480)
AvrII (514)
PmlI (679)
PaqCI (702)
(7061) SgrAI
(7049) PasI
(6597) PshAI
BssHII (1506)
RsrII (1625)
XbaI (1788)
PspXI (2066)
BstZ17I (2125
(5519) HpaI
(5443) BstBI
(5409) PfoI
(5404) PpuMI
(5303) NotI
(5302) BmtI
(5298) NheI
(5232) BsaBI*
(5230) BspDI* - ClaI*
(4910) SnaBI
(4804) NdeI
(4548) MluI
(4528) NruI
(4500) Bpu10I
(4481) MfeI
(4318) SgrDI
(3397) AhdI
IRES
NeoR
pBR322 origin
AmpR
CMV early promoter
CAG enhancer
T7 promoter
FLAG-HA
Ago2
1000
2000
3000
4000
5000
6000
7000

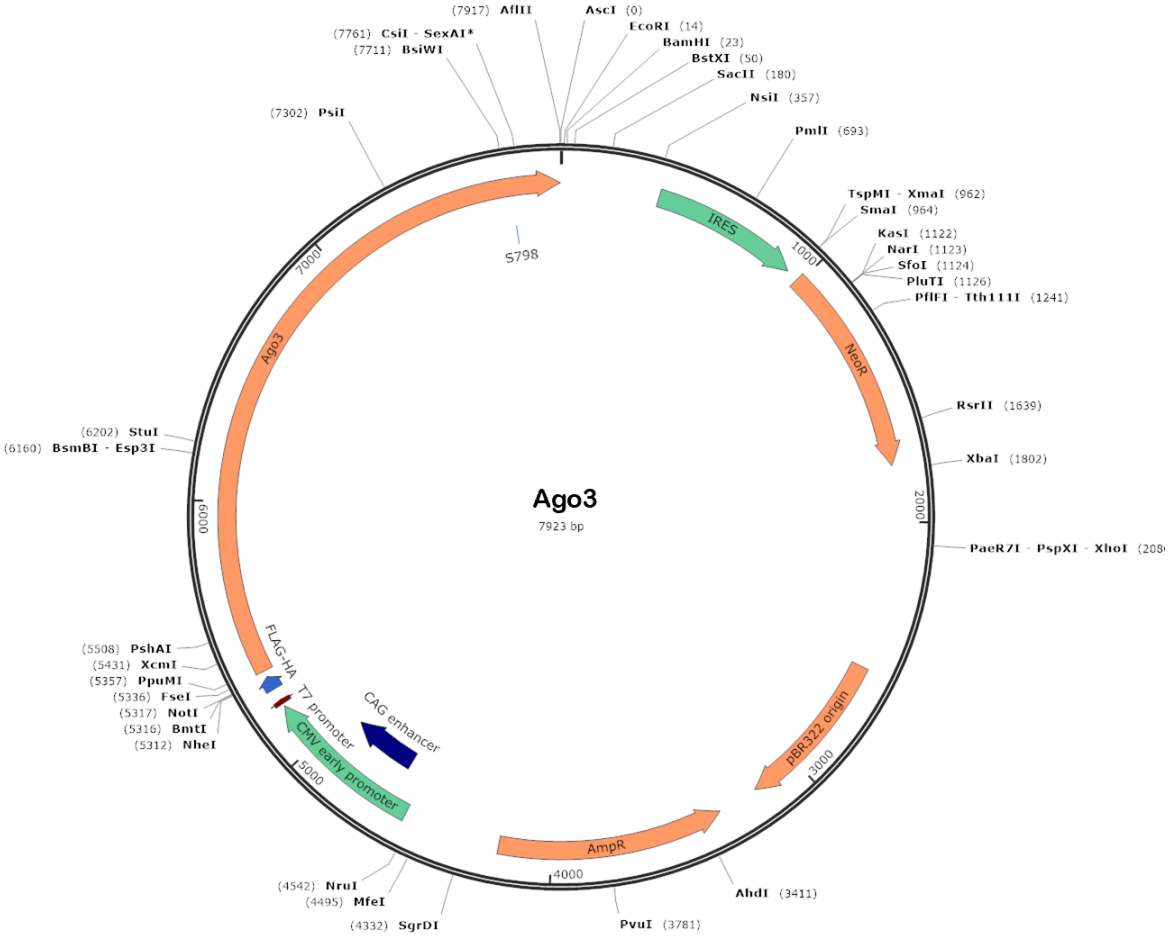
Ago3
7923 bp
(7917) AflII
AscI (0)
EcoRI (14)
BamHI (23)
BstXI (50)
SacII (180)
NsiI (357)
PmlI (693)
TspMI - XmaI (962)
SmaI (964)
KasI (1122)
NarI (1123)
SfoI (1124)
PluTI (1126)
PflFI - Tth111I (1241)
RsrII (1639)
XbaI (1802)
PaeR7I - PspXI - XhoI (208
(7761) CsiI - SexAI*
(7711) BsiWI
(7302) PsiI
S798
IRES
NeoR
Ago3
FLAG-HA
T7 promoter
CAG enhancer
CMV early promoter
pBR322 origin
AmpR
(6202) StuI
(6160) BsmBI - Esp3I
(5508) PshAI
(5431) XcmI
(5357) PpuMI
(5336) FseI
(5317) NotI
(5316) BmtI
(5312) NheI
(4542) NruI
(4495) MfeI
(4332) SgrDI
PvuI (3781)
AhdI (3411)
1000
2000
3000
4000
5000
6000
7000

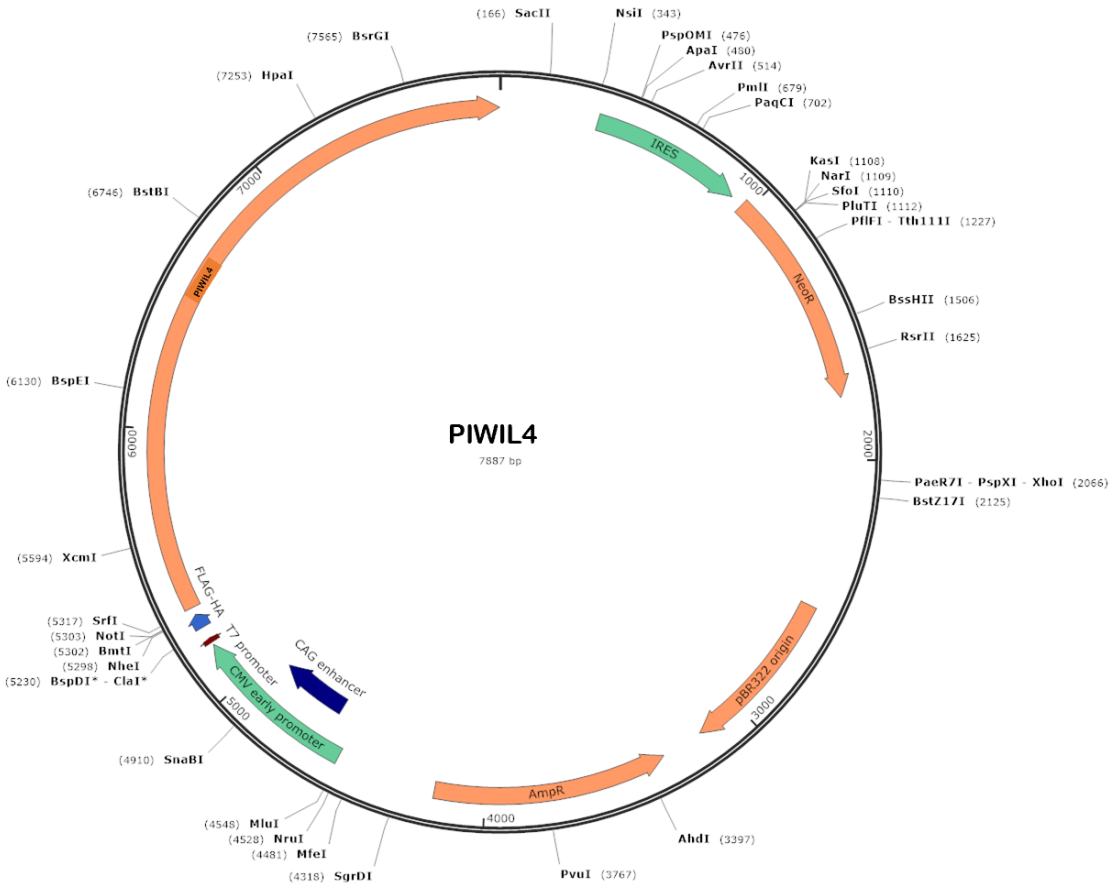
PIWIL4
7887 bp
(166) SacII
NsiI (343)
PspOMI (476)
ApaI (480)
AvrII (514)
PmlI (679)
PaqCI (702)
KasI (1108)
NarI (1109)
SfoI (1110)
PluTI (1112)
PflFI - Tth111I (1227)
BssHII (1506)
RsrII (1625)
PaeR7I - PspXI - XhoI (2066)
BstZ17I (2125)
pBR322 origin
AmpR
AhdI (3397)
PvuI (3767)
SgrDI (4318)
MfeI (4481)
NruI (4528)
MluI (4548)
SnaBI (4910)
CMV early promoter
CAG enhancer
T7 promoter
FLAG-HA
SrfI (5317)
NotI (5303)
BmtI (5302)
NheI (5298)
BspDI* - ClaI* (5230)
XcmI (5594)
BspEI (6130)
BsiBI (6746)
HpaI (7253)
BsrGI (7565)
PIWIL4
IRES
NeoR
1000
2000
3000
4000
5000
6000
7000

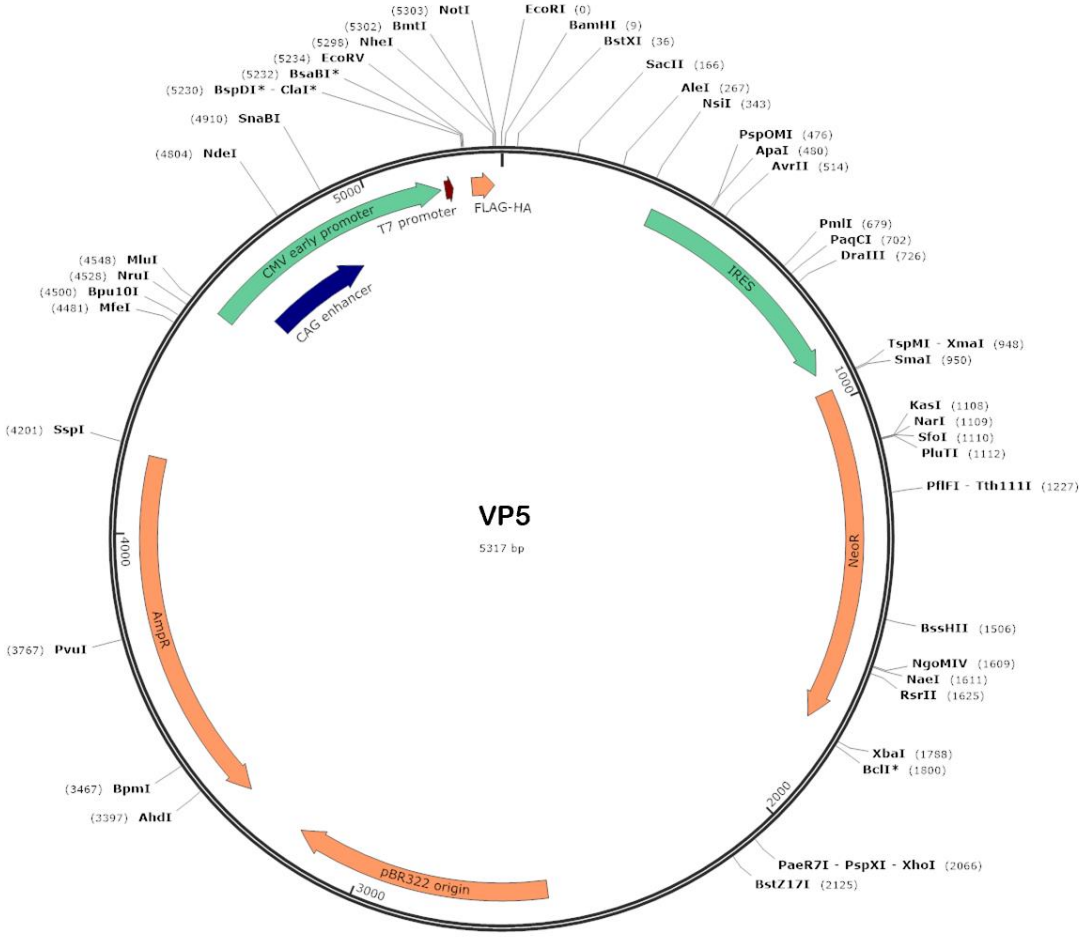

Supplementary Figure 6. **Plasmid cards of HA-tagged Plasmids.**
Plasmid cards of HA-tagged Plasmids Ago2-HA, Ago3-HA, PIWIL4-HA, and VP5-HA provided by AG Meister.

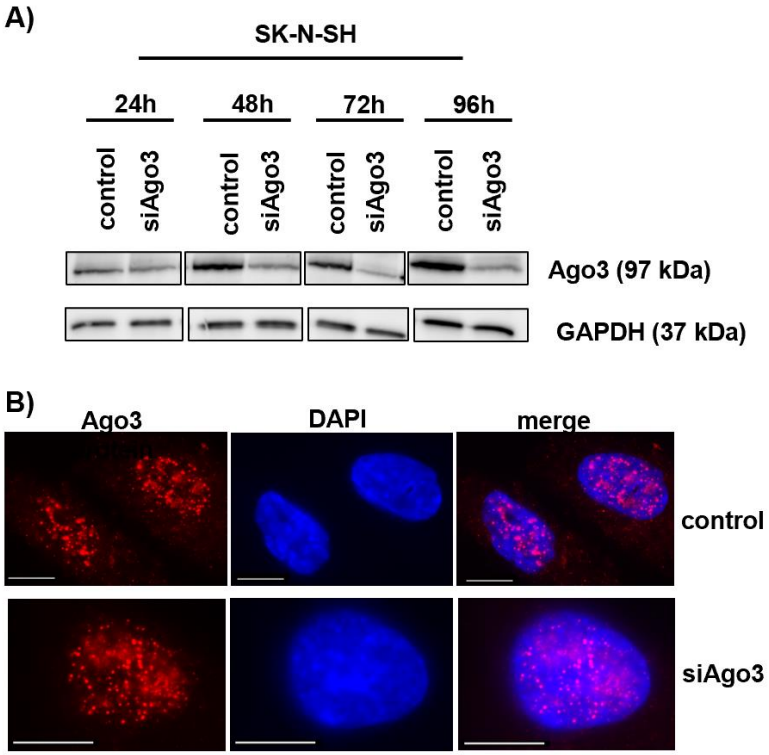

Supplementary Figure 7. Localization of Ago3 protein and Ago3 depletion in SK-N-SH cells.
(A) Western Blot analysis of Ago3 protein expression in Ago3 depleted SK-N-SH cells at different time points. **(B)** Immunofluorescence of SK-N-SH cells fixated 72h after Ago3 depletion and its respective control cells. No difference of signal between the two different groups could be visualized, as determined in two independent experiments.

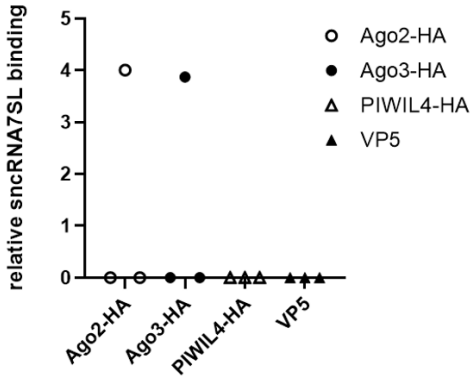

Supplementary Figure 8. The binding of FAM-sncRNA7SL to Argonaute proteins cannot be reproduced reliably.
Results of fluorescence measurements of FAM-sncRNA7SL binding assays in three independent experiments. In one Experiment Ago2-HA and Ago2-HA show FAM-sncRNA7SL binding. In two other experiments there is no bindnig between FAM-sncRNA7SL and

Argnoaute proteins. The results of FAM-sncRNA7SL binding of Ago2-HA and Ago3-HA could not be reproduced. All results were determined with Prism 8.4 (Graph Pad Software).

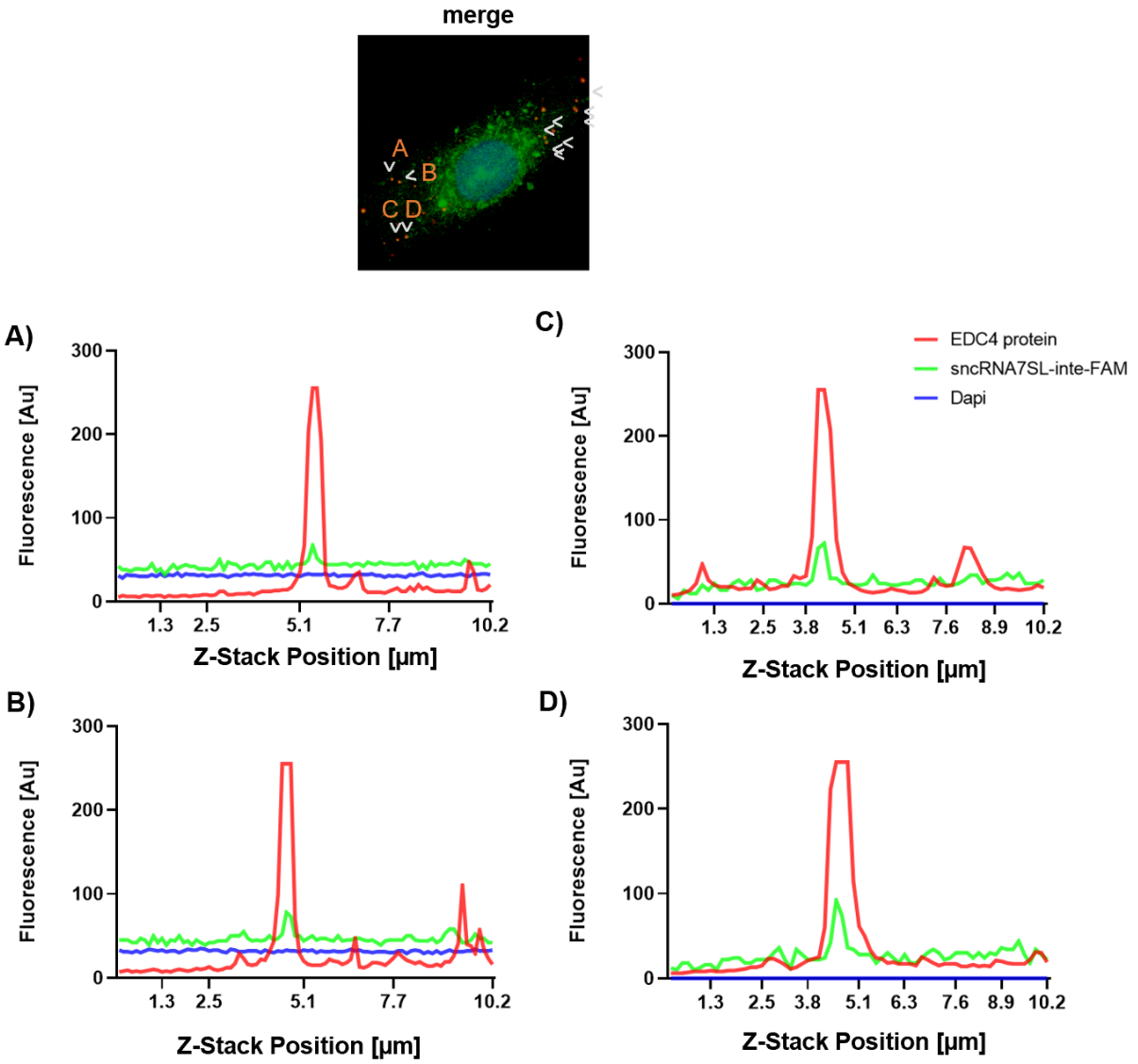

Supplementary Figure 9. Partial colocalization of internally fluorescent labeled sncRNA7SL and EDC4 protein in the cytoplasm.
(A, B, C, D) Line Profiles of colocalized sncRNA7SL-inte-FAM and EDC4 protein in the cytoplasm of SK-NSH cells. Orange letters with white arrows in the picture on the left indicate which line profile belongs to which point of colocalization.

6.2 Abbreviations

A	
A	Adenine
ADAR	Adenosine Deaminase acting on RNA
Ago	Argonaute
Amp	Ampicillin
APS	Ammonium persulfate
A-to-I	Adenosine to Inosine
B	
BHQ2	Black Hole Quencher 2
BMI1	B-lymphoma Moloney murine leukemia virus insertion region-1
BSA	Bovine serum albumin
C	
C	Cytosine
Casp3	Caspase 3
CCR4-NOT	Carbon catabolite repressor 4-negative on TATA
cDNA	Complementary DNA
Con	Control
C-terminus	Carboxyl-terminus
Ctrl	Control
Cy5	Cyanine 5
D	
DAB	Dabcyl
DAPI	4',6-Diamidino-2-phenylindole
DCML	Detergent cytoplasmic membrane lysis buffer
DCP	Decapping protein
DGCR8	DiGeorge syndrome critical region 8
DMEM	Dulbecco’s modified Eagle’s medium
DMSO	Dimethylsulfoxide
DNA	Desoxyribonucleic acid
DTT	Dithiothreitol
E	
E.coli	*Escherichia coli*
EDC4	Enhancer of mRNA Decapping 4
EDTA	Ethylenediaminetetraacetic acid
eIF	Eukaryotic translation initiation factor
EMEM	Eagle’s minimum essential medium
ER	Endoplasmatic Reticulum
EtOH	Ethanol
F	
FACS	Fluorescence-activated cell sorting
FAM	Carboxyfluorescein
FBS	Fetal Bovine Serum
G	
g	Gram

G	Guanine
GAPDH	Glycerinaldehyd-3-phosphate-dehydrogenase
GFP	Green fluorescent protein
GW182/TNRC6A	Trinucleotide repeat-containing 6
H	
h	Hour
HA	Human influenza hemagglutinin
Ham's F12	F12 Nutrient Medium
HEK293	Human embryonic kidney 293
HCl	Hydrochloric acid
HDAC	Histon-Deacetylase
HEPES	4-(2-hydroxyethyl)-1-piperazineethanesulfonic acid
H_2O	Water
I	
I	Inosine
IRAlu	Inverted repeat Alu
K	
kb	Kilo base pair
kDa	Kilodalton
KCl	Potassium chloride
Kelly	Human MYCN-amplified neuroblastoma cell line
KNL1	Kinetochor Scaffold 1
L	
l	Liter
LB	Lysogeny Broth
M	
M	Molar
mA	Milliampere
MB	Molecular Beacon
$MgCl_2$	Magnesium Chloride
ml	Mililiter
mM	Milimolar
MID domain	Middle domain
min	Minute
miRBase	MiRNA database
miRNA	MicroRNA
mRNA	Messenger RNA
MTT	Thiazolyl Blue Tetrazolium Bromide
N	
NADH	Nicotinamideadenindinucleotid
NADPH	Nicotinamideadenindinucleotidphophate
NB	Nuclear bodies
NEAT1	Nuclear Paraspeckle Assembly Transcript 1
ng	Nanogram
nM	Nanomolar
NONO	Non-POU domain-containing octamer-binding protein

Nt	Nucleotide
N-terminus	Amino-terminus
NP40	Nonident P-40
O	
Oligo	Oligonucleotide
Opti-MEM	Improved minimal essential medium
ORF	Open reading frame
P	
P	Phosphate
p21	CDK-Inhibitor 1
TP53	Tumor suppressor gen 53
PABP	Poly(A)-binding protein
PAGE	Polyacrylamide gel electrophoresis
PAN2 –PAN3	Poly (A)-binding protein-dependent poly (A) ribonuclease 2-3
PAZ	PIWI-ARGONAUTE-ZWILLE
PBS	Phosphate buffered saline
PCR	Polymerase chain reaction
PI	Propidium iodide
piRNA	PIWI-interacting RNA
PIWI	P-element induced wimpy testis
pmol	Picomolar
Pol III	RNA Polymerase III
PSPC1	Paraspeckle Component 1
Pre	Precursor
PTGS	Post-transcriptional gene silencing
Q	
qPCR	Quantitative polymerase chain reaction
R	
RCD	RNA Chaperone Domain
RBP	RNA binding protein
RIP	RNA immunoprecipitation
RISC	RNA-induced silencing complex
RNA	Ribonucleic acid
RNase	Ribonuclease
RNP	Ribonucleoprotein
rpm	Rounds per minute
RPMI 1640	Roswell Park Memorial Institute 1640
RRM	RNA recognition motif
RT	Room Temperature
RT	Realtime
S	
s	Second
SC35	Serine/arginine-rich splicing factor-like protein
SD	Standard deviation
SDS	Sodium dodecyl sulfate
siRNA	Small interfering RNA

SINE	Short interspersed nuclear element
siRNAs	Small interfering RNA
SK-N-AS	Human Myc-N not amplified neuroblastoma cell line
SK-N-MC	Human brain neuroepithelioma cell line (Ewing Sarcoma)
SK-N-SH	Human Myc-N not amplified neuroblastoma cell line
sncRNA	Small non-coding RNA
snRNA	Small nuclear RNA
SOC-Medium	Super Optimal Broth medium with glucose
SRP	Signal recognition particle
T	
T	Thymine
TEMED	Tetraacetylethylenediamine
TGS	Transcriptional gene silencing
tRNA	Transfer RNA
Tris	Tris(hydroxymethyl)aminomethane
TSA	Trichostatin A
TxRED	Texas RED
U	
U	Unit
U	Uracil
U2-OS	Human Bone Osteosarcoma Epithelial cell line
UTR	Untranslated region
V	
V	Volt
W	
WB	Western Blot
X	
xg	Times gravity
XRN	5’-3’ exoribonuclease
µ	
µg	Microgram
µl	Microliter
µM	Micromolar
3’	Three prime
5’	Five prime
3CholTEG	3’cholesterol-TEG
2D	Two-dimensional
3D	Three-dimensional
%	Percent
°C	Degree Celsius

6.3 List of Figures

6.4 List of Tables

7. References

Abdelmohsen, Kotb; Panda, Amaresh C.; Kang, Min-Ju; Guo, Rong; Kim, Jiyoung; Grammatikakis, Ioannis et al. (2014): 7SL RNA represses p53 translation by competing with HuR. In: *Nucleic Acids Research* 42 (15), S. 10099–10111. DOI: 10.1093/nar/gku686.

Alshaer, Walhan; Zureigat, Hadil; Al Karaki, Arwa; Al-Kadash, Abdulfattah; Gharaibeh, Lobna; Hatmal, Ma'mon M. et al. (2021): siRNA: Mechanism of action, challenges, and therapeutic approaches. In: *European journal of pharmacology* 905, S. 174178. DOI: 10.1016/j.ejphar.2021.174178.

An, Haiyan; Tan, Jing Tong; Shelkovnikova, Tatyana A. (2019): Stress granules regulate stress-induced paraspeckle assembly. In: *The Journal of cell biology* 218 (12), S. 4127–4140. DOI: 10.1083/jcb.201904098.

Andersen, Jens S.; Lyon, Carol E.; Fox, Archa H.; Leung, Anthony K. L.; Lam, Yun Wah; Steen, Hanno et al. (2002): Directed proteomic analysis of the human nucleolus. In: *Current biology : CB* 12 (1), S. 1–11. DOI: 10.1016/S0960-9822(01)00650-9.

Anzelon, Todd A.; Chowdhury, Saikat; Hughes, Siobhan M.; Xiao, Yao; Lander, Gabriel C.; MacRae, Ian J. (2021): Structural basis for piRNA targeting. In: *Nature* 597 (7875), S. 285–289. DOI: 10.1038/s41586-021-03856-x.

Aravin, Alexei; Gaidatzis, Dimos; Pfeffer, Sébastien; Lagos-Quintana, Mariana; Landgraf, Pablo; Iovino, Nicola et al. (2006): A novel class of small RNAs bind to MILI protein in mouse testes. In: *Nature* 442 (7099), S. 203–207. DOI: 10.1038/nature04916.

Athanasiadis, Alekos; Rich, Alexander; Maas, Stefan (2004): Widespread A-to-I RNA editing of Alu-containing mRNAs in the human transcriptome. In: *PLoS biology* 2 (12), e391. DOI: 10.1371/journal.pbio.0020391.

Ausserlechner, M. J.; Obexer, P.; Geley, S.; Kofler, R. (2005): G1 arrest by p16INK4A uncouples growth from cell cycle progression in leukemia cells with deregulated cyclin E and c-Myc expression. In: *Leukemia* 19 (6), S. 1051–1057. DOI: 10.1038/sj.leu.2403729.

Bahmad, Hisham F.; Chamaa, Farah; Assi, Sahar; Chalhoub, Reda M.; Abou-Antoun, Tamara; Abou-Kheir, Wassim (2019): Cancer Stem Cells in Neuroblastoma: Expanding the Therapeutic Frontier. In: *Frontiers in molecular neuroscience* 12, S. 131. DOI: 10.3389/fnmol.2019.00131.

Bahn, Jae Hoon; Lee, Jae-Hyung; Li, Gang; Greer, Christopher; Peng, Guangdun; Xiao, Xinshu (2012): Accurate identification of A-to-I RNA editing in human by transcriptome sequencing. In: *Genome research* 22 (1), S. 142–150. DOI: 10.1101/gr.124107.111.

Bai, Tianliang; Zhao, Yalei; Liu, Yabin; Cai, Bindan; Dong, Ning; Li, Binghui (2019): Effect of KNL1 on the proliferation and apoptosis of colorectal cancer cells. In: *Technology in cancer research & treatment* 18, 1533033819858668. DOI: 10.1177/1533033819858668.

Bao, Jianqiang; Yan, Wei (2012): Male germline control of transposable elements. In: *Biology of reproduction* 86 (5), 162, 1-14. DOI: 10.1095/biolreprod.111.095463.

Barnes, Claire; Kanhere, Aditi (2016): Identification of RNA-Protein Interactions Through In Vitro RNA Pull-Down Assays. In: *Methods in molecular biology (Clifton, N.J.)* 1480, S. 99–113. DOI: 10.1007/978-1-4939-6380-5_9.

Bauer, D. W.; Gall, J. G. (1997): Coiled bodies without coilin. In: *Molecular biology of the cell* 8 (1), S. 73–82. DOI: 10.1091/mbc.8.1.73.

Bayfield, Mark A.; Maraia, Richard J. (2009): Precursor-product discrimination by La protein during tRNA metabolism. In: *Nature structural & molecular biology* 16 (4), S. 430–437. DOI: 10.1038/nsmb.1573.

Berridge, M. V.; Tan, A. S. (1993): Characterization of the cellular reduction of 3-(4,5-dimethylthiazol-2-yl)-2,5-diphenyltetrazolium bromide (MTT): subcellular localization, substrate dependence, and involvement of mitochondrial electron transport in MTT reduction. In: *Archives of biochemistry and biophysics* 303 (2), S. 474–482. DOI: 10.1006/abbi.1993.1311.

Bhattacharya, Resham; Mustafi, Soumyajit Banerjee; Street, Mark; Dey, Anindya; Dwivedi, Shailendra Kumar Dhar (2015): Corrigendum to 'Bmi-1: At the crossroads of physiological and pathological biology' Genes & Diseases 2 (2015) 225-239. In: *Genes & diseases* 2 (4), S. 353. DOI: 10.1016/j.gendis.2015.11.001.

Bohmert, K.; Camus, I.; Bellini, C.; Bouchez, D.; Caboche, M.; Benning, C. (1998): AGO1 defines a novel locus of Arabidopsis controlling leaf development. In: *The EMBO journal* 17 (1), S. 170–180. DOI: 10.1093/emboj/17.1.170.

Boland, Andreas; Huntzinger, Eric; Schmidt, Steffen; Izaurralde, Elisa; Weichenrieder, Oliver (2011): Crystal structure of the MID-PIWI lobe of a eukaryotic Argonaute protein. In: *Proceedings of the National Academy of Sciences of the United States of America* 108 (26), S. 10466–10471. DOI: 10.1073/pnas.1103946108.

Bossé, Gabriel D.; Simard, Martin J. (2010): A new twist in the microRNA pathway: Not Dicer but Argonaute is required for a microRNA production. In: *Cell research* 20 (7), S. 735–737. DOI: 10.1038/cr.2010.83.

Bousquet-Antonelli, Cécile; Deragon, Jean-Marc (2009): A comprehensive analysis of the La-motif protein superfamily. In: *RNA (New York, N.Y.)* 15 (5), S. 750–764. DOI: 10.1261/rna.1478709.

Bratu, Diana P.; Cha, Byeong-Jik; Mhlanga, Musa M.; Kramer, Fred Russell; Tyagi, Sanjay (2003): Visualizing the distribution and transport of mRNAs in living cells. In: *Proceedings of the National Academy of Sciences of the United States of America* 100 (23), S. 13308–13313. DOI: 10.1073/pnas.2233244100.

Braun, Joerg E.; Huntzinger, Eric; Fauser, Maria; Izaurralde, Elisa (2011): GW182 proteins directly recruit cytoplasmic deadenylase complexes to miRNA targets. In: *Molecular Cell* 44 (1), S. 120–133. DOI: 10.1016/j.molcel.2011.09.007.

Brennecke, Julius; Aravin, Alexei A.; Stark, Alexander; Dus, Monica; Kellis, Manolis; Sachidanandam, Ravi; Hannon, Gregory J. (2007): Discrete small RNA-generating loci as master regulators of transposon activity in Drosophila. In: *Cell* 128 (6), S. 1089–1103. DOI: 10.1016/j.cell.2007.01.043.

Brodeur, Garrett M. (2003): Neuroblastoma: biological insights into a clinical enigma. In: *Nature reviews. Cancer* 3 (3), S. 203–216. DOI: 10.1038/nrc1014.

Brümmer, Anneke; Yang, Yun; Chan, Tracey W.; Xiao, Xinshu (2017): Structure-mediated modulation of mRNA abundance by A-to-I editing. In: *Nature communications* 8 (1), S. 1255. DOI: 10.1038/s41467-017-01459-7.

Cardinale, Stefano; Cisterna, Barbara; Bonetti, Paolo; Aringhieri, Chiara; Biggiogera, Marco; Barabino, Silvia M. L. (2007): Subnuclear localization and dynamics of the Pre-mRNA 3' end processing factor mammalian cleavage factor I 68-kDa subunit. In: *Molecular biology of the cell* 18 (4), S. 1282–1292. DOI: 10.1091/mbc.e06-09-0846.

Carmell, Michelle A.; Xuan, Zhenyu; Zhang, Michael Q.; Hannon, Gregory J. (2002): The Argonaute family: tentacles that reach into RNAi, developmental control, stem cell maintenance, and tumorigenesis. In: *Genes & development* 16 (21), S. 2733–2742. DOI: 10.1101/gad.1026102.

Carmo-Fonseca, M.; Ferreira, J.; Lamond, A. I. (1993): Assembly of snRNP-containing coiled bodies is regulated in interphase and mitosis--evidence that the coiled body is a kinetic nuclear structure. In: *The Journal of cell biology* 120 (4), S. 841–852. DOI: 10.1083/jcb.120.4.841.

Chalbatani, Ghanbar Mahmoodi; Dana, Hassan; Memari, Feridon; Gharagozlou, Elahe; Ashjaei, Shirin; Kheirandish, Peyman et al. (2019): Biological function and molecular mechanism of piRNA in cancer. In: *Practical laboratory medicine* 13, e00113. DOI: 10.1016/j.plabm.2018.e00113.

Chang, Chung-Te; Bercovich, Natalia; Loh, Belinda; Jonas, Stefanie; Izaurralde, Elisa (2014): The activation of the decapping enzyme DCP2 by DCP1 occurs on the EDC4 scaffold and involves a conserved loop in DCP1. In: *Nucleic acids research* 42 (8), S. 5217–5233. DOI: 10.1093/nar/gku129.

Cheeseman, Iain M.; Hori, Tetsuya; Fukagawa, Tatsuo; Desai, Arshad (2008): KNL1 and the CENP-H/I/K complex coordinately direct kinetochore assembly in vertebrates. In: *Molecular biology of the cell* 19 (2), S. 587–594. DOI: 10.1091/mbc.E07-10-1051.

Chen, Ling-Ling; Carmichael, Gordon G. (2008): Gene regulation by SINES and inosines: biological consequences of A-to-I editing of Alu element inverted repeats. In: *Cell cycle (Georgetown, Tex.)* 7 (21), S. 3294–3301. DOI: 10.4161/cc.7.21.6927.

Chen, Ling-Ling; DeCerbo, Joshua N.; Carmichael, Gordon G. (2008): Alu element-mediated gene silencing. In: *The EMBO journal* 27 (12), S. 1694–1705. DOI: 10.1038/emboj.2008.94.

Chen, Ling-Ling; Carmichael, Gordon G. (2009): Altered nuclear retention of mRNAs containing inverted repeats in human embryonic stem cells: functional role of a nuclear noncoding RNA. In: *Molecular Cell* 35 (4), S. 467–478. DOI: 10.1016/j.molcel.2009.06.027.

Chen, Ying; Boland, Andreas; Kuzuoğlu-Öztürk, Duygu; Bawankar, Praveen; Loh, Belinda; Chang, Chung-Te et al. (2014): A DDX6-CNOT1 complex and W-binding pockets in CNOT9 reveal direct links between miRNA target recognition and silencing. In: *Molecular Cell* 54 (5), S. 737–750. DOI: 10.1016/j.molcel.2014.03.034.

Chen, Ling-Ling; Yang, Li (2017): ALUternative Regulation for Gene Expression. In: *Trends in cell biology* 27 (7), S. 480–490. DOI: 10.1016/j.tcb.2017.01.002.

Cheng, Jia; Guo, Jun-Ming; Xiao, Bing-Xiu; Miao, Ying; Jiang, Zhen; Zhou, Hui; Li, Qing-Ning (2011): piRNA, the new non-coding RNA, is aberrantly expressed in human cancer cells. In: *Clinica chimica acta; international journal of clinical chemistry* 412 (17-18), S. 1621–1625. DOI: 10.1016/j.cca.2011.05.015.

Chu, Haiyan; Hui, Gaoyun; Yuan, Lin; Shi, Danni; Wang, Yubang; Du, Mulong et al. (2015): Identification of novel piRNAs in bladder cancer. In: *Cancer letters* 356 (2 Pt B), S. 561–567. DOI: 10.1016/j.canlet.2014.10.004.

Clemson, Christine M.; Hutchinson, John N.; Sara, Sergio A.; Ensminger, Alexander W.; Fox, Archa H.; Chess, Andrew; Lawrence, Jeanne B. (2009): An architectural role for a nuclear noncoding RNA: NEAT1 RNA is essential for the structure of paraspeckles. In: *Molecular Cell* 33 (6), S. 717–726. DOI: 10.1016/j.molcel.2009.01.026.

Cui, Hongjuan; Hu, Bo; Li, Tai; Ma, Jun; Alam, Goleeta; Gunning, William T.; Ding, Han-Fei (2007): Bmi-1 is essential for the tumorigenicity of neuroblastoma cells. In: *The American journal of pathology* 170 (4), S. 1370–1378. DOI: 10.2353/ajpath.2007.060754.

Czech, Benjamin; Munafò, Marzia; Ciabrelli, Filippo; Eastwood, Evelyn L.; Fabry, Martin H.; Kneuss, Emma; Hannon, Gregory J. (2018): piRNA-Guided Genome Defense: From Biogenesis to Silencing. In: *Annual review of genetics* 52, S. 131–157. DOI: 10.1146/annurev-genet-120417-031441.

Darling, April L.; Uversky, Vladimir N. (2023): Known types of membrane-less organelles and biomolecular condensates. In: Droplets of Life: Elsevier, S. 271–335.

Dash, Sabyasachi; Balasubramaniam, Muthukumar; Dash, Chandravanu; Pandhare, Jui (2018): Biotin-based Pulldown Assay to Validate mRNA Targets of Cellular miRNAs. In: *Journal of visualized experiments : JoVE* (136). DOI: 10.3791/57786.

Deininger, Prescott (2011): Alu elements: know the SINEs. In: *Genome biology* 12 (12), S. 236. DOI: 10.1186/gb-2011-12-12-236.

Dewannieux, Marie; Esnault, Cécile; Heidmann, Thierry (2003): LINE-mediated retrotransposition of marked Alu sequences. In: *Nature genetics* 35 (1), S. 41–48. DOI: 10.1038/ng1223.

Ding, Hongliu; Schwarz, Dianne S.; Keene, Alex; Affar, El Bachir; Fenton, Laura; Xia, Xugang et al. (2003): Selective silencing by RNAi of a dominant allele that causes amyotrophic lateral sclerosis. In: *Aging cell* 2 (4), S. 209–217. DOI: 10.1046/j.1474-9728.2003.00054.x.

Dock-Bregeon, Anne-Catherine; Lewis, Karen A.; Conte, Maria R. (2021): The La-related proteins: structures and interactions of a versatile superfamily of RNA-binding proteins. In: *RNA biology* 18 (2), S. 178–193. DOI: 10.1080/15476286.2019.1695712.

Dong, Peixin; Xiong, Ying; Yue, Junming; Hanley, Sharon J. B.; Kobayashi, Noriko; Todo, Yukiharu; Watari, Hidemichi (2018): Long Non-coding RNA NEAT1: A Novel Target for Diagnosis and Therapy in Human Tumors. In: *Frontiers in genetics* 9, S. 471. DOI: 10.3389/fgene.2018.00471.

Doyle, Michael; Badertscher, Lukas; Jaskiewicz, Lukasz; Güttinger, Stephan; Jurado, Sabine; Hugenschmidt, Tabea et al. (2013): The double-stranded RNA binding domain of human Dicer functions as a nuclear localization signal. In: *RNA (New York, N.Y.)* 19 (9), S. 1238–1252. DOI: 10.1261/rna.039255.113.

Dragomir, Mihnea Paul; Knutsen, Erik; Calin, George Adrian (2018): SnapShot: Unconventional miRNA Functions. In: *Cell* 174 (4), 1038-1038.e1. DOI: 10.1016/j.cell.2018.07.040.

Du, Lili; Zhou, Junhui; Meng, Lingwei; Wang, Xiaoxia; Wang, Changrong; Huang, Yuanyu et al. (2017): The pH-Triggered Triblock Nanocarrier Enabled Highly Efficient siRNA Delivery for Cancer Therapy. In: *Theranostics* 7 (14), S. 3432–3445. DOI: 10.7150/thno.20297.

Duchaine, Thomas F.; Fabian, Marc R. (2019): Mechanistic Insights into MicroRNA-Mediated Gene Silencing. In: *Cold Spring Harb Perspect Biol* 11 (3), a032771. DOI: 10.1101/cshperspect.a032771.

el-Deiry, W. S.; Tokino, T.; Velculescu, V. E.; Levy, D. B.; Parsons, R.; Trent, J. M. et al. (1993): WAF1, a potential mediator of p53 tumor suppression. In: *Cell* 75 (4), S. 817–825. DOI: 10.1016/0092-8674(93)90500-P.

Ernst, Christina; Odom, Duncan T.; Kutter, Claudia (2017): The emergence of piRNAs against transposon invasion to preserve mammalian genome integrity. In: *Nature communications* 8 (1), S. 1411. DOI: 10.1038/s41467-017-01049-7.

Fabian, Marc R.; Cieplak, Maja K.; Frank, Filipp; Morita, Masahiro; Green, Jonathan; Srikumar, Tharan et al. (2011): miRNA-mediated deadenylation is orchestrated by GW182 through two conserved motifs that interact with CCR4-NOT. In: *Nat Struct Mol Biol* 18 (11), S. 1211–1217. DOI: 10.1038/nsmb.2149.

Faehnle, Christopher R.; Elkayam, Elad; Haase, Astrid D.; Hannon, Gregory J.; Joshua-Tor, Leemor (2013): The making of a slicer: activation of human Argonaute-1. In: *Cell reports* 3 (6), S. 1901–1909. DOI: 10.1016/j.celrep.2013.05.033.

Fan, Jiahui; Zhang, Xudong; Nie, Xiang; Li, Huaping; Yuan, Shuai; Dai, Beibei et al. (2020): Nuclear miR-665 aggravates heart failure via suppressing phosphatase and tensin homolog transcription. In: *Science China. Life sciences* 63 (5), S. 724–736. DOI: 10.1007/s11427-018-9515-1.

Fazio, Serena de; Bartonicek, Nenad; Di Giacomo, Monica; Abreu-Goodger, Cei; Sankar, Aditya; Funaya, Charlotta et al. (2011): The endonuclease activity of Mili fuels piRNA amplification that silences LINE1 elements. In: *Nature* 480 (7376), S. 259–263. DOI: 10.1038/nature10547.

Felsenfeld, G.; Miles, H. T. (1967): The physical and chemical properties of nucleic acids. In: *Annual review of biochemistry* 36, S. 407–448. DOI: 10.1146/annurev.bi.36.070167.002203.

Feng, Peifu; Li, Ling; Deng, Tanggang; Liu, Yan; Ling, Neng; Qiu, Siyuan et al. (2020): NONO and tumorigenesis: More than splicing. In: *Journal of cellular and molecular medicine* 24 (8), S. 4368–4376. DOI: 10.1111/jcmm.15141.

Fenger-Grøn, Martin; Fillman, Christy; Norrild, Bodil; Lykke-Andersen, Jens (2005): Multiple processing body factors and the ARE binding protein TTP activate mRNA decapping. In: *Molecular cell* 20 (6), S. 905–915. DOI: 10.1016/j.molcel.2005.10.031.

Fox, Archa H.; Bond, Charles S.; Lamond, Angus I. (2005): P54nrb forms a heterodimer with PSP1 that localizes to paraspeckles in an RNA-dependent manner. In: *Molecular biology of the cell* 16 (11), S. 5304–5315. DOI: 10.1091/mbc.E05-06-0587.

Fox, Archa H.; Lam, Yun Wah; Leung, Anthony K. L.; Lyon, Carol E.; Andersen, Jens; Mann, Matthias; Lamond, Angus I. (2002): Paraspeckles: a novel nuclear domain. In: *Current biology : CB* 12 (1), S. 13–25. DOI: 10.1016/S0960-9822(01)00632-7.

Fox, Archa H.; Lamond, Angus I. (2010): Paraspeckles. In: *Cold Spring Harb Perspect Biol* 2 (7), a000687. DOI: 10.1101/cshperspect.a000687.

Frank, Filipp; Fabian, Marc R.; Stepinski, Janusz; Jemielity, Jacek; Darzynkiewicz, Edward; Sonenberg, Nahum; Nagar, Bhushan (2011): Structural analysis of 5′-mRNA–cap interactions with the human AGO2 MID domain. In: *EMBO Rep* 12 (5), S. 415–420. DOI: 10.1038/embor.2011.48.

Frank, Filipp; Sonenberg, Nahum; Nagar, Bhushan (2010): Structural basis for 5'-nucleotide base-specific recognition of guide RNA by human AGO2. In: *Nature* 465 (7299), S. 818–822. DOI: 10.1038/nature09039.

Friedrich, Juergen; Seidel, Claudia; Ebner, Reinhard; Kunz-Schughart, Leoni A. (2009): Spheroid-based drug screen: considerations and practical approach. In: *Nature protocols* 4 (3), S. 309–324. DOI: 10.1038/nprot.2008.226.

Fukaya, Takashi; Iwakawa, Hiro-Oki; Tomari, Yukihide (2014): MicroRNAs block assembly of eIF4F translation initiation complex in Drosophila. In: *Molecular Cell* 56 (1), S. 67–78. DOI: 10.1016/j.molcel.2014.09.004.

Gamble, L. D.; Kees, U. R.; Tweddle, D. A.; Lunec, J. (2012): MYCN sensitizes neuroblastoma to the MDM2-p53 antagonists Nutlin-3 and MI-63. In: *Oncogene* 31 (6), S. 752–763. DOI: 10.1038/onc.2011.270.

Ginjala, Vasudeva; Nacerddine, Karim; Kulkarni, Atul; Oza, Jay; Hill, Sarah J.; Yao, Ming et al. (2011): BMI1 is recruited to DNA breaks and contributes to DNA damage-

induced H2A ubiquitination and repair. In: *Molecular and cellular biology* 31 (10), S. 1972–1982. DOI: 10.1128/MCB.00981-10.

Girard, Angélique; Sachidanandam, Ravi; Hannon, Gregory J.; Carmell, Michelle A. (2006): A germline-specific class of small RNAs binds mammalian Piwi proteins. In: *Nature* 442 (7099), S. 199–202. DOI: 10.1038/nature04917.

Gorospe, M.; Wang, X.; Holbrook, N. J. (1999): Functional role of p21 during the cellular response to stress. In: *Gene expression* 7 (4-6), S. 377–385.

Gunawardane, Lalith S.; Saito, Kuniaki; Nishida, Kazumichi M.; Miyoshi, Keita; Kawamura, Yoshinori; Nagami, Tomoko et al. (2007): A slicer-mediated mechanism for repeat-associated siRNA 5' end formation in Drosophila. In: *Science (New York, N.Y.)* 315 (5818), S. 1587–1590. DOI: 10.1126/science.1140494.

Gundelfinger, E. D.; Krause, E.; Melli, M.; Dobberstein, B. (1983): The organization of the 7SL RNA in the signal recognition particle. In: *Nucleic acids research* 11 (21), S. 7363–7374. DOI: 10.1093/nar/11.21.7363.

Gussakovsky, Daniel; McKenna, Sean A. (2021): Alu RNA and their roles in human disease states. In: *RNA biology* 18 (sup2), S. 574–585. DOI: 10.1080/15476286.2021.1989201.

Hanahan, D.; Weinberg, R. A. (2000): The hallmarks of cancer. In: *Cell* 100 (1), S. 57–70. DOI: 10.1016/s0092-8674(00)81683-9.

Handwerger, Korie E.; Cordero, Jason A.; Gall, Joseph G. (2005): Cajal Bodies, Nucleoli, and Speckles in the Xenopus Oocyte Nucleus Have a Low-Density, Sponge-like Structure. In: *Molecular biology of the cell* 16 (1), S. 202–211. DOI: 10.1091/mbc.E04-08-0742.

Harper, J. W.; Adami, G. R.; Wei, N.; Keyomarsi, K.; Elledge, S. J. (1993): The p21 Cdk-interacting protein Cip1 is a potent inhibitor of G1 cyclin-dependent kinases. In: *Cell* 75 (4), S. 805–816. DOI: 10.1016/0092-8674(93)90499-G.

Hashimoto, C.; Steitz, J. A. (1983): Sequential association of nucleolar 7-2 RNA with two different autoantigens. In: *Journal of Biological Chemistry* 258 (3), S. 1379–1382. DOI: 10.1016/S0021-9258(18)32990-9.

Hasler, Daniele; Lehmann, Gerhard; Murakawa, Yasuhiro; Klironomos, Filippos; Jakob, Leonhard; Grässer, Friedrich A. et al. (2016): The Lupus Autoantigen La Prevents Mis-channeling of tRNA Fragments into the Human MicroRNA Pathway. In: *Molecular cell* 63 (1), S. 110–124. DOI: 10.1016/j.molcel.2016.05.026.

Häsler, Julien; Strub, Katharina (2006): Alu elements as regulators of gene expression. In: *Nucleic acids research* 34 (19), S. 5491–5497. DOI: 10.1093/nar/gkl706.

Hauptmann, Judith; Kater, Lukas; Löffler, Patrick; Merkl, Rainer; Meister, Gunter (2014): Generation of catalytic human Ago4 identifies structural elements important for RNA cleavage. In: *RNA (New York, N.Y.)* 20 (10), S. 1532–1538. DOI: 10.1261/rna.045203.114.

He, Kang; Li, Jingze; Huang, Xuemiao; Zhao, Weixin; Wang, Kai; Wang, Taiwei et al. (2023): KNL1 is a prognostic and diagnostic biomarker related to immune infiltration in patients with uterine corpus endometrial carcinoma. In: *Frontiers in oncology* 13, S. 1090779. DOI: 10.3389/fonc.2023.1090779.

Holcik, Martin; Sonenberg, Nahum (2005): Translational control in stress and apoptosis. In: *Nature reviews. Molecular cell biology* 6 (4), S. 318–327. DOI: 10.1038/nrm1618.

Hu, QiDong; Tanasa, Bogdan; Trabucchi, Michele; Li, Wenbo; Zhang, Jie; Ohgi, Kenneth A. et al. (2012): DICER- and AGO3-dependent generation of retinoic acid-induced DR2 Alu RNAs regulates human stem cell proliferation. In: *Nature structural & molecular biology* 19 (11), S. 1168–1175. DOI: 10.1038/nsmb.2400.

Hu, Zhiquan; Ma, Siquan; Sun, Yi; Long, Gongwei; Chen, Ke (2022): Identification of Long Non-Coding RNA MIR4435-2HG as a Prognostic Biomarker in Bladder Cancer. In: *Genes* 13 (8). DOI: 10.3390/genes13081462.

Huang, Ying; Bayfield, Mark A.; Intine, Robert V.; Maraia, Richard J. (2006): Separate RNA-binding surfaces on the multifunctional La protein mediate distinguishable activities in tRNA maturation. In: *Nature structural & molecular biology* 13 (7), S. 611–618. DOI: 10.1038/nsmb1110.

Huntzinger, Eric; Izaurralde, Elisa (2011): Gene silencing by microRNAs: contributions of translational repression and mRNA decay. In: *Nature reviews. Genetics* 12 (2), S. 99–110. DOI: 10.1038/nrg2936.

Iwakawa, Hiro-Oki; Tomari, Yukihide (2022): Life of RISC: Formation, action, and degradation of RNA-induced silencing complex. In: *Molecular Cell* 82 (1), S. 30–43. DOI: 10.1016/j.molcel.2021.11.026.

Iwasaki, Shintaro; Sasaki, Hiroshi M.; Sakaguchi, Yuriko; Suzuki, Tsutomu; Tadakuma, Hisashi; Tomari, Yukihide (2015): Defining fundamental steps in the assembly of the Drosophila RNAi enzyme complex. In: *Nature* 521 (7553), S. 533–536. DOI: 10.1038/nature14254.

Jakymiw, Andrew; Lian, Shangli; Eystathioy, Theophany; Li, Songqing; Satoh, Minoru; Hamel, John C. et al. (2005): Disruption of GW bodies impairs mammalian RNA interference. In: *Nature cell biology* 7 (12), S. 1267–1274. DOI: 10.1038/ncb1334.

Jie, Minwen; Feng, Tong; Huang, Wei; Zhang, Moran; Feng, Yuliang; Jiang, Hao; Wen, Zhili (2021): Subcellular Localization of miRNAs and Implications in Cellular Homeostasis. In: *Genes* 12 (6). DOI: 10.3390/genes12060856.

Kaess, Carina; Matthes, Marie; Gross, Jonas; Waetzig, Rebecca; Heise, Tilman; Corbacioglu, Selim; Sommer, Gunhild (2023): Evaluating the RIST Molecular-Targeted Regimen in a Three-Dimensional Neuroblastoma Spheroid Cell Culture Model. In: *Cancers* 15 (6). DOI: 10.3390/cancers15061749.

Kellogg, Morgana K.; Miller, Sarah C.; Tikhonova, Elena B.; Karamyshev, Andrey L. (2021): SRPassing Co-translational Targeting: The Role of the Signal Recognition Particle in Protein Targeting and mRNA Protection. In: *International journal of molecular sciences* 22 (12). DOI: 10.3390/ijms22126284.

Kidner, Catherine A.; Martienssen, Robert A. (2004): Spatially restricted microRNA directs leaf polarity through ARGONAUTE1. In: *Nature* 428 (6978), S. 81–84. DOI: 10.1038/nature02366.

Kim, Seong-Jin; Ju, Jin-Sung; Kang, Myoung-Hee; Eun, Ji Won; Kim, Young Ha; Raninga, Prahlad V. et al. (2020): RNA-binding protein NONO contributes to cancer cell growth and confers drug resistance as a theranostic target in TNBC. In: *Theranostics* 10 (18), S. 7974–7992. DOI: 10.7150/thno.45037.

Kirino, Yohei; Mourelatos, Zissimos (2007): Mouse Piwi-interacting RNAs are 2'-O-methylated at their 3' termini. In: *Nature structural & molecular biology* 14 (4), S. 347–348. DOI: 10.1038/nsmb1218.

Kiyomitsu, Tomomi; Obuse, Chikashi; Yanagida, Mitsuhiro (2007): Human Blinkin/AF15q14 Is Required for Chromosome Alignment and the Mitotic Checkpoint through Direct Interaction with Bub1 and BubR1. In: *Developmental cell* 13 (5), S. 663–676. DOI: 10.1016/j.devcel.2007.09.005.

Knuckles, Philip; Vogt, Miriam A.; Lugert, Sebastian; Milo, Marta; Chong, Mark M. W.; Hautbergue, Guillaume M. et al. (2012): Drosha regulates neurogenesis by controlling neurogenin 2 expression independent of microRNAs. In: *Nature neuroscience* 15 (7), S. 962–969. DOI: 10.1038/nn.3139.

Kostrikis, L. G.; Tyagi, S.; Mhlanga, M. M.; Ho, D. D.; Kramer, F. R. (1998): Spectral genotyping of human alleles. In: *Science (New York, N.Y.)* 279 (5354), S. 1228–1229. DOI: 10.1126/science.279.5354.1228.

Kozloski, Goldi A.; Jiang, Xiaoyu; Bhatt, Shruti; Ruiz, Jose; Vega, Francisco; Shaknovich, Rita et al. (2016): miR-181a negatively regulates NF-κB signaling and affects activated B-cell-like diffuse large B-cell lymphoma pathogenesis. In: *Blood* 127 (23), S. 2856–2866. DOI: 10.1182/blood-2015-11-680462.

Kramerov, D. A.; Lekakh, I. V.; Samarina, O. P.; Ryskov, A. P. (1982): The sequences homologous to major interspersed repeats B1 and B2 of mouse genome are present in mRNA and small cytoplasmic poly(A) + RNA. In: *Nucleic acids research* 10 (23), S. 7477–7491. DOI: 10.1093/nar/10.23.7477.

Kramerov, D. A.; Vassetzky, N. S. (2011): Origin and evolution of SINEs in eukaryotic genomes. In: *Heredity* 107 (6), S. 487–495. DOI: 10.1038/hdy.2011.43.

Kucera, Nathan J.; Hodsdon, Michael E.; Wolin, Sandra L. (2011): An intrinsically disordered C terminus allows the La protein to assist the biogenesis of diverse noncoding RNA precursors. In: *Proceedings of the National Academy of Sciences of the United States of America* 108 (4), S. 1308–1313. DOI: 10.1073/pnas.1017085108.

Kuehnert, Julia; Sommer, Gunhild; Zierk, Avery W.; Fedarovich, Alena; Brock, Alexander; Fedarovich, Dzmitry; Heise, Tilman (2015): Novel RNA chaperone domain of RNA-binding protein La is regulated by AKT phosphorylation. In: Nucleic Acids Research 43 (1), S. 581–594. DOI: 10.1093/nar/gku1309.

Kuramochi-Miyagawa, Satomi; Watanabe, Toshiaki; Gotoh, Kengo; Totoki, Yasushi; Toyoda, Atsushi; Ikawa, Masahito et al. (2008): DNA methylation of retrotransposon

genes is regulated by Piwi family members MILI and MIWI2 in murine fetal testes. In: *Genes & development* 22 (7), S. 908–917. DOI: 10.1101/gad.1640708.

Kutter, Claudia; Svoboda, Petr (2008): miRNA, siRNA, piRNA: Knowns of the unknown. In: *RNA biology* 5 (4), S. 181–188. DOI: 10.4161/rna.7227.

Lander, E. S.; Linton, L. M.; Birren, B.; Nusbaum, C.; Zody, M. C.; Baldwin, J. et al. (2001): Initial sequencing and analysis of the human genome. In: *Nature* 409 (6822), S. 860–921. DOI: 10.1038/35057062.

Lattmann, Evelyn; Deng, Ting; Hajnal, Alex (2020): To Divide or Invade: A Look Behind the Scenes of the Proliferation-Invasion Interplay in the Caenorhabditis elegans Anchor Cell. In: *Frontiers in cell and developmental biology* 8, S. 616051. DOI: 10.3389/fcell.2020.616051.

Lee, Yoontae; Jeon, Kipyoung; Lee, Jun-Tae; Kim, Sunyoung; Kim, V. Narry (2002): MicroRNA maturation: stepwise processing and subcellular localization. In: *The EMBO journal* 21 (17), S. 4663–4670. DOI: 10.1093/emboj/cdf476.

Lee, Youn Jung; Moon, Sung Ung; Park, Min Geun; Jung, Woon Yong; Park, Yong Keun; Song, Sung Kyu et al. (2016): Multiplex bioimaging of piRNA molecular pathway-regulated theragnostic effects in a single breast cancer cell using a piRNA molecular beacon. In: *Biomaterials* 101, S. 143–155. DOI: 10.1016/j.biomaterials.2016.05.052.

Leung, Anthony K. L.; Calabrese, J. Mauro; Sharp, Phillip A. (2006): Quantitative analysis of Argonaute protein reveals microRNA-dependent localization to stress granules. In: *Proceedings of the National Academy of Sciences of the United States of America* 103 (48), S. 18125–18130. DOI: 10.1073/pnas.0608845103.

Li, Ruohan; Harvey, Alan R.; Hodgetts, Stuart I.; Fox, Archa H. (2017): Functional dissection of NEAT1 using genome editing reveals substantial localization of the NEAT1_1 isoform outside paraspeckles. In: *RNA (New York, N.Y.)* 23 (6), S. 872–881. DOI: 10.1261/rna.059477.116.

Li, Yinuo; Zhang, Yue; Liu, Mingxi (2021): Knockout Gene-Based Evidence for PIWI-Interacting RNA Pathway in Mammals. In: *Frontiers in cell and developmental biology* 9, S. 681188. DOI: 10.3389/fcell.2021.681188.

Li, Yuping; Wu, Xiwei; Gao, Hanlin; Jin, Jennifer M.; Li, Arthur X.; Kim, Young S. et al. (2015): Piwi-Interacting RNAs (piRNAs) Are Dysregulated in Renal Cell Carcinoma and Associated with Tumor Metastasis and Cancer-Specific Survival. In: *Molecular medicine (Cambridge, Mass.)* 21 (1), S. 381–388. DOI: 10.2119/molmed.2014.00203.

Liang, Jun; Wang, Peng; Xie, Shao; Wang, Weifeng; Zhou, Xiuping; Hu, Jinxia et al. (2015): Bmi-1 regulates the migration and invasion of glioma cells through p16. In: *Cell biology international* 39 (3), S. 283–290. DOI: 10.1002/cbin.10390.

Lin, Yuan; Protter, David S. W.; Rosen, Michael K.; Parker, Roy (2015): Formation and Maturation of Phase-Separated Liquid Droplets by RNA-Binding Proteins. In: *Molecular cell* 60 (2), S. 208–219. DOI: 10.1016/j.molcel.2015.08.018.

Lingel, Andreas; Simon, Bernd; Izaurralde, Elisa; Sattler, Michael (2003): Structure and nucleic-acid binding of the Drosophila Argonaute 2 PAZ domain. In: *Nature* 426 (6965), S. 465–469. DOI: 10.1038/nature02123.

Lingel, Andreas; Simon, Bernd; Izaurralde, Elisa; Sattler, Michael (2004): Nucleic acid 3′-end recognition by the Argonaute2 PAZ domain. In: *Nat Struct Mol Biol* 11 (6), S. 576–577. DOI: 10.1038/nsmb777.

Liu, Jidong; Valencia-Sanchez, Marco Antonio; Hannon, Gregory J.; Parker, Roy (2005): MicroRNA-dependent localization of targeted mRNAs to mammalian P-bodies. In: *Nature cell biology* 7 (7), S. 719–723. DOI: 10.1038/ncb1274.

Liu, Xiaoying; Sun, Yu; Guo, Jianping; Ma, Hong; Li, Jiyou; Dong, Bin et al. (2006): Expression of hiwi gene in human gastric cancer was associated with proliferation of cancer cells. In: *International journal of cancer* 118 (8), S. 1922–1929. DOI: 10.1002/ijc.21575.

Livak, K. J.; Schmittgen, T. D. (2001): Analysis of relative gene expression data using real-time quantitative PCR and the 2(-Delta Delta C(T)) Method. In: *Methods (San Diego, Calif.)* 25 (4), S. 402–408. DOI: 10.1006/meth.2001.1262.

Lu, Ting; Lin, Zongwei; Ren, Jianwei; Yao, Peng; Wang, Xiaowei; Wang, Zhe; Zhang, Qunye (2016): The Non-Specific Binding of Fluorescent-Labeled MiRNAs on Cell Surface by Hydrophobic Interaction. In: *PloS one* 11 (3), e0149751. DOI: 10.1371/journal.pone.0149751.

Ma, Jin-Biao; Ye, Keqiong; Patel, Dinshaw J. (2004): Structural basis for overhang-specific small interfering RNA recognition by the PAZ domain. In: *Nature* 429 (6989), S. 318–322. DOI: 10.1038/nature02519.

Maas, Stefan; Rich, Alexander; Nishikura, Kazuko (2003): A-to-I RNA editing: recent news and residual mysteries. In: *The Journal of biological chemistry* 278 (3), S. 1391–1394. DOI: 10.1074/jbc.R200025200.

Mao, Shiqi; Ying, Yachen; Wu, Xiaotian; Chen, Antony K. (2020): Delivering Molecular Beacons via an Electroporation-Based Approach Enables Live-Cell Imaging of Single RNA Transcripts and Genomic Loci. In: Methods in molecular biology (Clifton, N.J.) 2106, S. 241–252. DOI: 10.1007/978-1-0716-0231-7_15.

Maquat, Lynne E. (2020): Short interspersed nuclear element (SINE)-mediated post-transcriptional effects on human and mouse gene expression: SINE-UP for active duty. In: *Philosophical transactions of the Royal Society of London. Series B, Biological sciences* 375 (1795), S. 20190344. DOI: 10.1098/rstb.2019.0344.

Maraia, Richard J.; Intine, Robert V. (2002): La protein and its associated small nuclear and nucleolar precursor RNAs. In: *Gene expression* 10 (1-2), S. 41–57.

Maraia, Richard J.; Mattijssen, Sandy; Cruz-Gallardo, Isabel; Conte, Maria R. (2017): The La and related RNA-binding proteins (LARPs): structures, functions, and evolving perspectives. In: *Wiley interdisciplinary reviews. RNA* 8 (6). DOI: 10.1002/wrna.1430.

Matera, A. G. (1999): Nuclear bodies: multifaceted subdomains of the interchromatin space. In: *Trends in cell biology* 9 (8), S. 302–309. DOI: 10.1016/s0962-8924(99)01606-2#.

Mattioli, M.; Reichlin, M. (1974): Heterogeneity of RNA protein antigens reactive with sera of patients with systemic lupus erythematosus. Description of a cytoplasmic nonribosomal antigen. In: *Arthritis and rheumatism* 17 (4), S. 421–429. DOI: 10.1002/art.1780170413.

McCluggage, Finn; Fox, Archa H. (2021): Paraspeckle nuclear condensates: Global sensors of cell stress? In: *BioEssays : news and reviews in molecular, cellular and developmental biology* 43 (5), e2000245. DOI: 10.1002/bies.202000245.

Mei, Yuping; Wang, Yuyan; Kumari, Priti; Shetty, Amol Carl; Clark, David; Gable, Tyler et al. (2015): A piRNA-like small RNA interacts with and modulates p-ERM proteins in human somatic cells. In: *Nature communications* 6, S. 7316. DOI: 10.1038/ncomms8316.

Meier, U. Thomas (2017): RNA modification in Cajal bodies. In: *RNA biology* 14 (6), S. 693–700. DOI: 10.1080/15476286.2016.1249091.

Meister, Gunter; Landthaler, Markus; Patkaniowska, Agnieszka; Dorsett, Yair; Teng, Grace; Tuschl, Thomas (2004): Human Argonaute2 Mediates RNA Cleavage Targeted by miRNAs and siRNAs. In: *Molecular Cell* 15 (2), S. 185–197. DOI: 10.1016/j.molcel.2004.07.007.

Meister, Gunter; Landthaler, Markus; Peters, Lasse; Chen, Po Yu; Urlaub, Henning; Lührmann, Reinhard; Tuschl, Thomas (2005): Identification of novel argonaute-associated proteins. In: *Current biology : CB* 15 (23), S. 2149–2155. DOI: 10.1016/j.cub.2005.10.048.

Miller, Douglas K. (1997): The role of the Caspase family of cysteine proteases in apoptosis. In: *Seminars in Immunology* 9 (1), S. 35–49. DOI: 10.1006/smim.1996.0058.

Mircsof, Dennis; Langouët, Maéva; Rio, Marlène; Moutton, Sébastien; Siquier-Pernet, Karine; Bole-Feysot, Christine et al. (2015): Mutations in NONO lead to syndromic intellectual disability and inhibitory synaptic defects. In: *Nature neuroscience* 18 (12), S. 1731–1736. DOI: 10.1038/nn.4169.

Misteli, T.; Cáceres, J. F.; Spector, D. L. (1997): The dynamics of a pre-mRNA splicing factor in living cells. In: *Nature* 387 (6632), S. 523–527. DOI: 10.1038/387523a0.

Modic, Miha; Grosch, Markus; Rot, Gregor; Schirge, Silvia; Lepko, Tjasa; Yamazaki, Tomohiro et al. (2019): Cross-Regulation between TDP-43 and Paraspeckles Promotes Pluripotency-Differentiation Transition. In: *Molecular Cell* 74 (5), 951-965.e13. DOI: 10.1016/j.molcel.2019.03.041.

Molofsky, Anna V.; He, Shenghui; Bydon, Mohammad; Morrison, Sean J.; Pardal, Ricardo (2005): Bmi-1 promotes neural stem cell self-renewal and neural development but not mouse growth and survival by repressing the p16Ink4a and p19Arf senescence pathways. In: *Genes & development* 19 (12), S. 1432–1437. DOI: 10.1101/gad.1299505.

Moretti, Francesca; Kaiser, Constanze; Zdanowicz-Specht, Agnieszka; Hentze, Matthias W. (2012): PABP and the poly(A) tail augment microRNA repression by facilitated miRISC binding. In: *Nat Struct Mol Biol* 19 (6), S. 603–608. DOI: 10.1038/nsmb.2309.

Morris, Glenn E. (2008): The Cajal body. In: *Biochimica et biophysica acta* 1783 (11), S. 2108–2115. DOI: 10.1016/j.bbamcr.2008.07.016.

Moyano, Miguel; Stefani, Giovanni (2015): piRNA involvement in genome stability and human cancer. In: *Journal of hematology & oncology* 8, S. 38. DOI: 10.1186/s13045-015-0133-5.

Naeeni, Amir R.; Conte, Maria R.; Bayfield, Mark A. (2012): RNA chaperone activity of human La protein is mediated by variant RNA recognition motif. In: *The Journal of biological chemistry* 287 (8), S. 5472–5482. DOI: 10.1074/jbc.M111.276071.

Naganuma, Takao; Nakagawa, Shinichi; Tanigawa, Akie; Sasaki, Yasnory F.; Goshima, Naoki; Hirose, Tetsuro (2012): Alternative 3'-end processing of long noncoding RNA initiates construction of nuclear paraspeckles. In: *The EMBO Journal* 31 (20), S. 4020–4034. DOI: 10.1038/emboj.2012.251.

Nakanishi, Kotaro (2016): Anatomy of RISC: how do small RNAs and chaperones activate Argonaute proteins? In: *Wiley interdisciplinary reviews. RNA* 7 (5), S. 637–660. DOI: 10.1002/wrna.1356.

Nakanishi, Kotaro; Weinberg, David E.; Bartel, David P.; Patel, Dinshaw J. (2012): Structure of yeast Argonaute with guide RNA. In: *Nature* 486 (7403), S. 368–374. DOI: 10.1038/nature11211.

Nakano, S.; Fujimoto, M.; Hara, H.; Sugimoto, N. (1999): Nucleic acid duplex stability: influence of base composition on cation effects. In: *Nucleic acids research* 27 (14), S. 2957–2965. DOI: 10.1093/nar/27.14.2957.

Nakatake, M.; Monte-Mor, B.; Debili, N.; Casadevall, N.; Ribrag, V.; Solary, E. et al. (2012): JAK2(V617F) negatively regulates p53 stabilization by enhancing MDM2 via La expression in myeloproliferative neoplasms. In: *Oncogene* 31 (10), S. 1323–1333. DOI: 10.1038/onc.2011.313.

Naruse, Ken; Matsuura-Suzuki, Eriko; Watanabe, Mariko; Iwasaki, Shintaro; Tomari, Yukihide (2018): In vitro reconstitution of chaperone-mediated human RISC assembly. In: *RNA (New York, N.Y.)* 24 (1), S. 6–11. DOI: 10.1261/rna.063891.117.

Naveed, Alina; Cooper, Jack A.; Li, Ruohan; Hubbard, Alysia; Chen, Jingwei; Liu, Tao et al. (2021): NEAT1 polyA-modulating antisense oligonucleotides reveal opposing functions for both long non-coding RNA isoforms in neuroblastoma. In: *Cellular and molecular life sciences : CMLS* 78 (5), S. 2213–2230. DOI: 10.1007/s00018-020-03632-6.

Nishikura, Kazuko (2016): A-to-I editing of coding and non-coding RNAs by ADARs. In: *Nature reviews. Molecular cell biology* 17 (2), S. 83–96. DOI: 10.1038/nrm.2015.4.

Nitin, Nitin; Santangelo, Philip J.; Kim, Gloria; Nie, Shuming; Bao, Gang (2004): Peptide-linked molecular beacons for efficient delivery and rapid mRNA detection in living cells. In: *Nucleic acids research* 32 (6), e58. DOI: 10.1093/nar/gnh063.

Nolan, J. C.; Frawley, T.; Tighe, J.; Soh, H.; Curtin, C.; Piskareva, O. (2020): Preclinical models for neuroblastoma: Advances and challenges. In: *Cancer letters* 474, S. 53–62. DOI: 10.1016/j.canlet.2020.01.015.

Nowak, Katrin; Kerl, Kornelius; Fehr, Daniel; Kramps, Christoph; Gessner, Christine; Killmer, Katrin et al. (2006): BMI1 is a target gene of E2F-1 and is strongly expressed in primary neuroblastomas. In: *Nucleic acids research* 34 (6), S. 1745–1754. DOI: 10.1093/nar/gkl119.

Nunes, Ana S.; Barros, Andreia S.; Costa, Elisabete C.; Moreira, André F.; Correia, Ilídio J. (2019): 3D tumor spheroids as in vitro models to mimic in vivo human solid tumors resistance to therapeutic drugs. In: *Biotechnology and bioengineering* 116 (1), S. 206–226. DOI: 10.1002/bit.26845.

Pampaloni, Francesco; Reynaud, Emmanuel G.; Stelzer, Ernst H. K. (2007): The third dimension bridges the gap between cell culture and live tissue. In: *Nature reviews. Molecular cell biology* 8 (10), S. 839–845. DOI: 10.1038/nrm2236.

Park, Mi Seul; Phan, Hong-Duc; Busch, Florian; Hinckley, Samantha H.; Brackbill, James A.; Wysocki, Vicki H.; Nakanishi, Kotaro (2017): Human Argonaute3 has slicer activity. In: *Nucleic Acids Research* 45 (20), S. 11867–11877. DOI: 10.1093/nar/gkx916.

Parker, Roy; Sheth, Ujwal (2007): P bodies and the control of mRNA translation and degradation. In: *Molecular cell* 25 (5), S. 635–646. DOI: 10.1016/j.molcel.2007.02.011.

Paz, Nurit; Levanon, Erez Y.; Amariglio, Ninette; Heimberger, Amy B.; Ram, Zvi; Constantini, Shlomi et al. (2007): Altered adenosine-to-inosine RNA editing in human cancer. In: *Genome research* 17 (11), S. 1586–1595. DOI: 10.1101/gr.6493107.

Pessina, Fabio; Giavazzi, Fabio; Yin, Yandong; Gioia, Ubaldo; Vitelli, Valerio; Galbiati, Alessandro et al. (2019): Functional transcription promoters at DNA double-strand breaks mediate RNA-driven phase separation of damage-response factors. In: *Nature cell biology* 21 (10), S. 1286–1299. DOI: 10.1038/s41556-019-0392-4.

Pisani, Gabriel; Baron, Byron (2019): Nuclear paraspeckles function in mediating gene regulatory and apoptotic pathways. In: *Non-coding RNA research* 4 (4), S. 128–134. DOI: 10.1016/j.ncrna.2019.11.002.

Pitchiaya, Sethuamasundaram; Mourao, Marcio D. A.; Jalihal, Ameya; Xiao, Lanbo; Jiang, Xia; Chinnaiyan, Arul M. et al. (2018): Dynamic Recruitment of Single RNAs to Processing Bodies Depends on RNA Functionality. In: *SSRN Journal*. DOI: 10.2139/ssrn.3224532.

Pitchiaya, Sethuramasundaram; Androsavich, John R.; Walter, Nils G. (2012): Intracellular single molecule microscopy reveals two kinetically distinct pathways for microRNA assembly. In: *EMBO reports* 13 (8), S. 709–715. DOI: 10.1038/embor.2012.85.

Pitchiaya, Sethuramasundaram; Heinicke, Laurie A.; Park, Jun I.; Cameron, Elizabeth L.; Walter, Nils G. (2017): Resolving Subcellular miRNA Trafficking and Turnover at Single-Molecule Resolution. In: *Cell reports* 19 (3), S. 630–642. DOI: 10.1016/j.celrep.2017.03.075.

Pitchiaya, Sethuramasundaram; Krishnan, Vishalakshi; Custer, Thomas C.; Walter, Nils G. (2013): Dissecting non-coding RNA mechanisms in cellulo by Single-molecule High-Resolution Localization and Counting. In: *Methods (San Diego, Calif.)* 63 (2), S. 188–199. DOI: 10.1016/j.ymeth.2013.05.028.

Platani, M.; Goldberg, I.; Swedlow, J. R.; Lamond, A. I. (2000): In vivo analysis of Cajal body movement, separation, and joining in live human cells. In: *The Journal of cell biology* 151 (7), S. 1561–1574. DOI: 10.1083/jcb.151.7.1561.

Rehwinkel, Jan; Behm-Ansmant, Isabelle; Gatfield, David; Izaurralde, Elisa (2005): A crucial role for GW182 and the DCP1:DCP2 decapping complex in miRNA-mediated gene silencing. In: *RNA (New York, N.Y.)* 11 (11), S. 1640–1647. DOI: 10.1261/rna.2191905.

Ren, Yong-Feng; Li, Guiling; Wu, Jianmin; Xue, Yong-Feng; Song, Yi-Jiang; Lv, Lu et al. (2012): Dicer-dependent biogenesis of small RNAs derived from 7SL RNA. In: *PloS one* 7 (7), e40705. DOI: 10.1371/journal.pone.0040705.

Rojas-Ríos, Patricia; Simonelig, Martine (2018): piRNAs and PIWI proteins: regulators of gene expression in development and stem cells. In: *Development (Cambridge, England)* 145 (17). DOI: 10.1242/dev.161786.

Roovers, Elke F.; Rosenkranz, David; Mahdipour, Mahdi; Han, Chung-Ting; He, Nannan; Chuva de Sousa Lopes, Susana M. et al. (2015): Piwi proteins and piRNAs in mammalian oocytes and early embryos. In: *Cell reports* 10 (12), S. 2069–2082. DOI: 10.1016/j.celrep.2015.02.062.

Roy, Jyoti; Mallick, Bibekanand (2018): Investigating piwi-interacting RNA regulome in human neuroblastoma. In: *Genes, chromosomes & cancer* 57 (7), S. 339–349. DOI: 10.1002/gcc.22535.

Santangelo, Philip J.; Nix, Brent; Tsourkas, Andrew; Bao, Gang (2004): Dual FRET molecular beacons for mRNA detection in living cells. In: *Nucleic acids research* 32 (6), e57. DOI: 10.1093/nar/gnh062.

Sasaki, Yasnory T. F.; Hirose, Tetsuro (2009): How to build a paraspeckle. In: *Genome biology* 10 (7), S. 227. DOI: 10.1186/gb-2009-10-7-227.

Sasaki, Yasnory T. F.; Ideue, Takashi; Sano, Miho; Mituyama, Toutai; Hirose, Tetsuro (2009): MENepsilon/beta noncoding RNAs are essential for structural integrity of nuclear paraspeckles. In: *Proc. Natl. Acad. Sci. U.S.A.* 106 (8), S. 2525–2530. DOI: 10.1073/pnas.0807899106.

Sawyer, Iain A.; Bartek, Jiri; Dundr, Miroslav (2018): Phase separated microenvironments inside the cell nucleus are linked to disease and regulate epigenetic state, transcription and RNA processing. In: *Seminars in cell & developmental biology* 90, S. 94–103. DOI: 10.1016/j.semcdb.2018.07.001.

Sawyer, Iain A.; Sturgill, David; Sung, Myong-Hee; Hager, Gordon L.; Dundr, Miroslav (2016): Cajal body function in genome organization and transcriptome diversity. In: *BioEssays : news and reviews in molecular, cellular and developmental biology* 38 (12), S. 1197–1208. DOI: 10.1002/bies.201600144.

Schirle, Nicole T.; Sheu-Gruttadauria, Jessica; MacRae, Ian J. (2014): Structural basis for microRNA targeting. In: *Science (New York, N.Y.)* 346 (6209), S. 608–613. DOI: 10.1126/science.1258040.

Schwab, M.; Alitalo, K.; Klempnauer, K. H.; Varmus, H. E.; Bishop, J. M.; Gilbert, F. et al. (1983): Amplified DNA with limited homology to myc cellular oncogene is shared by human neuroblastoma cell lines and a neuroblastoma tumour. In: *Nature* 305 (5931), S. 245–248. DOI: 10.1038/305245a0.

Seeger, R. C.; Brodeur, G. M.; Sather, H.; Dalton, A.; Siegel, S. E.; Wong, K. Y.; Hammond, D. (1985): Association of multiple copies of the N-myc oncogene with rapid progression of neuroblastomas. In: *The New England journal of medicine* 313 (18), S. 1111–1116. DOI: 10.1056/NEJM198510313131802.

Seto, Eri; Yoshida-Sugitani, Reiko; Kobayashi, Toshihiko; Toyama-Sorimachi, Noriko (2015): The Assembly of EDC4 and Dcp1a into Processing Bodies Is Critical for the Translational Regulation of IL-6. In: *PloS one* 10 (5), e0123223. DOI: 10.1371/journal.pone.0123223.

Sharma, A. K.; Nelson, M. C.; Brandt, J. E.; Wessman, M.; Mahmud, N.; Weller, K. P.; Hoffman, R. (2001): Human CD34(+) stem cells express the hiwi gene, a human homologue of the Drosophila gene piwi. In: *Blood* 97 (2), S. 426–434. DOI: 10.1182/blood.V97.2.426.

Shelkovnikova, Tatyana A.; Kukharsky, Michail S.; An, Haiyan; Dimasi, Pasquale; Alexeeva, Svetlana; Shabir, Osman et al. (2018): Protective paraspeckle hyper-assembly downstream of TDP-43 loss of function in amyotrophic lateral sclerosis. In: *Molecular neurodegeneration* 13 (1), S. 30. DOI: 10.1186/s13024-018-0263-7.

Shiromoto, Yusuke; Sakurai, Masayuki; Qu, Helen; Kossenkov, Andrew V.; Nishikura, Kazuko (2020): Processing of Alu small RNAs by DICER/ADAR1 complexes and their RNAi targets. In: *RNA (New York, N.Y.)* 26 (12), S. 1801–1814. DOI: 10.1261/rna.076745.120.

Sienski, Grzegorz; Dönertas, Derya; Brennecke, Julius (2012): Transcriptional silencing of transposons by Piwi and maelstrom and its impact on chromatin state and gene expression. In: *Cell* 151 (5), S. 964–980. DOI: 10.1016/j.cell.2012.10.040.

Sommer, G.; Dittmann, J.; Kuehnert, J.; Reumann, K.; Schwartz, P. E.; Will, H. et al. (2011): The RNA-binding protein La contributes to cell proliferation and CCND1 expression. In: *Oncogene* 30 (4), S. 434–444. DOI: 10.1038/onc.2010.425.

Sommer, Gunhild; Heise, Tilman (2021): Role of the RNA-binding protein La in cancer pathobiology. In: *RNA biology* 18 (2), S. 218–236. DOI: 10.1080/15476286.2020.1792677.

Song, Ji-Joon; Liu, Jidong; Tolia, Niraj H.; Schneiderman, Jonathan; Smith, Stephanie K.; Martienssen, Robert A. et al. (2003): The crystal structure of the Argonaute2 PAZ

domain reveals an RNA binding motif in RNAi effector complexes. In: *Nature structural biology* 10 (12), S. 1026–1032. DOI: 10.1038/nsb1016.

Sonoda, Yuki; Kano, Fumi; Murata, Masayuki (2021): Applications of cell resealing to reconstitute microRNA loading to extracellular vesicles. In: *Scientific reports* 11 (1), S. 2900. DOI: 10.1038/s41598-021-82452-5.

Spector, D. L. (2001): Nuclear domains. In: *Journal of cell science* 114 (Pt 16), S. 2891–2893. DOI: 10.1242/jcs.114.16.2891.

Spector, David L.; Lamond, Angus I. (2011): Nuclear speckles. In: *Cold Spring Harb Perspect Biol* 3 (2). DOI: 10.1101/cshperspect.a000646.

Stafman, Laura L.; Beierle, Elizabeth A. (2016): Cell Proliferation in Neuroblastoma. In: *Cancers* 8 (1). DOI: 10.3390/cancers8010013.

Su, Chang; Ren, Zhong-Jie; Wang, Fang; Liu, Min; Li, Xin; Tang, Hua (2012): PIWIL4 regulates cervical cancer cell line growth and is involved in down-regulating the expression of p14ARF and p53. In: *FEBS letters* 586 (9), S. 1356–1362. DOI: 10.1016/j.febslet.2012.03.053.

Sugimoto, Keiki; Kage, Hidenori; Aki, Naomi; Sano, Atsushi; Kitagawa, Hiroshi; Nagase, Takahide et al. (2007): The induction of H3K9 methylation by PIWIL4 at the p16Ink4a locus. In: *Biochemical and biophysical research communications* 359 (3), S. 497–502. DOI: 10.1016/j.bbrc.2007.05.136.

Swarts, Daan C.; Makarova, Kira; Wang, Yanli; Nakanishi, Kotaro; Ketting, René F.; Koonin, Eugene V. et al. (2014): The evolutionary journey of Argonaute proteins. In: *Nat Struct Mol Biol* 21 (9), S. 743–753. DOI: 10.1038/nsmb.2879.

Tan, Liping; Mai, Dongmei; Zhang, Bailin; Jiang, Xiaobing; Zhang, Jialiang; Bai, Ruihong et al. (2019): PIWI-interacting RNA-36712 restrains breast cancer progression and chemoresistance by interaction with SEPW1 pseudogene SEPW1P RNA. In: *Molecular cancer* 18 (1), S. 9. DOI: 10.1186/s12943-019-0940-3.

Taubert, H.; Greither, T.; Kaushal, D.; Würl, P.; Bache, M.; Bartel, F. et al. (2007): Expression of the stem cell self-renewal gene Hiwi and risk of tumour-related death in patients with soft-tissue sarcoma. In: *Oncogene* 26 (7), S. 1098–1100. DOI: 10.1038/sj.onc.1209880.

Tian, Yuan; Simanshu, Dhirendra K.; Ma, Jin-Biao; Patel, Dinshaw J. (2011): Structural basis for piRNA 2'-O-methylated 3'-end recognition by Piwi PAZ (Piwi/Argonaute/Zwille) domains. In: *Proceedings of the National Academy of Sciences of the United States of America* 108 (3), S. 903–910. DOI: 10.1073/pnas.1017762108.

Tolia, Niraj H.; Joshua-Tor, Leemor (2007): Slicer and the argonautes. In: *Nature chemical biology* 3 (1), S. 36–43. DOI: 10.1038/nchembio848.

Treiber, Thomas; Treiber, Nora; Meister, Gunter (2019): Regulation of microRNA biogenesis and its crosstalk with other cellular pathways. In: *Nature reviews. Molecular cell biology* 20 (1), S. 5–20. DOI: 10.1038/s41580-018-0059-1.

Tripathi, Kaushlendra; Parnaik, Veena K. (2008): Differential dynamics of splicing factor SC35 during the cell cycle. In: *Journal of biosciences* 33 (3), S. 345–354. DOI: 10.1007/s12038-008-0054-3.

Trotta, Rossana; Vignudelli, Tatiana; Candini, Olivia; Intine, Robert V.; Pecorari, Luisa; Guerzoni, Clara et al. (2003): BCR/ABL activates mdm2 mRNA translation via the La antigen. In: *Cancer cell* 3 (2), S. 145–160. DOI: 10.1016/S1535-6108(03)00020-5.

Tsuboyama, Kotaro; Tadakuma, Hisashi; Tomari, Yukihide (2018): Conformational Activation of Argonaute by Distinct yet Coordinated Actions of the Hsp70 and Hsp90 Chaperone Systems. In: *Molecular Cell* 70 (4), 722-729.e4. DOI: 10.1016/j.molcel.2018.04.010.

Turunen, Tiia A.; Roberts, Thomas C.; Laitinen, Pia; Väänänen, Mari-Anna; Korhonen, Paula; Malm, Tarja et al. (2019): Changes in nuclear and cytoplasmic microRNA distribution in response to hypoxic stress. In: *Scientific reports* 9 (1), S. 10332. DOI: 10.1038/s41598-019-46841-1.

Tyagi, S.; Bratu, D. P.; Kramer, F. R. (1998): Multicolor molecular beacons for allele discrimination. In: *Nature biotechnology* 16 (1), S. 49–53. DOI: 10.1038/nbt0198-49.

Tyagi, S.; Kramer, F. R. (1996): Molecular beacons: probes that fluoresce upon hybridization. In: *Nature biotechnology* 14 (3), S. 303–308. DOI: 10.1038/nbt0396-303.

Ullu, E.; Tschudi, C. (1984): Alu sequences are processed 7SL RNA genes. In: *Nature* 312 (5990), S. 171–172. DOI: 10.1038/312171a0.

van Mierlo, Joël T.; Bronkhorst, Alfred W.; Overheul, Gijs J.; Sadanandan, Sajna A.; Ekström, Jens-Ola; Heestermans, Marco et al. (2012): Convergent evolution of argonaute-2 slicer antagonism in two distinct insect RNA viruses. In: *PLoS pathogens* 8 (8), e1002872. DOI: 10.1371/journal.ppat.1002872.

Vautrot, Valentin; Heckler, Géraud; Aigueperse, Christelle; Behm-Ansmant, Isabelle (2021): Fluorescence In Situ Hybridization of Small Non-Coding RNAs. In: *Methods in molecular biology (Clifton, N.J.)* 2300, S. 73–85. DOI: 10.1007/978-1-0716-1386-3_8.

Walter, P.; Blobel, G. (1983): Disassembly and reconstitution of signal recognition particle. In: *Cell* 34 (2), S. 525–533. DOI: 10.1016/0092-8674(83)90385-9.

Walter, P.; Johnson, A. E. (1995): Signal sequence recognition and protein targeting to the endoplasmic reticulum membrane. In: *Harvey lectures*.

Walter, P.; Lingappa, V. R. (1986): Mechanism of protein translocation across the endoplasmic reticulum membrane. In: *Annual review of cell biology* 2, S. 499–516. DOI: 10.1146/annurev.cb.02.110186.002435.

Wang, Wang-Xia; Prajapati, Paresh; Nelson, Peter T.; Springer, Joe E. (2020): The Mitochondria-Associated ER Membranes Are Novel Subcellular Locations Enriched for Inflammatory-Responsive MicroRNAs. In: *Molecular neurobiology* 57 (7), S. 2996–3013. DOI: 10.1007/s12035-020-01937-y.

Wang, Wei; Han, Bo W.; Tipping, Cindy; Ge, Daniel Tianfang; Zhang, Zhao; Weng, Zhiping; Zamore, Phillip D. (2015): Slicing and Binding by Ago3 or Aub Trigger Piwi-

Bound piRNA Production by Distinct Mechanisms. In: *Molecular cell* 59 (5), S. 819–830. DOI: 10.1016/j.molcel.2015.08.007.

Wang, Yanli; Sheng, Gang; Juranek, Stefan; Tuschl, Thomas; Patel, Dinshaw J. (2008): Structure of the guide-strand-containing argonaute silencing complex. In: *Nature* 456 (7219), S. 209–213. DOI: 10.1038/nature07315.

Wei, Yao; Li, Limin; Wang, Dong; Zhang, Chen-Yu; Zen, Ke (2014): Importin 8 regulates the transport of mature microRNAs into the cell nucleus. In: *The Journal of biological chemistry* 289 (15), S. 10270–10275. DOI: 10.1074/jbc.C113.541417.

Weigert, Nina; Schweiger, Anna-Lena; Groß, Jonas; Matthes, Marie; Corbacioglu, Selim; Sommer, Gunhild; Heise, Tilman (2023): Detection of 7SL RNA-derived small non-coding RNA using Molecular Beacons *in vitro* and in cells. Manuscript submitted for publication.

Weinberg, Marc S.; Morris, Kevin V. (2016): Transcriptional gene silencing in humans. In: *Nucleic acids research* 44 (14), S. 6505–6517. DOI: 10.1093/nar/gkw139.

White, Eleanor; Schlackow, Margarita; Kamieniarz-Gdula, Kinga; Proudfoot, Nick J.; Gullerova, Monika (2014): Human nuclear Dicer restricts the deleterious accumulation of endogenous double-stranded RNA. In: *Nat Struct Mol Biol* 21 (6), S. 552–559. DOI: 10.1038/nsmb.2827.

Willis, I. M. (1993): RNA polymerase III. Genes, factors and transcriptional specificity. In: *European journal of biochemistry* 212 (1), S. 1–11. DOI: 10.1111/j.1432-1033.1993.tb17626.x.

Wong, Justin J. L.; Ritchie, William; Gao, Dadi; Lau, Katherine A.; Gonzalez, Maria; Choudhary, Anupma et al. (2014): Identification of nuclear-enriched miRNAs during mouse granulopoiesis. In: *Journal of hematology & oncology* 7, S. 42. DOI: 10.1186/1756-8722-7-42.

Xi, Xiaochen; Li, Tianxiao; Huang, Yiming; Sun, Jiahui; Zhu, Yumin; Yang, Yang; Lu, Zhi John (2017): RNA Biomarkers: Frontier of Precision Medicine for Cancer. In: *Non-coding RNA* 3 (1). DOI: 10.3390/ncrna3010009.

Xiong, Qunli; Zhang, Yaguang; Li, Junjun; Zhu, Qing (2022): Small Non-Coding RNAs in Human Cancer. In: *Genes* 13 (11). DOI: 10.3390/genes13112072.

Yan, Kelley S.; Yan, Sherry; Farooq, Amjad; Han, Arnold; Zeng, Lei; Zhou, Ming-Ming (2003): Structure and conserved RNA binding of the PAZ domain. In: *Nature* 426 (6965), S. 469–474. DOI: 10.1038/nature02129.

Yi, Rui; Qin, Yi; Macara, Ian G.; Cullen, Bryan R. (2003): Exportin-5 mediates the nuclear export of pre-microRNAs and short hairpin RNAs. In: *Genes & development* 17 (24), S. 3011–3016. DOI: 10.1101/gad.1158803.

Young, Alexander P.; Jackson, Daniel J.; Wyeth, Russell C. (2020): A technical review and guide to RNA fluorescence in situ hybridization. In: *PeerJ* 8, e8806. DOI: 10.7717/peerj.8806.

Yu, Jiang Hong; Yang, Wei-Hong; Gulick, Tod; Bloch, Kenneth D.; Bloch, Donald B. (2005): Ge-1 is a central component of the mammalian cytoplasmic mRNA processing body. In: *RNA (New York, N.Y.)* 11 (12), S. 1795–1802. DOI: 10.1261/rna.2142405.

Yu, Xin; Li, Zheng; Zheng, Heyi; Chan, Matthew T. V.; Wu, William Ka Kei (2017): NEAT1: A novel cancer-related long non-coding RNA. In: *Cell proliferation* 50 (2). DOI: 10.1111/cpr.12329.

Zhang, Z.; Carmichael, G. G. (2001): The fate of dsRNA in the nucleus: a p54(nrb)-containing complex mediates the nuclear retention of promiscuously A-to-I edited RNAs. In: *Cell* 106 (4), S. 465–475. DOI: 10.1016/S0092-8674(01)00466-4.

Zhang, Donglei; Tu, Shikui; Stubna, Michael; Wu, Wei-Sheng; Huang, Wei-Che; Weng, Zhiping; Lee, Heng-Chi (2018): The piRNA targeting rules and the resistance to piRNA silencing in endogenous genes. In: *Science (New York, N.Y.)* 359 (6375), S. 587–592. DOI: 10.1126/science.aao2840.

Zhang, Xinyang; Yang, Siqi; Chen, Wenbo; Dong, Xin; Zhang, Rongyu; Ye, Haidong et al. (2021): Circular RNA circYPEL2: A Novel Biomarker in Cervical Cancer. In: *Genes* 13 (1). DOI: 10.3390/genes13010038.B.

Zhang, Zhao; Zhang, Jian; Diao, Lixia; Han, Leng (2021): Small non-coding RNAs in human cancer: function, clinical utility, and characterization. In: *Oncogene* 40 (9), S. 1570–1577. DOI: 10.1038/s41388-020-01630-3.A.

Zuker, Michael (2003): Mfold web server for nucleic acid folding and hybridization prediction. In: *Nucleic acids research* 31 (13), S. 3406–3415. DOI: 10.1093/nar/gkg595.

8. Danksagung

An dieser Stelle möchte ich allen Personen bedanken, ohne die es diese Arbeit niemals gegeben hätte.
Mein erster großer Dank gilt natürlich PD Dr. Gunhild Sommer und Dr. Tilman Heise, für die Betreuung dieser Arbeit, die vielen Ideen und Gespräche und dafür, dass ihr den Ergebnissen immer etwas Gutes abgewinnen konnten, auch wenn ich es nicht sehen konnte. Außerdem will ich mich bedanken, dass ihr mir die Möglichkeit gegeben habt mit euch einmal um die halbe Welt zu Konferenzen zu reisen.
Natürlich bedanke ich auch meinem Mentorat, Prof. Markus Kretz, Prof. Gunter Meister und Prof. Selim Corbacioglu für die zahlreichen Ideen und dem kritischen Blick der mich aus so mancher Sackgasse herausgeführt hat.
Mein nächster großer Dank gilt natürlich dem gesamten Laborteam, besonders Marie. Du warst so oft mein Fels in der Brandung, standest immer mit Rat und Tat zur Seite und bist einfach eine tolle Freundin.
Ein weiterer Dank gilt meiner Familie, Papa, der mir so manches Mal Mut gesprochen hat und sich meine Sorgen stehts mit großer Geduld angehört hat. Besonders Danke an meine Schwester Andrea, danke, dass du mich immer unterstützt hast und sogar mit mir um die halbe Welt geflogen bist, damit ich mich nicht alleine in der Wüste verlaufe. Natürlich meine Mama, die nicht mehr hier sein kann aber der einzige Grund ist warum ich es bis hierhin geschafft habe.
Ein weiteres Danke gilt natürlich meinen Freunden, vor allem Rich, Lari und Franzi, die immer Zeit hatten mich aufzuheitern und stets ein offenes Ohr für mich haben. Ganz besonders will ich mich hier bei Ecki bedanken, der mich viel zu oft nach Feierabend unangekündigt in seiner Wohnung vorgefunden hat, sich die Nächte um die Ohren geschlagen hat um mir mit dieser Arbeit zu helfen und trotzdem noch mit mir um die Häuser gezogen ist.
Zuletzt will ich mich noch bei einem ganz besonderen Menschen bedanken. Carina, du hast mir gezeigt, dass Familie wenig mit Blut zu tun hat, hast mich durch die schwerste Zeit meines Lebens geführt und für mich weitergekämpft, wenn ich aufgeben wollte.

9. SELBSTÄNDIGKEITSERKLÄRUNG

Ich, Nina Weigert geboren am 13.04.1995 in Burglengenfeld, erkläre hiermit, dass ich die vorliegende Arbeit ohne unzulässige Hilfe Dritter und ohne Benutzung anderer als der angegebenen Hilfsmittel angefertigt habe.
Die aus anderen Quellen direkt oder indirekt übernommenen Daten und Konzepte sind unter Angabe der Quelle gekennzeichnet. Insbesondere habe ich nicht die entgeltliche Hilfe von Vermittlungs- bzw. Beratungsdiensten (Promotionsberater*innen oder andere Personen) in Anspruch genommen.
Die Arbeit wurde bisher weder im In- noch im Ausland in gleicher oder ähnlicher Form einer anderen Prüfungsbehörde vorgelegt.

Ort, Datum

eigenhändige Unterschrift
des/r Promovenden*in